An investigation into the role of OCRL1 in polarised epithelial cells

Rachel Dorothy Daniels

This Thesis is submitted to University College London for the Degree of Doctor of Philosophy

August 2013

Department of Cell Biology
UCL Institute of Ophthalmology

Bath Street
London
EC1V 9EL

Declaration

I, Rachel Daniels, confirm that the work presented in this thesis is my own. Where information has been derived from other sources, I confirm that this has been indicated in the thesis.

Rachel D. Daniels

20th August 2013

Acknowledgments

First and foremost I would like to acknowledge the Lowe Syndrome Trust for funding my project and organising the symposiums I enjoyed attending. The effort that goes into funding research like my own is inspiring and I sincerely hope it yields the progress you seek.

I would like to thank my supervisors Dr. Tim Levine and Prof. Karl Matter for taking me on as a student and for all the support over the past three years. I am particularly grateful to Tim for always being available when I needed advice and guidance. Your input throughout my research and during the writing of this thesis has been invaluable.

It would not have been possible to complete this work without kind assistance from many others. I would like to thank the students and staff at the Institute of Ophthalmology, past and present, for making it such a great place to work. A big thank you to Adam Grieve, whose previous project on OCRL1 gave rise to mine. Thanks for staying in touch, your enthusiasm for OCRL1 was infectious and your suggestions and feedback have been a huge help. Special thanks to Matt Hayes for mentoring me in the lab and for the many insightful discussions about my results. I would like to thank Ceniz for being somebody I could always turn to for advice and several others in the Matter lab who helped me along the way; Elena for helping with the Co-IP's and Emily and Ahmed for providing me with everything I needed to complete the paper. Thank you to Jenny for her friendly advice on all matters relating to PhD life and everybody in the office including Alberto, Apostolis, Hui, Ingrid, Katharina, Louise, Simon, Sterenn and Vineeta. Without you all, this PhD would have been a lot less fun.

Lastly, I would like to thank my family for their unequivocal support throughout, especially my mother and father for always believing in me and my grandfather for all his care and love. The mere expression of thanks does not suffice for the support provided by my partner Lawrence. Thank you for being there through the

frustrations of failed experiments and for motivating me when I found it particularly challenging. For a non-scientist, your impressive understanding of my project reveals just how much I have talked about OCRL1 for the past three years. Thank you for listening, I love you and like we always say; we did it!

Abstract

Mutations in the phosphoinositide 5-phosphatase OCRL1 cause Lowe Syndrome and Dents-2 disease, both involving selective renal proximal tubulopathy. Epithelial cells lining renal proximal tubules are highly polarised with distinct apical and basolateral membranes separated by intercellular junctions. Using Madin Darby canine kidney (MDCK) cells as a model of the renal tubular epithelium, we found a pool of OCRL1 targeted intercellular junctions and was required for the correct organisation of apical and basolateral membranes. One of the first events when cells were depleted of OCRL1 was a block in apical recycling. Apical cargo accumulated in exaggerated Rab11 positive recycling compartments with ectopic accumulation of the OCRL1 substrate PI(4,5)P_2. Among the apical cargo were Gp135 and key regulators of apical membrane formation, including Cdc42 and the Par6-aPKC polarity complex. Rescue of recycling required the 5-phosphatase domain of OCRL1, suggesting down-regulation of 5-phosphoinositides is necessary for cargo exit from apical recycling endosomes. Eventually, the Rab11 positive vesicles containing apical cargo were targeted to the plasma membrane to re-form the apical domain. However, instead of being targeted to the cell apex, the apical vesicles were trafficked towards the lateral membrane where lumens formed, resembling the bile canaliculi in hepatocytes. This process was co-ordinated with cell division. Lateral lumens formed close to the midbody formed during cytokinesis. During cytokinesis Rab11 normally regulates a trafficking pathway to the midbody. Therefore, in cells lacking OCRL1 apical cargo held up in Rab11 positive compartments may be aberrantly trafficked along this pathway when cells divide. We also found that the orientation and subsequent resolution of mitoses was altered in cells lacking OCRL1, which may contribute to improper positioning of the midbody and subsequent failure to polarise correctly. In summary, these results implicate OCRL1 in multiple steps of the process that co-ordinates apical recycling and cell division in polarised cells.

Table of Contents

Table of Figures

Chapter One: Introduction

Chapter Three: OCRL1 is involved in the maturation of epithelial cells

Chapter Four: MDCK cells without OCRL1 form lateral apical lumens

Chapter Five: OCRL1 regulates apical recycling pathways in MDCK cells

Chapter Six: OCRL1 and Cell Division in MDCK cells

Abbreviations

AEE	Apical early endosomes
AMIS	Apical membrane initiation site
ANTH	AP180 N-terminal homology
AP-2	Adaptor protein 2
aPKC	Atypical protein kinase C
APPL1	Adaptor protein, phosphotyrosine interaction, PH domain and leucine zipper containing 1
ARE	Apical recycling endosome
ARF	ADP-ribosylation factor
ARP2/3	Actin-related protein2/3
ASH	ASPM-SPD-2-Hydin
ASPM	Abnormal spindle-like, microcephaly-associated
BAR	Bin-Amphiphysin-Rvs
BEE	Basolateral early endosomes
C. elegans	*Caenorhabditis elegans*
Caco-2	Colorectal adenocarcinoma
Cdc42	Cell division cycle 42
CI-MPR	Cation-independent mannose-6-phosphate receptor
CLCN5	Chloride channel, voltage-sensitive 5
CRE	Common recycling endosome
DAG	1,2-Diacylglycerol
DAPI	4',6-diamidino-2-phenylindole
Dlg	Discs large
DMEM	Dulbecco's modified eagle medium
DNA	Deoxyribonucleic acid
E. coli	*Escherichia coli*
E-cadherin	Epithelial cadherin
ECL	Enhanced chemiluminescence
ECM	Extracellular medium
EDTA	Ethylenediaminetetraacetic acid
EEA1	Early endosome antigen 1
EGFR	Epidermal growth factor receptor
ENTH	Epsin N-terminal homology domain
ERM	Ezrin, Radixin, Moesin
ESCRT	Endosomal sorting complex required for transport
FBS	Fetal bovine serum
FRAP	Fluorescence recovery after photobleaching
FYVE	Fab-1, YGL023, Vps27, and EEA1
GAP	GTPase activating protein
GDP	Guanosine diphosphate

GEF	Guanine exchange factor
GFP	Green fluorescent protein
GIPC	GAIP-interacting protein, C terminus
Gp135	Glycoprotein 135
Grp1	General receptor for phosphoinositides 1
GST	Glutathione S-transferase
GTP	Guanosine triphosphate
GTPase	Guanosine triphosphatase
HeLa	Henrietta Lacks, cervical immortalised cancer cell line
hTERT	Human telomerase reverse transcriptase
IgG	Immunoglobulin G
INPP5B	Inositol polyphosphate-5-phosphatase B
IP3	Inositol(1,4,5)P3
IPIP27A/B	inositol polyphosphate phosphatase interacting protein of 27 kDa A/B
IPTG	Isopropyl β-D-1-thiogalactopyranoside
IRSp53	insulin receptor tyrosine kinase substrate p53
LB	Lysogeny broth
Lgl	Lethal giant larvae
LMW	Low molecular weight
MAGI-2	Membrane-associated guanylate kinase inverted-2
MARK2	Microtubule affinity-regulating kinase 2
MDCK	Madin Darby canine kidney
MPR	mannose-6-phosphate receptor
MTM	Myotubularin
OCRL	Oculocerebrorenal syndrome of Lowe
PAGE	Polyacrylamide gel electrophoresis
PALS1	protein associated with Lin-7
PAP	pre-apical patch
Par	Partitioning defective protein
PATJ	PALS1-associated tight junction protein
PBS	Phosphate buffered saline
PDZ	Postsynaptic density protein-95, Disc-large tumor suppressor protein, Zonula occludens-1
PFA	Paraformaldehyde
PH	Pleckstrin Homology
PI(3)P	Phosphatidylinositol 3-phosphate
PI(3,4,5)P3	Phosphatidylinositol 3,4,5-trisphosphate
PI(3,5)P2	Phosphatidylinositol 3,4-bisphosphate
PI(4)P	Phosphatidylinositol 4-phosphate
PI(4,5)P2	Phosphatidylinositol 4,5-bisphosphate
PIP5K	Phospholipid kinase phosphatidylinositol 4-phosphate 5-kinase
PLC	Phospholipase C
PTEN	Phosphatase and tensin Homolog
PVDF	Polyvinylidene fluoride

PX	Phox homology
Rab	Ras-like protein in brain
Rac1	Ras-related C3 botulinum toxin substrate 1
Rho	Ras homolog
RNAi	Ribonucleic acid interference
ROCK1	Rho-associated, coiled-coil containing protein kinase 1
SDS	Sodium dodecyl sulfate
SEM	Standard error of the mean
Ses1/2	Sesquipedalian1/2
SH3	Src Homology 3
SHIP	SH2 containing inositol 5-phoshatase
siRNA	Small interfering ribonucleic acid
SKIPP	Skeletal muscle and kidney enriched inositol polyphosphate phosphatase
SNARE	Soluble NSF attachment protein receptor
SNX18	Sorting nexin 18
TER	Transepithelial resistance
TGN	Trans golgi network
Tmod3	Tropomodulin 3
VAC	Vacuolar apical compartment
VAP	vesicle-associated membrane protein-associated protein
WASP	Wiscott-Aldrich Syndrome protein
WAVE	Wiskott-Aldrich Syndrome protein family verprolin-homologous protein
ZO-1	Zonula Occludens-1

Chapter One

Introduction

OCRL1 and human disease

Overview

Mutations in the OCRL1 gene are associated with Lowe Syndrome and a subset of Dent's disease. Lowe Syndrome is a rare X-linked disorder affecting the eyes, the kidneys, and the central nervous system (Loi, 2006; Lowe et al., 1952). Lowe Syndrome patients present with cataracts at birth and frequently develop additional ocular abnormalities such as glaucoma. The central nervous system (CNS) involvement is attributed by low muscle tone (hypotonia), cognitive delay and behavioural problems. However the most fatal aspect of the disease is the renal selective proximal tubulopathy, characterised by low molecular weight proteinuria and hypercalciuria. Dent-2 disease has similar renal defects but only mild neurological and ocular symptoms (Shrimpton et al., 2009; Utsch et al., 2006).

All Lowe Syndrome patients display loss of function mutations in the OCRL1 gene, coding for a phosphoinositide phosphatase. The majority of Dent's patients have mutations in the CLCN5 gene, coding for a chloride transporter. However approximately 15% of all Dent's patients have mutations in OCRL1 and not CLCN5, when it is known as Dents-2 disease (Hoopes et al., 2005). The overlapping renal symptoms of Lowe Syndrome and Dent's disease suggest OCRL1 and CLCN5 may be involved in similar reabsorption pathways in the renal proximal tubule.

Phosphoinositides

OCRL1 is involved in the metabolism of phosphoinositides, these are minor but essential components of all eukaryotic cell membranes. Phosphoinositides contain two fatty acyl chains and a glycerol backbone esterified to a polar inositol head group that extends into the cytoplasm. There are seven different combinations which are formed by differential phosphorylation of the inositol ring at positions

D3, D4 and D5 (Liu and Bankaitis, 2010). A single phosphorylation event at one of these sites forms either PI(3)P, PI(4)P, or PI(5)P, and multiple phosphorylations can give rise to PI(3,4)P_2, PI(4,5)P_2, PI(3,5)P_2, or PI(3,4,5)P_3. The different combinations of phosphoinositides can be interconverted in a manner that is spatially and temporally regulated by phosphoinositide kinases and phosphatases. In addition, phospholipases hydrolyse some phosphoinositide species to produce a variety of inositol phosphates.

Phosphoinositide metabolising enzymes are heterogeneously localised in the cell, which in turn results in the accumulation of different species at distinct organelles (figure 1.1). PI(3)P is typically enriched on early endocytic membranes and the multivesicular body (MVB) compartment (Gillooly et al., 2000). The Golgi apparatus has a high PI 4-kinase activity (Wang et al., 2003) and therefore PI(4)P is the dominant species on membranes of the Golgi apparatus (Roy and Levine., 2004). PI(4,5)P_2 and PI(3,4,5)P_3 are particularly enriched at the plasma membrane (Czech et al., 2000). Most of the plasma membrane PI(4,5)P_2 is generated by phosphorylation of PI(4)P by PIP 5-kinases which localise there (Mao and Yin, 2007). PI(3,5)P_2 concentrates on late compartments of the endocytic pathway, the MVB, and the lysosome (Ikonomov et al., 2006). PI(5)P is also present on endosomes and is thought to localise to the nucleus (Clarke et al., 2001). This pattern of phosphoinositide distribution represents the most abundant species at each organelle but small functionally relevant pools of other phosphoinositides are present in membrane micro-domains; for example, pools of PI(4)P exist at the plasma membrane which is predominantly rich in PI(4,5)P_2 (Balla et al., 2005; Roy and Levine, 2004) and small pools of PI(4,5)P_2 are thought to be present on intracellular membranes that predominantly contain PI(3)P or PI(4)P (Watt et al., 2002).

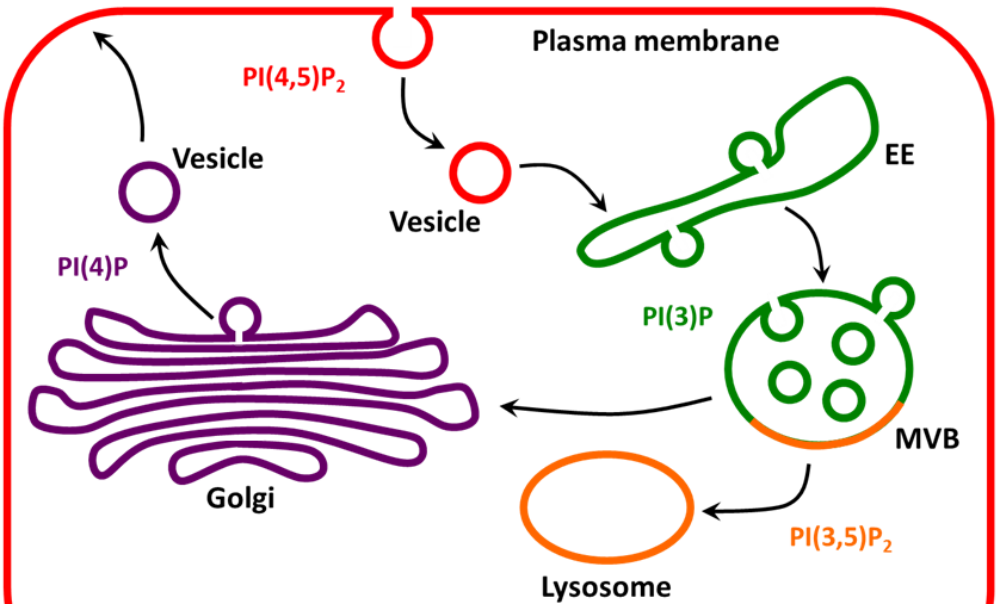

Figure 1.1: Predominant localisation of the major phosphoinositides in the cell. The main phosphoinositide species in the plasma membrane is PI(4,5)P_2. Golgi membranes are enriched in PI(4)P. Early endosomes mostly contain PI(3)P and late compartments in the endocytic pathway are enriched in PI(3,5)P_2.

A number of human diseases have been linked to phosphoinositide metabolising enzymes, emphasising the importance of this process in cell function. Mutations in myotubularin (MTM) 3-phosphatases have been linked to myotubular myopathy and Charcot-Marie-Tooth disease (Clague et al., 2005). In addition the 3-phosphatase PTEN (phosphatase and tensin homologue) is a potent tumour suppressor mutated in many human cancers (Ali et al., 1999). Of the 10 members of the 5-phosphatase family, several have been linked to human disease. SHIP2 (SH2 containing inositol 5-phoshatase 2) has been implicated in diabetes through its role in regulating the cellular response to insulin (Clement et al., 2001) and synaptojanin-1 may play a role in the onset of Down Syndrome associated Alzheimer's disease (Voronov et al., 2008). As mentioned above, OCRL1 is the 5-phosphatase associated with Lowe Syndrome and Dents-2 disease. Pathological mutations in the OCRL1 gene cause complete loss of the protein product either because of gene deletion mutations or because mutations cause the protein to be unstable and subsequently enzymatically degraded. Therefore a lack of enzyme activity is thought to underlie the disease and not truncated protein induced

dominant effects. OCRL1 removes the phosphate group at the 5th position of both PI(4,5)P_2 and PI(3,4,5)P_3 (Lowe et al., 2005). Skin fibroblasts derived from Lowe Syndrome patients have reduced 5-phosphatase activity (Suchy et al., 1995) and concurrently elevated levels of PI(4,5)P_2, suggesting that this may contribute to the symptoms of the disease (Wenk et al., 2003; Zhang et al., 1998).

Phosphoinositide binding domains

One of the main functions of phosphoinositides is the recruitment and regulation of effector proteins that contain phosphoinositide binding domains. Each species of phosphoinositide recruits a specific complement of proteins appropriate for each membrane compartment. Binding of proteins to phosphoinositides is often through electrostatic interactions with the negative charges of the phosphate groups on the inositol ring (Lemmon, 2008). Some proteins, including the small GTPases interact with phosphoinositides through unstructured cytoplasmic regions rich in basic residues (Heo et al., 2006), while other proteins contain highly conserved modular domains (Lemmon, 2008). The best studied of these domains are the PH, PX, ANTH/ENTH and FYVE families (Lemmon, 2003). Most PH (pleckstrin homology) domains interact with multiple phosphoinositides, however a subset of PH domains are specific for PI(3,4)P_2, PI(4,5)P_2 or PI(3,4,5)P_3 (Lietzke et al., 2000). The majority of PX (phox homology) domains, and all FYVE (Fab-1, YGL023, Vps27, and EEA1) domains specifically recognise endosomal PI(3)P (Kutateladze, 2010), while the ANTH (AP180 N-terminal homology) and ENTH (Epsin N-terminal homology) domains are specific for plasma membrane PI(4,5)P_2 (Itoh et al., 2006). Proteins containing phosphoinositide binding domains become associated with a particular membrane in part because of its phosphoinositide composition, however other factors co-operate with phosphoinositides to recruit peripheral proteins to membranes, particularly GTPase proteins, discussed next.

Phosphoinositides and GTPases

Phosphoinositides do not function alone to specify membrane identity, members of the Ras superfamily of small GTPases including the Rab and Arf (ADP-ribosylation factor) families act together with phosphoinositides to create distinct membrane domains (Mizuno-Yamasaki et al., 2012). In a similar manner to phosphoinositides, GTPases are heterogeneously localised in the cell and function to recruit a specific repertoire of effector proteins to the membrane (Hutagalung and Novick, 2011). Another parallel between phosphoinositides and GTPase proteins involves their dynamic regulation. GTPases can exist in either an active (GTP bound) or inactive (GDP) state. Guanine nucleotide exchange factors (GEFs) convert the inactive GDP bound protein to an active GTP bound form, whilst GTPase activating proteins (GAPs) promote GTP hydrolysis to deactivate the protein (Barr and Lambright, 2010). Effector proteins only interact with the active form of the GTPase and therefore effector proteins can be recruited to membranes temporally by switching the GTPase to an active state. Membrane recruitment of OCRL1 5-phosphatase is thought to be mediated by interactions with Rab proteins (Hyvola et al., 2006), discussed in more detail below (Cellular roles of OCRL1).

The spatiotemporal regulation of phosphoinositides and the Rab GTPases is critical for membrane trafficking and organelle maturation. The transport of cargo through successive membrane compartments either through vesicle fusion or membrane maturation requires the membrane to change identity by modifying its phosphoinositide and Rab GTPase composition. As one species of phosphoinositide is replaced by another during vesicle trafficking or membrane maturation, a different set of peripheral proteins is recruited to the membrane. To achieve such a transition, some phosphoinositides and Rab GTPases have been shown to recruit regulators that lead to production of the next phosphoinositide or activation of the downstream Rab (Jean and Kiger, 2012). In addition Rab and phosphoinositide activities can lead to the recruitment of enzymes that inactivate their own function, which ensures a sequential progression of membrane identity (Jean and Kiger, 2012). For example, during endosome maturation, Rab5 on early endosomes

recruits a Rab7 GEF to contribute to Rab7 activation on late endosomes (Rink et al., 2005). Similarly, phosphoinositide regulating enzymes can be recruited as phosphoinositide effectors. For example, PI(3)P on early endosomes facilitates its own down-regulation by recruiting a set of MTM proteins (myotubularins) with 3-phosphatase activity (Jean et al., 2012). The MTM proteins are recruited to PI(3)P on membranes through FYVE domains (Jean et al., 2012).

Some Rab GTPases and phosphoinositides have common effectors, strengthening membrane specificity further. Many of these effector proteins require both the Rab and phosphoinositide for membrane recruitment (Jean and Kiger, 2012). These effector proteins have only weak and transient interactions with phosphoinositides but the presence of another binding partner, such as a Rab GTPase, increases the binding strength of the effector protein to the membrane (Carlton et al., 2005). For example, recruitment of EEA1 (early endosome antigen 1) to endosomes requires both PI(3)P and Rab5 (Simonsen et al., 1998). In this way, Rab GTPases and phosphoinositides co-operate to maintain distinct identities of organelles and ensure the correct timing and location of a variety of events. Some examples of proteins regulated by phosphoinositides, as well as their cellular function are given next.

Cellular roles of phosphoinositides

The ability to rapidly turnover phosphoinositides makes them optimal mediators in signalling pathways. At the plasma membrane, PI(4,5)P_2 and PI(3,4,5)P_3 are involved in the intracellular transduction of extracellular signals. Upon stimulation of G-protein coupled receptors, phospholipase C (PLC) hydrolyses PI(4,5)P_2 into second messengers Inositol(1,4,5)P3 (IP3) and 1,2-Diacylglycerol (DAG) which activate downstream signalling pathways that promote transcription factor activation (Czech, 2000). PI(3,4,5)P_3 is normally present at very low levels in cells at rest but upon growth factor stimulation the levels of this phosphoinositide rapidly rise where it recruits effectors of numerous signalling pathways (Cantley, 2002).

Phosphoinositides, particularly $PI(4,5)P_2$ and $PI(3,4,5)P_3$ are key regulators of the organisation and dynamics of the actin cytoskeleton (Czech, 2000). These phosphoinositides act as platforms to recruit regulators of the actin cytoskeleton as well as actin binding proteins to the membrane. Membrane associated actin dynamics contribute to the force required for events such as shape change, migration and endocytosis. One way phosphoinositides affect actin dynamics is through regulating the activities of Rho GTPases, which activate signalling cascades involved in actin organisation. For example, GEFs of Rac1 (Sos1 and Vav) are activated by interactions with $PI(3,4,5)P_3$ through PH domains (Das et al., 2000). $PI(3,4,5)P_3$ mediated Rac1 activation leads to the induction of actin filament assembly near membranes containing this phosphoinositide. In addition, most of the Rho family members contain a cluster of positively charged residues which may bind to acidic phospholipids, for example, Rho1 and Cdc42 become associated with the membrane in part through interactions of their polybasic sequence with $PI(4,5)P_2$ (Johnson et al., 2012; Yoshida et al., 2009). As well as regulating the Rho family of GTPases, these phosphoinositides also regulate the actin nucleating Arp2/3 complex. In one mechanism, $PI(4,5)P_2$ acts together with the GTPase Cdc42 to recruit N-WASP to the plasma membrane, resulting in the activation of Arp2/3 (Rohatgi et al., 2000). $PI(4,5)P_2$ further contributes to actin filament assembly by directly interacting with numerous actin binding proteins, as well as negatively regulating proteins that inhibit actin filament assembly (Yin et al., 2003). As a consequence of these activities, membranes rich in $PI(4,5)P_2$ are usually associated with actin filament assemblies and disrupting the levels of this phosphoinositide affects the organisation of these structures (Raucher et al., 2000).

As well as cytoskeletal dynamics, phosphoinositides are involved in multiple stages of membrane trafficking including cargo selection, vesicle budding, tethering and fusion. At the plasma membrane, $PI(4,5)P_2$ regulates both endocytosis and exocytosis (Czech, 2000). $PI(4,5)P_2$ interacts with numerous components of the clathrin mediated endocytic machinery such as the adaptor protein AP-2 (Gaidarov and Keen, 1999), and epsin (Itoh et al., 2001). Similarly, PI(4)P recruits components of the clathrin machinery to the Golgi apparatus. Without PI(4)P, the clathrin

adaptor protein AP-1 dissociates from the TGN and all AP-1 dependent trafficking events are inhibited (Wang et al., 2003). Phosphoinositides can facilitate vesicle budding by recruiting effector proteins with BAR domains (Bin, Amphiphysin, Rvs-homology) which dimerize and form a curved structure to drive membrane deformation (van Weering et al., 2010). In addition, PI(4,5)P_2 mediated actin filament assembly (discussed above) contributes to the force required to induce membrane curvature and scission of endocytic vesicles (Sun et al., 2007). In addition, phosphoinositides can facilitate membrane trafficking specificity by recruiting tethering proteins to particular membrane compartments. PI(3)P recruits EEA1 which functions to dock incoming vesicles to the endosome and PI(4,5)P_2 interacts with several components of the exocyst complex to target vesicles to the plasma membrane (He et al., 2007; Zhang et al., 2008).

OCRL1 domain organisation and binding partners

OCRL1 is a member of the type II family of inositol polyphosphate 5-phosphatases which include synaptojanins 1 and 2, SHIP (SH2 containing inositol 5-phoshatase) 1 and 2, SKIPP (Skeletal muscle and kidney enriched inositol polyphosphate phosphatase) and INPP5B (Inositol polyphosphate-5-phosphatase B) (Astle et al., 2006). Members of this family share the central 5-phosphatase domain, but differ in additional domain structures.

The N-terminus of OCRL1 contains a PH-like domain (figure 1.2), which lacks residues required for phosphoinositide recognition and therefore does not bind to membranes (Mao et al., 2009). Adjacent to the PH domain is the central 5-phosphatase domain followed by a short helix connecting to a ASPM-SPD-2-Hydin (ASH) domain (Ponting, 2006) and a Rho GAP-like domain (Faucherre et al., 2003), indicated in figure 1.2. The ASH domain has an immunoglobulin-like fold similar to VAP (vesicle-associated membrane protein-associated protein) and is frequently associated with cilia and centrosomal proteins (Ponting et al., 2006). The RhoGAP domain lacks the catalytic arginine residue and is enzymatically inactive but is able

to interact with various small GTPases, such as Cdc42, Rac1 and Arf family members Arf1 and Arf6 (Lichter-Konecki et al., 2006). The Rho GAP-like domain and ASH domain is required for OCRL1 to associate with several members of the Rab GTPase family. OCRL1 has a broad specificity of Rab binding partners including Rab1, Rab5, Rab6, Rab8, Rab14 (Hyvola et al., 2006), as well as Rab3, Rab13, Rab22, Rab35 (Fukuda et al., 2008) and Rab31 (Rodriguez-Gabin et al., 2010). Interactions of OCRL1 with Rab5, Rab6 and Rab35 have been confirmed by functional and co-localisation studies (Dambournet et al., 2011; Hyvola et al., 2006) and OCRL1 has recently been crystallised in complex with Rab8a (Hou et al., 2011). Interactions with Rab8 require the complete ASH domain of OCRL1 and one α-helix from the 5-phosphatase domain (Hou et al., 2011). This binding mode is unusual, whereas other known Rab effectors bind their Rab through α-helical structural elements, OCRL1 interacts with Rab8a through the β-sheets of the ASH domain as well as the one α-helix (Hou et al., 2011).

As well as interacting with Rab GTPases, the ASH domain of OCRL1 is also required for interactions with the endocytic proteins APPL1 (adaptor protein, phosphotyrosine interaction, PH domain and leucine zipper containing 1) and IPIP27A/B (inositol polyphosphate phosphatase interacting protein of 27 kDa A/B), also known as Ses1/2, for sesquipedalian (Erdmann et al., 2007; Noakes et al, 2011; Swan et al, 2010). These proteins interact with OCRL1 through an F&H motif, a short amino acid sequence within a α-helix containing phenylalanine and histidine residues essential for binding to OCRL1 (Noakes et al, 2011; Swan et al, 2010). The ASH-RhoGAP-like domain of OCRL1 has been crystallised in complex with the F&H peptide of IPIP27A/Ses1 (Pirruccello et al., 2011). The binding site for IPIP27A/Ses1 is distinct from the binding site for Rab proteins, with F&H proteins interacting with the RhoGAP-like domain and not the ASH domain of OCRL1. However, the requirement of the ASH domain for binding of OCRL1 to F&H proteins might be due to the ASH domain stabilising the RhoGAP-like domain fold (Hagemann et al., 2012). Interestingly the F&H binding surface in OCRL1 is evolutionary conserved in organisms that do not have homologues of IPIP/Ses proteins or APPL1 (Pirruccello

et al., 2011), indicating the presence of additional proteins containing the F&H motif.

As well as the modular domains, OCRL1 also contains several short motifs that co-ordinate interactions with additional binding partners. On either side of the central 5-phosphatase domain are several clathrin box motifs: LIDLE and LIDIA which interact with clathrin heavy-chain. In the linker between the PH domain and 5-phosphatase domain is a short motif (FEDNEF) that binds to the adaptor protein AP-2. These interactions have been shown to facilitate the formation of clathrin cages in vitro (Choudhury et al., 2005).

Figure 1.2: Schematic diagram showing domain structure of OCRL1. At the C-terminus of the protein are a catalytically inactive Rho GAP-like domain and an ASH domain which facilitates Rab GTPase binding. At the N-terminus is a PH-like domain and in the centre is the catalytic 5-phosphatase domain. OCRL1 contains several short motifs: LIDLE and LIDIA interact with clathrin heavy chain and FEDNF binds to adaptor protein 2 (AP-2).

OCRL1 and INPP5B are the only members of the type II 5-phosphatase family that contain the ASH domain and RhoGAP-like domain at the C-terminus. INPP5B has no clathrin or AP-2 binding sites (Jefferson and Majerus, 1995) but shares all other binding partners of OCRL1, suggesting the possibility that OCRL1 and INPP5B have partially overlapping functions. Lowe Syndrome cannot be reproduced in OCRL1-knockout mice, probably due to compensation by INPP5B (Jänne et al., 1998). Evidence for INPP5B compensating for loss of OCRL1 in mice comes from the observation that loss of INPP5B and OCRL1 singularly produces only minor phenotypes but loss of both INPP5B and OCRL1 together is lethal (Jänne et al.,

1998). Splice site variation between species may explain the lack of compensation in humans (Bothwell et al., 2010). However, the potential for INPP5B to compensate for OCRL1 is a possible explanation for the tissue specificity of Lowe Syndrome. Variations in the level of expression of INPP5B in the relevant tissues may affect the severity of the OCRL1 loss of function phenotype.

OCRL1 exists as two splice isoforms (a and b) that differ by the presence or absence of eight amino acids (EDSFLEKE) downstream of the LIDLE clathrin box motif (Nussbaum, 1999). The longest isoform (Isoform a) is only expressed in the brain, whilst both isoforms are present in all other tissues, with the shorter isoform usually the most abundant (Johnson et al., 2003). Alternative splicing of OCRL1 modifies it's interaction with clathrin; OCRL1 isoform a binds clathrin heavy chain with higher affinity than isoform b (Choudhury et al., 2009).

Cellular roles of OCRL1

Membrane localisation of OCRL1 is thought to be primarily mediated by interactions with Rab proteins, with Rab1 and Rab6 recruiting OCRL1 to the Golgi apparatus, Rab5 recruiting OCRL1 to endocytic membranes (Hyvola et al., 2006) and Rab8 recruiting OCRL1 to other trafficking intermediates (Coon et al., 2012). Point mutations of OCRL1 that render the protein defective in Rab binding fail to target intracellular membranes (Hyvola et al., 2006). Furthermore, binding to Rab GTPases has been reported to stimulate the 5-phosphatase activity of OCRL1 (Hyvola et al, 2006), suggesting that OCRL1 is recruited to membrane compartments by Rab GTPases at least in part to regulate the levels of $PI(4,5)P_2$. However, OCRL1 also localises to clathrin coated trafficking intermediates by directly interacting with components of the clathrin machinery (Choudhury et al., 2005; Ungewickell et al, 2004) and has been found to translocate to plasma membrane ruffles after growth factor stimulation in a Rac-1 dependent manner (Faucherre et al, 2003; Hyvola et al, 2006). OCRL1 has also been found to localise to the tight Junctions of epithelial cells (Grieve et al., 2011). However, the protein interactions that mediate junctional

recruitment of OCRL1 and its cellular function there are not currently known. These findings are explained in more detail in the second section of this introduction: Epithelial cell polarity.

The subcellular localisations of OCRL1 and its confirmed binding partners indicate a role in regulating membrane trafficking. Furthermore, the interaction of OCRL1 with numerous Rab proteins suggests that OCRL1 may regulate multiple trafficking pathways. Numerous studies have defined roles for OCRL1 in the endocytic pathway. Firstly, OCRL1 has been implicated to regulate traffic from endosomes to the Golgi apparatus (Choudhury et al., 2005; Cui et al., 2010; Ungewickell et al., 2004; van Rahden et al., 2012). For example, overexpression or depletion of OCRL1 in HeLa cells results in the redistribution the cation-independent mannose 6-phosphate receptor (CI-MPR) to enlarged endosomes that are defective in trafficking to the TGN (Choudhury et al., 2005). In agreement with OCRL1 binding to Rab5 and components of the clathrin machinery, OCRL1 also associates with endocytic clathrin coated pits and to peripheral early endosomes (Erdmann et al., 2007). At early endosomes, OCRL1 interacts with the Rab5 effector APPL1, and IPIP27A/B through an F&H motif that binds the C-terminal ASH-RhoGAP domain of OCRL1 (Noakes et al, 2011; Swan et al, 2010), as explained in the previous section. These interactions are mutually exclusive; APPL1 and IPIP27A/B compete for binding to OCRL1 as vesicles progress along the endocytic pathway (Noakes et al, 2011; Swan et al., 2010). As early endosomes acquire PI(3)P and mature, the OCRL1-APPL1 interaction is replaced by the OCRL1-IPIP interaction (Swan et al., 2010), suggesting a regulatory mechanism whereby membrane maturation is coupled to the modification of OCRL1 binding partners.

Given the localisation pattern and pathways regulated by binding partners of OCRL1, there may be additional roles for OCRL1 in the endocytic pathway. For example, as well as the TGN and early endosomes, the IPIPs also localise to Rab11 positive recycling endosomes and participate in trafficking of the transferrin receptor from these compartments to the cell surface (Noakes et al., 2011). APPL1 has been implicated in signalling and sorting of cell surface receptors such as the

nerve growth factor receptor TrkA and its binding partner GPIC (GAIP-interacting protein, C terminus) (Lin et al., 2006). OCRL1 may regulate this protein complex since pull downs of OCRL1 from rat brain extracts contain GIPC and APPL1 (Erdmann et al., 2007). In addition, GIPC has been found to be a binding partner of megalin (Lou et al., 2002), a protein less abundant on the cell surface in Lowe Syndrome (Norden et al., 2000). Megalin is a multi-ligand receptor that mediates reabsorption of low molecular weight (LMW) proteins from the ultrafiltrate. The accumulation of LMW proteins in the ultrafiltrate of Lowe Syndrome patients is consistent with a recycling defect of megalin (Christensen et al., 2002). In addition, many of the Rab binding partners of OCRL1 are involved in recycling pathways, including Rab8 and Rab35 (Hutagalung and Novick, 2011), further suggesting a possible role for OCRL1 in regulating recycling routes to the plasma membrane.

A recent study directly implicates OCRL1 in plasma membrane recycling pathways. In cells derived from Lowe Syndrome patients and OCRL1 depleted renal cell lines, trafficking of megalin and the transferrin receptor to the cell surface was reduced (Vicinanza et al., 2011). In addition to reduced plasma membrane recycling, this study also demonstrated a requirement for OCRL1 in trafficking of epidermal growth factor receptor (EGFR) to late endosomes and confirmed the previous finding that OCRL1 regulates recycling of CI-MPR to the Golgi apparatus (Vicinanza et al., 2011). Without OCRL1, these receptors accumulated in large early endosomes, suggesting OCRL1 regulates cargo exit from these compartments. The block in recycling appeared to be caused by elevated levels of $PI(4,5)P_2$ on endosomes which in turn increased the levels of filamentous actin associated with endosomal membranes, as shown in figure 1.3.

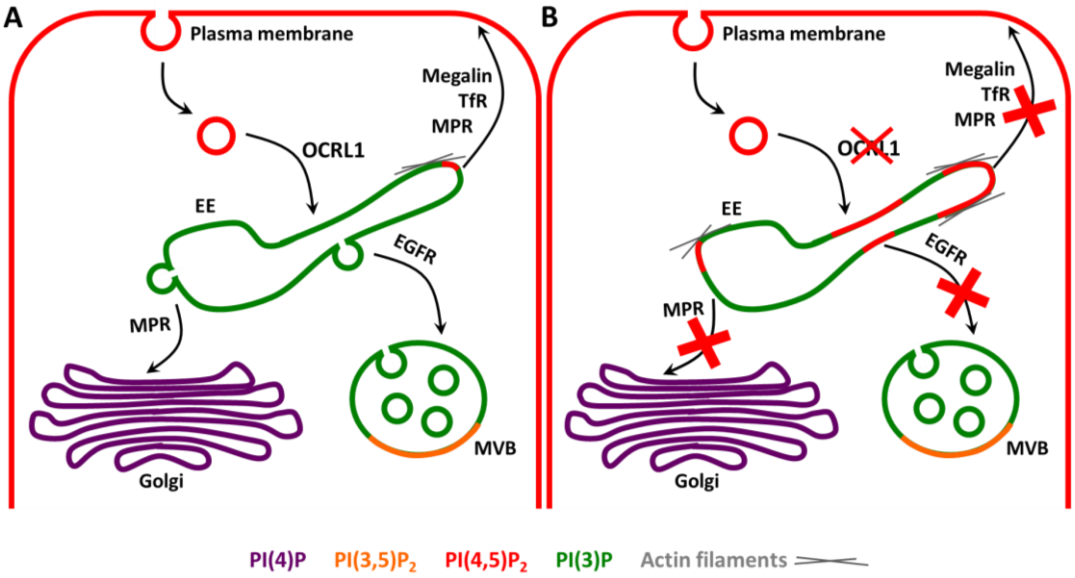

Figure 1.3: Loss of OCRL1 alters trafficking from early endosomes. A: OCRL1 removes PI(4,5)P_2 on endocytosed vesicles and early endosomes. Removal of PI(4,5)P_2 facilitates a phosphoinositide switch towards PI(3)P which is required for early endosome organelle identity. B: Without OCRL1, PI(4,5)P_2 levels remain high on these compartments. PI(4,5)P_2 activates N-WASP dependent F-actin polymerisation which compromises cargo exit and trafficking to the plasma membrane, late endosomes/multi-vesicular body (MVB) and lysosome is impaired. Adapted from Vicinanza et al., 2011.

However, a subsequent study found trafficking of the transferrin receptor and EGFR was normal in Lowe Syndrome fibroblasts, but defects were observed in the intracellular sorting of MPRs (van Rahden et al., 2012). Interestingly, OCRL1 depletion resulted in reduced levels of active Rac1 and increased levels of active RhoA, affecting the activities of downstream actin regulatory substrates cofilin and PAK3 (van Rahden et al., 2012), suggesting OCRL1 might similarly regulate trafficking of MPRs through modulating cellular actin dynamics.

A specific trafficking pathway regulated by OCRL1 has been described involving cilia assembly. Primary cilia are cell surface projections that sense the extracellular environment and are involved in multiple signal transduction pathways (Goetz and Anderson, 2010). The primary cilium is composed of a basal body differentiated from the centrosome and a ciliary axoneme consisting of 9 microtubule doublets

(Sorokin, 1962). OCRL1 has been found to localise to the basal body by numerous studies (Coon et al., 2012; Luo et al., 2012; Rbaibi et al., 2012). However, different effects have been reported on cilia length in the absence of OCRL1, with no clear consensus as to whether they are shorter than normal (Coon et al., 2012; Luo et al., 2012) or elongated (Rbaibi et al., 2012). OCRL1 appears to effect cilia length by regulating a trafficking pathway involving Rab8 that carries ciliary proteins from the TGN to the primary cilium. In addition, OCRL1 regulates trafficking to the primary cilium from recycling endosomes through interactions with the IPIPs (Coon et al., 2012). Interestingly, INPP5E is a member of the 5-phosphatase family and is mutated in Joubert Syndrome and MORM Syndrome, characterised by structure and function defects of cilia (Bielas et al., 2009; Jacoby et al., 2009). INPP5E shares substrates with OCRL1, down regulating the levels of $PI(4,5)P_2$ and $PI(3,4,5)P_3$. The prevalence of human disease with mutations in INPP5E highlights the importance of phosphoinositide metabolism in the function of cilia. Although not a ciliopathy, Lowe Syndrome affects the same organs as ciliopathy syndromes (Adams et al., 2008), suggesting disrupted ciliary trafficking may play a role in aspects of Lowe Syndrome pathogenesis.

The substrates of OCRL1 are key regulators of the actin cytoskeleton, linking OCRL1 to the regulation of cytoskeletal dynamics. In addition to regulating endosomal actin (figure 1.3), cells from Lowe Syndrome patients have fewer stress fibres and increased punctate actin staining that co-localises with actin binding proteins regulated by $PI(4,5)P_2$ (Suchy and Nussbaum, 2002). Analysis of these cells also indicated that OCRL1 is involved in cell migration, although it is not clear whether this is a consequence of altered actin dynamics or membrane trafficking (Coon et al., 2009; Suchy and Nussbaum, 2002). Recently aberrant actin phenotypes have been observed in cells undergoing cytokinesis in the absence of OCRL1. When HeLa cells divide, OCRL1 localises to the abscission site formed during the late stages of cytokinesis (Dambournet et al., 2011). Recruitment of OCRL1 to the abscission site is dependent on interactions with Rab35 (Dambournet et al., 2011). At the abscission site, OCRL1 hydrolyses $PI(4,5)P_2$, which is thought to contribute to the removal of F-actin required to complete cytokinesis (Dambournet et al., 2011). Cells

from Lowe Syndrome patients frequently fail to complete cytokinesis due to the ectopic accumulations of F-actin at abscission sites (Dambournet et al., 2011). In addition, depletion of an OCRL1 homologue in *Drosophila* results in a high rate of cytokinesis failure. In these cells, loss of dOCRL1 disrupts furrowing of the contractile ring (Ben El Kadhi et al., 2011), which occurs at an earlier stage of cytokinesis than abscission. The furrowing defect seen in the absence of OCRL1 is thought to be caused by mis-targeting of contractile ring components to intracellular membranes with aberrant accumulations of $PI(4,5)P_2$ and F-actin (Ben El Kadhi et al., 2011). By regulating the levels of $PI(4,5)P_2$, OCRL1 may be involved in numerous cellular events that require dynamic actin pools.

These studies demonstrate that OCRL1 regulates similar pathways in multiple cellular processes. Although loss of OCRL1 affects a wide range of cellular events such as membrane trafficking, cytokinesis and cilia assembly, common mechanisms of disruption exist. OCRL1 is recruited to various different sites in the cell by interacting with organelle specific Rab GTPases and their effector proteins. At these locations, OCRL1 functions to couple dephosphorylation of $PI(4,5)P_2$ with membrane identity or cytoskeletal dynamics. One function of OCRL1 may be to remove $PI(4,5)P_2$ on intracellular membranes, allowing the plasma membrane to maintain the identity of being $PI(4,5)P_2$ rich and therefore allowing intracellular membranes to acquire alternative phosphoinositides. Disrupting this basic function of OCRL1 can explain many of the trafficking defects as well as the cytokinesis defects seen in *Drosophila*. For example, the contractile ring formed during cytokinesis becomes enriched in $PI(4,5)P_2$, which aids recruitment of furrowing proteins to the site. Such a local enrichment of $PI(4,5)P_2$ requires proteins such as OCRL1 to remove $PI(4,5)P_2$ elsewhere. Disrupting this balance by depletion of dOCRL1 resulted in accumulations of $PI(4,5)P_2$ on endosomes and the recruitment of the cytokinetic machinery away from the furrow site (Ben El Kadhi et al., 2011). Similar functions of OCRL1 may be required to facilitate the directionality of membrane trafficking. Disrupted phosphoinositide switches may explain the many trafficking problems reported in the absence of OCRL1. In addition, the removal of $PI(4,5)P_2$ by OCRL1 functions to down-regulate F-actin such as post endocytosis or

during abscission. The spatial and temporal down-regulation of $PI(4,5)P_2$ by OCRL1 allows for the progression of these cellular events and loss of OCRL1 tends to result in a blockage at a particular stage in one of these processes.

Epithelial cell polarity

Overview

Through the common mechanism of $PI(4,5)P_2$ hydrolysis, OCRL1 has been implicated to regulate numerous cellular processes, however it is not currently known which of these contribute to the pathology of Lowe Syndrome. Most of the cell types affected by Lowe Syndrome are highly polarised, neurons in the central nervous system, lens epithelial cells in the eye and renal proximal tubule epithelial cells in the kidney. Epithelial cell polarity is essential for the morphological and functional asymmetries that underlie these tissues. Polarised cells maintain an asymmetric distribution of proteins and lipids within the plasma membrane, as well as distinct spatial organisations of the cytoskeleton and organelles (Rodriguez-Boulan et al., 1989).

The renal failure in Lowe Syndrome and Dents disease can often be fatal (Loi et al., 2006). The epithelial cells of the kidney form tubules where single monolayers of tightly packed cells are arranged around a central lumen (Hogan et al., 2002). The cells within the proximal tubule develop a distinct apical surface that faces the lumen and a basal domain that contacts the underlying extracellular matrix. The apical and basolateral domains are morphologically and compositionally different. The apical domain is covered in microvilli and contains proteins involved in absorption and secretion, the basal domain is specialised to form interactions with the underlying tissue (O'Brien et al., 2002). Separating the apical and basal domains is the lateral membrane which is similar to the basal domain but contains junctions involved in cell-cell adhesions and the maintenance of cell polarity.

Failure of epithelial cells to polarise appropriately leads to a variety of diseases including polycystic kidney disease, cystic fibrosis and some metastatic cancers (McConkey et al., 2009; Wilson, 1997). Polarisation has a large functional

importance in the renal proximal tubule. The loss of proteins and metabolites in the urine of Lowe Syndrome and Dents-2 disease patients indicate abnormal reabsorption in the kidney, suggesting a possible role for disordered polarisation in the pathology of the disease. In addition, many of the cellular processes implicated to involve OCRL1 in the previous section have specific functions in polarised cells. For example, membrane trafficking and cytoskeletal dynamics are critical for the establishment and maintenance of cell polarity, suggesting polarisation may be disrupted in Lowe Syndrome.

Intercellular junctions

As mentioned previously, OCRL1 has been found to localise to the intercellular junctions of several epithelial cell lines (Grieve et al., 2011). During epithelial development, adjacent cells form intercellular junctions to facilitate the structural integrity of the tissue and to enable apical-basolateral polarity. In addition, intercellular junctions act as dynamic signalling complexes regulating the expression of genes involved in proliferation, differentiation and apoptosis (Jamora et al., 2002; Matter and Balda, 2003).

Strong cell adhesion is mediated by adherens junctions, characterised by the cadherin family of transmembrane proteins (Hartsock et al., 2008). The adhesive strength of adherens junctions is provided by calcium dependent homotypical interactions between the extracellular domains of E-cadherin proteins (Hartsock et al., 2008). In addition, the cytoplasmic domain of E-cadherin forms complexes with catenins that link the adherens junction to the actin cytoskeleton (Yonemura, 2011). The lateral domains of epithelial cells are also linked by desmosomes and gap junctions. Gap junctions form channels to connect the cytoplasm of adjacent cells, allowing molecules and ions to be exchanged between neighbours (Kumar et al., 1985). In contrast, tight junctions create a diffusion barrier for the movement of molecules between cells. Tight junctions are composed of multiple integral membrane proteins linked to a cytoplasmic network of adaptor proteins that link

the junction to the actin cytoskeleton (Green et al., 2010). As well as maintaining a paracellular barrier, tight junctions also prevent diffusion of proteins and lipids between membrane domains (Dragsten et al., 1981). This junction is formed at the boundary between the apical and basolateral surface domains, preventing mixing of apical and basolateral membrane components.

Intercellular junction formation occurs in a strictly sequential manner (Knust and Bossinger, 2002). Initially a primordial junction is formed that contains components of both adherens junctions and tight junctions. As the epithelium matures, the cells change morphology, gain height and resolve separate adherens junctions and tight junctions (Matter and Balda, 2003). In mature polarised epithelial cells, the tight junction forms a ring beneath the apical domain and the adherens junction is usually found on the basolateral side of the tight junction. Maturation of junctions is mediated by reorganisation of the actin cytoskeleton and vesicular delivery of junctional components to the plasma membrane (Green et al., 2010).

Once junctions have matured, the junctions remain highly dynamic and are continuously remodelled through vesicular trafficking (Green et al., 2010). The dynamic nature of junctions is essential for their role in signalling and is also required during morphological changes such as cell division or cell extrusion. The dynamic nature of tight junctions was visualised by Shen and colleagues by imaging GFP-tagged tight junction proteins in live cells (Shen et al., 2008). The movement of the GFP signal was monitored by using fluorescence recovery after photobleaching (FRAP) as well as photoactivatable GFP probes (Shen et al., 2008). This study revealed that the junctional proteins ZO-1 (Zonula occludens-1), occludin and claudin-1 each have different stabilities at the tight junction, the majority of claudin-1 was stably localised to the tight junction, occludin was motile within the region of the junction while ZO-1 continuously moved between plasma membrane and intracellular pools (Shen et al., 2008). Therefore multiple mechanisms must exist for regulating the dynamics of junctional components.

OCRL1 localises to the tight junctions of multiple polarised epithelial cell lines in culture (Grieve et al., 2011). Immunoprecipitations of OCRL1 suggest that it exists in the same complex as junctional components ZO-1 and α-catenin early in junction formation (Grieve et al., 2011). Depletion of OCRL1 in these cells inhibited maturation, the cells were flatter than normal and failed to reach a columnar shape. Depletion of OCRL1 in more physiologically relevant 3-dimensional cultures prevented proper lumen formation (Grieve et al., 2011), further suggesting OCRL1 is necessary for epithelial morphology. Other studies of OCRL1 in epithelial cells have not found the protein at junctions (Cui et al., 2010; Dressman et al., 2000), however OCRL1 is thought to target junctions temporally during early development as junctional OCRL1 was not detected in fully mature cells (Grieve et al., 2011). At junctions OCRL1 might regulate actin organisation. Alternatively, through its recognised role in regulating endocytic recycling, OCRL1 might be involved in pathways that turnover junctional proteins.

Polarised membrane trafficking

The dynamic nature of intercellular junctions is supported in part by vesicular trafficking. In addition, the apical and basolateral domains of epithelial cells are continuously remodelled via multiple trafficking pathways. Newly synthesised proteins can be directly delivered to the plasma membrane from the TGN as they are produced in the biosynthetic pathway (Rodriguez-Boulan et al., 2005). However, the route to the cell surface from the TGN is not always direct; some newly synthesised apical proteins traffic through recycling endosomes positive for Rab8a and Rab11a GTPases before being delivered to the plasma membrane (Ang et al., 2004; Cramm-Behrens et al., 2008). After surface delivery, proteins at the plasma membrane can be internalised for entry along multiple trafficking pathways. Internalised cargo first enters domain specific early endosomes: apical early endosomes and basolateral early endosomes. From early endosomes, some proteins are trafficked to the lysosome or TGN, while other proteins undergo rapid recycling to plasma membrane. Many proteins are delivered to the common

recycling endosome, a Rab8 and Rab10 positive compartment localised to the perinuclear region where apical and basolateral cargoes are sorted for delivery to their respective domain (Wang et al., 2000). In addition, proteins destined for the apical domain may be further routed through the Rab11a positive apical recycling endosome before delivery to the cell surface (Leung et al., 2000), although whether the apical recycling endosome and common recycling endosome are separate entities or subdomains of the same structure is controversial (Leung et al., 2000; Thompson et al., 2007). There is some evidence to suggest a subset of apical proteins may be delivered first to the basolateral domain before routing to the apical surface (Hua et al., 2006). This transcytosis route is particularly used by epithelial cells of the liver, intestine and the retinal pigment epithelium (Bonilha et al, 1997; Matter et al., 1990, Maurice et al., 1994). The multiple pathways involved in polarised membrane trafficking are summarised in figure 1.4. These pathways help to maintain the different compositions of apical and basolateral domains and also have functional roles such as receptor mediated uptake of nutrients from the extracellular environment and the regulation of signalling receptors at the plasma membrane.

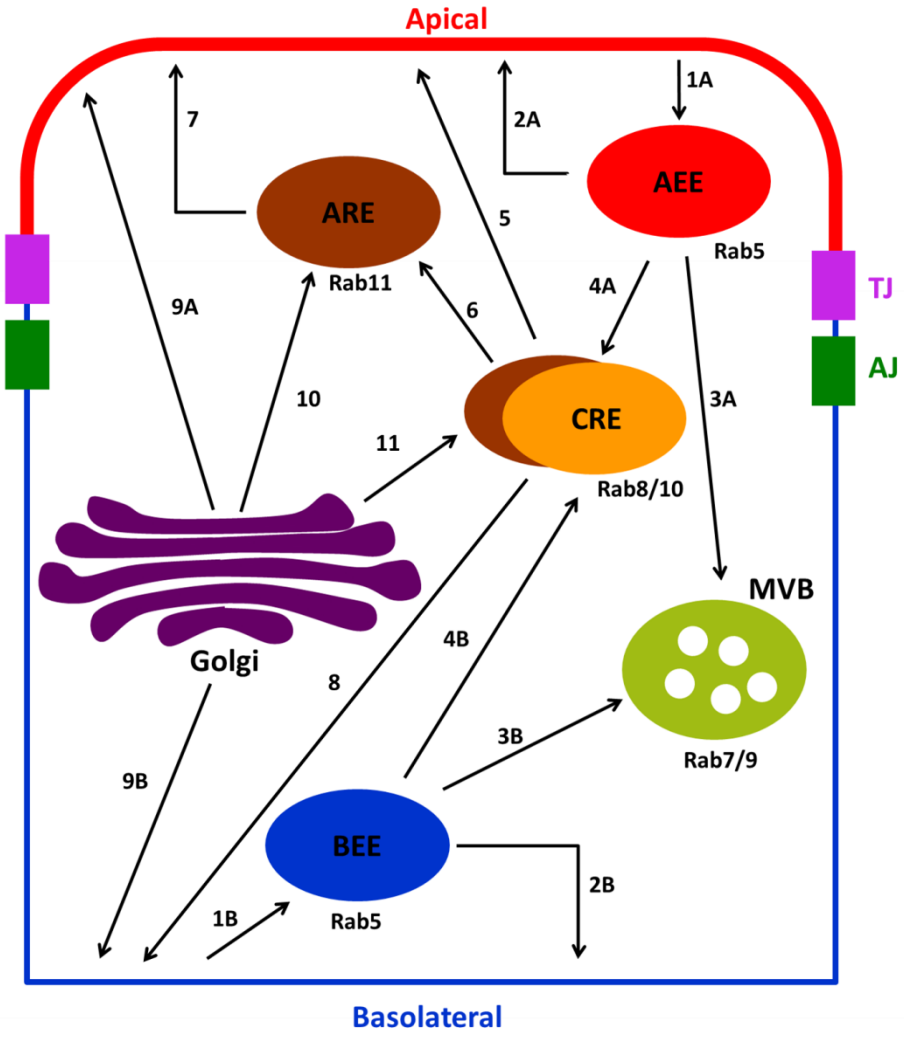

Figure 1.4: Membrane trafficking pathways in polarised epithelial cells. Proteins and lipids internalised either from the basolateral (blue) or apical (red) surface (1A and 1B), are delivered to basolateral early endosomes (BEEs) and apical early endosomes (AEEs). At EE, cargo can recycle to the plasma membrane (2A and 2B), or be directed in the degradation pathway to the multi-vesicular body, MVB (3A and 3B). Alternatively, basolateral and apical proteins are sorted into a recycling route and meet in the common recycling endosome, CRE (4A and 4B). At the CRE, cargo is sorted directly to the apical membrane (5) or indirectly via the ARE (6 and 7). Cargo can also be sorted to the basolateral membrane from the CRE (8). In the biosynthetic pathway, plasma membrane targeting can occur directly from the Golgi (9A and 9B) or indirectly via recycling endosomes (10 and 11). TJ: tight junctions, AJ: adherens junctions. Adapted from Apodaca et al., 2012

Proteins destined for the junction, apical or basal membrane must be trafficked in different carriers selectively to these sites. Sorting is driven by multiple mechanisms at the TGN and recycling endosomes. For example, some proteins contain short sequence motifs that interact with adaptor proteins that are involved in specific trafficking pathways to ensure a particular sorting route (Pandey, 2010). In addition, lipid rafts are thought to play a role in the sorting of apical cargo. Some apical proteins may have an affinity for cholesterol and sphingolipids which make up lipid rafts. The association of apical proteins with lipid rafts could mediate clustering and incorporation into apical carriers (Cao et al., 2012). During sorting of apical and basolateral proteins, the membrane of the sorting organelle is organised into tubules or buds that assist in the formation of carriers. Membrane curvature is supported by BAR domain containing proteins (Habermann, 2004). In addition, membrane bending can be facilitated by the insertion of protein regions into the lipid bilayer (McMahon and Gallop, 2005). The membrane associated actin network also contributes to membrane deformation and scission (Lanzetti et al., 2007), along with motor proteins such as the dynamin family (Ferguson et al., 2012).

Most of the events at sorting organelles are regulated by Rab GTPases and phosphoinositides. For example, the Rab11 GTPase recruits FIP5 (family interacting protein 5) and its binding partner SNX18 (sorting nexin 18) to apical recycling endosomes (Willenborg et al., 2011). SNX18 Is a BAR domain containing protein and FIP5 is required for scission, both proteins interact with $PI(4,5)P_2$ which acts together with Rab11 to recruit them to the membrane (Willenborg et al., 2011). As carrier formation progresses from cargo selection to tubule formation, budding and scission, the proteins recruited to the membrane change to allow one stage to be completed and the next to be initiated. The sequential stages of endocytosis have been studied using fluorescence-based real-time imaging in yeast (Kaksonen et al., 2005). Clathrin and coat proteins arrive at the site of endocytosis within the first 10 seconds which is followed by a burst of actin polymerisation and recruitment of proteins able to bind curved membranes (Kaksonen et al., 2005). Once a bud is formed of appropriate size (approximately 30 seconds), the F-actin is down-regulated and the vesicle is released (Kaksonen et al., 2005). Similar results were

found for clathrin mediated endocytosis in mammalian cells (Taylor et al., 2011). In this study the 5-phosphatases synaptojanin-2β1 and OCRL1 were recruited transiently to budding and post scission vesicles, indicating down-regulation of phosphoinositides during late stage endocytosis (Taylor et al., 2011). Removal of $PI(4,5)P_2$ from late stage endocytic buds might facilitate actin depolymerisation and separation of the bud from the membrane of origin. Although these studies were carried out in yeast and fibroblasts, similar molecular dynamics are likely to occur for cargo exit of sorting organelles in polarised epithelial cells.

Fully formed cargo carrying vesicles are trafficked to the plasma membrane along the actin and microtubule cytoskeleton by motor proteins that are recruited to carriers by Rab proteins and phosphoinositides. Different motor proteins drive membrane traffic to the apical or basolateral domain. The actin binding motor protein myosin-5b is recruited to apical recycling endosomes by Rab11 and Rab8 and is essential for exit of apical cargo from the recycling endosomes to the plasma membrane (Lapierre et al., 2001; Roland et al., 2011). Mutations of myosin-5b can cause microvillus inclusion disease, characterized by the accumulation of large intracellular vacuoles enriched in microvilli (Müller et al., 2008). A similar phenotype is observed in Rab8 knockout mice (Sato et al., 2007). Trafficking of vesicles across the cytosol also depends on microtubule driven transport by the kinesin family of motor proteins, for example, the kinesin KIFC3 delivers the apical protein annexin-13b to the apical domain (Noda et al., 2001), while basolateral targeting of cargo carrying vesicles is driven by different members of the family (Lafont et al., 1994).

Further membrane specificity of cargo delivery is achieved by tethering proteins once the vesicle is in the vicinity of the target membrane. Tethering proteins ensure vesicles fuse with appropriate membrane domains. The exocyst is a complex of eight proteins some of which are localised to the target plasma membrane while others are localised to the transport vesicle (Oztan et al., 2007; Yeaman et al., 2001). Assembly of the complex when the vesicle meets the plasma membrane drives vesicle fusion (TerBush et al., 1996). Loss of exocyst function blocks the

recycling of internalised cargos and results in their accumulation in recycling endosomes (Prigent et al., 2003). The exocyst complex localises to secretory vesicles by interacting with Rab GTPases (Zhang et al., 2001) and targets them to plasma membranes rich in $PI(4,5)P_{2,}$ which is recognised by exocyst subunits EXO70 and Sec3 (He et al., 2007, Zhang et al., 2008). Another type of tethering complex involves annexins which are present on apical transport vesicles and the target apical membrane. Annexins have the capacity to aggregate in a $PI(4,5)P_2$ and calcium dependent manner, which might facilitate fusion of apical vesicles in the vicinity of the $PI(4,5)P_2$ rich apical membrane (Gerke et al., 2005). In addition, polarised cells have different distributions of t-SNARES on the apical and basolateral membrane that complement different v-SNARES on apical and basolateral vesicles.

The actin and microtubule cytoskeleton in polarised cells

Membrane polarity is highly influenced by the orientation and organisation of cytoskeletal actin and microtubule filaments. Apical and basolateral cargo carrying vesicles are trafficked to the plasma membrane by motor proteins that utilise the polarity of the cytoskeleton for directional information, therefore polarised trafficking is dependent on the polarised organisation of actin and microtubule arrays. Molecular motor proteins were discussed in the previous section (Polarised membrane trafficking). Briefly, myosins are motor proteins that interact with actin filaments whilst microtubule motors encompass the kinesin and dynein families. In addition to regulating polarised membrane trafficking, the cytoskeleton also has a structural role within the cell and is required to maintain the tall cuboidal shape of polarised epithelial cells.

Fully polarised epithelial cells have a dense network of actin filaments throughout the cell cortex. In the lateral domain, short actin filaments are part of the spectrin network that maintains the columnar shape of epithelial cells (Kizhatil and Bennett, 2004). In the apical domain, actin filaments are specially arranged to form microvilli that increase membrane surface area for absorption of nutrients from the

extracellular fluid. The actin filament organisation in microvilli may also help retain apical cargo in the apical membrane (Revenu et al., 2012). Epithelial cells also develop a circumferential actin belt associated with tight junctions and adherens junctions which is essential for junction stability (Cavey and Lecuit, 2009). Actin reorganisation plays an important role in initiating cell-cell contacts and in the expansion required for the cuboidal morphology. Actin polymerisation produces membrane protrusions to generate new sites of E-cadherin based contacts (Bershadsky, 2004). Following these initial contacts, acto-myosin tension near contacting membranes generates a pulling force to facilitate the lateral expansion (Yamada and Nelson, 2007). Actin dynamics are regulated by Rac, Rho and Cdc42 GTPases (Ridley, 2006) as well as phosphoinositides (Yin et al., 2003).

The microtubule cytoskeleton in un-polarised cells typically displays a centrosomal arrangement of dynamic microtubules with the plus ends directed towards the cell periphery (Müsch, 2004). In polarised cells the arrangement of the microtubules is dependent on the specific cell type. Epithelial cell lines derived from the kidney maintain a population of stable microtubules organised vertically along the polarity axis with the minus end facing apically and the plus end basolaterally in addition to more dynamic apical and basal networks (Bartolini and Gundersen, 2006; Müsch, 2004). This rearrangement of microtubules is regulated by the polarity protein kinase Par1b (Partitioning protein-1b), also known as MARK2 (Cohen et al., 2004). Depletion of Par1b from the Madin Darby Canine Kidney (MDCK) epithelial cell line prevented the organisation of microtubules normally associated with polarisation, whilst over-expression of Par1b resulted in rearrangement of the microtubules of MDCK cells to a liver-like phenotype, with microtubule arrays emanating from bile canaliculi-like lumina at the lateral membrane (Cohen et al., 2004). Cells over-expressing Par1b re-routed their apical membrane traffic in accordance with the microtubule cytoskeleton (Cohen et al., 2004). In addition, disruption of microtubules with nocodazole or colchicine prevents plasma membrane localisation of apical proteins, which instead accumulate intracellularly in large vacuolar apical compartments (Gilbert et al., 1991; van Zeijl and Matlin, 1990). These vacuoles are thought to form from frustrated apical carriers unable to traffic to the plasma

membrane (Vega-Salas et al., 1987), highlighting the importance of microtubules in routing apical traffic.

Phosphoinositides and polarised membranes

The apical-basal polarity of the plasma membrane in epithelial cells includes phosphoinositides as well as proteins. The asymmetric distribution of phosphoinositides is critical for maintaining apical-basal polarity since domain specific phosphoinositides regulate trafficking and cytoskeletal dynamics appropriate for the membrane. In polarised epithelial cells, $PI(3,4,5)P_3$ localises to the basolateral membrane, whereas $PI(4,5)P_2$ is enriched apically (Martín-Belmonte et al., 2007). The segregation of these two phosphoinositides occurs during the early stages of polarisation, although it is not clear whether basal enrichment of $PI(3,4,5)P_3$ is maintained in mature cells. $PI(3,4,5)P_3$ becomes enriched basally when β1-integrins activate PI(3)-kinase which phosphorylates $PI(4,5)P_2$ at the third position to generate $PI(3,4,5)P_3$ (King et al., 1997). In addition, a significant source of $PI(3,4,5)P_3$ is produced in the basolateral domain when cell-cell contacts are made since PI(3)-kinase is activated downstream of E-cadherin signalling (Kovacs et al., 2002). $PI(4,5)P_2$ is maintained in the apical domain by the 3-phosphatase PTEN which dephosphorylates $PI(3,4,5)P_3$. PTEN is recruited to tight junctions by interacting with the tight junction proteins MAGI-2 (membrane-associated guanylate kinase inverted-2) and Par3, known as Bazooka in Drosophila (Von Stein et al., 2005; Wu et al., 2000).

The separation of apical and basolateral phosphoinositides is crucial for polarity homeostasis. Ectopic delivery of $PI(4,5)P_2$ to the basolateral membrane results in a rapid redistribution of apical proteins to this compartment (Martin-Belmonte et al., 2007). In addition, depletion of the 3-phosphatase PTEN prevents proper apical lumen formation due to lack of apical $PI(4,5)P_2$ (Martin-Belmonte et al., 2007), further suggesting polarisation of $PI(4,5)P_2$ is critical for apical membrane identity. Similarly, proper polarisation of $PI(3,4,5)P_3$ is required for basal membrane identity.

Insertion of PI(3,4,5)P_3 apically results in transcytosis of basolateral proteins to the apical membrane (Gassama-Diagne et al., 2006). Blocking endocytosis in these cells by expression of a dominant negative dynamin prevented the apical accumulation of basolateral proteins, highlighting the ability of phosphoinositides to regulate polarised membrane traffic. In addition, treatment of epithelial cells with PI(3)-kinase inhibitors to limit production of PI(3,4,5)P_3 reduced cell height due to inhibition of basolateral membrane expansion (Jeanes et al., 2009).

As well as regulating polarised membrane trafficking, phosphoinositides also regulate cytoskeleton organisation beneath the plasma membrane. In the basolateral domain PI(3,4,5)P_3 regulates Rac1 activation (Kovacs et al., 2002) and the recruitment of WAVE (Wiskott-Aldrich Syndrome protein family verprolin-homologous protein) actin nucleating proteins (Padrick and Rosen, 2010). In the apical domain PI(4,5)P_2 recruits the Cdc42 binding protein annexin-2 (Rescher et al., 2004) and the WASP (Wiscott-Aldrich Syndrome protein) family of proteins which activate Arp2/3 to promote nucleation of filamentous actin (Padrick and Rosen 2010). In addition PI(4,5)P_2 interacts with the ERM proteins, ezrin, radixin and moesin, promoting the association of actin fibres and bundles to PI(4,5)P_2 rich regions of the plasma membrane (Pearson et al., 2000). OCRL1 may be involved in the maintenance of plasma membrane phosphoinositide asymmetries by down-regulating the levels of 5-phosphoinositides on intracellular membranes.

Polarity complexes and polarised membranes

Phosphoinositides co-operate with a set of evolutionarily conserved polarity complexes to regulate apical-basal polarity (Margolis and Borg, 2005). In a similar manner to phosphoinositides, polarity complexes associate with particular membrane domains and promote expansion of the domain they associate with. Apical membrane development is regulated by two polarity complexes: the Crumbs complex and the Par complex. The apical Crumbs complex consists of three major proteins, crumbs, PALS1 (protein associated with Lin-7) and PATJ (PALS1-associated

tight junction protein). The mammalian Par complex is comprised of two scaffold proteins: Par-3 (partitioning defective-3) and Par-6 (partitioning defective-6) and an atypical protein kinase C (aPKC). In addition, the Par complex exists as two separate complexes: Cdc42-Par6-aPKC and Par3-aPKC. The basolateral Scribble complex is associated with the lateral membrane and contains discs large (Dlg), lethal giant larvae (Lgl) and scribble proteins (Assémat et al., 2008).

The apical polarity complexes Crumbs and Par are involved in generating apical-basal polarity as well as tight junction formation, while the lateral Scribble complex appears to be required for the formation of adherens junctions. Modulating the protein levels of the Crumbs complexes affects the balance between apical and basolateral membrane expansion and the formation of tight junctions, highlighting the essential role of the Crumbs complex in regulating these activities. For example, overexpression of crumbs leads to an expansion of the apical membrane and reduction of the basolateral membrane (Roh et al., 2003) while loss of PALS1 expression delays the formation of tight junctions (Straight et al., 2004). Modulating the levels of the Par complex appears to particularly affect the apical membrane. Depletion of Par3 in monolayer cultures of MDCK cells resulted in the formation of the apical domain in the lateral membrane and a similar phenotype in 3D cultures (Horikoshi et al., 2009). In addition, deletion of the Par3 gene in *C. elegans* leads to the defective segregation of apical and basal proteins during the first cell division of the zygote (Kemphues et al., 1988). Depletion of scribble has little effect on apicobasal polarity but reduces the integrity of cell-cell adhesions and leads to increased cell motility (Qin et al., 2005).

These polarity complexes initiate apicobasal polarity by recruiting functionally important proteins to the plasma membrane. In addition, some polarity proteins have enzymatic kinase activity and are involved in signalling cascades. The Crumbs complex acts as a scaffold to recruit and retain junctional proteins in the plasma membrane. The Crumbs component PATJ contains 10 PDZ domains that interact with tight junction proteins such as ZO-3 and claudin-1 (Roh et al., 2002). Further scaffolding activity is provided by the Crumbs component PALS1 which contains at

least six different domains that engage in protein interactions (Kamberov et al., 2000). The GTPase Cdc42 is considered to play a central role in establishing cell polarity, regulating the orientation of the actin and microtubule cytoskeleton and organisation of membrane traffic (Etienne-Manneville, 2004). Cdc42 is recruited to the apical domain by interacting with Par6. In addition, the binding of Cdc42 to Par6 induces a conformational change in Par6 that activates its binding partner aPKC (Garrard et al., 2003). Polarity proteins also regulate phosphoinositide turnover by recruiting phosphoinositide metabolising proteins to the plasma membrane. For example, a PDZ domain of Par3 has been shown to bind the PI-3-phosphatase *PTEN (*Von Stein et al., 2005), contributing to PI(4,5)P_2 production in the apical domain. Although polarity proteins integrate a host of processes critical for apical-basal polarity, there is some evidence to suggest the asymmetric distribution of polarity complexes itself depends on phosphoinositide metabolism and polarised membrane trafficking, suggesting a feedback loop. For example, the exocyst complex, which regulates polarised membrane trafficking is required for Par3 localisation (Lalli et al., 2009), suggesting that polarised membrane trafficking operates both upstream and downstream of polarity complexes. The earliest events known to initiate epithelial cell polarity are discussed in more detail next.

Polarity orientation cues

The segregation of apical and basolateral polarity complexes generates an axis of polarity that determines where on the membrane the apical and basolateral domains will form. Orientation of the polarity axis is influenced by positional information received from the surrounding micro-environment. Cells in culture are typically grown in an asymmetric environment with a plastic support on one side and growth media on the other. The presence of asymmetry in the environment is thought to assist in the formation of a polarity axis; the basal membrane is formed at the site of adhesion to the underlying support and the apical domain is formed where the plasma membrane contacts the growth media. When cells are immersed in a uniform environment surrounded by extra cellular matrix (ECM) they

proliferate and assemble into cysts of spherical monolayers with central lumens (O'Brien et al., 2002), more closely resembling epithelial organisation in vivo. Apical membrane formation in 3D culture is thought to be initiated at the two cell stage. A single cell fully immersed in ECM has no external polarity cues but asymmetry is introduced upon the first cell division, while the free plasma membrane remains in contact with the environment, a region of the plasma membrane can no longer sense the ECM due to the formation of cell-cell contacts. This suggests that cells initiate apical membrane formation during cell division, which is the topic of the section towards the end of this chapter entitled 'Co-ordinating polarity and cell division'.

Even after the first cell division, the apical membrane appears to be identified by the absence of adhesion. The apical membrane faces the inside of the lumen which forms no adhesive contacts, in contrast the basolateral membrane adheres to adjacent cells and the underlying matrix. One way in which cells might identify the absence of adhesion is through the activation state of integrin proteins. Cells distribute integrins in both the apical and basal membrane, however apical integrins remain inactive due to absence of collagen in the extracellular environment. When the apical membrane is covered with collagen, apical integrins become active and the cells re-assemble into tubules and develop the apical membrane in the new free surface (Schwimmer and Ojakian, 1995). These findings suggest the activation state of integrin receptors influences the orientation of the apical-basal polarity axis.

Activated integrins initiate the formation of the basolateral membrane. Activated integrins promote deposition and re-modelling of a laminin rich basement membrane between the plasma membrane and the ECM. The basement membrane formed serves to enforce and further develop basal membrane identity. The serine/threonine kinase Par1b is activated downstream of integrin signalling and promotes laminin reorganisation by directly interacting with laminin receptors and inducing their aggregation at the basal surface (Masuda-Hirata et al., 2009; Yamashita et al., 2010). In addition, Par1b regulates the localisation of the

scaffolding protein IRSp53 (Insulin receptor substrate p53). IRSp53 links Rac1 and Cdc42 to their effector proteins in the basement membrane (Cohen et al., 2011, Scita et al., 2008). Active Rac1 and Cdc42 at the basal membrane further facilitate laminin remodelling by inducing sub-membranous cytoskeletal organisation. These signalling events downstream of integrin activation are required for proper positioning of the apical membrane. Depletion of β1-Integrin results in the abnormal localisation of the apical membrane to a region in-between neighbouring cells through inappropriate activation of a RhoA–ROCKI–myosin2 pathway (Yu et al., 2008), suggesting that ECM-derived signals influence polarity orientation by regulating cytoskeletal tension. In addition, lumen positioning in MDCK cells is regulated by Par1b mediated cytoskeletal organisation (Cohen et al., 2011). In these studies, impaired ECM signalling and basal cytoskeletal organisation triggered inappropriate positioning of the apical membrane but did not perturb polarity and intercellular junction formation, suggesting the orientation of cell polarity and apicobasal polarisation can be molecularly uncoupled.

Early stages of apical membrane formation

Once the orientation of apical-basal polarity has been established, the apical membrane is formed by polarised trafficking of apical components to the plasma membrane. When a single epithelial cell divides in 3D culture, the apical lumen is typically formed by exocytosis of apical cargo carrying vesicles to a specific site on the plasma membrane between the two cells (Martin-Belmonte et al., 2008). At the single cell stage, apical membrane components are distributed throughout the plasma membrane. The boundary that forms between daughter cells when the single cell divides acts as the precursor apical domain for the delivery of apical vesicles. The apical components that were uniformly distributed on the plasma membrane are endocytosed into Rab11a positive recycling endosomes and sorted for transport to this site (Bryant et al., 2010), see figure 1.5. The precursor apical domain or apical membrane initiation site (AMIS) is marked by Par3 and aPKC (Bryant et al., 2010). The mechanism of Par3 targeting to the AMIS is not clear,

however membrane recruitment may be mediated by interactions with the phosphoinositide $PI(4,5)P_2$ (Horikoshi et al., 2011; Krahn et al., 2010; Wu et al., 2007). Par3 is thought to recruit the lipid phosphatase PTEN to the AMIS (Feng et al., 2008; von Stein et al., 2005) which facilities enrichment of $PI(4,5)P_2$ in the forming apical membrane by dephosporylation of $PI(3,4,5)P_3$. Therefore Par3 utilises $PI(4,5)P_2$ for membrane recruitment and also facilitates the production of more $PI(4,5)P_2$. This is another example of Par3 participating in a feedback loop to rapidly promote expansion of the apical membrane.

Rab11a drives apical trafficking to the AMIS by recruiting Rabin8, a Rab8 GEF to apical vesicles (Bryant et al., 2010), which associates with motor proteins such as myosin-5b (Roland et al., 2011). In addition, trafficking of luminal vesicles also depends on microtubule driven transport. For example, the kinesin KIF3b is recruited to the membrane of apical vesicles through interactions with the Rab11 binding protein FIP5 (Schonteich et al., 2008). Luminal targeting of apical vesicles requires the tethering exocyst complex. Rab11a on apical vesicles interacts with sec15a exocyst subunit (Wu et al., 2005) whilst sec8 and sec10 exocyst components are recruited to the AMIS (Bryant et al., 2010). In addition, enrichment of $PI(4,5)P_2$ at the AMIS is likely to facilitate membrane association of additional exocyst subunits (He et al., 2007; Zhang et al., 2008). Therefore a functional exocyst complex is formed when vesicle bound subunits interact with target apical membrane bound subunits, ensuring specificity of apical vesicles and apical membrane. Other tethering proteins such as SNAREs are likely to facilitate targeting of apical vesicles with the developing lumen; syntaxin-3 appears to play a key role in this process (Sharma et al., 2006).

The Rab11a/Rab8 apical trafficking pathway functions upstream to deliver essential components required for lumen formation to the plasma membrane. One of the first proteins known to localise to lumens at the earliest visible stage is Gp135 (glycosylated protein-135), also known as podocalyxin (Bryant et al., 2010). Gp135 is a member of the CD34 family of anti-adhesins. Heavy sialylation of Gp135 gives the protein a negative charge which helps to repulse opposing membranes during

lumen expansion. In addition to Gp135, the Cdc42-Par6-aPKC polarity complex is also delivered to the AMIS via the Rab11a/Rab8a apical trafficking pathway (Bryant et al., 2010). Cdc42 is recruited to apical vesicles by its interaction with annexin-2, a $PI(4,5)P_2$ binding protein (Martin-Belmonte et al., 2007) and is activated on apical vesicles via the GEF protein Tuba (Bryant et al., 2010). Par3 at the AMIS might act as an additional tethering factor by associating with Cdc42-Par6-aPKC on apical vesicles and completing the formation of the Par polarity complex (figure 1.5). However, association of Par3 and Par6 is thought to occur only temporally and is disrupted by delivery of the Crumbs polarity complex to the AMIS. This complex is also delivered to early forming lumens via the same Rab11a/Rab8a trafficking pathway (Walther and Pichaud, 2010). Arrival of the Crumbs complex at the AMIS is thought to dissociate Par3 from Cdc42-Par6-aPKC and facilitate relocation of Par3 to apicolateral borders, where junctions form (Morais-de-Sá et al., 2010 and Walther and Pichaud, 2010), also shown in figure 1.5.

Expansion of the AMIS into a lumen requires separation of opposing plasma membranes which is achieved by multiple mechanisms, as mentioned above, negatively charged sialic acids in apical glycoproteins such as Gp135 repel adjacent apical membranes (Strilić et al., 2010). Gp135 also contributes to the organisation of the sub-apical actin network by recruiting ERM proteins (Meder at al., 2005), which together with ROCK (Rho-associated protein kinase) generates the force required for lumen expansion through contraction of actin (Ferrari et al., 2008). In addition, delivery of ion pumps to the forming lumen creates an ionic gradient that encourages water to enter through the paracellular pathway. The exocytosis of fluid filled endocytic vesicles at the AMIS further contributes to lumen expansion (Martin-Belmonte et al., 2008). The formation of a lumen by exocytosis of luminal components occurs in developing mouse aorta (Strilić et al., 2009) and in MDCK cysts (Martin-Belmonte et al., 2008). However, other mechanisms for generating a luminal space exist. For example, some cells cluster and generate a lumen by apoptosis of cells not in contact with the ECM, generating luminal space. This occurs for example in mammary terminal end buds (Mailleux et al., 2008). Although multiple mechanisms exist for generating the space for a lumen, polarisation must

still occur as the membrane facing the luminal space is developed to specialise in apical membrane activities.

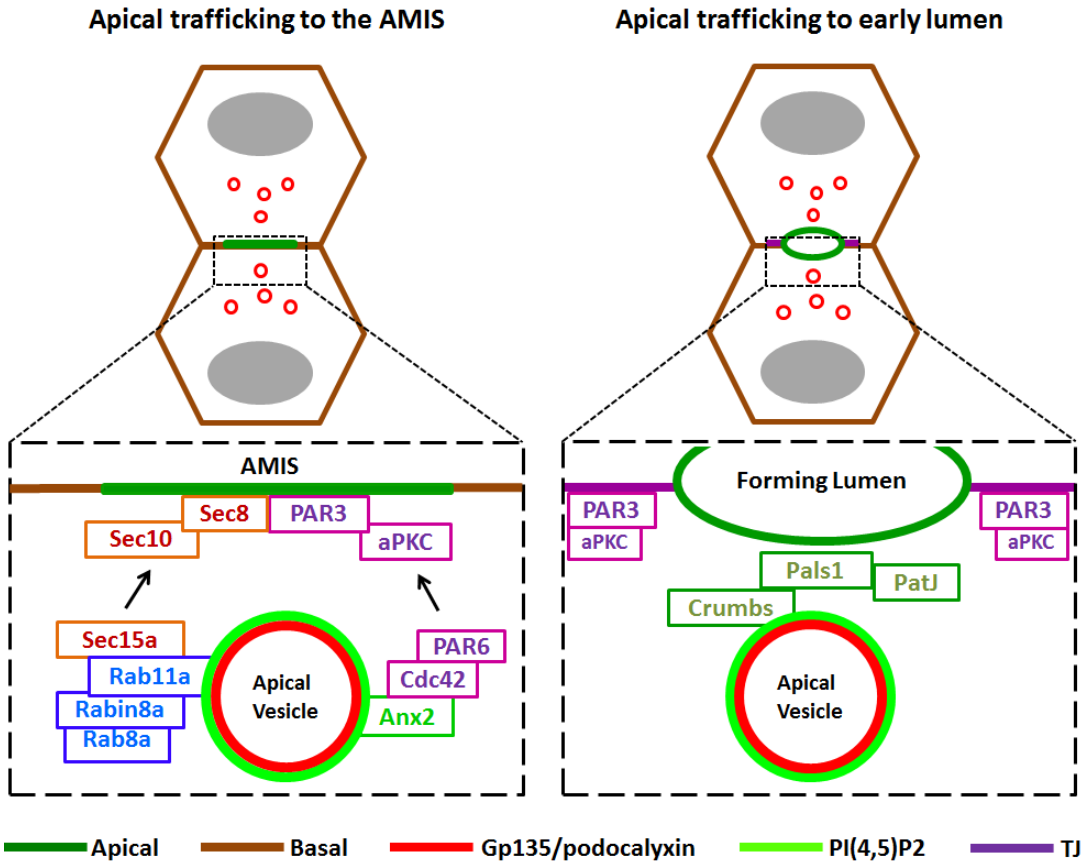

Figure 1.5: Model for apical lumen formation in cysts. The apical membrane initiation site (AMIS) is marked by the Par3-aPKC polarity complex. Apical components such as Gp135/podocalyxin (red) are trafficked in Rab11a and Rab8a positive vesicles. Formation of the Par complex (Cdc42-Par6-aPKC) and the Exocyst complex (containing Sec subunits) drive trafficking of apical vesicles to the AMIS. Delivery of fluid filled vacuoles as well as heavily sialylated proteins such as Gp135 to the AMIS induce membrane expansion of the forming lumen. Arrival of the Crumbs complex (Crumbs-Pals1-Patj) to the early forming lumen re-locates Par3-aPKC to the periphery enabling tight junction formation (purple) to occur around the forming lumen. Adapted from Bryant et al., 2010.

Cytokinesis

Overview

Cytokinesis is the final stage of cell division that results in the separation of two cells after the completion of mitosis. Cytokinesis in mammalian cells is achieved through the formation of an actomyosin ring that contracts to divide the cell into two. The assembly of the actin ring is in turn regulated by the microtubule cytoskeleton which plays an important role in defining the cleavage plane. Vesicular trafficking is required for the final stages of cytokinesis when the two daughter cells become physically separated.

A homologue of OCRL1 has been implicated to regulate contractile ring formation in *Drosophila* (Ben El Kadhi et al., 2011). In addition, OCRL1 is required for the final stage of cytokinesis in human non-polarised epithelial cell lines (Dambournet et al., 2011). The final stage of cytokinesis is referred to as abscission, when the intercellular microtubule bridge is severed. Whether OCRL1 regulates cytokinesis in polarised epithelial cell lines is not currently known.

Cytoskeletal dynamics during cytokinesis

Cytokinesis in mammalian cells involves rearrangement of the mitotic spindle to define the plane of division and extensive actin polymerisation to facilitate abscission (figure 1.6). The mitotic spindle is organised by the centrosomes which replicate and separate at the beginning of mitosis. Each centrosome nucleates an array of microtubules such that a bipolar spindle is formed (Cassimeris and Skibbens, 2003). In metaphase, the positive ends of the spindle microtubules align the chromosomes whilst the negative ends of microtubules focus near the centrosome (Cassimeris and Skibbens, 2003).

Cytokinesis begins in anaphase when the mitotic spindle rearranges to separate the chromosomes and initiate division into two pronuclei. During this process the mitotic spindle reassembles to form the central spindle (figure 1.6), a dense array of antiparallel microtubules between the two spindle poles (Fededa and Gerlich, 2012). Astral microtubules extend from spindle poles to the cell cortex which helps define the cleavage plane (Fededa and Gerlich, 2012). In symmetric division, this occurs midway between segregated chromosomes so that the cytoplasm is equally divided between daughter cells.

Once the cleavage plane has been identified, the contractile ring is assembled. The small GTPase RhoA becomes activated at the boundary of the cleavage plane (Bement et al., 2005) and recruits effector proteins that organise contractile ring assembly (Watanabe et al., 2008). The contractile ring is composed of three structural components: actin, myosin-2 and septins. Activated RhoA stimulates actin polymerisation by activating formins (Watanabe et al., 2008). In addition, the production of $PI(4,5)P_2$ at the cleavage furrow further stimulates actin polymerisation. The actin binding motor protein myosin-2 hydrolyses ATP to exert force on the actin filaments and promote constriction of the ring during the furrowing stage (Glotzer, 2005). The septins are GTP binding proteins that associate to form oligomeric filaments (Sirajuddin et al., 2007). In addition to these three components, the peripheral plasma membrane protein anillin appears to be critical for assembly of the contractile ring. Anillin is able to bind both myosin-2 and the septins, potentially functioning as a cross linker of the actomyosin and septin cytoskeletons (D'Avino, 2009). $PI(4,5)P_2$ at the cleavage furrow may contribute to recruitment of key components of the contractile ring, for example both anillin and the septins interact with $PI(4,5)P_2$ (Field et al., 2005).

As cytokinesis progresses, the contractile ring constricts and compacts the midzone microtubule array until an intercellular cytoplasmic bridge is formed (figure 1.6). These microtubules overlap at the midbody, which also contains numerous proteins required for abscission (Skop et al., 2004). Abscission proceeds by disassembly of the actin contractile ring and plasma membrane fission. Actin filament disassembly

during abscission requires inactivation of RhoA at the midbody (Saurin et al., 2008). In addition, down-regulation of $PI(4,5)P_2$ may be required to remove the actin filaments associated with the intercellular bridge. This process may involve OCRL1 and is discussed in the section entitled 'OCRL1 in cytokinesis'.

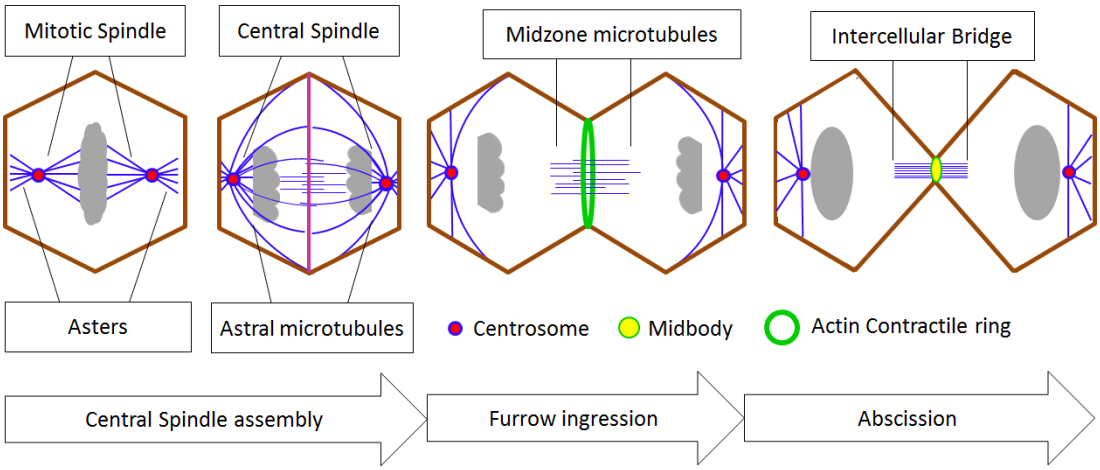

Figure 1.6: Organisation of the cytoskeleton during the different stages of cytokinesis. Cytokinesis begins by assembly of the central spindle consisting of midzone microtubules and astral microtubules that contact the cell cortex. Interaction of the central spindle with the cell cortex defines the cleavage site (purple line) and initiates assembly of the actin contractile ring (green). Furrow ingression is mediated by contraction of the actin ring which condenses midzone microtubules to form the intercellular bridge. At the centre of the intercellular bridge is the midbody (yellow) that contains numerous proteins required for abscission. At the end of cytokinesis, the intercellular bridge is cleaved which occurs asymmetrically on one side of the midbody (not shown).

Membrane trafficking during cytokinesis

As well as rearranging the actin and microtubule cytoskeleton, specific membrane trafficking pathways are altered during mitosis and cytokinesis to accommodate fluctuations in cell volume and plasma membrane surface area. In addition, the delivery of new membrane to the abscission site during the final stages of cytokinesis is essential for completing this process (Schweitzer et al., 2005).

During interphase, the Golgi complex and endocytic compartments localise near the centrosome in the perinuclear region of the cell. At this stage in the cell cycle, the rate of recycling to and from the plasma membrane is balanced and a constant cell size is maintained. As cells enter prophase, clathrin mediated endocytosis (CME) is inhibited, though the mechanism underlying this inhibition is unclear (Fielding and Royle, 2013). However, recent evidence suggests the inhibition may be due to the unavailability of the actin machinery, which assembles into a stiff cortex in mitotic cells (Kaur et al., 2014). Furthermore, the increased membrane tension during mitosis would add to the requirement of actin to assist endocytosis and overcome the inhibition (Kaur et al., 2014). As cells enter late anaphase and telophase, CME resumes to normal levels (Fielding and Royle, 2013). In addition to altering the rate of endocytosis, the rate of recycling to the plasma membrane slows during metaphase and anaphase, resulting in an intracellular accumulation of endosomes (Boucrot and Kirchhausen, 2007). These endosomes accumulate into four clusters, two pools of endosomes localise around each centrosome, while additional clusters of endosomes accumulate at the furrow side of the two pronuclei formed during anaphase. These endosomes are positioned proximal to the minus end of the midzone microtubules (Dunster et al., 2002). As mitosis progresses to telophase, recycling resumes, with most of the traffic directed towards the furrow (Boucrot and Kirchhausen, 2007). In this study, the recovery of plasma membrane surface area did not require the Golgi apparatus, suggesting that modulation of plasma membrane surface area during mitosis is mostly achieved through regulating endosomal recycling and not the secretory pathway (Boucrot and Kirchhausen, 2007). Therefore, endocytosis and recycling appear to be regulated spatially and

temporarily during mitosis, however the mechanism adjusting the rate of endosomal exit during early stages of mitosis remains to be elucidated.

During cytokinesis, endocytic recycling is essential for the final separation of the two daughter cells. Disruption of clathrin mediated endocytosis results in significant defects in cytokinesis (Schweitzer et al., 2005; Smith and Chircop, 2012), suggesting the accumulation of intracellular membrane is critical for this process. During cytokinesis, Rab11 positive vesicles traffic from proximal clusters along midzone microtubules and accumulate in the midbody of the intercellular bridge (Simon and Prekeris, 2008). Vesicles in the intercellular bridge fuse with the plasma membrane before abscission (Schiel et al., 2011) and depletion of Rab11 or expression of a dominant-negative mutant induces significant abscission defects (Wilson et al., 2005). In addition, secretory vesicles derived from the Golgi apparatus may also be required for abscission (Gromley et al., 2005). Although vesicle trafficking is involved in completing cytokinesis, the exact role of vesicles in the mechanism of abscission remain unclear. Fusion of vesicles with the plasma membrane of the intercellular bridge might cause thinning of the intercellular bridge, bringing opposing plasma membranes closer together (Neto and Gould, 2011). The final abscission step is thought to involve further constriction of the bridge by a helical arrangement of the ESCRT (endosomal sorting complexes required for transport) complex until direct fission of the opposing membranes occur (Guizetti et al., 2011).

OCRL1 in cytokinesis

OCRL1 has been implicated via its phosphatase activity to be involved in cytokinesis. In *Drosophila*, a homologue of OCRL1 is required for furrowing of the contractile ring. Depletion of dOCRL1 causes increased intracellular levels of $PI(4,5)P_2$ on giant endocytic vacuoles (Ben El Kadhi et al., 2011). Consequently, in dividing cells, components of the cleavage furrow including anillin were mis-localised to the $PI(4,5)P_2$ rich vacuoles (Ben El Kadhi et al., 2011). Mis-localisation of the furrowing machinery led to unsuccessful furrowing and a high frequency of bi-nucleate cells (Ben El Kadhi et al., 2011). Therefore, OCRL1 in *Drosophila* is required to down-regulate $PI(4,5)P_2$ on intracellular membranes so that the contractile ring in dividing cells has the identity of being rich In $PI(4,5)P_2$ which is important for correct targeting of contractile ring components.

In HeLa cells, OCRL1 removes 5-phosphoinositides to facilitate abscission during the final stages of cytokinesis. In these cells, depletion of OCRL1 blocked abscission due to abnormal accumulations of $PI(4,5)P_2$ and associated actin filaments in the intercellular bridge, highlighting the requirement for lipid and F-actin removal for the final physical separation of daughter cells (Dambournet et al., 2011). OCRL1 localises to the intercellular bridge in a Rab35 dependent manner (Dambournet et al., 2011), therefore OCRL1 is likely delivered to the abscission site by direct interactions with Rab35, which regulates a fast recycling endocytic pathway that is essential for abscission (Kouranti et al., 2006).

Coordinating polarity and cell division

Overview

During epithelial development, cell division is co-ordinated with polarisation so that the morphology of the tissue and the integrity of the epithelial barrier are maintained as cells within the epithelium divide. Unsurprisingly, there appears to be significant cross-talk between cell division and polarisation mechanisms (Hehnly and Doxsey, 2012). In addition, many key regulatory proteins and complexes required for polarisation also have functional roles in cell division, particularly during cytokinesis (Hehnly and Doxsey, 2012). If OCRL1 regulates cytokinesis in polarised epithelial cells, this could have consequences for polarisation and the morphology of the epithelium.

Apical membrane formation and cytokinesis

In epithelial cysts, apical membrane formation occurs at the late stages of the first cell division. Daughter cells co-ordinate delivery of apical membrane vesicles to a common site that lies between the cell pair. The molecular landmark for apical membrane insertion at this particular site is not currently known but one possibility is for cells to utilise products of the cytokinesis machinery to initiate lumenogenesis. In yeast, a complex of proteins retained from the previous cytokinesis event provides the landmark for membrane delivery required for the formation of the next bud (Nelson, 2003). In mammalian cells, a number of observations support the idea that apical membrane insertion occurs at the site of cytokinesis. In epithelial cysts, apical cargo such as Gp135 and crumbs3a accumulate in Rab11a positive recycling endosomes at the onset of mitosis (Bryant et al., 2010; Schlüter et al., 2009). During metaphase, apical cargo carrying vesicles localise around the poles of the mitotic spindle and are subsequently partitioned

into each daughter cell during telophase (Hobdy-Henderson et al., 2003). At the latest stages of mitosis, Rab11 positive apical vesicles are trafficked to the site of abscission along the midzone microtubule bundle (Schlüter et al., 2009), suggesting that lumen formation is co-ordinated with mitosis and the abscission site localises the formation of the first apical membrane. Expression of dominant negative Rab11a in MDCK cells blocked the trafficking of apical cargo such as Crumbs3a and prevented early apical membrane formation (Schlüter et al., 2009). Therefore, polarised cells appear to have utilised a common Rab11 vesicular trafficking pathway during cytokinesis to co-ordinate cell division with apical-basal polarity.

At the two cell stage of epithelial cysts, the orientation of the polarity axis is aligned with the spindle axis and the apical membrane forms in the plane of cell division (figure 1.7). In subsequent cell divisions, the apico-basal polarity axis is aligned perpendicular to the spindle axis so that apical membrane formation reinforces the lumen formed following the first cell division (figure 1.7). Therefore as epithelial cells develop from two cells to multicellular cysts, the orientation of polarisation changes relative to the plane of cell division. In 2D monolayer cultures of epithelial cells, the relative orientations of the polarity axis and the plane of cell division are similar to multicellular cysts, where cells divide in a horizontal plane and polarise in a vertical plane (figure 1.7).

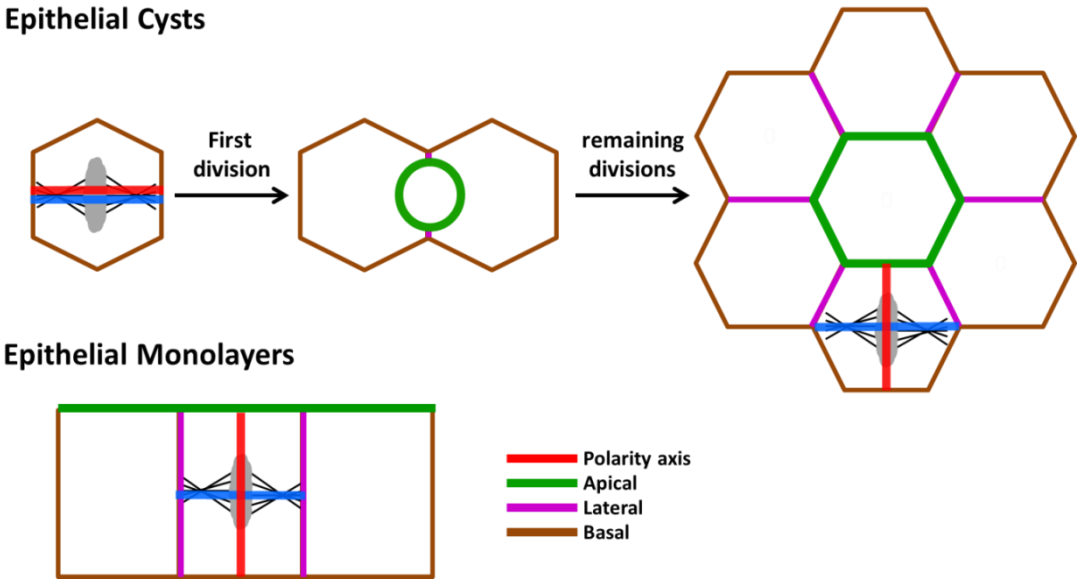

Figure 1.7: Orientation of the apical-basal axis relative to the spindle axis in cyst and monolayer epithelial development. In the first cell division within a cyst the apical-basal axis (red line) and the spindle axis (blue line) are aligned so that formation of the apical lumen is co-ordinated with mitosis. In subsequent cell divisions within a cyst, the apical-basal axis is aligned perpendicular to the spindle axis so that apical membrane formation reinforces lumen formation. Similarly, in 2D monolayer cultures of epithelial cells the apical-basal axis and plane of cell division are aligned at right angles.

The mechanism of shifting the orientation of the apical-basal axis from a horizontal plane in two cells to a vertical place in multicellular cysts is not known. One possibility is that apical membrane formation might utilise mitotic machinery only in the first cell division but not in subsequent divisions, so that the mechanism of apical membrane formation becomes dissociated from cell division once an apical membrane has already been established. For example, in one study trafficking of crumbs3a to spindle poles was not observed in cell divisions occurring in cysts larger than two cells, instead crumbs3a remained in the plasma membrane and the apical domain established at the two cell stage was kept intact (Schlüter et al., 2009). These findings suggest that apical membrane trafficking along the spindle and midzone microtubules to form the apical membrane is unique to the very first division only. However, disrupting spindle orientation of dividing cells in multicellular cysts leads to a multi-lumen phenotype; cells fail to traffic apical membrane to a common lumen and subsequently form multiple lumens in the lateral membranes between cells (Jaffe et al., 2008). This suggests that even at later stages of development, cell division influences the orientation of apicobasal polarity and that the mitotic apparatus directs apical membrane formation in all cell division events.

Several polarity proteins have been implicated recently in spindle pole orientation during epithelial cell division. Silencing of Cdc42 causes spindle orientation defects in the MDCK cell line (Jaffe et al., 2008; Rodriguez-Fraticelli et al., 2010, Qin et al., 2010) and in the developing neural tube of *Xenopus laevis* (Kieserman and Wallingford, 2009). In all cases, loss of Cdc42 and spindle mis-orientation severely disrupted morphogenesis of the epithelium. In MDCK cysts, depletion of the Cdc42 GEFs Intersectin-2 and Tuba caused multiple lumen formation (Rodriguez-Fraticelli et al., 2010, Qin et al., 2010), suggesting that regulation of spindle orientation by Cdc42 is required for proper lumenogenesis. Tuba localises to intracellular membranes and is necessary for the apical localisation of Cdc42, while Intersectin-2 localises to the centrosome, where it may activate Cdc42 in the pericentrosomal region during mitosis.

Spindle orientation is regulated by the G-alpha binding protein Pins (Siller and Doe, 2009). When cells within a cyst or monolayer divide, the mitotic spindle is initially orientated parallel to the vertical apicobasal axis but subsequently rotates 90° aligning parallel to the ECM. Pins localises to the lateral membrane where it captures astral microtubules and anchors them to the plasma membrane (Zheng et al., 2010). Disruption or mis-localisation of Pins causes spindle mis-orientation and disrupts lumen formation (Hao et al., 2010). Pins segregation to the lateral membrane appears to be regulated by the Par6–Par3–aPKC Par polarity complex (Hao et al., 2010). Pins is phosphorylated by aPKC at the apical membrane, which causes it to be sequestered by 14-3-3, excluding Pins from the apical cortex and restricting its localisation to the lateral membrane (Clarke, 2009). Disruption of any of the components of the Par6–Par3–aPKC complex affects polarised localisation of Pins, induces abnormal spindle orientation and results in multiple lumen formation (Hao et al., 2010). Activated Cdc42 can bind to the Par6-aPKC complex and activates aPKC (Goldstein et al., 2007), therefore the role of Cdc42 in spindle orientation could involve apical activation of aPKC and sequestering of Pins.

The orientation of the mitotic spindle during cell division may affect the positioning of the mid body during abscission, since the midbody and intercellular bridge is formed from spindles derived from the mitotic spindle apparatus. The midbody is thought to mark the site of apical membrane formation and therefore midbody localisation may affect apical membrane trafficking. For example, apical cargo such as aPKC and crumbs3a are trafficked along midzone microtubules (Schlüter et al., 2009). In the intestinal cyst model (caco-2), depletion of Cdc42 caused the position of the midbody to be mis-localised due to random orientations of the mitotic spindle (Jaffe et al., 2008). Interestingly, the localisation of the midbody coincided with lumen development in both normal cysts and in Cdc42 depleted cysts which formed multiple lumens, suggesting the multiple lumen phenotype of Cdc42 depletion could be due to mis-localised midbodies. The formation of multiple lateral lumens in multicellular cysts with mis-localised midbodies further suggests that apical trafficking along the midzone microtubules is not unique to the first cell division and on-going apical membrane trafficking is co-ordinated with abscission.

In epithelial cells growing as cysts and in two dimensional cultures, the midbody localises asymmetrically near the apical domain (Fleming et al., 2007; Reinsch and Karsenti, 1994). Apical localisation of the midbody ensures apical cargo is trafficked towards the apical membrane. The analysis of MDCK cells in two dimensional culture and mouse intestinal epithelial cells in vivo has revealed that cleavage furrowing is asymmetric (figure 1.8), proceeding from the basal side to the apical side. Asymmetric furrowing of the contractile ring positions the midbody apically and ensures abscission occurs near the surface of the monolayer (Fleming et al., 2007; Reinsch and Karsenti, 1994). However, in the case of the first cell division of epithelial cysts, abscission appears to be symmetric and apical membrane formation is initiated in the middle of the cleavage plane.

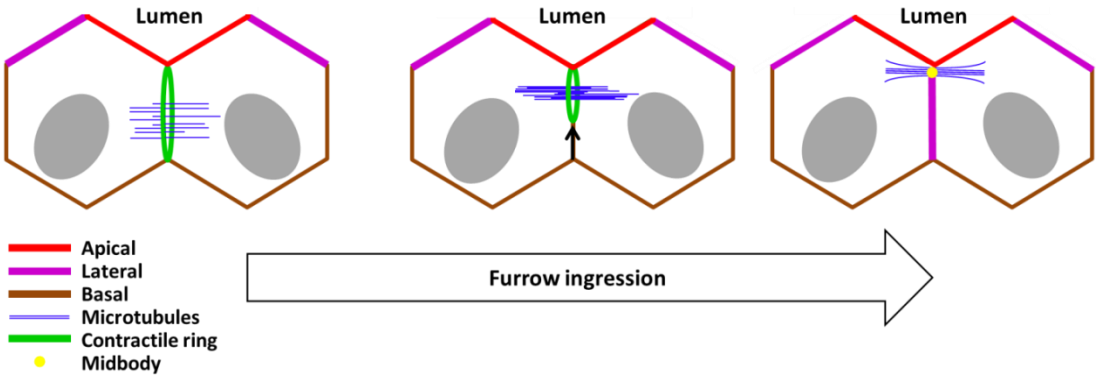

Figure 1.8: Asymmetric furrow ingression positions the midbody apically. During cytokinesis, furrowing of the contractile ring (green) occurs asymmetrically, from the basal membrane (brown) towards the apical surface (red). The directional movement of the contractile ring is indicated with an arrow. In cyst cultures of epithelial cells, the midbodies (yellow) are located beneath the developing lumen whilst in to two dimensional cultures the midbodies are positioned beneath the apical side of the monolayer (not shown). Asymmetric abscission ensures the structure of the tissue is not disrupted by cells undergoing division.

The mechanism regulating asymmetric furrow ingression is not clear. However, in the *C. elegans* embryo, depletion of anillin and the septins blocked asymmetric furrowing and cytokinesis subsequently occurred midway in the cleavage plane (Maddox et al., 2007). Anillin and the septins promote a differential distribution of contractile ring components around the circumference of the ring (Maddox et al., 2007; Tse et al., 2011), thus strengthening constriction of the ring from one side. For example, myosin-2 is more concentrated on the side of the ring that ingresses the most and depletion of either anillin or the septins results in a loss of this asymmetric distribution (Maddox et al., 2007). Asymmetric abscission in polarised cells might function to limit disruption of apical junctional complexes and maintain the integrity of the epithelium.

Project aims and objectives

The cell types most affected in Lowe Syndrome are highly polarised but whether OCRL1 is involved in establishing or maintaining polarity is not currently known. The overall aim of this project was to study the role of OCRL1 in polarisation which is critical for the function and architecture of the tissues affected by Lowe Syndrome.

The reasoning behind this objective was that OCRL1 has been implicated by numerous studies to regulate processes important for cell polarity, such as membrane trafficking and cytoskeletal dynamics. Several groups have used the MDCK cell line or renal cells derived from Lowe Syndrome patients to examine the effects of OCRL1 loss on these processes. One study reported defects in the trafficking of receptors such as megalin and transferrin to the cell surface (Vicinanza et al., 2011), while another study found no effect on biosynthetic or endocytic pathways but instead reported changes in trafficking from the TGN to lysosomes (Cui et al., 2010). Therefore the role of OCRL1 in regulating polarised trafficking remains unclear. However, the multiple reports of OCRL1 function in ciliogenesis suggest a role for OCRL1 in apical trafficking. The formation of the primary cilium is a hallmark of apical membrane biogenesis. OCRL1 regulates trafficking of ciliary proteins in a Rab8 dependent pathway (Coon et al., 2012) and apical trafficking in renal cells also occurs through Rab8 dependent transport. Rab8 was shown to be one of the preferred in vitro binding partners of OCRL1 (Hyvola et al., 2006) and it has recently been crystallised in complex with Rab8 (Hagemann et al., 2012), therefore other Rab8 dependent apical trafficking pathways may be regulated by OCRL1 as well as the ciliary specific route. Lastly, OCRL1 facilitates cytokinesis in *Drosophila* and non-polarised cell lines (Ben El Kadhi et al., 2011; Dambournet et al., 2011). It is not known whether OCRL1 similarly functions in renal cell cytokinesis, but should OCRL1 affect cytokinesis in polarised epithelial cells, polarisation might in turn be affected.

In addition to a possible role of OCRL1 in regulating polarised trafficking pathways, several of its interaction partners play crucial roles in polarised epithelial cell development such as the Rho GTPases Rac1 and Cdc42. Additionally, phosphoinositides regulate multiple processes in polarised cell types, particularly the substrate of OCRL1; $PI(4,5)P_2$, which is expected to be elevated in Lowe Syndrome. The strongest evidence suggesting a role for OCRL1 in cell polarity was the finding that OCRL1 depletion disrupted lumen formation in MDCK cysts (Grieve et al., 2011), although the mechanism behind this remains unclear.

Given the previous findings with OCRL1 outlined above, it is possible that OCRL1 has a role in polarisation and that polarisation may be disrupted when OCRL1 is absent. This project studies the role of OCRL1 in the polarisation of cell lines derived from the kidney, which is the organ most affected in Lowe Syndrome as well as Dents-2 disease. Firstly, we detail the effects of OCRL1 loss on the appearance of epithelial monolayers in Chapter 3. Whether OCRL1 plays a role in polarised trafficking pathways is examined in Chapter 4 and chapter 5. Chapter 4 focuses on the localisation of polarity markers in cells allowed to fully mature without OCRL1. The emphasis of Chapter 5 is on the role of OCRL1 in the earliest stages of polarisation when an apical-basal polarity axis is established. Lastly, Chapter 6 examines a role for OCRL1 in renal cell cytokinesis which is intricately linked to polarisation in this cell type. One possibility is that these aspects of renal tubular cell function are disrupted in Lowe Syndrome and Dents-2 disease, where loss of OCR1 causes selective renal proximal tubulopathy and eventually renal failure.

Chapter Two

Materials and Methods

DNA methods

Bacterial strains

BL21 *Escherichia coli (E. coli)* competent bacteria were used for GST fusion protein expression. *E. coli* strain MC1061 was used for plasmid DNA amplification. Competent bacteria were stored at -80 ^{o}C.

DNA Constructs

GFP tagged human OCRL1 (wild-type, isoform b, 893 amino acids) and GFP-OCRL1Δphosphatase Δ237–539) were a gift from Prof. Martin Lowe (University of Manchester Faculty of Life Sciences, UK). Human GFP-AKT-PH (1–167), and GFP-Grp1-PH were a kind gift from Dr. Tamas Balla (National Institute of Health, Bethesda, USA). GFP-PLCδ-PH was prepared previously in our lab (Dr. Tim Levine, Institute of Ophthalmology, University College London, UK). Cdc42-GFP was a gift from Prof. Catherine Rabouille (Hubrecht Institute, Utrecht, Netherlands). GST-zebrafish-OCRL1 and GST-human-OCRL1 were also gifts from Prof. Martin Lowe. GFP/EGFP plasmids were Kanamycin resistant and GST plasmids were Ampicillin resistant.

Bacterial transformation

Competent bacteria were thawed on ice. 10 ng plasmid DNA was incubated with 15 µl MC1061 or 500 ng plasmid DNA was incubated with 30 µl BL21 on ice for 5 minutes. Bacteria were heat shocked at 42 ^{o}C for 45 seconds and immediately put back on ice. 5x volume (75 µl for BL21, 150 µl for MC1061) of LB medium without antibiotics was added and the bacteria were incubated at 37 ^{o}C for 30 minutes. After resting at 37 ^{o}C the bacteria were diluted into 4 ml LB containing appropriate antibiotic (100 µg/ml Ampicillin or Kanamycin) and grown shaking at 30 ^{o}C (MC1061) or 37 ^{o}C (BL21) overnight.

Bacterial glycerol stocks

For long term storage of transformed bacteria, overnight cultures were diluted in glycerol and stored at -80 ^{o}C. 0.5 ml of overnight culture was diluted in 0.5 ml sterile 50% (v/v) glycerol solution in a sterile eppendorf tube. To recover the bacteria a small amount of frozen culture was extracted with a sterile inoculating needle and added to LB medium containing appropriate antibiotic. Inoculated cultures were grown at 30 ^{o}C (MC1061) or 37 ^{o}C (BL21) overnight before DNA extraction.

Plasmid DNA extraction

2 ml overnight transformed bacterial cultures were pelleted by centrifugation at 3000-4000 x g for 10 minutes. Plasmid DNA was extracted using QUIAGEN Spin Miniprep Kit according to manufacturer's instructions. Briefly, bacterial cells were lysed by alkali and the lysate was applied to a silica column that selectively binds plasmid DNA. Contaminants were removed with wash buffers and the plasmid DNA was eluted with 40 µl of ddH_2O. Concentration and purity of plasmid DNA samples were obtained with a Nanodrop (Thermo Fisher Scientific).

Protein methods

SDS-PAGE

Cell lysates were prepared for SDS-PAGE analysis by washing cells twice with Dulbecco's phosphate buffered saline (PBS, Invitrogen) and then adding directly to the cells 2x sample buffer (4% SDS, 20% glycerol, 0.003% bromophenol blue, 0.125 M Tris pH 6.8, 10 % β-mercaptoethanol and 1% Sigma protease inhibitor cocktail). 200 µL sample buffer was added per well of cells on a 6 well plate. Cell lysates were heated at 95 °C for 2 minutes before loading. Resolving gels were 0.375 M Tris pH 8.8, 10% Acrylamide/Bis-acrylamide, 0.1% SDS. Stacking gels were 0.125 M Tris pH 6.8, 4% Acrylamide/Bis-acrylamide, 0.1% SDS. Gels were polymerised with 0.05% ammonium persulphate and 0.1% TEMED (tetramethylethylenediamine). Gels were run in 1 x SDS-PAGE buffer (25 mM Tris, 192 mM glycine, 0.1% SDS) for 90 minutes at 150 V.

Coomassie staining

Following electrophoresis the protein gels were stained with coomassie blue (0.1% (w/v) coomassie blue, 20% (v/v) methanol, and 10% (v/v) acetic acid) and resolved with de-stain solution (50% (v/v) methanol in water with 10% (v/v) acetic acid).

Electrophoretic transfer

PVDF membrane (GE Healthcare) was pre-soaked in 100% methanol for 10 seconds and immersed in ddH_2O. After SDS-PAGE, polyacrylamide gels and Whatman filter paper was soaked in transfer buffer (25 mM Tris, 250 mM glycine pH 8.3, 0.1% SDS, 20% MeOH) for 10 minutes. Gels were transferred using a wet transfer apparatus (BioRad) assembled according to manufactures instructions. Transfer was at 300 mA for 45 minutes at 4 °C.

Immunoblotting

After electrophoretic transfer, PVDF membranes were blocked in PBST (PBS 0.05% Tween-20) containing 5% skimmed milk for 60 minutes at room temperature (RT) with agitation. Primary antibody incubations were for 2 hours at RT or overnight at 4 °C diluted in blocking solution. The membrane was washed five times for 10 minutes with PBST and then incubated with an appropriate HRP conjugated secondary antibody in blocking solution for 1 hour. After secondary antibody incubations, the membrane was washed again five times for 10 minutes each with PBST and then washed once with PBS for an additional 10 minutes. Protein bands were detected with Pierce ECL Western Blotting Substrate and Fuji x-ray film.

Immunoprecipitations

A confluent 15 cm plate of cells were washed three times with cold PBS and lysates were harvested by direct addition on ice of 3 ml extraction buffer to the plate (10 mM Hepes pH 7.4, 150 mM NaCl, 1% Triton X-100, 0.5% Na-deoxycholate, 0.2% SDS, Sigma protease inhibitor cocktail). The cells were scraped at 4 °C. 1 ml extract was incubated with protein G sepharose beads rotating for 30 minutes at 4 °C. Previously the beads were washed three times in extraction buffer and centrifuged at 7,500 x g. The pre-cleared lysates were added to immunobeads (1.5 µg of antibody conjugated overnight to protein G sepharose beads). Lysate was incubated with immunobeads for 2 hours at 4 °C. Beads were washed once with PBS containing 0.5% Triton-X100 followed by an additional wash with just PBS. The beads were suspended in 2x sample buffer and boiled before loading onto SDS-PAGE gels or storing at -80 °C.

Expression of GST fusion proteins

BL21 *E. coli* was transformed with pGEX vectors coding for the amino-terminal fragment of OCRL1 (1-237) tagged to GST or zebrafish GST-OCRL1 (1-297). 5 ml of overnight cultures of BL21 were diluted into 500 ml LB medium and 100 mg/ml ampicillin. Cultures were incubated at 37 °C for approximately 2 hours at 250 rpm until A600 reached 0.8-1.0 at which point 0.2 mM IPTG was added to induce protein expression. Cultures were placed at 30 °C at 250 rpm for 5 hours to allow protein expression. Bacteria were centrifuged at 7,500 x g for 15 minutes at 4 °C to pellet the cells which were re-suspended in 30 ml of cold NETN (0.5% NP-40, 20 mM Tris pH 8.0, 100 mM NaCl, 1 mM EDTA, 1 mM DTT, 0.1 mg/ml lysozyme and Sigma protease inhibitor cocktail) and incubated on ice for 30 minutes. The DNA was sheared by sonication with a microprobe 5 x 10 seconds on ice. Insoluble cell debris was pelleted by centrifugation at 12000 x g for 20 minutes at 4 °C. Protein expression was checked by running the clarified supernatant on 10% polyacrylamide gels and stained with coomassie blue. If successful the supernatant was stored at -80 °C or immediately processed for purification.

GST and GST-fusion protein column preparation

30 ml total soluble protein prepared from bacteria expressing GST fusion proteins was incubated with 1.5 ml of 50% slurry of glutathione-sepharose beads (1:1 suspension in NETN) for 2 hours on a rotor at 4 °C. The glutathione-sepharose beads were pre-equilibrated with NETN. The beads were washed twice with 0.1 M borate buffer pH 8.0, once each with 0.1 M borate buffer pH 9.0, and once with 0.2 M borate buffer pH 9.0. The GST and GST fusion protein was cross-linked to the beads using 40 mM dimethypimelimidate (DMP) for one hour at 4 °C. Beads were again washed in 0.1 M borate buffer pH 8.0 before incubation with 40 mM ethanolamine in 0.1 M borate buffer pH 8.0 for 45 min at 4 °C. Additional washes were carried out once each with PBS, 0.2 M glycine-HCl (pH 2.5), 1 M K_2HPO_4 and 2 final washes in PBS.

Affinity purification of anti-OCRL1 antibodies

10 ml sheep serum raised against human GST-OCRL1 (1-237) was diluted 1:1 in PBS containing 0.2% Tween-20. The anti-GST antibodies in the serum were first removed by affinity purification using a GST column. The glutathione-sepharose beads cross-linked to GST were incubated with the serum for 2 hours at 4 °C. The beads were spun and the remaining serum was incubated with glutathione-sepharose beads cross-linked to zebrafish GST-OCRL1 (1-297) overnight at 4 °C. The beads were placed in a 2 ml Biorad column and the flow through was allowed to pass. The beads in the column were washed with 120 ml of PBS containing 0.2% Tween-20, followed by 10 ml of just PBS. After washing, the antibody was eluted with 0.2 M glycine-HCl (pH 2.5) into eppendorf tubes already containing 1 M K_2HPO_4. This was repeated so that 10 fractions were collected. The fractions were run on a 10% acrylamide gel and stained with coomassie blue to identify which fraction the antibody was eluted in.

Mammalian cell culture

Cell lines

Madin-Darby canine kidney epithelial cells (MDCK) clone 2 and Caco-2 (human caucasian colon adenocarcinoma epithelial cells) were gifts from Prof. Karl Matter (Institute of Ophthalmology, University College London, UK). MDCK clone 2 cells stably expressing GFP-Gp135 (Meder et al., 2005) was a kind gift from Prof. Joachim Fullekrug (Max Planck Institute of Molecular Cell Biology and Genetics, Dresden, Germany). The renal tubular cell line RCC4 stably transfected with wild-type pVHL was kindly provided by Prof. Patrick Maxwell (Division of Medicine, Rayne Institute, University College London, UK). The hTERT immortalised human renal tubular cell line NHPTK (Herbert et al., 2013) was a kind gift from Prof. Robert Bacallao (Department of Medicine, Indiana University School of Medicine, Indianapolis, USA). The transformed trabecular meshwork human cell lines NTM5 and GTM3 were kind gifts from Prof. Ian Grierson (Eye and Vision Science, University of Liverpool, UK). LoweB fibroblasts were a kind gift from Prof. William O'Brien (Department of Molecular and Human Genetics, Baylor College of Medicine, Houston, USA).

Growth conditions

All cell lines were grown at 37 °C with 5% CO_2. MDCK, Caco-2, GTM3, NTM5, and VHL+ RCC4 cells were cultured in Dulbecco's modified Eagle's medium (DMEM, Invitrogen) containing 10% heat inactivated foetal bovine serum (FBS, Invitrogen). LoweB fibroblasts were cultured in DMEM medium containing 20% FBS. NHPTK cells were cultured in Lonza's REBM medium containing Lonza's supplements for renal cells (bullet kit) and 10% FBS. All cell culture media was supplemented with 100 µg/ml streptomycin and 100 µg/ml penicillin.

Passaging cells

Prior to passaging MDCK, Caco-2, LoweB, NTM5, GTM3 and VHL+ RCC4 cell lines, the cells were washed once in calcium and magnesium free PBS (Invitrogen). NHPTK cells were washed in HDF buffer (8 g NaCl, 0.4 g KCl, 1 g Glucose Dextrose/monohydrate, 0.35 g $NaHCO_3$ in 992 ml endotoxin free H_2O). All cells were detached from the tissue culture flask with 0.25% Trypsin (w/v) in 0.5 mM EDTA (disodium ethylenediaminetetraacetic acid). Detached MDCK, Caco-2, NTM5, GTM3, LoweB and VHL+ RCC4 cells were split directly into appropriate medium without additional washing and centrifugation steps at a ratio of 1:6. Detached NHPTK cells were suspended in growth medium, pelleted by centrifugation and re-suspended in fresh medium prior to plating at a ratio of 1:5.

Freezing cells

For storage, cells were grown to approximately 70% confluence, washed and trypsinised according to the passaging protocol. Once detached, cells were suspended in appropriate growth medium and transferred to a 15 ml sterile centrifuge tube. Cells were pelleted at 1000 rpm for 4 minutes and re-suspended in cold freezing medium (20% (v/v) dimethylsulphoxide (DMSO) in FBS). Freezing medium was added to trypsinised cells at 6x volume and the cells in freezing medium were aliquoted into 1 ml storage vials. Cells were frozen slowly, initially at -20 °C for an hour, followed by -80 °C overnight before permanent storage in liquid nitrogen at -80 °C. For short term storage (several months) cells were maintained at -80 °C.

Thawing cells

Recovery of cells from frozen stocks was carried out as quickly as possible. Growth medium was pre-warmed to 37 °C in advance. Vials of cells were taken from storage and immediately placed in a 37 °C water bath until approximately 80% had thawed. The thawed cells were washed in growth medium and pelleted at 1000

rpm for 4 minutes to remove the DMSO. The cell pellet was re-suspended in fresh growth medium appropriate for the cell line and plated into tissue culture flasks.

Calcium switch assay

Cells were grown in appropriate medium for the cell line (see growth conditions). At approximately 80% confluence the cells were washed and trypsinised according to the passaging cells protocol. Detached cells were diluted in pre-warmed calcium free DMEM (Invitrogen) containing 10% FBS in a 15 ml centrifuge tube. The cells were spun down at 1000 rpm for 5 minutes and washed for a second time by re-suspending the cell pellet in calcium free DMEM and centrifuging again at 1000 rpm for 5 minutes. After washing, the cells were re-suspended in calcium free DMEM containing 10% FBS and re-plated in a 6 well plate containing glass coverslips and incubated at 37 ^{o}C 5% CO_2 overnight. To carry out the switch, cells were washed twice in PBS and incubated with pre-warmed complete DMEM (containing normal high calcium content) and 10% FBS. Cells were fixed and observed at various time points after calcium recovery.

Apoptosis assay

Cells were grown on 13 mm coverslips in 24 well plates to approximately 60% confluence. As a positive contol for apoptosis, a control group of cells were treated with 1 μM staurosporine (Invitrogen) in the extracellular growth medium for 2 hours before analysis. To detect apopotic bodies the cells were incubated with a number of fluorescent stains in the extracellular growth medium for 1 hour prior to analysis. The membrane permeable DNA marker Hoechst 33342 (final concentration of 1 μg/ml) labels live cells. Propidium iodide (final concentration of 2 μg/ml) labels necrotic cells. YO-PRO-1 idodide dye (Molecular probes, Invitrogen) was used at 1/1000 and labels specifically apoptotic cells. Samples were fixed in 3% PFA but not permeabilised.

Plasmid DNA transfection with JetPEI

This protocol was carried out for experiments in Chapter 3 (3.9-3.10) and Chapter 4 (4.9-4.11) because cells were grown over the course of 5 days and therefore siRNA and DNA transfection could be carried out separately. Cells were transfected with DNA 24 hours after the second siRNA dose (section 'siRNA transfection with Oligofectamine') when they were approximately 70% confluent. For cells in figure 3.1 which were wild type and untreated with siRNA, the cells were transfected with plasmid after 3 days growth at approximately 70% confluence. To prepare the transfection mix, 0.4 µg of plasmid DNA was add to 150 µl of sterile NaCl JetPEI buffer (polyplus transfection), vortexed and spun down. In a separate tube 4 µl of JetPEI reagent (polyplus transfection) was diluted in 150 µl of sterile NaCl JetPEI buffer, vortexed and spun down. After resting for 5 minutes, the JetPEI reagent solution was added to the DNA solution to give a final transfection mix of 300 µl. After 20 minutes of additional resting, the transfection mix was added drop wise to cells containing 1.5 ml of appropriate growth medium for the cell line containing antibiotic.

siRNA transfection with Oligofectamine

Cells in all experiments were grown on 22 mm square coverslips in 6-well plates in appropriate medium containing antibiotic (see growth conditions). The siRNA protocol used varied depending on the stage of cell growth when treating with siRNA.

Cells growing as monolayers (Chapter 3 and Chapter 4) were treated twice with siRNA over the course of 4-5 days growth. In this protocol, cells were plated at approximately 20% confluence on day 1. On day 2 cells were treated with one dose of siRNA at approximately 40% confluence and again on day 3 at approximately 60% confluence. Cells were allowed to rest until fixing on day 4 or 5, 48 hours or 72 hours post the first siRNA treatment respectively. Whether cells were fixed at 48 hours or 72 hours is indicated in the figure legends.

When cells were treated with siRNA and subsequently transfected with a plasmid, a modified version of this siRNA protocol was carried out to allow time for DNA transfection before becoming fully confluent. This protocol was performed in the experiments for Figures 3.10, 4.9, 4.10, 4.11. For this protocol, cells were plated on the morning of day 1 and treated to the first dose of siRNA 8 hours later on the same day, when they had reached approximately 30% confluence. The cells were treated again to a second dose of siRNA 24 hours later at approximately 50% confluence on day 2 and transfected with plasmid DNA separately 24 hours later on day 3. Cells were allowed to rest and fixed on day 4 or 5, 48 hours or 72 hours after the second dose of siRNA.

For RNAi treatment of cells plated at very low confluence (Chapter 5 and 6), the cells were plated onto coverslips for just a few hours before treatment with one dose of siRNA. In this protocol, cells were trypsinised well and pipetted gently to discourage cell clumping prior to plating. Cells were plated for 4 hours, treated once with siRNA and analysed 17-24 hours later.

In all protocols using MDCK cells, the cells were treated with a mix of 4 canine specific OCRL1 siRNA sequences. All protocols using human cell lines were treated with a mix of 2 human specific OCRL1 siRNA sequences and control cells were treated with non-targeting control siRNA. All siRNA was purchased from Invitrogen and the sequences are listed below in the section: siRNA sequences.

For both single and double siRNA transfections, the following method was used to prepare the siRNA for transfection. The siRNA was diluted into 175 µl of serum free Opti-MEM (Invitrogen) in a 1.5 ml tube so that the final concentration of siRNA was 120 nM (6 µl of a 20 µM stock). In a separate tube, 5 µl Oligofectamine transfection reagent (Invitrogen) was diluted into 15 µl serum free Opti-MEM. After 5 minutes incubating at room temperature the oligofectamine solution was gently mixed with the siRNA solution and incubated for an additional 20 minutes at room temperature. The cells were washed twice in PBS to remove antibiotics and plated in 800 µl of appropriate growth medium without antibiotics. The final siRNA:

Oligofectamine solution of 200 µl was added drop wise to a single well of a 6 well plate and mixed gently before returning to the incubator for 24 hours.

siRNA transfection with INTERFERin

INTERFERin transfection reagent was used for human cell lines, because Oligofectamine appeared toxic and resulted in cell death (data not shown). Therefore this protocol was used for Figures 3.11, 3.12, 3.13, 3.14, 5.24 and 5.24. Cells were plated on 22 mm glass coverslips in a 6 well plate and cultured to approximately 50% confluence, taking approximately 1-3 days depending on the cell line (indicated in figure legend). At 50% confluence, human siRNA was transfected with INTERFERin (Polyplus transfection). siRNA was diluted in 150 µl serum free Opti-MEM so that the final concentration was 40 nM (3 µl of a 20 µM stock) and incubated for 5 minutes. INTERFERin was vortexed and 2 µl was added to the siRNA solution and the mixture was left to rest for 10 minutes at room temperature. Cells were washed once in PBS and replaced with 1.35 ml appropriate medium containing antibiotics. The RNAi transfection mix was added drop wise to the cells, gently mixed and the cells were returned to the humidified chamber for a further 48 hours. The medium was replaced after 24 hours.

Plasmid DNA and siRNA co-transfection

This protocol was used in chapter 5 (Figures 5.18-5.23) where cells were only depleted of OCRL1 for less than 24 hours. Separate transfection of siRNA and plasmid in the course of 24 hours was toxic. For this protocol, cells were plated on 22 mm glass coverslips in a 6 well plate and cultured to approximately 60% confluence. Co-transfection of siRNA with plasmid DNA was carried out using JetPRIME reagent (Polyplus transfection). The siRNA was diluted in 150 µl JetPRIME buffer so that the final concentration was 50 nM (2.5 µl of a 20 µM stock), 2 µg of plasmid DNA in ddH_20 was added to the siRNA mix, vortexed, spun down and incubated for 5 minutes. After resting, 4 µl of JetPRIME reagent was added to the siRNA/DNA mix, vortexed, spun down and incubated for a further 15 minutes at

room temperature. The cells were washed once with PBS before adding 850 µl of appropriate growth medium for the cell line containing antibiotic. The transfection mix was added drop wise to the cells, 8 hours later it was washed off and the growth medium was replaced.

siRNA sequences

Canine OCRL1	CUUUCCGAUACCUCCGUUCUU
	GCUUAUUAGUCUUCAUCACUU
	UUUGAUGAGACCCUCCCGCUU
	UUUGAUGAGACCCUCCCGCUU
Human OCRL1	UUUGAUGAGACCCUCCCGCUU
	CUUUCCGGUACCUUCGUUCUU

Primary antibodies

Mouse anti-Ezrin, rabbit anti-Par6β, mouse anti-aPKCζ, goat anti-scribble (Santa Cruz Biotechnology, Inc.), rabbit anti-Par3 (EMD Millipore) and rabbit anti–ZO-1 (antigen: the peptide N-YTDQELDETLNDEVC-C) described previously (Benais-Pont et al., 2003) were all kind gifts from Prof. Karl Matter (Institute of Ophthalmology, University College London, UK). Polyclonal anti-OCRL1 antibody used for immunoblotting was a gift from Prof. Robert Nussbaum (Department of Medicine, UCSF, San Francisco, USA), described previously (Olivos-Glander et al. 1995). Affinity-purified rabbit antibodies to annexin-2 (Gerke and Weber, 1984) and mouse monoclonal anti-α-tubulin (Sigma) were gifts from Prof. Stephen Moss (Institute of Ophthalmology, University College London, UK). Rabbit polyclonal anti-Rab11a (Zymed) was a gift from Prof. Clare Futter (Institute of Ophthalmology, University College London, UK). Mouse anti-Gp135 secreted from hybridoma cell line 3F2 (Ojakian and Schwimmer, 1988) was a kind gift from Prof. George Ojakian (State University of New York Downstate Medical Center, Brooklyn, NY). Rat anti-

(CI)-M6PR (Reaves et al., 1996) and rabbit anti-Rab8a (Sigma) were kind gifts from Prof. Paul Luzio (Cambridge Institute for Medical Research, University of Cambridge, UK). Primary antibodies were diluted in PBS to a concentration of 1–5.0 μg/ml.

Immunostaining

For immunostaining the cells were either fixed with PFA or methanol. Methanol was only used when staining the microtubules, to better preserve the structures. Therefore methanol fixation was used in all microscopy figures in Chapter 6 and Figure 4.12. For PFA fixation, cells were washed once in PBS and fixed in 3% PFA (w/v) in PBS at room temperature for 30 minutes. Cells were permeabilised with 0.5% Triton X-100 in PBS for 2 minutes. For methanol fixation, cells were washed quickly in PBS and incubated with cold methanol on ice for 2 minutes. After fixation with both PFA and methanol, the cells were washed 5 times in PBS for 5 minutes. Primary antibodies were incubated with the cells in PBS either overnight at 4 °C or at room temperature for 2 hours. Primary antibodies were washed off the cells 5 x 5 minutes each with PBS. Secondary antibodies conjugated to FITC, TRITC or Cy3 (Molecular probes Alexafluor, Invitrogen) were incubated with the cells in PBS (1/2000) for 45 minutes. When DAPI or phalloidin was used, they were diluted according to manufacturers protocols (1/2000 for phalloidin and 1/5000 for DAPI) into the secondary antibody mix and incubated with cells at the same time. The cells were washed 5 x 5 minutes in PBS before mounting in vectashield (Vector Laboratories, Inc) on glass cover slides for imaging. Confocal images were acquired with an SP2 confocal microscope (Leica) using Apochromat 63×/1.4 immersion oil objectives. Immersion oil (Carl Zeiss) was used for all objectives.

Live cell imaging

Cells from Figures 5.6 and 5.18 were imaged live on a Leica confocal microscopy system pre-warmed to 37 °C. Cells were plated on 35 mm glass bottom MaTek dishes and imaged directly from the dish. Prior to imaging the cells were replaced with phenol free medium (Leibniz) containing 10% FBS and antibiotics.

Fluorescence recovery after photobleaching (FRAP)

FRAP experiments (Figure 5.6) were performed on transfected cells plated into 35 mm glass bottom MaTek dishes in phenol free medium. The Leica confocal microscopy system was pre-warmed to 37 °C prior to analysis. The pinhole size was set to maximum AU units to allow for large confocal sections to be imaged. Laser light was set to a low intensity for image recording to minimise background bleaching and high intensity for bleaching the flourophore. Specific regions of interested were selected for bleaching using the Leica software. Images were recorded pre-beaching, immediately post bleaching and every 2.5 minutes from then on. The images were aligned in ImageJ to account for movements in the plane using the StackReg plugin. Signal Intensity values for the regions of interest was calculated in ImageJ. Values were normalised against background fluorescence intensity.

Image editing

Microscopy images were adjusted for brightness and contrast with Adobe Photoshop. Stacks were compressed and XZ images were reconstructed using ImageJ. 3D reconstructions of stacks were created using ImageJ 3D Viewer.

Statistical analysis

T-test

T-tests on group means were carried out in Excel. Each group of data was first plotted in S+ (TIBCO) to check for normal distribution. The equality of the variances between compared groups was tested with a Fisher test in S+. Where variances were statistically different a Welch modified T-test was done in Excel. T-tests were carried out in S+ on linear regressions to confirm the gradients were statistically different from 0.

ANOVA

One-way ANOVA was performed to test whether multiple means were equal. This test was carried out in S+.

Chapter Three

OCRL1 is involved in the maturation of epithelial cells

Overview

Some of the symptoms of Lowe Syndrome manifest in polarised cells of the lens and kidney epithelium. Cells in an epithelium grow as a single layer and adhere to each other strongly through multiple junctions including adherens junctions, tight junctions and desmosomes. Another feature of the epithelium is the uniformity of cell size and shape, for example the simple epithelium of the kidney consists of sheets of cells which are tall and columnar in shape. Isolated epithelial cells are relatively flat, but upon initiating cell-cell contacts the sheet grows in height by extension of the lateral domain. Spatial control of the actin cytoskeleton in these cells is crucial for proper morphogenesis of the epithelium. In addition, formation of apical and basolateral domains relies on vesicular transport of domain specific cargo to the plasma membrane. Given the cell types most affected in Lowe Syndrome and the potential for OCRL1 to regulate actin dynamics or trafficking in polarised epithelial cells, OCRL1 could be involved in some aspect of epithelial maturation.

This chapter is a continuation of a previous doctoral project investigating the localisation and function of OCRL1 in polarised epithelial cell lines (Grieve et al., 2011). Most of the previous work was carried out in intestinal epithelial cells (Caco-2), derived from a human colonic adenocarcinoma. In addition, some results were reproduced in the renal MDCK cell line. In both Caco-2 and MDCK cells, OCRL1 was shown to target intercellular junctions, co-localising with the tight junction protein ZO-1 (Grieve et al., 2011). In addition, this work implicated OCRL1 to function in some aspect of epithelial maturation since monolayers of Caco-2 and MDCK cells depleted of the protein were flatter than normal (Grieve et al., 2011).

Firstly, this chapter reproduces the finding that OCRL1 targets intercellular junctions and then confirms that OCRL1 is required for maturation in a similar manner shown previously, in addition to accurately measuring the effect. In this chapter, we also investigate possible explanations for these findings and reveal the role of OCRL1 in epithelial development may extend to human renal cells and cells

derived from the trabecular meshwork of the lens, which is also affected by Lowe Syndrome.

OCRL1 targets intercellular junctions in MDCK cells

OCRL1 has been shown by numerous studies to localise to the Golgi apparatus and endosomes in non-polarised cells (Choudhury et al., 2005; Noakes et al., 2011; Swan et al., 2010; Vicinanza et al., 2011). Previous work in several polarised epithelial cell lines found a small pool of OCRL1 targeted primordial junctions (Grieve et al., 2011). Here, expression of OCRL1 tagged with green fluorescent protein (GFP) in MDCK cells showed OCRL1 to localise to the Golgi apparatus, numerous intracellular vesicles and the plasma membrane, marked by the tight junction marker ZO-1 (figure 3.1). XZ images suggested OCRL1 localised to the region of the plasma membrane engaged in intercellular junctions (data not shown).

The localisation of overexpressed recombinant OCRL1 might not reflect the localisation of the endogenous protein. To detect endogenous OCRL1, sheep antibodies raised against human-OCRL1 antibodies were purified with zebrafish-OCRL1 to reduce affinity of binding and enable efficient elution of the most useful antibodies from the column. These antibodies also detected a population of OCRL1 at intercellular junctions (figure 3.2), as shown with other antibodies previously which were no longer available (Grieve et al., 2011). The specificity of the antibody was confirmed in cells depleted of OCRL1 with silencing oligonucleotides (siRNA), which showed that both the junctional staining and the Golgi apparatus staining were dependent on the presence of the protein (figure 3.2). There was also a small amount of nuclear staining with the OCRL1 antibody which was likely to be non-specific as it was not lost when OCRL1 was depleted.

Previously, OCRL1 depletion did not affect the appearance of the tight junction (Grieve et al., 2011). However, when we repeated the RNAi experiment, the

localisation of ZO-1 no longer appeared normal. Here, the junctional bands of ZO-1 appeared to be thinner than controls and non-continuous in the absence of OCRL1 (figure 3.2). In addition, the broken appearance of the junctions in OCRL1 depleted cells was accompanied by a larger vesicular pool of ZO-1 (figure 3.2), which was not reported previously (Grieve et al., 2011). These differences may be explained by the use of different antibodies and optimisation of the levels of OCRL1 depletion in recent studies compared to previous studies.

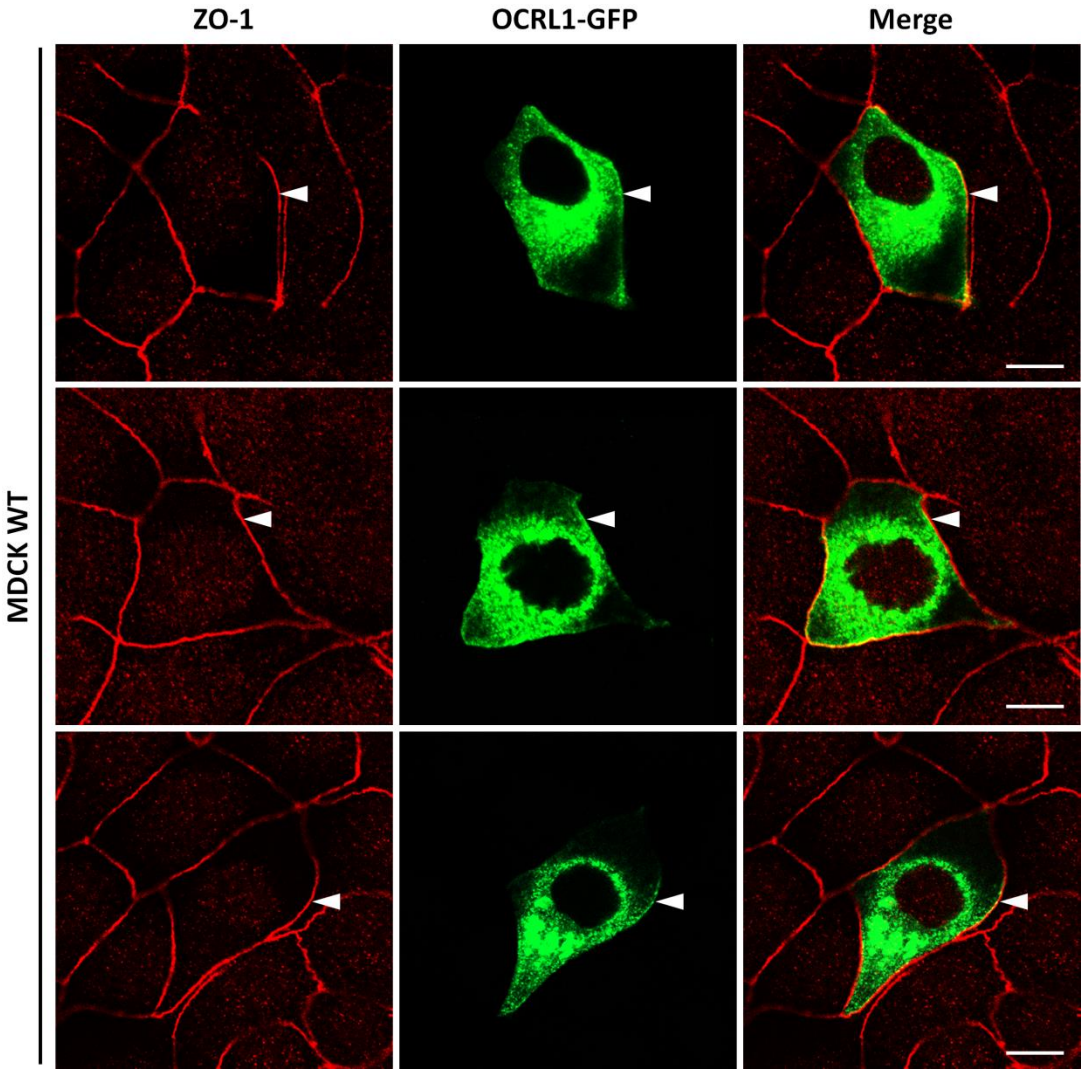

Figure 3.1: GFP-OCRL1 partially localises to junctions in MDCK cells. MDCK cells were grown for 3 days and were transfected with GFP-OCRL1 DNA at 60% confluence. 24 hours after transfection the cells were fixed and permeabilised for immunostaining with antibodies to the tight junction protein ZO-1. Representative images are shown from 3 experiments. White arrows indicate sites where GFP-OCRL1 (green) co-localised with ZO-1 (red). Single confocal sections are shown. Scale bar 10 μM.

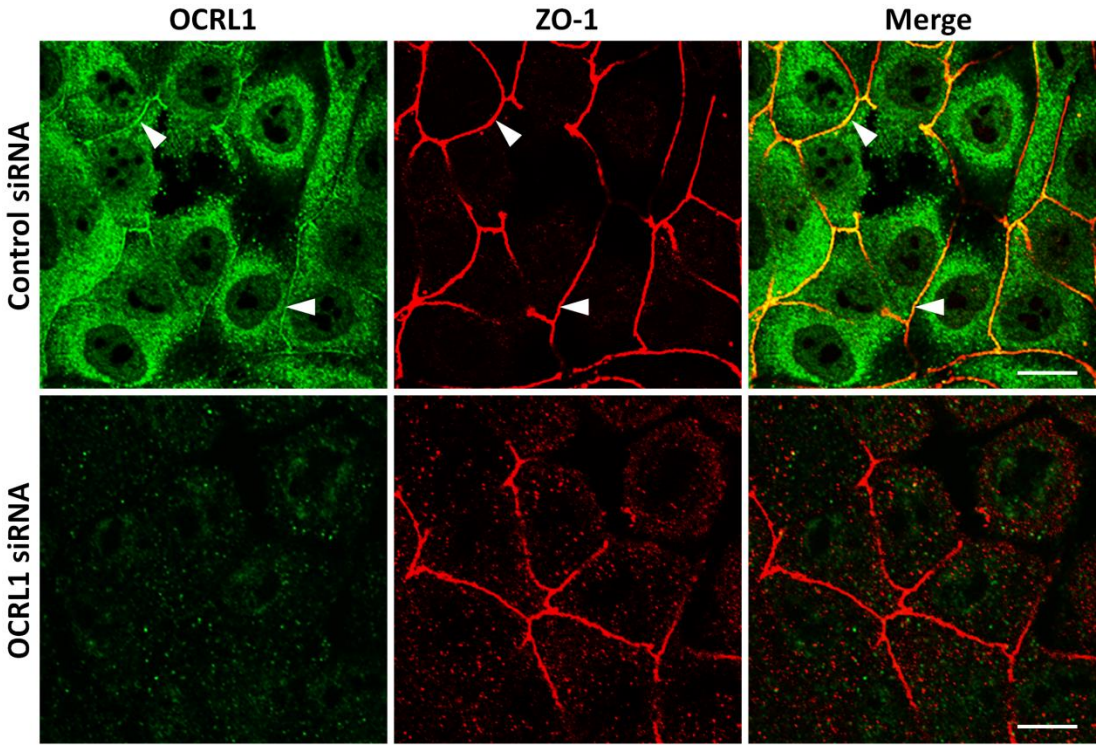

Figure 3.2: Endogenous OCRL1 partially localises to the tight junction. MDCK cells were grown overnight. At 40% and 60% confluence cells were transfected with non-targeting control or a pool of canine specific OCRL1 siRNA. After 48 hours, the cells were fixed and permeabilised for immunostaining with antibodies to the tight junction protein ZO-1 (red) and OCRL1 (green). Representative images are shown from 1 of 3 experiments. White arrows indicate sites where ZO-1 and OCRL1 co-localise which is absent from OCRL1 depleted cells. Single confocal sections are shown. Scale bar 10 µM.

OCRL1 forms a complex with tight junction protein ZO-1

The apparent co-localisation of OCRL1 with ZO-1 by immunofluorescence indicates a potential interaction. Supporting this possibility, it was previously shown that immunoprecipitates of OCRL1 complexes were positive for ZO-1 (Grieve et al., 2011). To confirm this interaction, we repeated the immunoprecipitation experiments in reverse, not carried out previously. Immunoprecipitated complexes of ZO-1 contained OCRL1 (figure 3.3), further suggesting that they exist in the same complex at the tight junction.

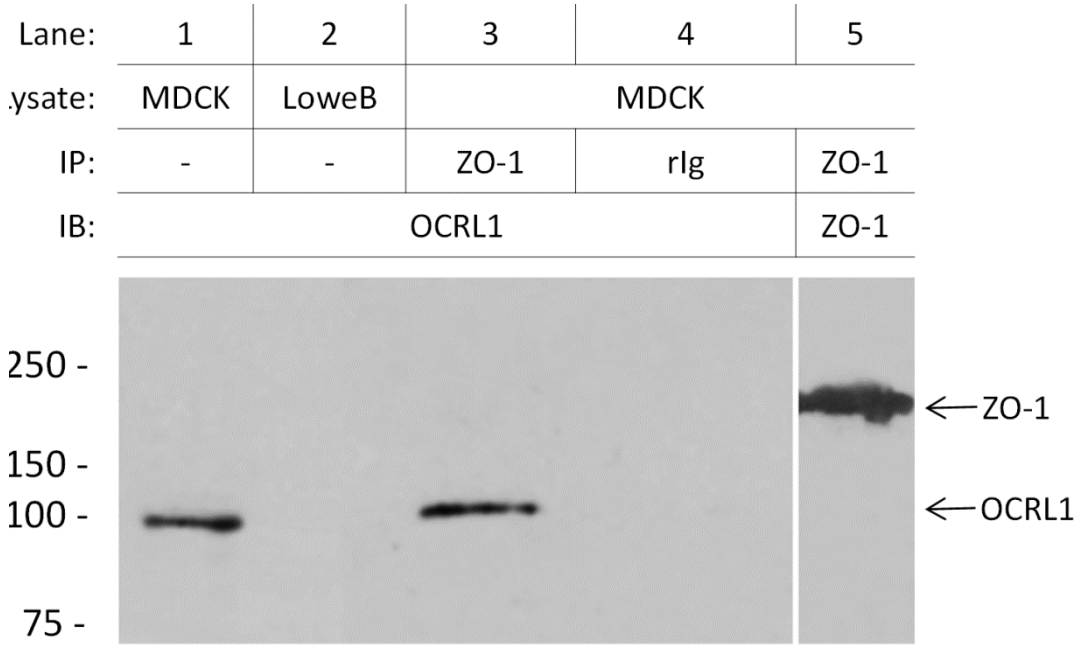

Figure 3.3: OCRL1 interacts with the tight junction ZO-1 complex. MDCK cells were grown on 10 cm dishes. LoweB fibroblasts were grown in a 6 well plate. Cell lysates were collected at 70% confluence. MDCK lysate was pre-cleared with negative beads before incubating overnight with protein G-sepharose beads linked to either ZO-1 or normal rabbit immunoglobulin (rIg). The precipitated proteins (Lanes 3, 4, 5) and MDCK input lysate (Lane 1) were run on SDS-PAGE gels and probed for OCRL1 (Lanes 1, 3, 4) and ZO-1 (Lane 5). LoweB fibroblasts from a patient with Lowe Syndrome lacking OCRL1 provided a negative control for OCRL1 immunoblotting (Lane 2). Arrows indicate OCRL1 (105kDa) and ZO-1 (220kDa).

OCRL1 is required for maturation of MDCK monolayers

Having reproduced the junctional localisation of OCRL1 in MDCK cells, we next investigated a role for OCRL1 in maturation. By using the filamentous actin (F-actin) stain phalloidin as a peripheral marker, MDCK cell monolayers were shown to be flatter when depleted of OCRL1 by RNA interference than control cell monolayers (figure 3.4A). In addition, we used the position of the tight junctions, normally localised apically, as a measure of cell height (figure 3.4B). The height of the tight Junction marker ZO-1 above the basal domain was reduced in OCRL1 depleted cells compared to control cells (figure 3.4B), further indicating inhibition of epithelial maturation in the absence of OCRL1. As well as appearing flatter, cells depleted of OCRL1 had a larger cross-sectional area compared to control cells (x1.67 ± 0.11 SEM), suggesting overall cell volume might be unaffected by loss of OCRL1 because a loss in cell height vertically was accompanied by an increased growth laterally (figure 3.5). MDCK cells grow as densely packed sheets, therefore in agreement with OCRL1 depleted cells having a larger cross-sectional area, there were less of these cells on the coverslip (figure 3.6). These findings suggest that OCRL1 depletion results in fewer cells that are flatter than controls.

OCRL1 depletion appears to reduce cell number, which could be due to increased levels of cell death or reduced proliferation rates, which was not investigated previously. To check for increased levels of cell death during OCRL1 RNAi experiments, OCRL1 depleted cells were stained with a combination of Hoechst 33342 (live cells), propidium iodide (necrotic cells) and YO-PRO-1 (apoptotic cells) at a number of time points after RNAi treatment. For comparison, some cells were treated with staurosporine instead of siRNA. The kinase inhibitor staurosporine induces apoptosis and was therefore used as a positive control. No excessive apoptosis was observed for up to 72 hours post RNAi compared to cells treated with staurosporine. The highest level of apoptosis was observed 48 hours post RNAi where 0.04% ± 0.0005 SEM of total cells treated with OCRL1 siRNA were apoptotic compared to 0.02% ± 0.001 SEM of cells treated with non-targeting control siRNA. Although significant ($p=0.004$, $n=3$, students T-test), the slightly elevated level of

apoptosis in OCRL1 depleted cells does not explain the 48% average reduction of cell number upon OCRL1 depletion compared to controls (figure 3.6). The reduced number of OCRL1 depleted cells appeared to be due to less cell division events (figure 3.8). Total cell number was counted regularly over the course of the RNAi assay. OCRL1 depleted cells continued to grow more slowly than control cells even when the cell number was normalised to control levels by re-plating both at a lower cell density (figure 3.8). Therefore MDCK cells continued to grow more slowly without OCRL1.

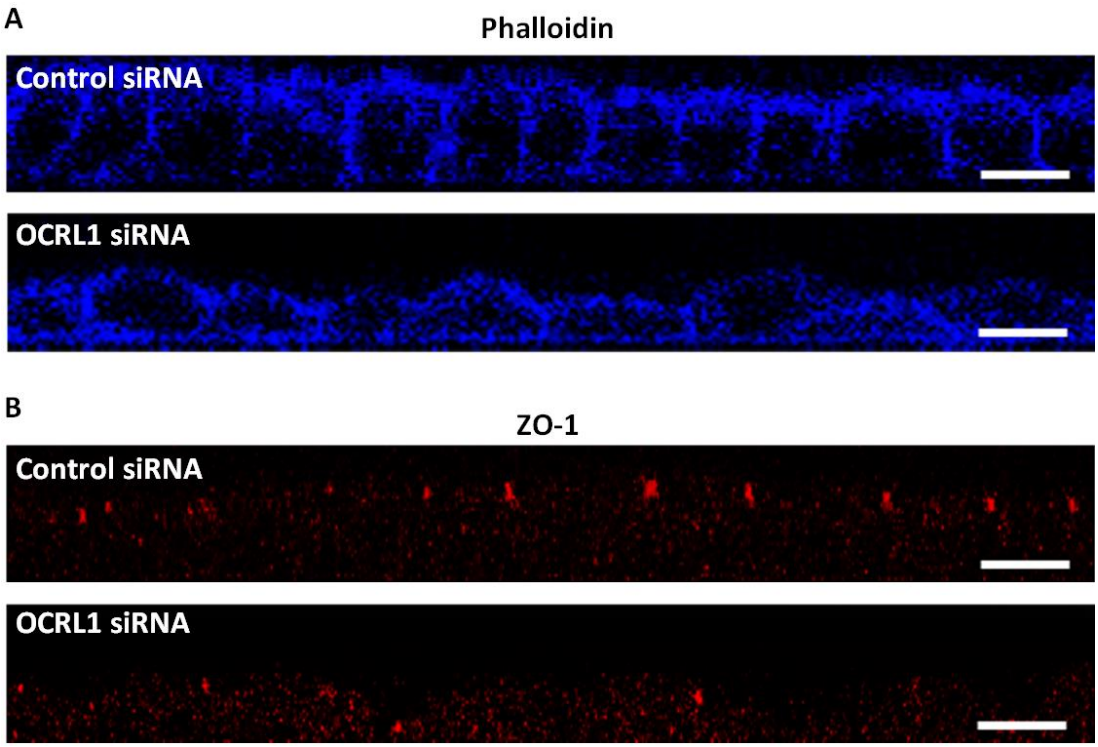

Figure 3.4: Depletion of OCRL1 reduces the height of MDCK monolayers. MDCK cells were grown overnight and treated with siRNA as in figure 3.2. After 48 hours, the cells were fixed and permeabilised for staining. A: Cells were stained with Cy5-phalloidin to identify filamentous actin (blue). B: Cells were immunostained with antibodies to the tight junction protein ZO-1 (red). Panels from A and B do not represent the same cells. XZ sections were reconstructed from Z-stacks containing 30 confocal sections spanning from the bottom to the top of the cell layer. Experiment was repeated twice and multiple XZ reconstructions were taken from each experiment (n=3). Scale bar 10 µM.

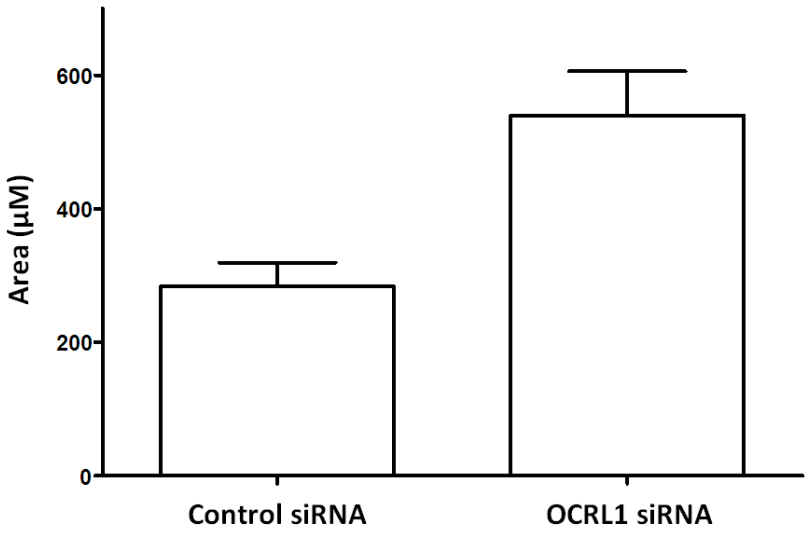

Figure 3.5: Depletion of OCRL1 increases cross sectional cell area. MDCK cells were grown overnight and treated with siRNA as in figure 3.2. After 48 hours, the cells were fixed, permeabilised and stained for the actin stain phalloidin as a peripheral cell marker and the DNA stain DAPI. Single confocal sections of the middle of the cell layer were taken across 6 different RNAi experiments. Approximate cell cross sectional area in each confocal section was calculated using the cell number and known dimensions of the frame. Using these two paramters it is posssible to estimate average cross sectional area per cell due to the intercellular contacts formed between MDCK cells and therefore tight packing of MDCK monolayers.
Plotted is the mean and SEM. P=0.001 (students T-test).

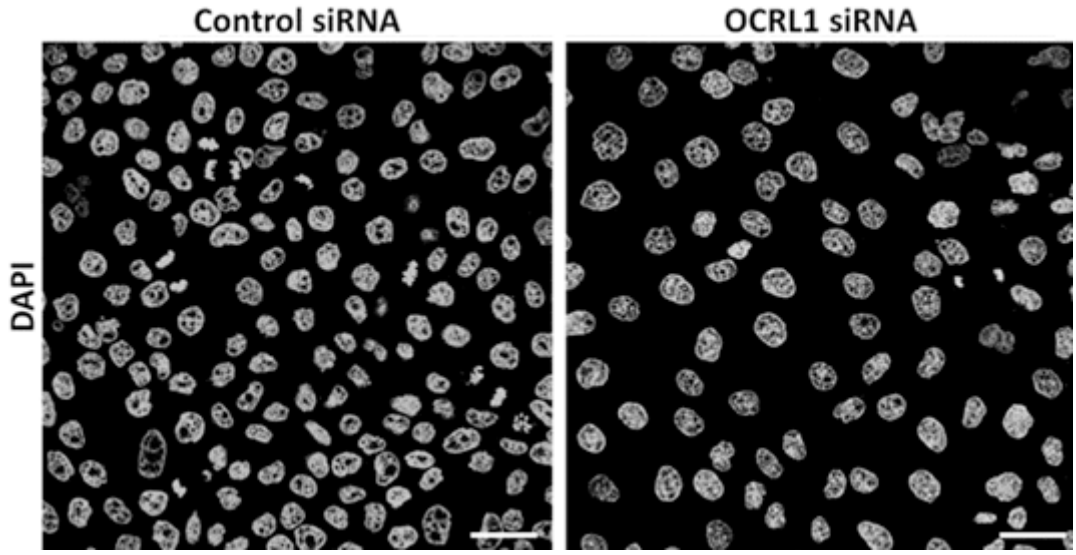

Figure 3.6: Depletion of OCRL1 reduces cell number. MDCK cells were grown overnight and treated with siRNA as in figure 3.2. After 48 hours, the cells were fixed, permeabilised and stained for the DNA stain DAPI. Single confocal sections of the middle of the cell layer were taken across 5 different RNAi experiments. Representative images are shown. The cell number in each frame was determined by the number of nuclei. There was an average of 187 ± 8 SEM cells in each frame treated with control siRNA compared to 97 ± 6 SEM in each frame of cells treated with OCRL1 siRNA ($p=8x10^{-9}$, students T-test). Scale bar 20 µM.

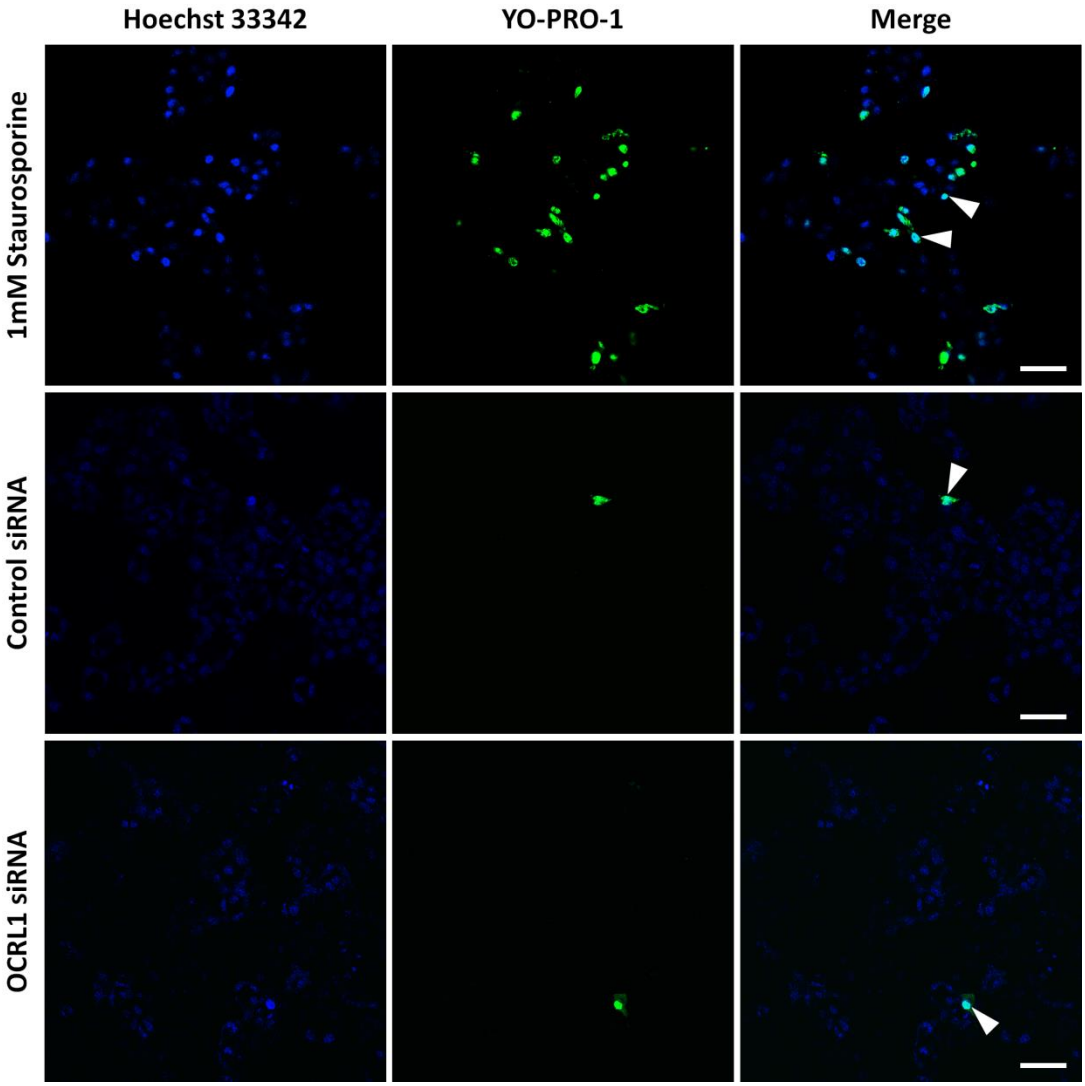

Figure 3.7: Depletion of OCRL1 does not induce significant apoptosis. MDCK cells were grown overnight and treated with siRNA as in figure 3.2. Cells were fixed at 0, 8, 24, 48 and 72 hours post RNAi treatment. For 1 hour before fixing the cells were incubated with a combination of Hoechst 33342 (live cells), propidium iodide (necrotic cells) and YO-PRO-1 (apoptotic cells) in the medium. Only Hoechst 33342 (blue) and YO-PRO-1 (green) are shown. In addition some MDCK cells were treated with 1 µM staurosporine for 2 hours as a positive control for apoptosis. Representative single confocal sections are shown of cells treated with siRNA for 48 hours from one set of three experiments. White arrows point to apoptotic cells. Scale bar 40 µM.

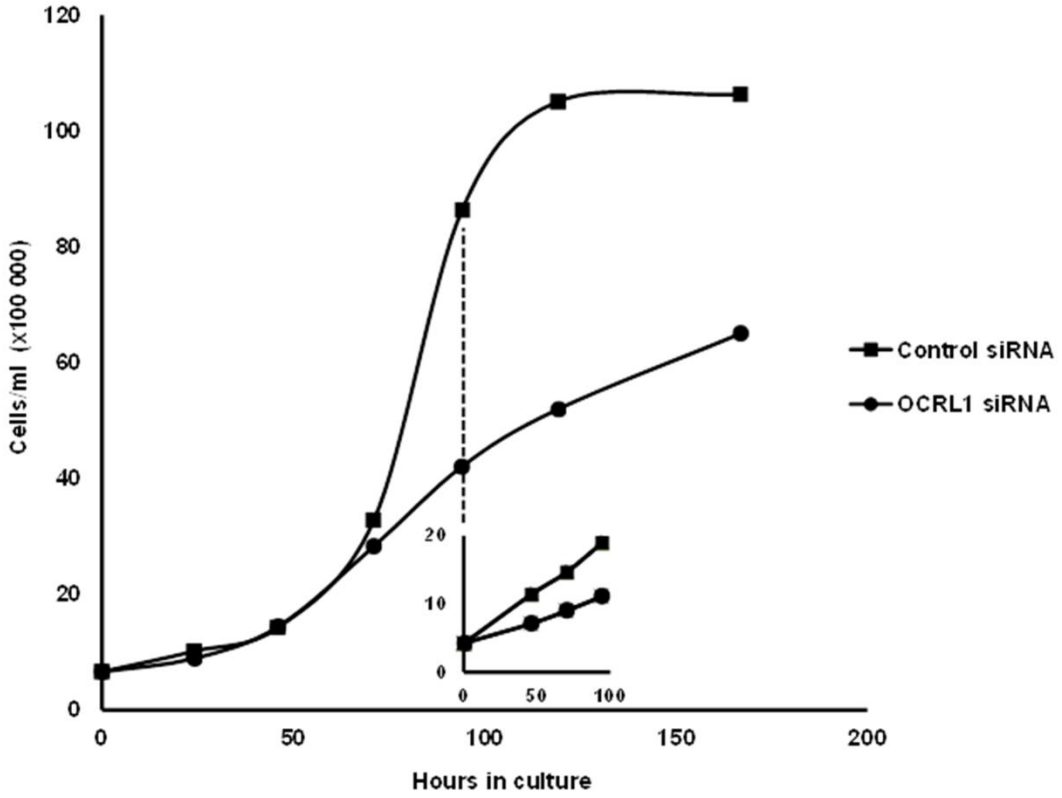

Figure 3.8: Depletion of OCRL1 reduces proliferation rate. Equal numbers of MDCK cells were plated at low density into the wells of a 24 well plate. At 48 and 72 hours the cells were treated with either non-targeting control siRNA or a pool of OCRL1 siRNA. Every 24 hours the cells were trypsinised and counted in a haemocytometer. Cell viability was confirmed by staining with trypan blue. At 96 hours in culture the cells were trypsinised and re-plated at a lower cell density. In this experiment the same number of cells from each sample was re-plated at low density and the proliferation rate was followed as before (inset graph). Results plotted are from a representative of 3 experiments.

The enzymatic activity of OCRL1 is required for maturation of MDCK monolayers

The results above suggest OCRL1 depletion may limit cell height, therefore we tested the effect of excess OCRL1 on cell height by expression of GFP-OCRL1 in untreated MDCK cells that still had endogenous OCRL1 (figure 3.9). Untreated MDCK cells over-expressing GFP-OCRL1 were slightly taller than cells expressing GFP alone (11.8 µm ± 0.32 SEM compared to 10.53 µm ± 0.17 SEM, n=50, p=0.001), suggesting OCRL1 has the capacity to induce expansion. The specificity of the effect on cell height with modulation of OCRL1 levels was further assessed by a series of rescue experiments. To carry out these experiments, the endogenous protein was first depleted with canine specific siRNA followed by reintroduction of OCRL1 by expression of human GFP-OCRL1. OCRL1 depleted cells re-expressing OCRL1 had cell heights comparable to normal levels (11.0 µm ± 0.27 SEM compared to 10.9 µm ± 0.16 SEM, n=50, p=0.88), suggesting re-expression of OCRL1 can rescue the loss of cell height caused by depletion of the endogenous protein. However a human GFP-OCRL1 construct lacking the 5-phosphatase domain caused no gain of cell height when re-expressed in OCRL1 depleted cells (8.8 µm ± 0.2 SEM compared to 10.93 µm ± 0.16 SEM, $p<0.001$). In addition, OCRL1 depleted cells re-expressing phosphatase null OCRL1 had cell heights comparable to OCRL1 depleted cells without re-expression (figure 3.4), further suggesting this construct was unable to induce any gain of height. These results suggest the enzyme activity of OCRL1 is required for maturation of MDCK cell monolayers.

The results of the rescue experiment can be seen in XZ sections taken of cells on the coverslips (figure 3.10). These images show OCRL1 depleted cells neighbouring cells re-expressing the full length protein or the null phosphatase mutant. The GFP positive cells re-expressing full length OCRL1 extend several microns above the height of the surrounding OCRL1 depleted monolayer (figure 3.10). In contrast, the GFP positive cells re-expressing the null phosphatase mutant have heights comparable to their OCRL1 depleted neighbours (figure 3.10). Additionally, when two neighbouring cells both re-expressed full length OCRL1, the tight junction

marker ZO-1 appeared several microns higher than in un-transfected neighbours, however this was not seen in cells expressing phosphatase null OCRL1 (figure 3.10). Similar observations were made previously (Grieve PhD, 2009), but the results here carry them further with accurate measurement of the effect in a large number of cells (250 cells per experiment, n=3). In addition, an effect of excess OCRL1 in wild-type MDCK cells was also observed (figure 3.9), which was not assessed previously.

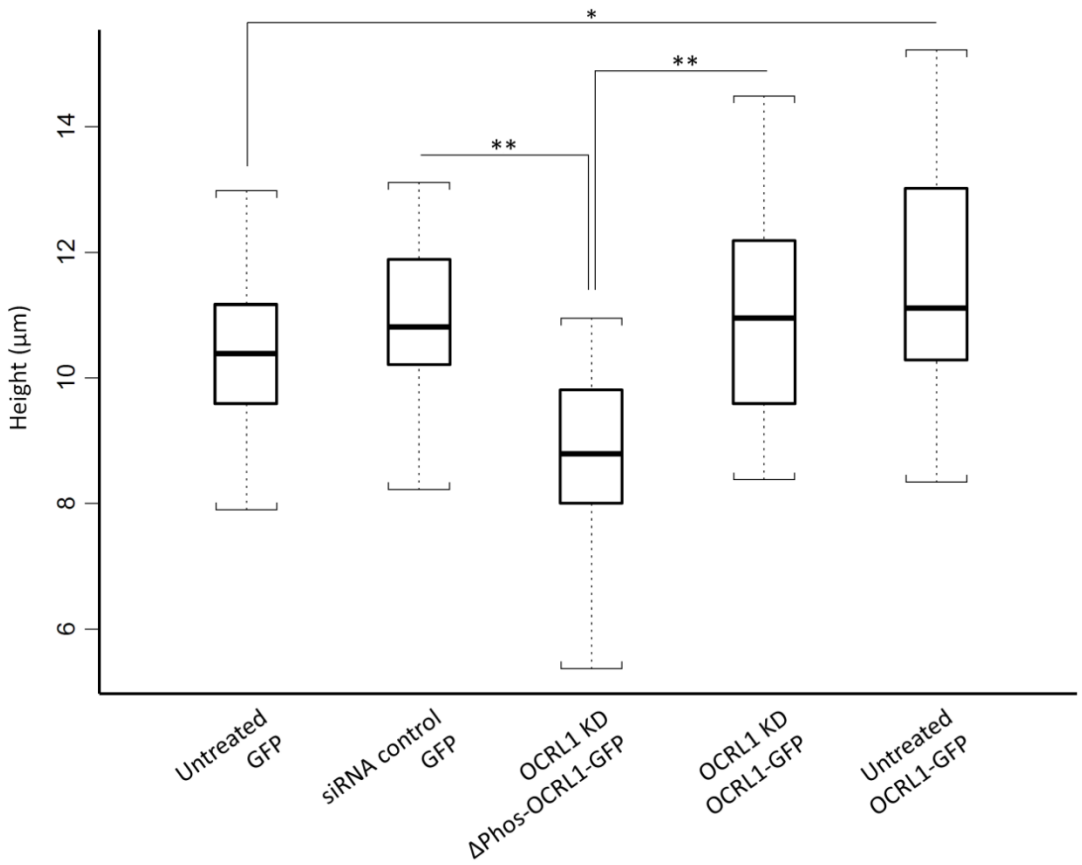

Figure 3.9: Quantification of the recovery of cell height when full length OCRL1 was expressed in OCRL1 depleted cells. MDCK cells were grown overnight. At 30% and 50% confluence, cells were treated with either non-targeting control siRNA or a pool of OCRL1 siRNA. Some samples were left untreated with siRNA (column 1, 5). At 70% confluence the cells were transfected with either empty vector (GFP), GFP-Δphosphatase-OCRL1 DNA (GFP-Δpase), or GFP-OCRL1 and grown for a further 24 hours. Cells were fixed and stained for F-actin as in figure 3.4. Z-stacks of 50 transfected cells per treatment were used to measure cell height. Plotted are the means (black line), upper and lower quartiles (white) and the range (dashed line). Results shown are from a representative of 3 data sets. * indicates $p<0.01$ and ** indicates $p<0.001$ (students T-test).

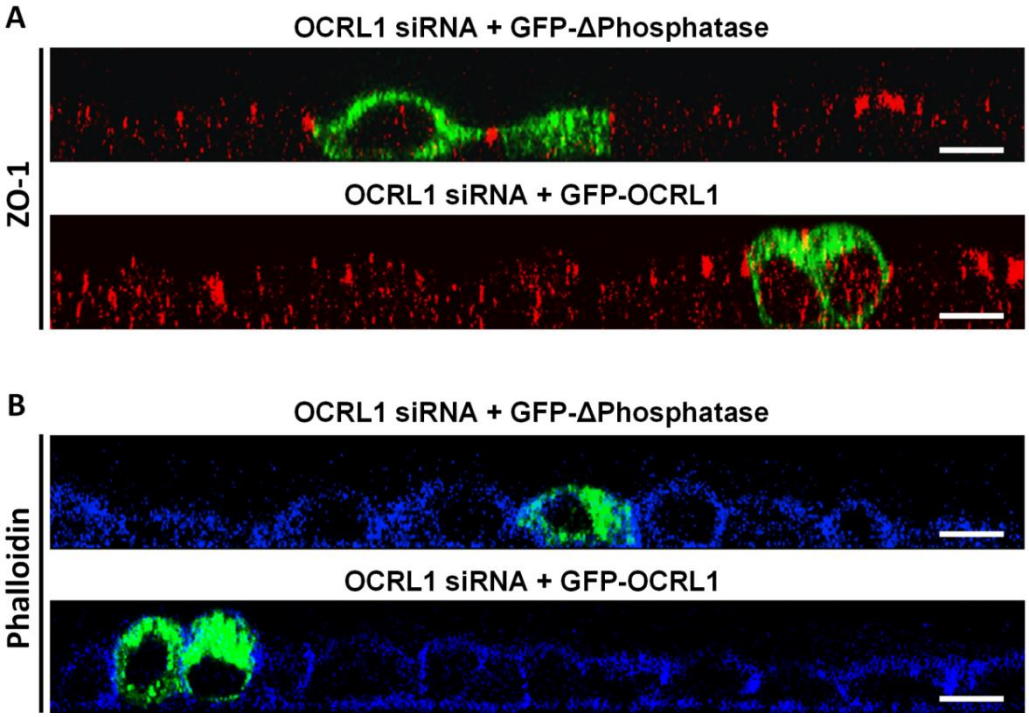

Figure 3.10: The cell height lost in OCRL1 depleted cells can be recovered by expression of full length OCRL1. MDCK cells were grown, transfected with siRNA and plasmid DNA as in figure 3.9. Cells were transfected with either GFP-OCRL1 DNA or GFP-Δphosphatase-OCRL1 DNA. After 24 hours the cells were fixed and permeabilised for staining. A: Cells were immunostained with antibodies to the tight junction protein ZO-1 (red). B: Cells were stained for F-actin with Cy5-phalloidin (blue). Panels in A and B do not represent the same cells. XZ sections were reconstructed from Z-stacks containing 40 confocal sections spanning from the bottom to the top of the cell layer. Experiment was repeated twice. Scale bar 10 µM.

OCRL1 is required for the development of other cell lines

The canine origin of MDCK cells limits any extension of the findings to human disease. Therefore, the affect of OCRL1 loss on cell shape was assessed in a hTERT immortalised human renal cell line NHPTK (Herbert et al., 2012), obtained from Prof. Robert Bacallao (Department of Medicine, Indiana University School of Medicine, Indianapolis, USA). These cells have not been used to study OCRL1 previously, so we first carried out immunofluorescence staining of OCRL1 to assess the localisation pattern. In human renal cells, OCRL1 localised to the Golgi apparatus and intracellular vesicles but no peripheral localisation of OCRL1 was apparent (figure 3.11), suggesting junctional recruitment of OCRL1 is specific to MDCK and Caco-2 cells. We used the same RNAi protocol for the human renal cell line as we used previously for the MDCK cell line, however the human cells took longer to mature and reach full confluence in culture compared to MDCK cells. Therefore, at the time of analysis, after 5 days of growth, the human renal cells were still sub-confluent and may not have completed junction formation. However, by immunofluorescence, we were able to confirm that OCRL1 could be depleted from the human renal cell line, the Golgi apparatus and vesicular staining seen with OCRL1 antibodies was lost when cells were treated with human specific OCRL1 siRNA (figure 3.11).

The human renal cells formed a tightly packed monolayer of columnar shaped cells after 8 days in culture, cell boundaries were visualised using the F-actin stain phalloidin (figure 3.12). We next tested whether OCRL1 depletion affected cell shape in a similar manner to MDCK cells. Monolayers of human renal cells treated with OCRL1 siRNA appeared less mature and failed to columnarise (figure 3.12). However, staining for F-actin revealed severe disruptions to monolayers of human renal cells not seen in MDCK cells. Instead of forming tight cell-cell and cell-ECM contacts, these interactions appeared perturbed (figure 3.12). Human renal cells depleted of OCRL1 formed large plasma membrane folds rich in F-actin where tight lateral contacts are normally made (figure 3.12), suggesting that OCRL1 might facilitate adhesive interactions in this cell line.

We next carried out similar experiments on a transformed human trabecular meshwork cell line. The trabecular meshwork is responsible for draining the aqueous humor from the eye, which may be disrupted in Glaucoma (Tektas and Lutjen-Drecoll, 2009). We obtained non-glaucomatous trabecular meshwork cells (NTM5) and glaucomatous (GTM3) cells from Prof. Ian Grierson (Eye and Vision Science, University of Liverpool, UK). In NTM5 cells, OCRL1 localised to the Golgi apparatus and vesicular pools (figure 3.13) and similar results were found for the GTM3 cell line (data not shown). OCRL1 could be depleted from this cell line, as shown by the loss of immunofluorescence staining with OCRL1 antibodies when cells were treated with a pool of human specific siRNA (figure 3.13). Staining with F-actin revealed that loss of OCRL1 appeared to have an effect on NTM5 cells, there were fewer cells that were not columnar-shaped like controls (figure 3.13). These results suggest that OCRL1 functions in multiple cell lines to promote shape change during columnar maturation.

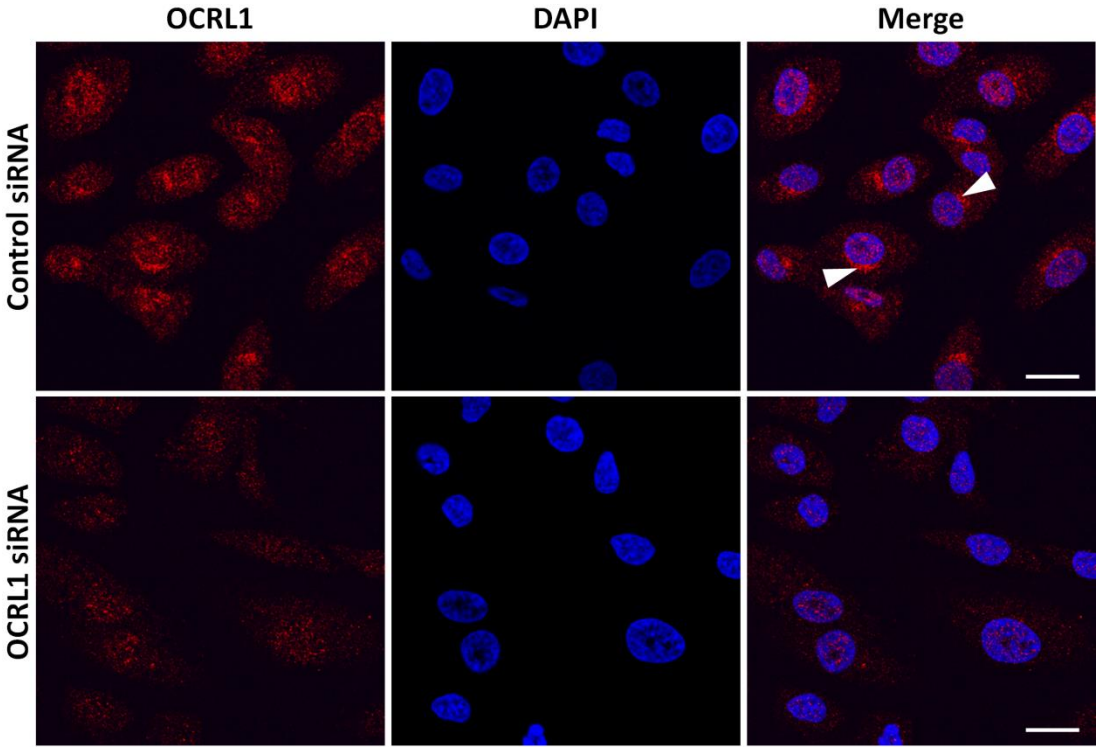

Figure 3.11: OCRL1 can be depleted from a human renal cell line. NHPTK cells were grown overnight. Cells were transfected with non-targeting control or a pool of human specific OCRL1 siRNA on the second and third day in culture and fixed 48 hours later. Cells were fixed and permeabilised for immunostaining with antibodies to OCRL1 (red) and stained with the DNA stain DAPI (blue). Single confocal sections are shown. Images shown are from a single experiment. White arrows indicate Golgi apparatus localisation of OCRL1. Scale bar 10 µM.

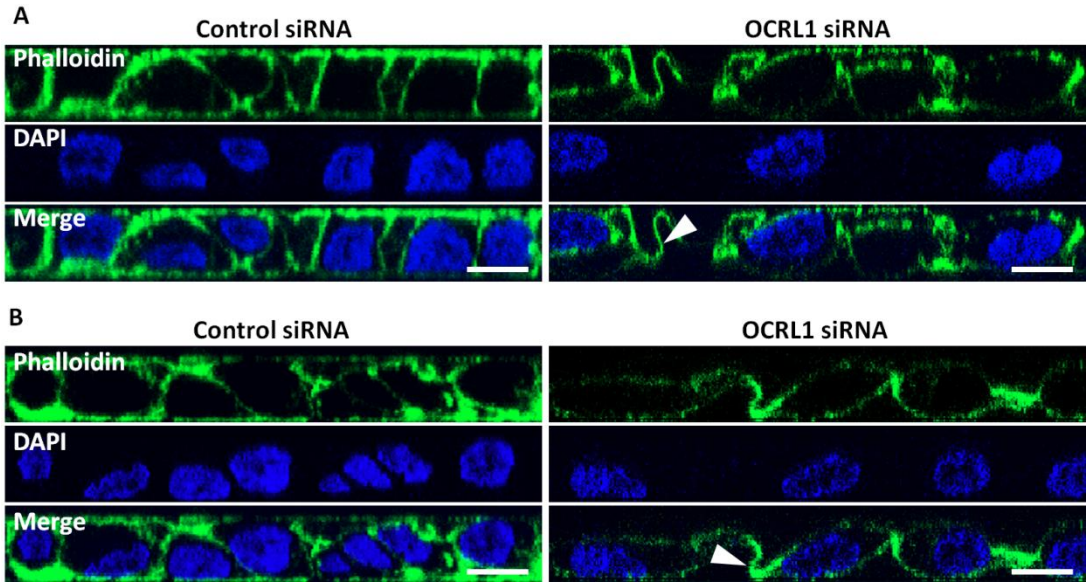

Figure 3.12: OCRL1 depletion disrupted the morphology of human renal cell monolayers. On the third and fourth day of culture, NHPTK cells were transfected with non-targeting control or a pool of human specific OCRL1 siRNA. After a total of 8 days in culture, the cells were fixed and permeabilised to stain for F-actin with phalloidin (green) the DNA stain DAPI (blue). XZ sections were reconstructed from Z-stacks containing 30 confocal sections spanning from the bottom to the top of the cell layer. Two XZ images from different regions on the coverslip are shown per treatment (panels A and B) from 2 experiments. White arrows indicate abnormal adhesions. Scale bar 10 µM.

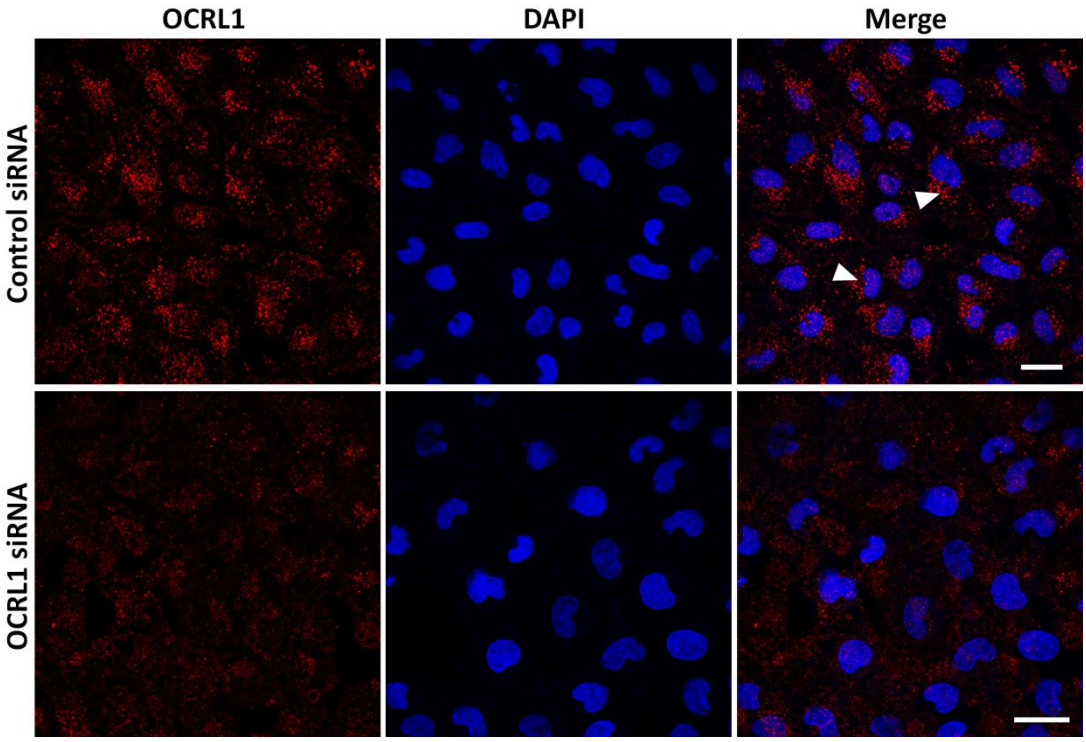

Figure 3.13: OCRL1 can be depleted from cells derived from the trabecular meshwork. Human NTM5 cells were grown overnight. At 40% and 60% confluence cells were transfected with non-targeting control or a pool of human specific OCRL1 siRNA. After 48 hours, the cells were fixed and permeabilised for immunostaining with antibodies to OCRL1 (red) and stained with the DNA stain DAPI (blue). Single confocal sections are shown. Images shown are from a single experiment. White arrows indicate Golgi apparatus localisation of OCRL1. Scale bar 10 µM.

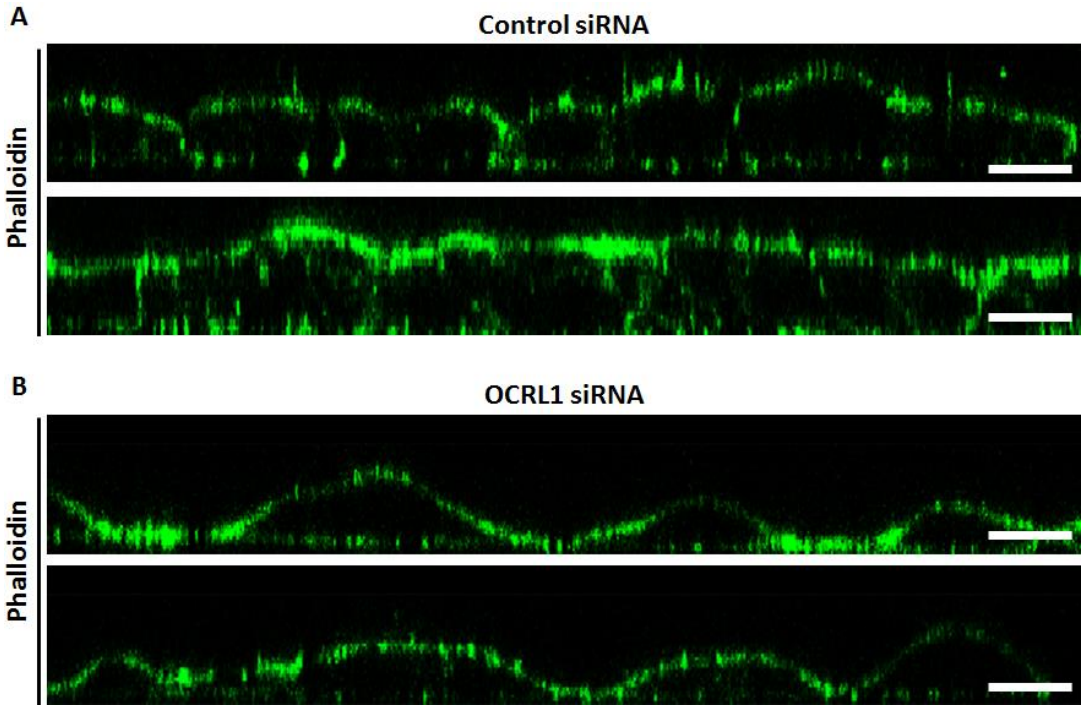

Figure 3.14: OCRL1 is required for the maturation of trabecular meshwork cells. NTM5 cells were grown overnight. At 40% and 60% confluence cells were transfected with non-targeting control or a pool of human specific OCRL1 siRNA. After 48 hours, cells were fixed and permeabilised for staining F-actin with phalloidin (green). XZ sections were reconstructed from Z-stacks containing 30 confocal sections spanning from the bottom to the top of the cell layer. Two XZ images are shown per RNAi treatment from two experiments (Panels A and B). Scale bar 10 µM.

Summary

This chapter aimed to investigate the localisation and function of OCRL1 in maturation of polarised epithelial cell lines derived from cell types that are affected by Lowe Syndrome. We confirmed the previous finding that a small pool of OCRL1 targeted apical tight junctions, existing in a complex with the tight junction protein ZO-1 (Grieve et al., 2011). OCRL1 appeared to be required to maintain the normal morphology of the tight junction which was thinner, partially broken and more punctate when OCRL1 was depleted. The disrupted appearance of the tight junction seen here when OCRL1 was depleted suggests OCRL1 may play a role in pathways that regulate junction integrity.

In addition to highlighting a potential role for OCRL1 at tight junctions, the results in this chapter support the previous work that suggested OCRL1 may be required for epithelial maturation. In MDCK cells, OCRL1 depletion inhibited the maturation of monolayers from flat to columnar shape. In addition, these affects were reproducible in a cell line derived from the trabecular meshwork of the lens (NTM5). More extensive disruptions of the monolayer were observed in a human kidney cell line (NHPTK). As well as reducing cell height, OCRL1 loss affected the ability of cells to form adhesive contacts with each other and the underlying matrix. These results indicate OCRL1 may be involved in the formation of intercellular contacts and is required for the shape change that normally accompanies epithelial development. In the MDCK cell line, extension of cell height during maturation required 5-phosphase activity, an intact enzyme domain in OCRL1 was necessary to rescue the phenotype, suggesting down-regulation of $PI(4,5)P_2$ mediates columnisation of cells in the monolayer. Growth of the monolayer in the vertical plane occurs by a combination of vesicular trafficking, intercellular junction formation and rearrangements of the actin cytoskeleton. OCRL1 has previously been implicated to regulate numerous processes in non-polarised cells which contribute to the maturation of polarised cell types, and these are discussed below.

Discussion

The results in this chapter confirm that OCRL1 targets apical junctions in MDCK cells (Grieve et al., 2011). Although OCRL1 has been reported to localise to peripheral membranes (Erdmann et al., 2007; Faucherre et al., 2005), several studies of OCRL1 in polarised epithelial cells failed to detect the protein at junctions (Cui et al., 2010; Dressman et al., 2010; Vicinanza et al., 2011). Similarly, in this chapter, endogenous OCRL1 was not observed at junctions in a human renal cell line (NHPTK) or a lens epithelial cell line (NTM5), suggesting the localisation pattern of OCRL1 is cell type specific and may not be relevant to Lowe Syndrome. An alternative possibility is that OCRL1 targets intercellular junctions only temporarily. Supporting this possibility is the previous finding that junctional localisation of OCRL1 was lost once monolayers reach maturity (Grieve et al., 2011). In addition, OCRL1 was absent from co-immunoprecipitated ZO-1 complexes when cells were grown to a higher density (Grieve et al., 2011). These findings suggest that OCRL1 may only function at tight junctions temporally during epithelial development.

Intercellular junction formation occurs early during development by vesicular trafficking of junctional components to the lateral membrane. OCRL1 regulates numerous trafficking pathways including biosynthetic and recycling routes (Choudhury et al., 2005; Erdmann et al., 2007; Vicinanza et al., 2011) and both of these pathways are involved in the formation of intercellular junctions. The finding in this chapter that OCRL1 depletion increases punctate intracellular staining of ZO-1 is consistent with OCRL1 regulating trafficking of vesicles carrying junctional proteins. If OCRL1 regulates membrane traffic of junctional components, the pool of OCRL1 at junctions may be delivered along with peripheral vesicular carriers originating from the Golgi apparatus or recycling endosomes.

Alternatively, OCRL1 might be recruited to junctions to maintain a balance in phosphoinositide composition or regulate functional pools of 5-phosphoinositides. The $PI(4,5)P_2$ synthesising enzyme PIP5Kγ has been found to target intercellular junctions in multiple cell lines, generating the $PI(4,5)P_2$ required for actin assembly

and adhesive strength (Akiyama et al., 2005; El Sayegh et al., 2007). By regulating the levels of $PI(4,5)P_2$, OCRL1 could have an important local role at intercellular junctions because of the ability of $PI(4,5)P_2$ to regulate actin binding proteins and therefore the organisation of actin filaments.

Although OCRL1 was found to complex with the tight junction protein ZO-1, the interaction may not be direct since ZO-1 exists in large complexes containing many proteins. Several confirmed binding partners of OCRL1 localise to the tight junction which could mediate OCRL1 recruitment. Several GTPases that interact with OCRL1 are known to target intercellular junctions, such Cdc42 and Rab8 (Rojas et al., 2001; Yamamura et al., 2008). Interestingly, Rab8 is involved in vesicular trafficking of tight junction proteins (Marzesco et al., 2002; Yamamura et al., 2008). Supporting the possibility that OCRL1 is recruited to junctions through interactions with junctional GTPases is the finding that the ASH-GAP domain of OCRL1 is required for OCRL1 to localise to junctions; expression of the C-terminal domain of OCRL1 showed junctional localisation, while the N-terminal portion of the protein was unable to target junctions (Grieve et al., 2011).

Alternatively, if OCRL1 localises to junctions to modulate the actin cytoskeleton, it may be interacting with actin binding proteins in the perijunctional actin pool. OCRL1 has been reported to interact with the GEF Frabin (also known as FGD4) which displays actin-bundling activity (Nakanishi and Takai, 2008). Frabin was identified as a potential OCRL1 binding partner due to the presence of an F&H motif in the amino acid sequence, resembling the interaction motif of the IPIPs/Ses proteins and APPL1 with OCRL1 (Daniels and Levine, unpublished observation). Frabin has since been confirmed as an OCRL1 binding protein (Laura E Swan, personal communication, 2012). Similarly, using an online bioinformatics tool (PROSI TE), we identified δ-catenin as another candidate protein containing a motif resembling the F&H motif found in OCRL1 binding proteins. Although this interaction remains unconfirmed, δ-catenin acts as a prominent adhesive protein and could potentially recruit OCRL1 to intercellular contacts. While the results of this chapter indicate OCRL1 localises to the vicinity of tight junctions in some cell

types, the relevance of junctional OCRL1 and its interactions with junctional proteins remains unclear, addressing these questions would require a molecular dissection of the interactions involved.

Although junctional localisation of OCRL1 has been inconsistent between cell types, we noticed that depletion of OCRL1 consistently reduced cell number and affected cell shape. One possible mechanism of delayed proliferation in OCRL1 depleted cells could involve cytokinesis, since OCRL1 has been implicated to regulate this stage of cell division (Ben El Kadhi et al., 2011; Dambournet et al., 2011). The role of OCRL1 in cytokinesis of MDCK cells is explored in chapter 6. The flattened appearance of OCRL1 depleted epithelial monolayers could be due to an indirect effect of slower proliferation rates. For example if OCRL1 delays proliferation and results in fewer cells on the coverslip, it is unsurprising that monolayers appear less mature than controls. However, rescue experiments demonstrated that OCRL1 had the ability to induce height gain in individual OCRL1 depleted cells. For example, OCRL1 depleted cells re-expressing OCRL1 as a GFP fusion protein extended several planes above the height of the monolayer. In addition, over-expression of OCRL1 in untreated cells also increased the height of cells above the rest of the monolayer indicating OCRL1 can directly induce shape change independently of affecting cell division. These rescue experiments also revealed that the 5-phosphatase activity of OCRL1 was required to induce cell height, suggesting down-regulation of 5-phosphoinositides by OCRL1 is involved in epithelial maturation. Similarly, inhibition of a phosphatidylinositol 3-kinase which is likely to cause elevated levels of its preferred substrate $PI(4,5)P_2$ also inhibited maturation of MDCK cells (Gassama-Diagne et al., 2006), further suggesting phosphoinositide metabolism is critical in the process by which epithelial cells develop.

The mechanism of OCRL1 regulation of cell shape change could involve a number of pathways. Expansion of lateral and apical membranes can facilitate shape change as new membrane is delivered by vesicular trafficking. The role of OCRL1 in regulating polarised trafficking pathways is explored in the next few chapters. It is also likely that OCRL1 affects maturation through regulation of the actin cytoskeleton. Loss of

OCRL1 has previously been shown to produce aberrant actin phenotypes in un-polarised cell types (Hayes et al., 2006; Suchy et al., 2002), and might therefore be involved in regulating cytoskeletal dynamics in polarised cells. OCRL1 may regulate the structural pool of perijunctional actin or regulate cytoskeletal dynamics at other sites in the cell to facilitate the mechanical tension necessary for columnarisation. Supporting the idea that OCRL1 acts via the cytoskeleton to induce cell height is the finding that depletion of the actin regulatory protein Tmod3 phenocopies OCRL1 loss, similarly inhibiting epithelial maturation (Weber et al., 2007). Through regulating the levels of $PI(4,5)P_2$, OCRL1 could potentially be involved in numerous processes important for cytoskeletal re-arrangements, $PI(4,5)P_2$ alters the function of a wide number of actin modulating proteins in addition to regulating actin nucleation through the Arp2/3 complex (Hilpelä et al., 2004). Given the large number of possible pathways downstream of OCRL1, further work would be required to determine the role of OCRL1 in the shape change that accompanies epithelial maturation. The next chapter focuses on another aspect of epithelial maturation, as cells columnarise they polarise and form distinct membrane domains. A potential role for OCRL1 in cell polarity is explored next in Chapter 4.

Chapter Four

MDCK cells without OCRL1 form lateral apical lumens

Overview

In the previous section, OCRL1 was implicated in epithelial cell maturation. Cells without OCRL1 were flatter than normal and pools of vesicular ZO-1 accumulated intracellularly, suggesting junctional remodelling and maturation may require turnover of 5-phosphoinositides. Columnar maturation occurs after cells make contacts and form junctions. In addition, columnar maturation occurs synonymously with polarisation. The loss of cell height that occurs without OCRL1 suggested the possibility that polarisation may also be affected. Therefore we examined the distribution of polarised lipids and proteins in sheets of MDCK cells depleted of OCRL1. MDCK cells were chosen as a model to study polarisation in the kidney epithelium as they express many polarity markers and polarise well in cell culture. In this chapter, OCRL1 was depleted to a greater extent than previously, and the results obtained with this level of depletion suggested OCRL1 may be required for correct orientation of apical-basal polarity.

Optimising OCRL1 RNAi

When MDCK cells were depleted of OCRL1 with a fresh batch of siRNA, we observed a different phenotype than in the previous chapter. Depleting OCRL1 with this siRNA inhibited maturation of MDCK monolayers as in Chapter 3 but in addition, cells accumulated large intracellular vacuoles and the ZO-1 pattern appeared to be more extensively broken (bottom panel figure 4.2). While disruptions to the ZO-1 pattern with OCRL1 depletion was observed previously (figure 3.2), the vacuoles were only observed with the siRNA used in this chapter. The differences in phenotype could be due to differing levels of OCRL1 depletion between batches of oligonucleotides. The siRNA used in this chapter efficiently depleted OCRL1, with approximately 75% of OCRL1 protein depleted 24 hours post RNAi and 90% of protein depleted 48 hours post RNAi (figure 4.1). Since the siRNA used in the previous chapter was no longer available to test depletion efficiency, it was not possible to directly compare protein levels between siRNA batches. However, halving the concentration of fresh siRNA reproduced the maturation defect seen in Chapter 3 but not the vacuole phenotype seen with higher concentrations of the same siRNA (figure 4.2), suggesting maximum OCRL1 depletion may be required for cells to form vacuoles. All four siRNAs produced the vacuole phenotype when used in isolation at maximum concentration, indicating the vacuoles did not arrive from off-target effects (figure 4.3). Therefore cells with very low levels of OCRL1 were flatter than controls and accumulated intracellular vacuoles (figure 4.2 blue arrows). In addition, we noticed intercellular spaces between the lateral borders of some OCRL1 depleted cells. These spaces appeared to disrupt the tight junction, with bands of ZO-1 absent from regions where lateral vacuoles localised (figure 4.2 white arrows). Both sets of vacuole structures, intracellular and lateral, (indicated with blue and white arrows respectively) were lined heavily with filamentous actin (F-actin).

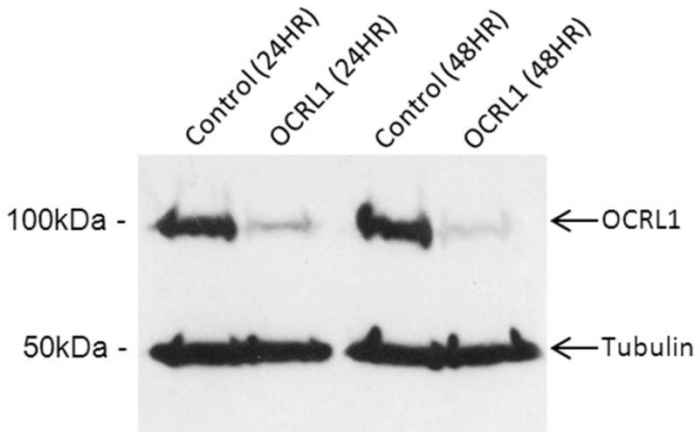

Figure 4.1: Endogenous OCRL1 can be depleted with siRNA. MDCK cells were grown on a 6 well plate overnight. At 40% and 60% confluence cells were transfected with non-targeting control or a pool of canine specific OCRL1 siRNA. Cell lysates were collected after 24 and 48 hours and loaded onto a 10% SDS-PAGE gel and processed for immunoblotting with anti-OCRL1 and anti-α-tubulin antibodies. Since OCRL1 depletion reduces cell proliferation rate (see figure 3.8), the amount of cell lysate loaded was normalised according to expected cell density. Arrows indicate OCRL1 (105kDa) and α-tubulin (50kDa). The relative protein levels were quantified using ImageJ gel analyzer and normalised against the loading control. Briefly, the relative amount of protein was estimated by density of the band. Compared to the control at 24 hours after RNAi, OCRL1 protein was reduced by 75% and at 48 hours after RNAi, OCRL1 was reduced by 90% compared to the 48 hour control.

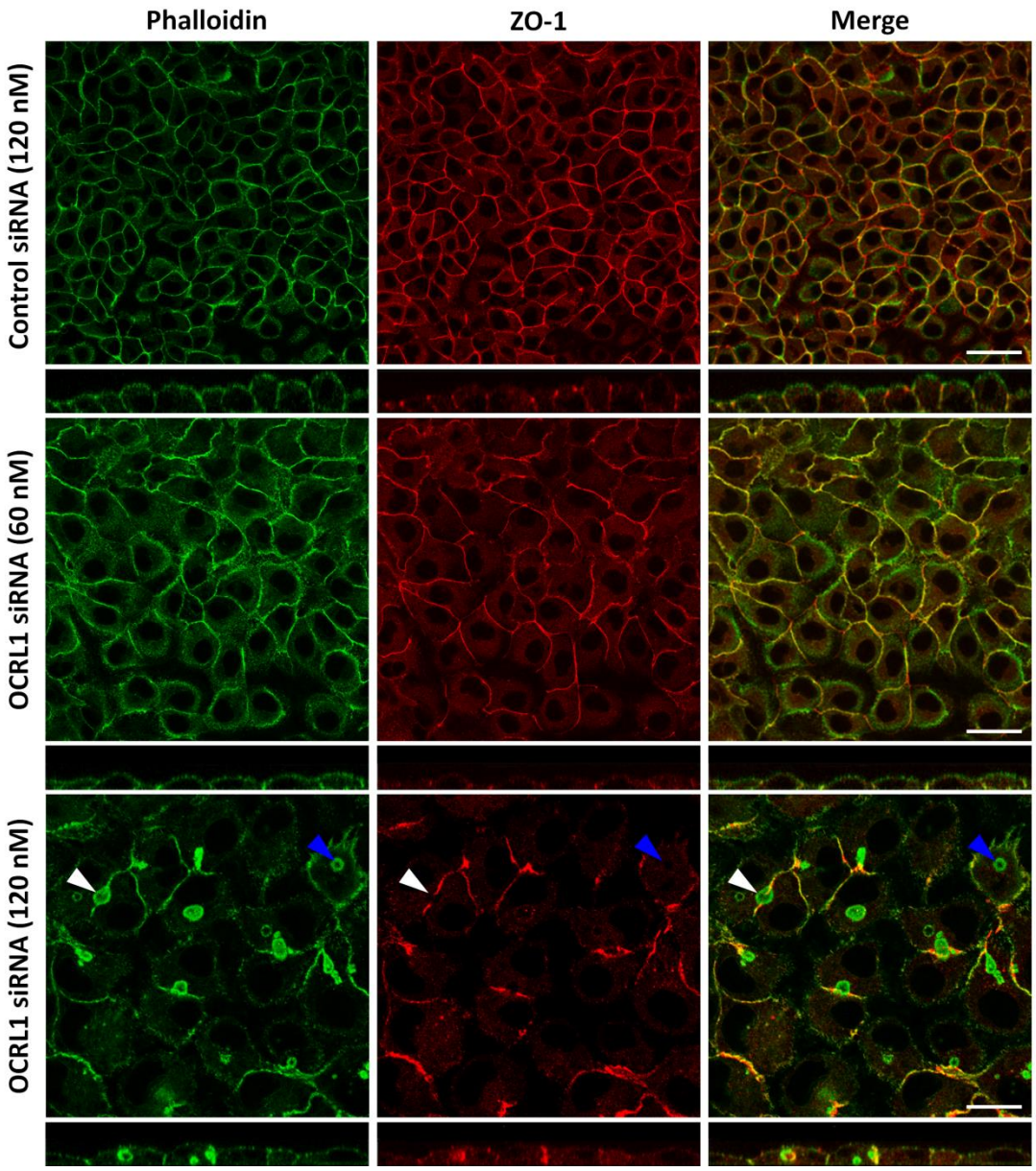

Figure 4.2: Maximum OCRL1 depletion is required for vacuole formation. MDCK cells were grown overnight. At 40% and 60% confluence the cells were transfected with non-targeting control or a pool of OCRL1 siRNA at a final concentration of 60 nM and 120 nM. After 48 hours with siRNA, the cells were fixed and permeabilised for immunostaining with antibodies to the tight junction marker ZO-1 (red) and the actin stain phalloidin (green). Single confocal sections and XZ sections are shown. XZ sections were constructed from Z-stacks of 30 confocal sections spanning from the bottom to the top of the cell layer. Blue arrows indicate intracellular vacuoles and white arrows indicate vacuoles between cells. Images shown are from a single experiment. Scale bar 20 µM.

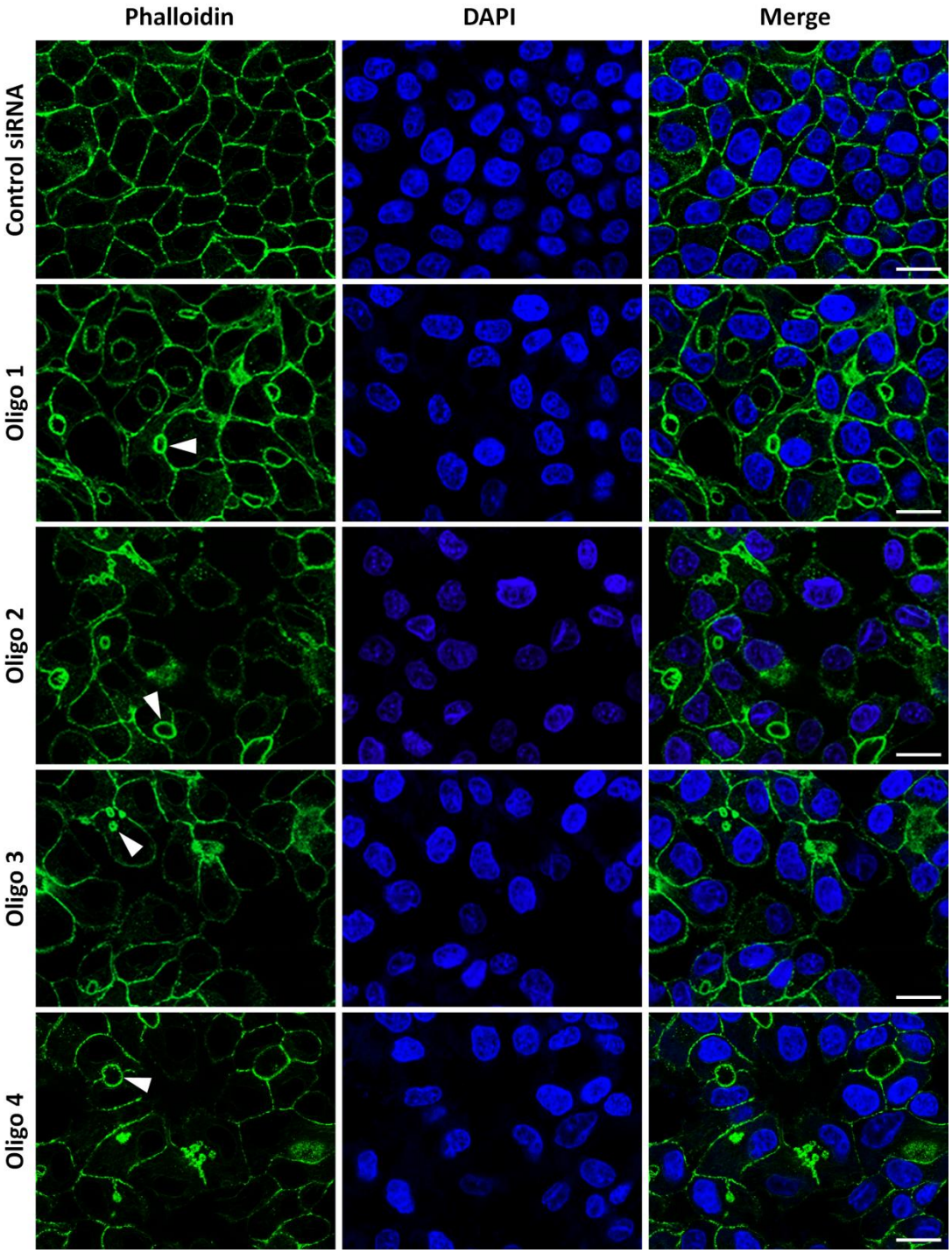

Figure 4.3: Confirmation of siRNA specificity. MDCK cells were grown overnight. At 40% and 60% confluence the cells were transfected with non-targeting control or with four individual OCRL1 siRNAs at a final concentration of 120 nM. The cells were fixed and permeabilised for visualising F-actin with phalloidin (green) and the DNA with DAPI (blue). White arrows indicate actin vacuoles, both intracellular and lateral. Single confocal sections are shown. Images shown are from a single experiment. Scale bar 20 µM

OCRL1 depletion results in redistribution of the apical membrane to vacuoles

Vacuoles in MDCK cells have been observed previously under certain conditions. Intracellular vacuoles appear in cells prevented from forming cell-cell contacts by removal of calcium from the extracellular media (Vega-Salas et al., 1988). These vacuoles contain microvilli and apical plasma membrane proteins but exclude basolateral proteins, and are therefore termed vacuolar apical compartments (VACs). Upon re-establishment of cell-cell contacts by re-addition of calcium, VACs are rapidly exocytosed towards intercellular spaces, after which the apical plasma membrane is re-formed (Vega-Salas et al., 1988). VACs are also formed when the microtubule cytoskeleton is disrupted and apical trafficking to the plasma membrane is perturbed (Gilbert et al., 1991; van Zeijl and Matlin, 1990). The structures seen upon depletion of OCRL1 have some properties of the VACs observed in these experiments, appearing similar in size and heavily enriched in F-actin. Therefore we tested to see whether apical cargo also localised to the vacuoles formed when OCRL1 was depleted, indicative of disrupted apical trafficking pathways.

To check the polarity status of OCRL1 depleted cells, we tested the localisation of a variety of apical and basolateral protein markers. Ezrin is a peripheral membrane protein that links the plasma membrane, where it interacts with $PI(4,5)P_{2,}$ to the actin cytoskeleton (Janke et al., 2008). Normally ezrin is enriched in the apical domain of MDCK cells. XZ images of MDCK cells treated with control siRNA showed the expected apical distribution of ezrin, lining the cell surface of monolayers (figure 4.4). However, ezrin was not localised to any peripheral domain in cells depleted of OCRL1 (figure 4.4). Higher magnification images of OCRL1 depleted cells revealed ezrin to be mostly cytosolic or present on large vacuoles intracellularly and between cells (figure 4.4 bottom panel). The aberrant pattern of ezrin staining resembled the pattern of F-actin staining shown above (figure 4.2), with ezrin localising to intracellular vacuoles or to the periphery of intercellular spaces in the lateral borders between cells (figure 4.4).

We found similar results with another apical marker frequently used when studying polarisation in MDCK cells. Gp135/podocalyxin is a heavily sialylated transmembrane protein that interacts with the actin cytoskeleton and is thought to be involved in expansion of the apical lumen (Ojakian and Schwimmer, 1988). OCRL1 depleted cells formed vacuoles rich in Gp135 and F-actin with the concomitant loss of these two components from the cell surface (figure 4.5).

For staining with Gp135, cells were grown in culture for 4 or 5 days and depleted of OCRL1 for 48 or 72 hours to assess the effect of OCRL1 depletion at different stages of polarisation. Monolayers of MDCK cells mature and polarise with time and therefore control cells grown for 5 days were taller and more compact than control cells grown for 4 days (figure 4.5 panel 1 compared to panel 2). Depleting cells of OCRL1 for different lengths of time revealed differences in vacuole localisation, cells grown for 4 days and depleted of OCRL1 for 48 hours mostly formed vacuoles that were intracellular (figure 4.5 blue arrows), whereas cells grown for 5 days and depleted of OCRL1 for 72 hours mostly formed lateral vacuoles between cells (figure 4.5 white arrows). The abundance the two types of vacuole with time can be seen in single XY sections of OCRL1 depleted cells (figure 4.5 panels 3 and 4). The intracellular vacuoles formed after 48 hours without OCRL1 appeared smaller and predominately localised to a perinuclear region (figure 4.5). The intercellular vacuoles formed after 72 hours without OCRL1 were larger and localised along the lateral borders between two or more cells (figure 4.5). Wild type MDCK cells that are fully polarised form a dense network of F-actin beneath the apical membrane. In addition, the formation of F-actin rich microvilli adds to the density of F-actin near the apical membrane which stains strongly with phalloidin. OCRL1 depleted cells lost this enrichment of F-actin in the cell apex, further indicating a loss of apical membrane development on the cell surface (figure 4.5).

To check whether the vacuoles observed in OCRL1 depleted cells were similar to the VACs formed in calcium switch experiments, we performed a calcium switch on untreated MDCK cells. The intracellular VACs formed upon loss of extracellular calcium were similar in appearance to the VACs formed when OCRL1 was depleted,

being of similar size and enriched in F-actin and Gp135 (figure 4.6). However in contrast to OCRL1 depletion, lateral vacuoles were not observed upon calcium depletion. In calcium switch experiments, the intracellular VACs are thought to fuse with the plasma membrane and re-form the apical surface when calcium is restored (Vega-Salas et al., 1988). Therefore in calcium switch experiments, lateral vacuoles are only observed temporarily, indicated with a blue arrow in figure 4.6.

The localisation of several apical components to the vacuoles formed in OCRL1 depleted cells suggested the membrane composition of vacuoles resembled the apical membrane normally found at the cell surface. To confirm this, an additional apical marker and a basolateral marker were tested for localisation to these structures. Annexin-2 is a sub-apical protein that also interacts with $PI(4,5)P_2$ (Lizarbe et al., 2011). Annexin-2 was strongly enriched on the vacuoles induced by loss of OCRL1 (figure 4.7). Conversely the basolateral marker Na^+/K^+ ATPase was not localised to these compartments (figure 4.8), further suggesting the apical nature of vacuole membranes. In summary, OCRL1 depleted MDCK cells formed intracellular and intercellular vacuoles. The vacuoles accumulated apical markers and excluded basolateral markers, resembling the VACs formed in calcium switch experiments and suggest OCRL1 is required for proper formation of the apical membrane.

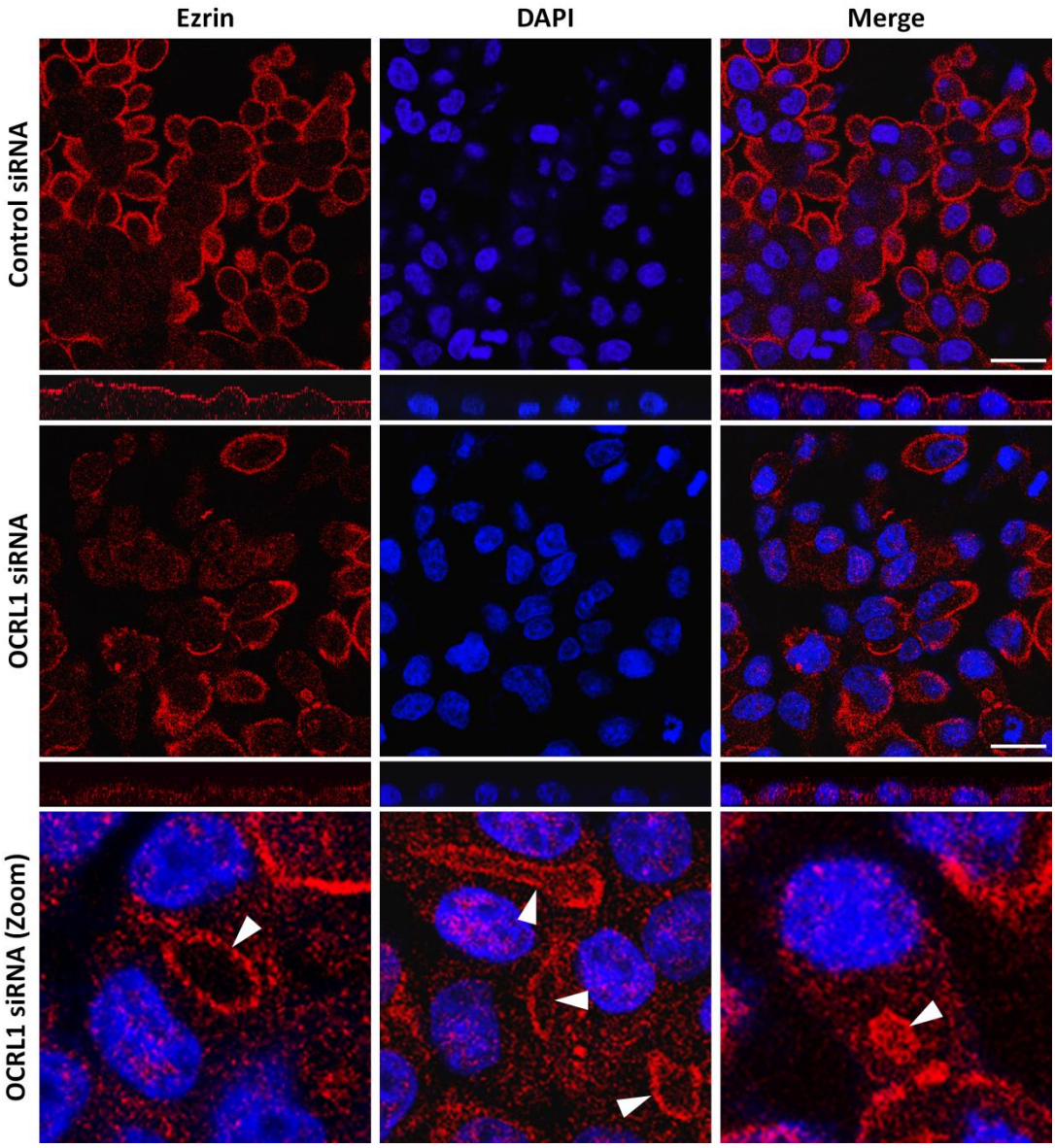

Figure 4.4: Ezrin localises to vacuoles in OCRL1 depleted cells. MDCK cells were grown overnight. At 40% and 60% confluence the cells were transfected with non-targeting control or a pool of OCRL1 siRNA. After 48 hours with siRNA, the cells were fixed and permeabilised for immunostaining with antibodies to the apical marker ezrin (red) and the DNA stain DAPI (blue). Single confocal sections and XZ images are shown. XZ sections were constructed from Z-stacks of 20 confocal sections spanning from the bottom to the top of the cell layer. The bottom panel shows higher magnification images of intracellular and intercellular ezrin (white arrows) taken from confocal sections in the same stack as the images above. Images shown are representative from two experiments. Scale bar 20 µM.

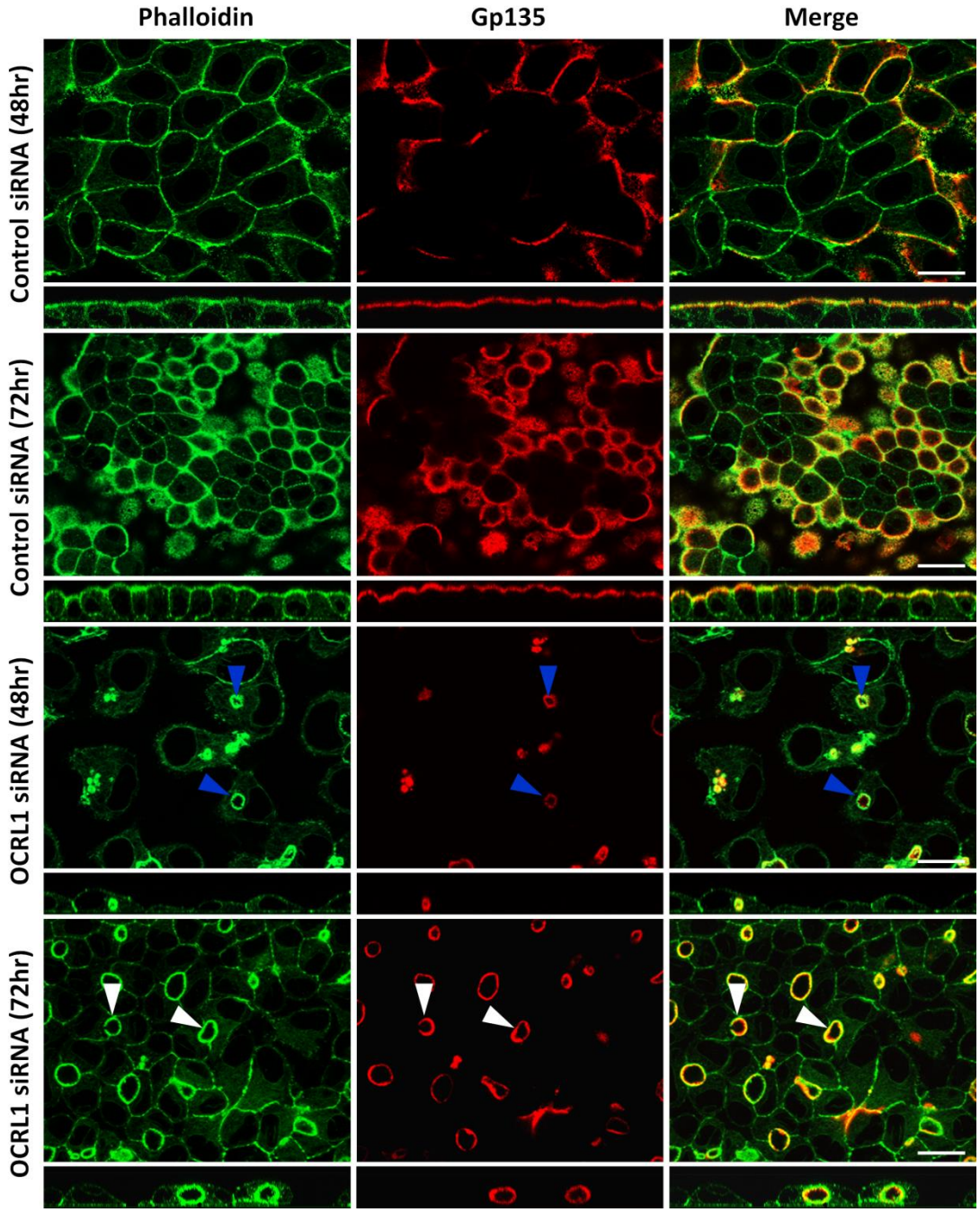

Figure 4.5: Gp135 localises to vacuoles in OCRL1 depleted cells. MDCK cells were grown overnight and transfected with siRNA as in figure 4.4. After 48 or 72 hours without siRNA, the cells were fixed and permeabilised for immunostaining with the apical marker Gp135 (red) and stained with phalloidin to label F-actin (green). XZ sections were constructed from Z-stacks of 40 confocal sections spanning from the bottom to the top of the cell layer. Single confocal sections from the top of the cell layer are shown. Blue arrows indicate intracellular vacuoles and white arrows indicate vacuoles in the lateral membrane between cells. Images shown are from a single experiment. Scale bar 20 μM.

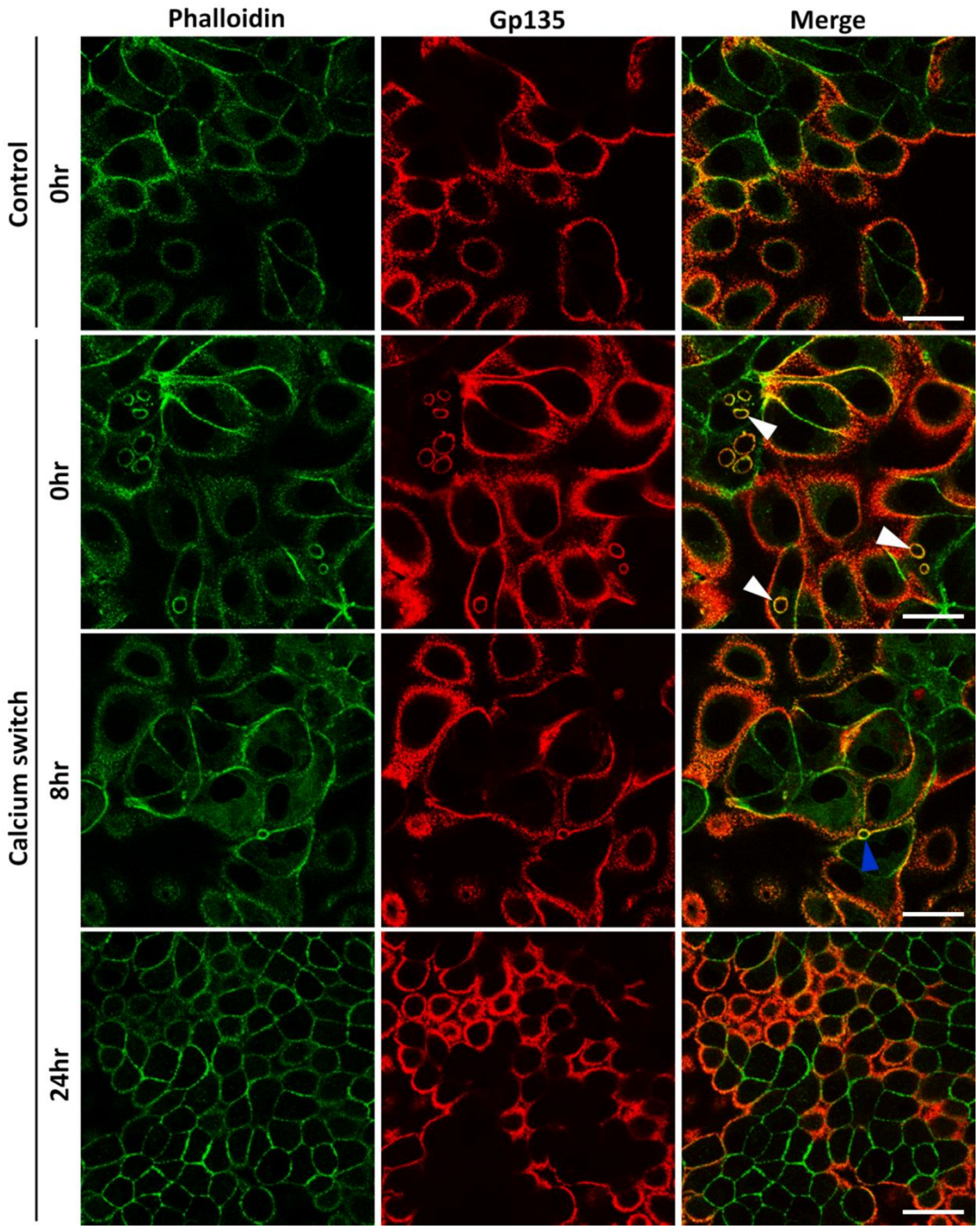

Figure 4.6: The VACs formed upon OCRL1 depletion resemble VACs in calcium switch experiments. Wild type MDCK cells were grown overnight in calcium free DMEM or calcium containing DMEM as a control. After 24 hours the cells were switched to calcium containing DMEM and fixed at various time points after recovery with calcium (0, 8 or 24 hours). The cells were permeabilised and stained for F-actin using phalloidin (green) and immunostained with antibodies to Gp135 (red). Single confocal sections are shown. White arrows indicate intracellular VACs and blue arrow indicates an exocytosed VAC in the lateral membrane. Images shown are from a single experiment. Scale bar 20 μM.

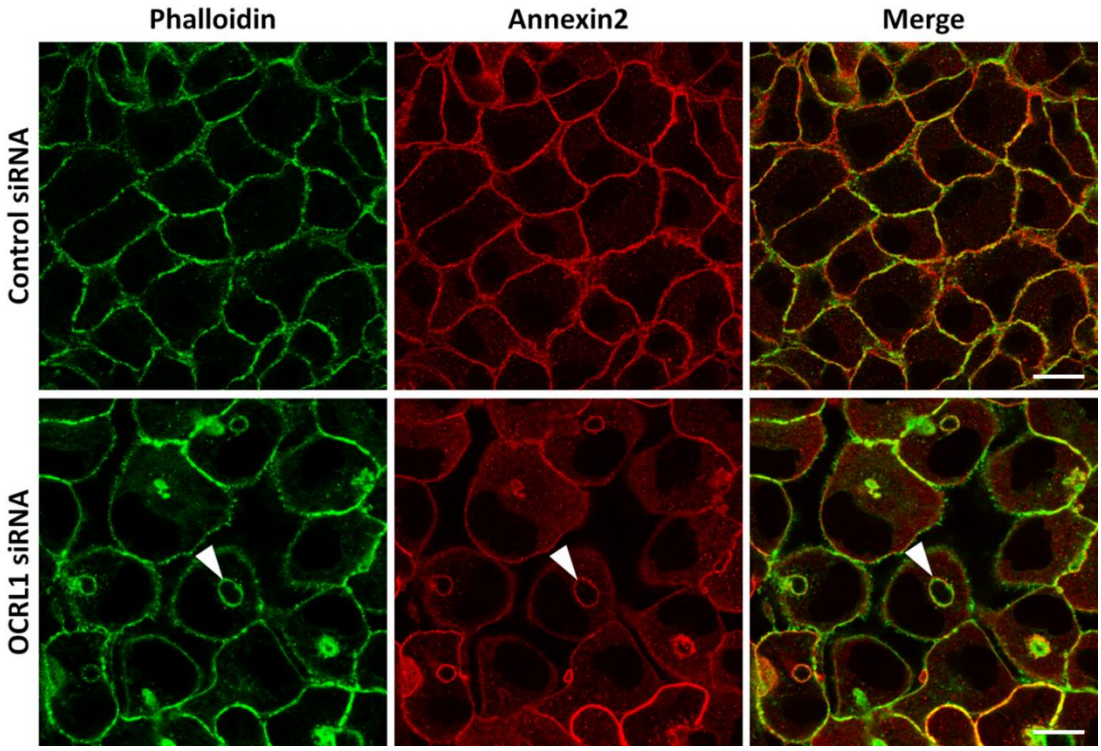

Figure 4.7: OCRL1 depletion redistributes Annexin-2 to intracellular vacuoles. MDCK cells were grown and treated with control or pooled OCRL1 siRNA as in figure 4.4. The cells were fixed and permeabilised for immunostaining with antibodies to Annexin-2 (red) and F-actin was labelled with FITC-phalloidin (green). Single confocal sections are shown. White arrows indicate the presence of Annexin-2 on actin rich intracellular vacuoles. Intercellular vacuoles showed the same properties. Images shown are representative from two experiments. Scale bar 10 µM.

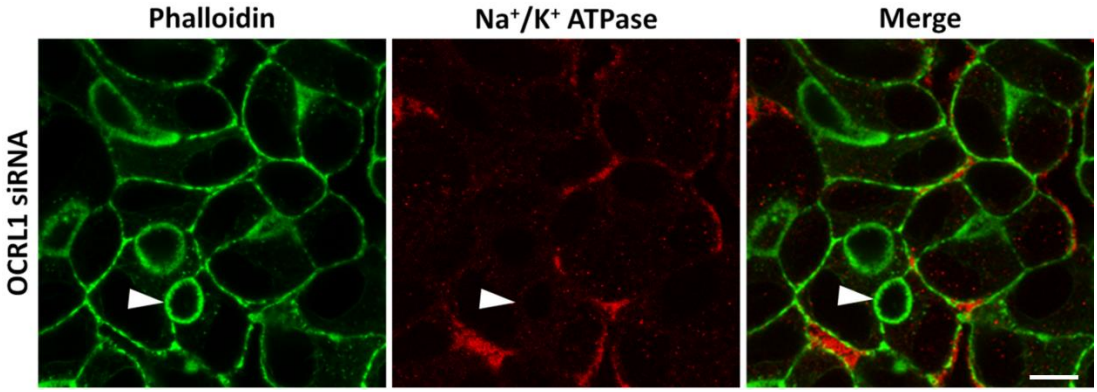

Figure 4.8: The vacuoles formed upon OCRL1 depletion exclude Na+/K+ ATPase. MDCK cells were grown and treated with pooled OCRL1 siRNA for 72 hours as in figure 4.5. The cells were fixed and permeabilised for immunostaining with antibodies to the basolateral marker Na^+/K^+ ATPase (red) and F-actin was labelled with FITC-phalloidin (green). Single confocal sections of OCRL1 depleted cells are shown. White arrows indicate the absence of Na^+/K^+ ATPase on actin rich lateral vacuoles, but intracellular vacuoles showed the same properties. Scale bar 10 µM.

Phosphoinositides polarise to vacuoles formed upon OCRL1 depletion

In addition to asymmetrically distributing proteins, polarised cell types also distribute phosphoinositides differentially on cell membranes. This is achieved by delivering specific lipids to target membranes and by localising lipid modifying enzymes spatially in the cell so that the production of a particular phosphoinositide is favoured on membranes where it is required. The asymmetric distribution of phosphoinositides in polarised cell types is a key aspect of maintaining domain identity. In MDCK cells $PI(4,5)P_2$ is apically localised while $PI(3,4)P_2$ and $PI(3,4,5)P_3$ are enriched basolaterally (Martín-Belmonte et al., 2007). To visualise where these lipids accumulate in the cell, a variety of phosphoinositide binding domains have been isolated, characterised for their phosphoinositide specificity and fused to green fluorescent protein (GFP) for expression in cells. The PH domain of phospholipase C delta (PLCδ-PH) is used to visualise $PI(4,5)P_2$ (Fujii et al., 1999), the PH domain of Grp1 is used to identify pools of $PI(3,4,5)P_3$ (Klarlund et al., 2000) and the PH domain of AKT recognises both $PI(3,4,5)P_3$ and $PI(3,4)P_2$ (Gassama-Diagne et al., 2006).

To assess whether OCRL1 depletion affects the distribution of apical and basolateral phosphoinositides, MDCK monolayers growing on glass coverslips were depleted of OCRL1 and transfected with GFP chimeras of the PH domains from AKT and PLCδ. XZ sections of OCRL1 depleted cells expressing the AKT-PH-GFP construct displayed an enrichment of $PI(3,4,5)P_3$ and $PI(3,4)P_2$ in the lateral compartment similar to controls (figure 4.9B), as well as nuclear localisation of AKT-PH-GFP. However XZ sections of OCRL1 depleted cells expressing PLCδ-PH-GFP revealed a loss of $PI(4,5)P_2$ from the apical surface (figure 4.9A). Instead, OCRL1 depleted cells displayed $PI(4,5)P_2$ enrichment exclusively in the lateral membrane (figure 4.9A). In control cells the reverse was true, $PI(4,5)P_2$ localised exclusively to the apical domain and was not apparent in the lateral compartment (figure 4.9A). Therefore loss of OCRL1 resulted in the redistribution of $PI(4,5)P_2$ from the apical membrane to the lateral membrane.

As well as the lateral localisation of $PI(4,5)P_2$, the vacuoles formed in OCRL1 depleted cells were also enriched in $PI(4,5)P_2$ (figure 4.10). Expression of Grp1-PH-GFP revealed the exclusion of the normally basolateral phosphoinositide $PI(3,4,5)P_3$ from these structures (figure 4.10). In OCRL1 depleted cells, the levels of $PI(4,5)P_2$ remaining on the apical surface were similar to the levels of $PI(4,5)P_2$ in the basal domain (figures 4.9 and 4.10), suggesting the normal apical-basal polarisation of $PI(4,5)P_2$ had been lost and polarisation of $PI(4,5)P_2$ had shifted towards vacuoles in these cells. The localisation of apical $PI(4,5)P_2$ to vacuoles and exclusion of basolateral phosphoinositides occurred whether the vacuole was formed intracellularly or localised between cells laterally (figure 4.11). Therefore loss of OCRL1 in MDCK cells promoted the formation of intracellular and intercellular compartments, not seen in control cells, with the phosphoinositide composition of the apical domain.

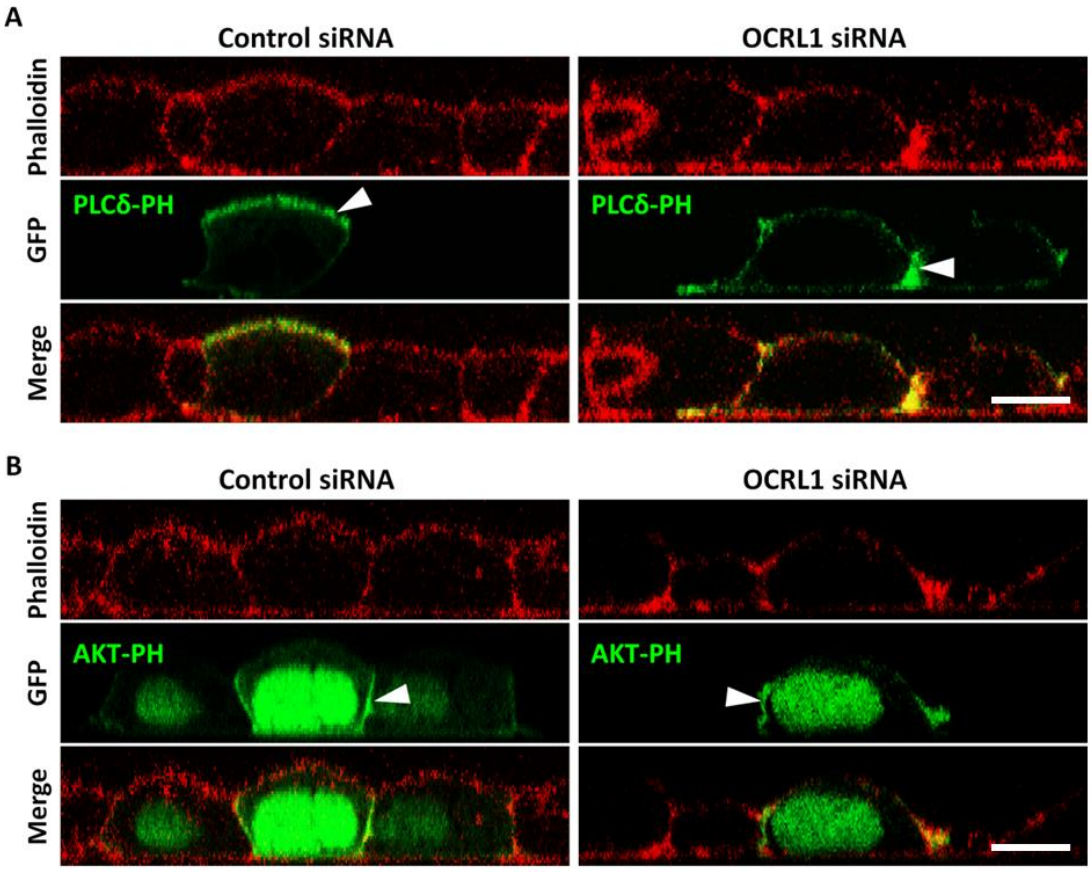

Figure 4.9: OCRL1 depletion redistributes PI(4,5)P_2 to the lateral membrane. MDCK cells were grown overnight. At 30% and 50% confluence the cells were transfected with non-targeting control or a pool of OCRL1 siRNA. 48 hours after the initial RNAi, the cells were transfected with PLCδ-PH-GFP DNA (PI(4,5)P_2 binding domain) or AKT-PH-GFP DNA (PI(3,4)P_2 and PI(3,4,5)P_3 binding domain) and left for a further 17 hours. Cells were fixed and permeabilised to stain F-actin with phalloidin (red). XZ sections were constructed from Z-stacks of 40 confocal sections spanning from the bottom to the top of the cell layer. Images shown are representative images from n=6 cells per treatment across 2 experiments. White arrows point to peripheral enrichment of phosphoinositides. Scale bar 10 µM.

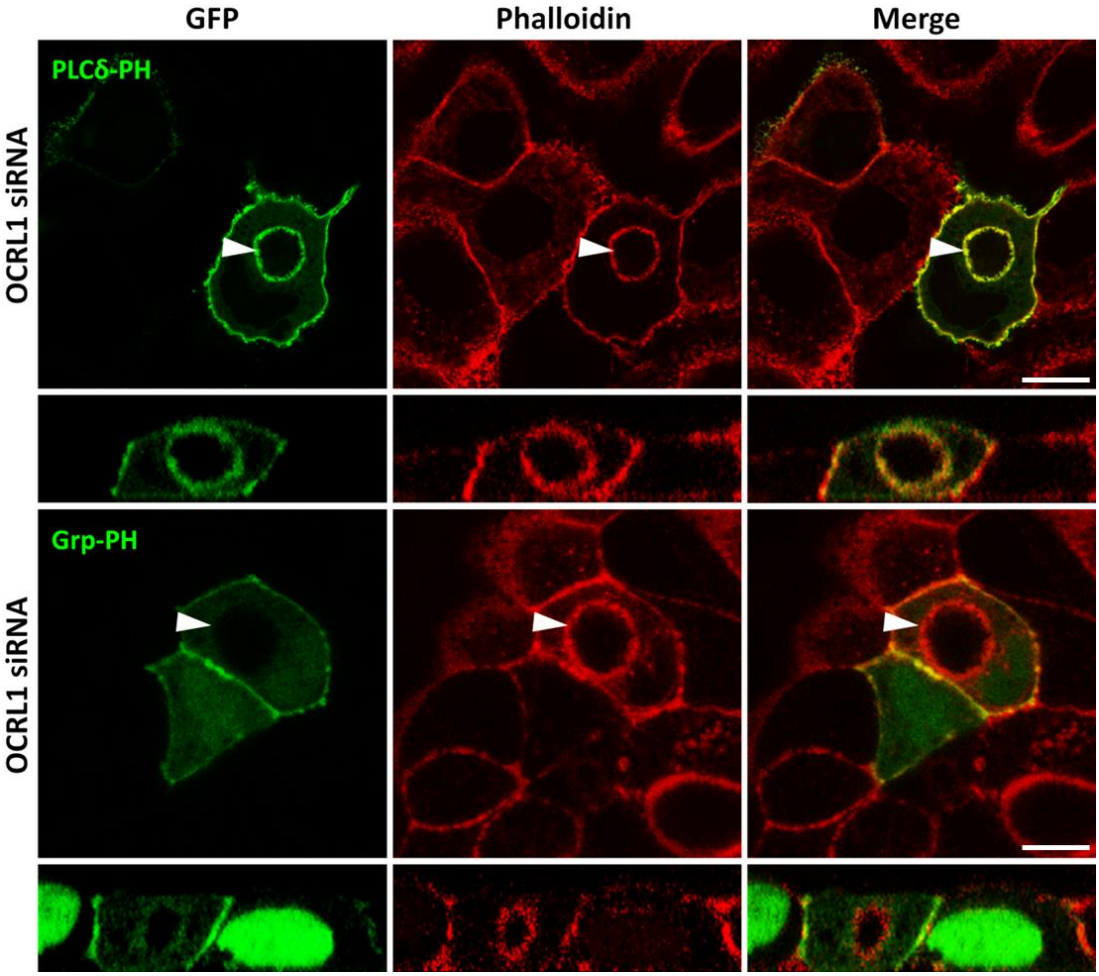

Figure 4.10: Intracellular vacuoles are enriched in apical phosphoinositides. MDCK cells were grown overnight and subjected to OCRL1 siRNA as in figure 4.9. After 48 hours with siRNA, the cells were transfected with PLCδ-PH-GFP DNA ($PI(4,5)P_2$ binding domain) or Grp-PH-GFP DNA ($PI(3,4,5)P_3$ binding domain) and left for a further 17 hours. Cells were fixed and permeabilised to stain F-actin with phalloidin (red). Single confocal sections and XZ images are shown. XZ images were created from Z-stacks containing 40 confocal sections. Arrows indicate the enrichment of PLCδ-PH-GFP and absence of Grp-PH-GFP on large intracellular vacuoles. Images shown are representative of all transfected cells in 2 experiments (n=20). Scale bar 10 µM.

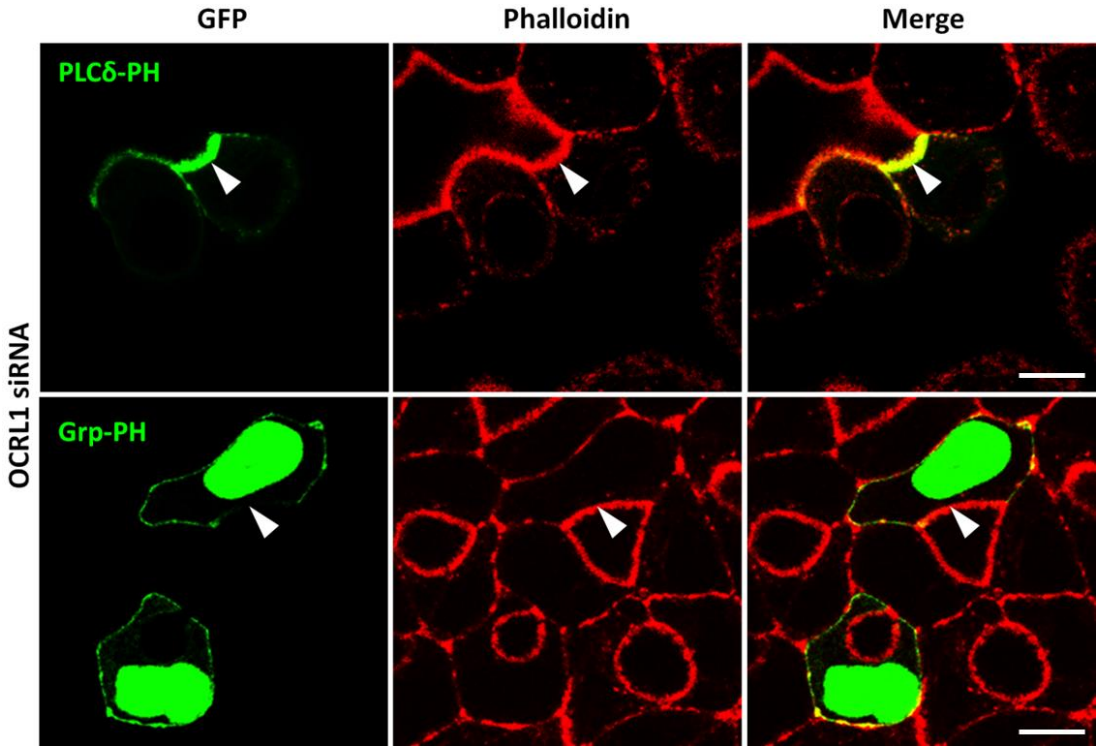

Figure 4.11: Lateral vacuoles are enriched in apical phosphoinositides. MDCK cells were grown and treated with OCRL1 siRNA as in figure 4.9. After 72 hours without siRNA, the cells were transfected with PLCδ-PH-GFP DNA ($PI(4,5)P_2$ binding domain) or Grp-PH-GFP DNA ($PI(3,4,5)P_3$ binding domain) and left for an additional 17 hours. Cells were fixed and permeabilised to stain F-actin with phalloidin (red). Single confocal sections from the middle of the cell layer are shown. Arrows indicate the enrichment of PLCδ-PH-GFP and absence of Grp-PH-GFP on large intercellular vacuoles. Images shown are representative of all transfected cells that had formed lumens in 2 experiments (n=10). Scale bar 10 µM.

Lateral lumens rearrange tight junctions and the microtubule cytoskeleton

The tight junction normally acts as a diffusion barrier to proteins and lipids, separating the apical and basolateral domains. In OCRL1 depleted cells PI(3,4,5)P_3 was found to be excluded from lateral vacuoles but present on the rest of the membrane, whilst PI(4,5)P_2 was abundant on lateral vacuoles and only weak detection of PI(4,5)P_2 was seen on the remaining plasma membrane (figure 4.11). In addition, the phalloidin and PI(4,5)P_2 staining of lateral vacuoles was relatively dense (figure 4.11), suggesting possible folding of the plasma membrane indicative of apical microvilli, as seen in microvillus inclusion disease (Müller et al., 2008). The effective segregation of apical and basal phosphoinositides suggested the integrity of the tight junction remained in OCRL1 depleted cells that had formed lateral lumens. However, previously we observed the tight junction to be disrupted by lateral lumens (figure 4.2). Therefore we looked more closely at the organisation of the tight junction in OCRL1 depleted cells with lateral lumens.

To visualise the tight junction, OCRL1 depleted cells were stained with the tight junction marker ZO-1. The tight junction was extensively reorganised in cells that had formed lateral vacuoles (figure 4.12). As shown previously (figure 4.2), lateral vacuoles appeared to form between tight junctions and ZO-1 was enriched at sites where the vacuole membrane contacted the lateral membrane (figure 4.12 panel 2). To study this further, a 3D reconstruction was created from a Z-stack of confocal images (figure 4.12 panel 3). The 3D image provided a complete view of the cell layer and revealed the entire structure of the tight junction in OCRL1 depleted cells. Bands of ZO-1 encompassed lateral vacuoles bordering the cell-cell contact (figure 4.12 panel 3), suggesting the tight junction maintains a distinct apical membrane within the vacuole and separates this membrane from the basolateral domain.

In addition to the tight junction, spatial organisation of the cytoskeleton is required for cells to maintain polarity. Cargo varying vesicles are trafficked along the microtubule cytoskeleton as a means of targeted transport. Normally MDCK cells polarise vertically with the apical domain formed at the top of the cell and the basal

domain facing the substratum. This arrangement of polarised membrane domains is supported by the underlying asymmetry of the microtubule network, with minus ends of microtubules facing the apical membrane and the plus ends facing the basal domain (Müsch, 2004). MDCK cells display a peripheral enrichment of vertical microtubules with this orientation and a dense network of microtubules beneath the apical surface.

Since OCRL1 depleted cells display an abnormal organisation of polarised membrane domains, we looked at the arrangement of the microtubule network in cells that had formed lateral lumens. The microtubules were visualised with antibodies to α-tubulin. In OCRL1 depleted cells, some of the microtubules were resolved in a single confocal image due to their horizontal alignment with the plane of the section (figure 4.13). However due to the vertical arrangement of the microtubules in control cells, the confocal section cut through the microtubules perpendicularly, appearing as punctate dots (figure 4.13). Therefore the microtubules appeared to be vertically arranged in control cells but were seen emanating more horizontally from the lateral lumens in OCRL1 depleted cells. This is further demonstrated in 3D reconstructions of Z-stacks taken of OCRL1 depleted cells. The 3D images revealed the entire arrangement of microtubules which were extensively organised around lateral lumens (figure 4.13 bottom 2 panels). The enrichment of microtubules near lateral lumens further supports the apical nature of these compartments.

In addition to the arrangement of tight junctions and microtubules, the positioning of the nuclei in OCRL1 depleted cells also supported a change in orientation. Normally MDCK cells gown in monolayer sheets position the nuclei centrally towards the bottom of the cell. However, in OCRL1 depleted cells, the nuclei were positioned at the maximum distance from the lateral vacuole near the opposite lateral membrane. Therefore the position of the apical membrane relative to the nuclei suggested OCRL1 depleted cells polarised horizontally. A similar orientation of polarity is observed in normal hepatocytes, these cells form lateral apical lumens (bile canaliculi) which are maintained by rings of tight junction and a dense network

of microtubules proximal to the lumen (Treyer and Müsch, 2013). One possibility is that MDCK cells depleted of OCRL1 adopt a hepatic mode of polarity. Similar results were shown for MDCK cells overexpressing Par1b, where cells appeared to convert from a normal columnar epithelial polarity to a hepatic mode of polarity (Cohen et al., 2004a, 2004b, 2007 and 2011). A schematic of polarity and junction organisation in cells depleted of OCRL1 is shown in figure 4.14.

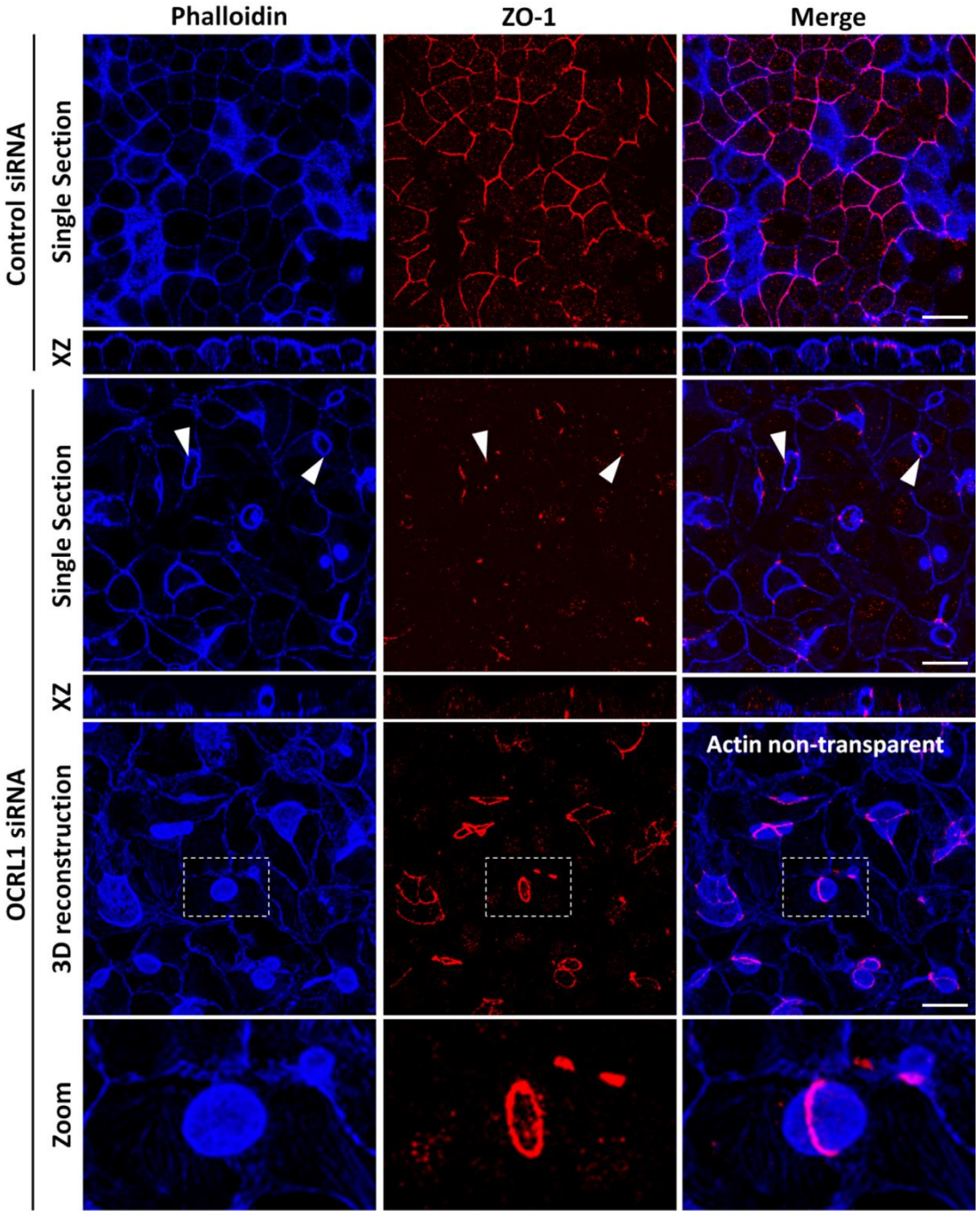

Figure 4.12: Tight junctions support lateral lumens. MDCK cells were grown overnight. Cells were treated with siRNA as in Figure 4.5. Cells were fixed after 72 hours and permeabilised for immunostaining with antibodies to the tight junction marker ZO-1 (red) and labelled F-actin with FITC-phalloidin (changed from green to blue). Single confocal sections are shown in the top 2 panels along with XZ sections. XZ sections were constructed from Z-stacks of 30 confocal sections spanning from the bottom to the top of the cell layer which were also used to create 3D reconstructions in ImageJ. The bottom panel shows a section of the 3D reconstruction at higher magnification. White arrows indicate regions of tight junction near lateral vacuoles. Experiment repeated twice. Scale bar 20 µM.

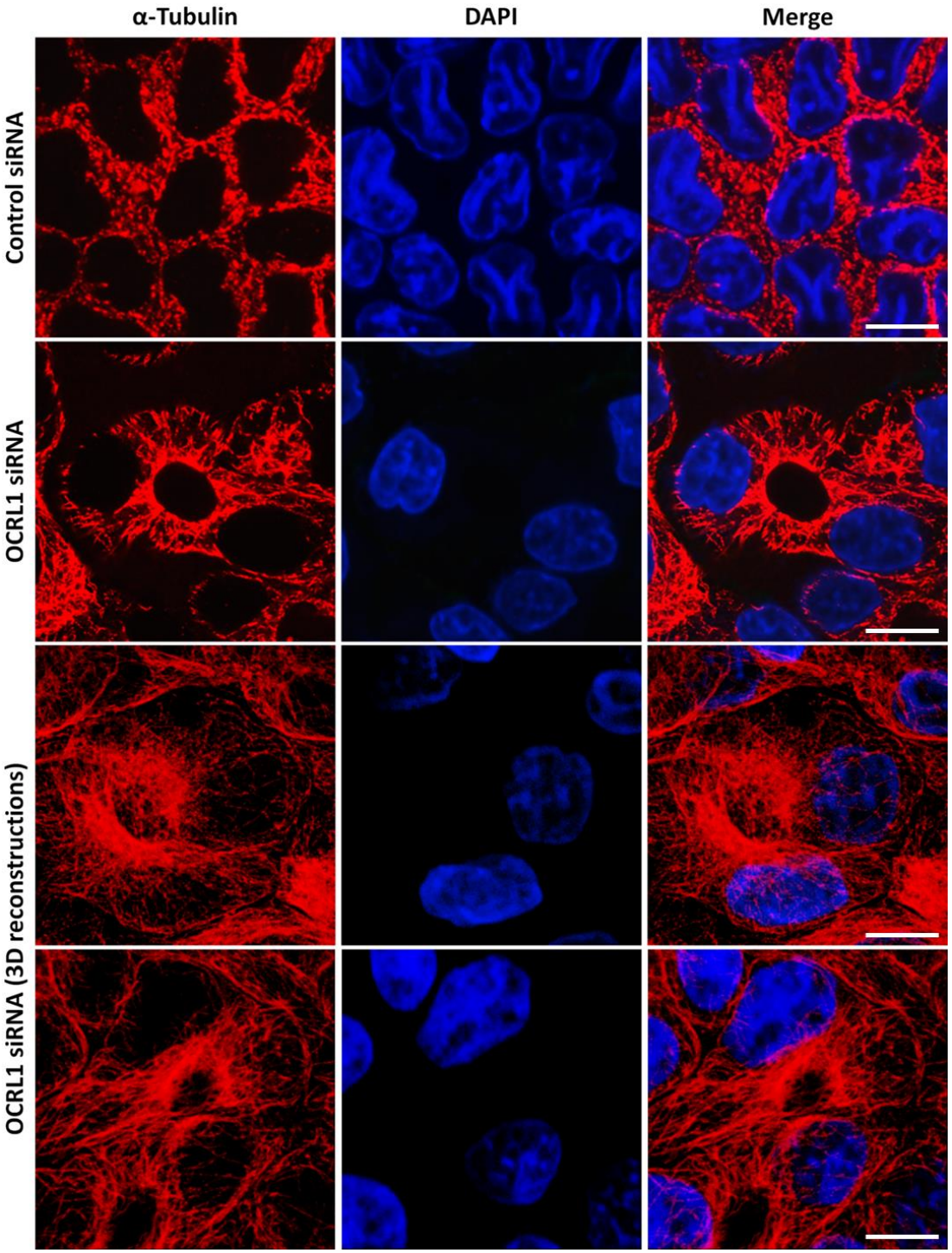

Figure 4.13: Microtubules reorganise around lateral lumens. MDCK cells were grown overnight and treated with siRNA as in figure 4.12. Cells were fixed 72 hours after initial RNAi and permeabilised for immunostaining with the microtubule marker α-tubulin (red), and the DNA was stained with DAPI (blue). Single confocal sections are shown through the middle of the cell layer. 3D reconstructions were made from Z-stacks containing 30 confocal sections in imageJ (bottom 2 panels). Experiment repeated twice. Scale bar 10 µM.

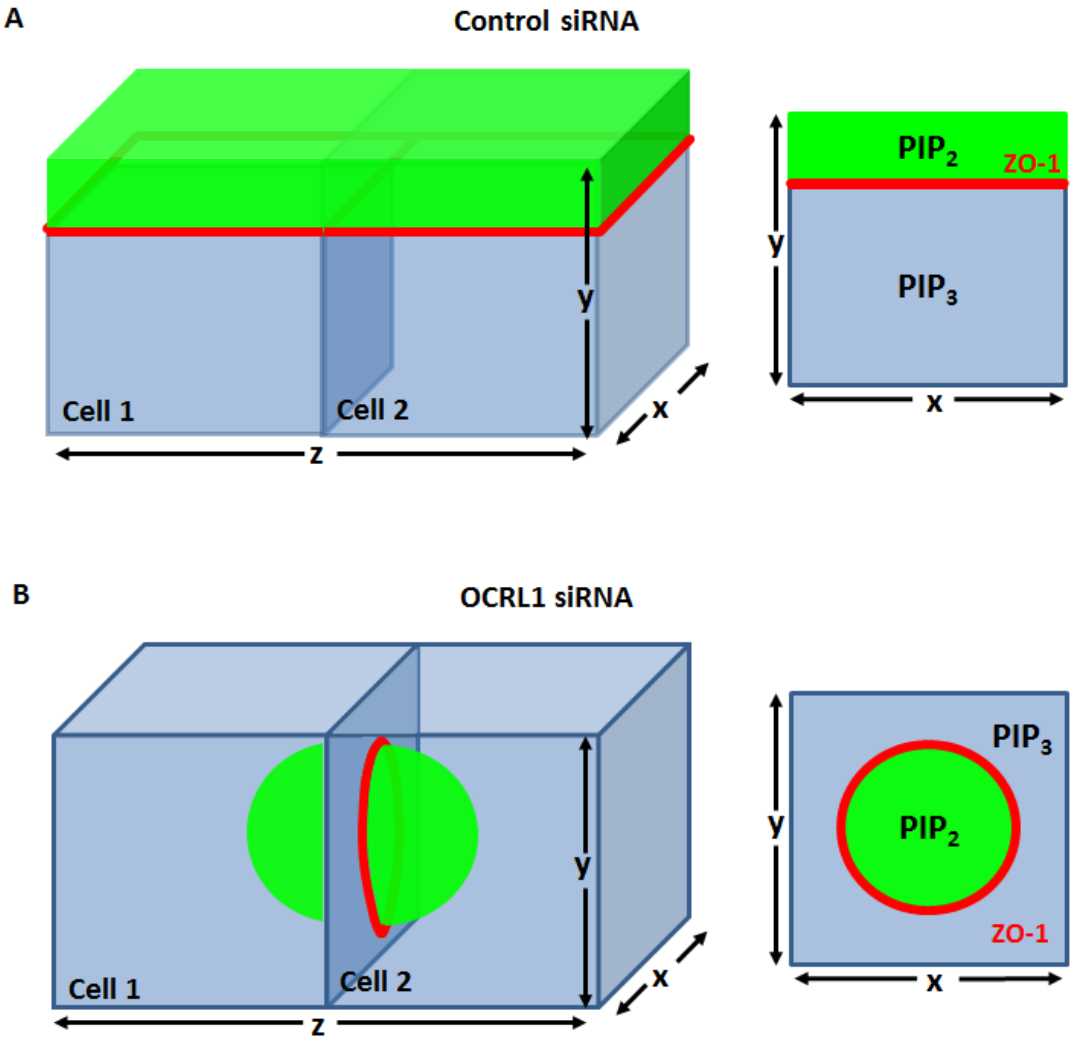

Figure 4.14 Schematic diagram of apical membrane formation in the absence of OCRL1. A: MDCK cells normally form an apical membrane enriched in PI(4,5)P_2 (green surface) at the apex of the monolayer, which is kept intact by junctional bands of ZO-1 (shown in red). B: Without OCRL1, MDCK cells form an apical membrane between neighbouring cells in the lateral membrane with encompassing rings of ZO-1.

Lateral lumens are formed from intracellular vacuoles

OCRL1 depletion induces the formation of intracellular apical vacuoles, however these vacuoles can also form between cells, resembling lateral lumens. The relative abundance of intracellular vacuoles compared to lateral lumens appeared to depend on the length of time spent without OCRL1 (figure 4.5), suggesting a possible time dependant relationship between the two species of vacuole.

To test whether the appearance of intracellular vacuoles preceded the appearance of lateral lumens, MDCK cells were depleted of OCRL1 and the position and size of vacuoles were measured at various time points after siRNA treatment. Over 300 vacuoles were counted and categorised according to cellular position at each time point after RNAi over a 6 day period (figure 4.15). Early after OCRL1 depletion, vacuoles were entirely intracellular, 57% of vacuoles counted at 24 hours post RNAi appeared to be budding from the plasma membrane and 37% were near the plasma membrane. Later after OCRL1 depletion, 44 hours post RNAi, vacuoles were almost completely lateral with only 9% intracellular vacuoles remaining. At this late stage, lateral vacuoles shared by three or more cells were also observed. At an intermediate stage of 72 hours post RNAi, vacuoles were largely perinuclear (30%) or between two cells (33%). Therefore looking in detail at position alone, these results were consistent with a series of gradual changes taking place over the 6 days. The first structures to appear were small vacuoles near the plasma membrane. These subsequently disappeared, with the appearance of perinuclear vacuoles. The fact that larger vacuoles appeared as the smaller ones disappeared suggested a precursor-product relationship, with the possibility that perinuclear vacuoles were formed by the fusion of smaller ones. Similarly perinuclear vacuoles declined as lateral lumens were formed, suggesting lateral lumens were formed from this perinuclear material.

To obtain supporting evidence for the idea that intracellular vacuoles develop into lateral lumens, the size of vacuoles were measured over the course of the RNAi experiment. The intracellular vacuoles formed early after OCRL1 depletion were

smaller than the lateral lumens formed at a later stage (figure 4.16). Vacuoles budding from the membrane were the smallest (2.5 μM ± 0.06 SEM), perinuclear vacuoles were of an intermediate size (5.8 μM ± 0.15 SEM), and lumens formed between two cells were larger (8.1 μM ± 0.2 SEM) and larger still when between three or more cells (12.9 μM ± 0.4 SEM). The relative size of these vacuoles supported the possibility that lateral lumens were formed from perinuclear vacuoles.

Furthermore it was also apparent that vacuoles at each cellular position increased in size over time; indicated in colour in figure 4.16 and plotted in figure 4.17. The lateral lumens first observed at 72 hours post RNAi were larger when observed at 96 hours and larger still at 144 hours (figure 4.17). The same was true of small intracellular vacuoles, however most of these vacuoles had diminished in number by 48 hours, therefore the plotted increase in size was only true of the small population of intracellular vacuoles remaining at later time points (9%). In summary, these results indicate that OCRL1 depletion resulted in the formation of small vacuoles which fused at a perinuclear site before being exocytosed at cell-cell contacts where they formed lumens between cells. However, these results only considered population changes of vacuoles over time. To confirm these findings it would be necessary to follow individual vacuoles over time by live cell imaging.

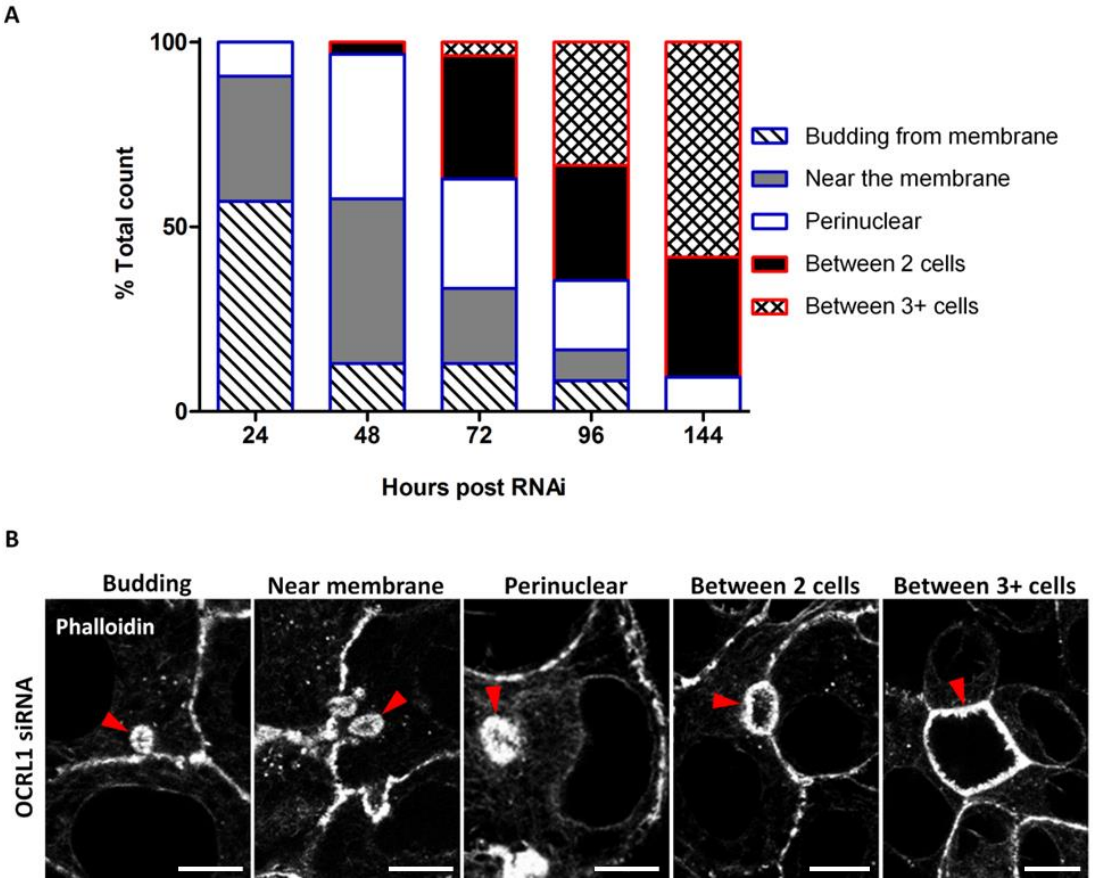

Figure 4.15: Vacuoles are internalised before becoming lateralised. MDCK cells were grown overnight and subjected to RNAi as in 4.5. The cells were fixed at various time points after RNAi. The cells were permeabilised and stained for F-actin using FITC-phalloidin. Over 300 vacuoles were categorised according to cellular position from Z-stacks taken across the coverslip. A: Plotted at each time point is the percentage of vacuoles found at each position within the cell or between cells. Highlighted in red are vacuoles found between neighbouring cells, highlighted in blue are vacuoles found intracellularly. B: High magnification images are shown of vacuoles (indicated by red arrows) in each category. Scale bar 5 µM.

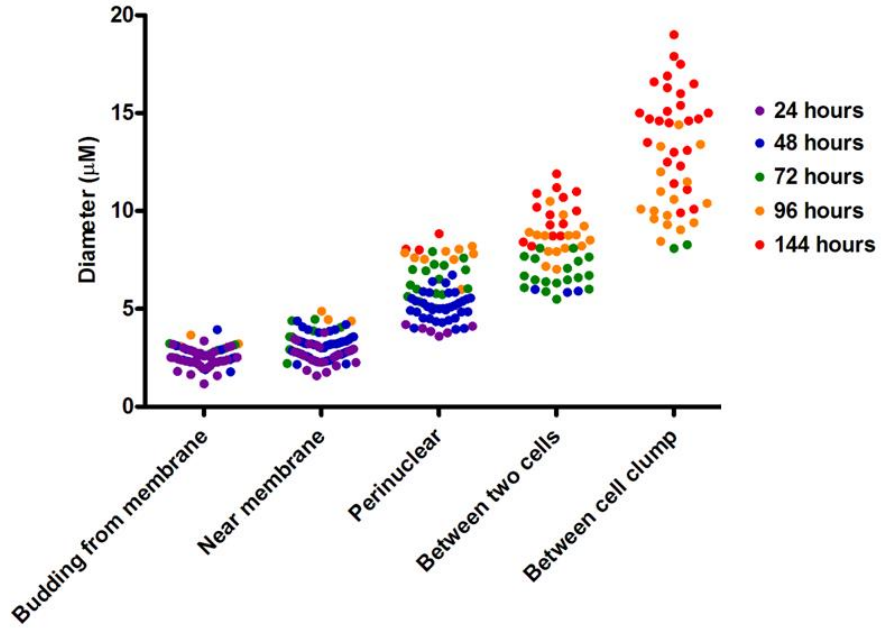

Figure 4.16: Vacuoles grow in size as they are internalised and lateralised. MDCK cells were grown overnight and subjected to RNAi as in figure 4.5. Cells were fixed at various time points post RNAi and permeabilised for staining F-actin with phalloidin. Confocal sections were taken from across the coverslip. Vacuole diameter was measured using Leica software and categorised according to cellular position. Plotted is the size of vacuoles at various cellular positions. Colours indicate the time of fixing after RNAi. One-way ANOVA analysis confirmed the mean diameter for each position was not equal, $p<0.001$.

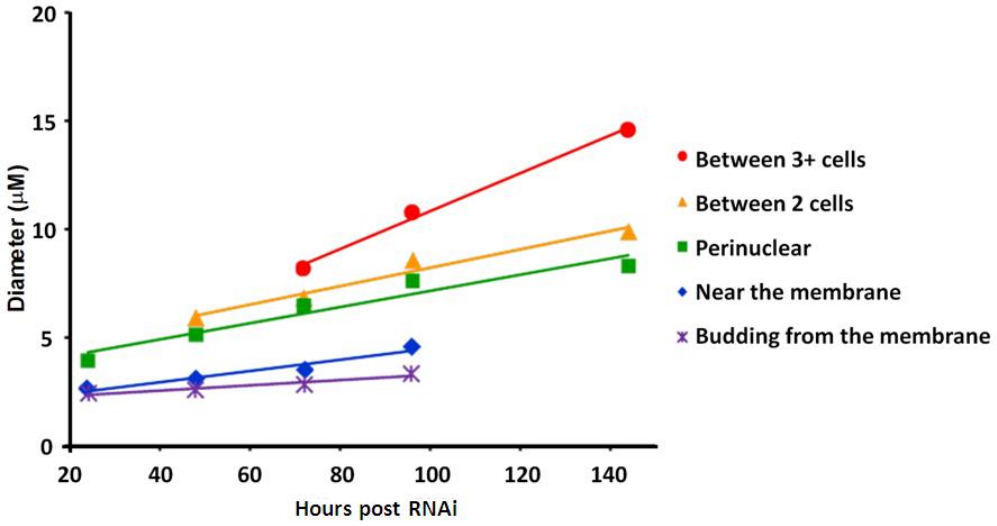

Figure 4.17: Vacuoles increase in size over time. MDCK cells were grown overnight and subjected to RNAi as in Figure 4.5. The data was collected as in figure 4.16. Plotted is the mean diameter of the vacuoles found at various cellular positions over time and line of best fits. The colours indicate different cellular positions. A student's T-test confirmed the gradients of all line of best fits plotted were not equal to zero, $p<0.05$.

Summary

A role for OCRL1 in polarisation has not previously been investigated although Lowe Syndrome affects cell types in which polarisation is critical to cellular function. In Chapter 3, loss of OCRL1 hindered the maturation of epithelial cells. Maturation was studied in terms of cell shape, however as cells mature they also polarise to form distinct apical and basolateral membranes. The finding that loss of OCRL1 hindered maturation suggested polarisation may also be affected. This chapter investigated whether OCRL1 was required for polarisation in the MDCK cell line, which was also used in Chapter 3 to show OCRL1 was involved in epithelial maturation.

The effects on maturation shown previously were observed in monolayers of MDCK cells grown without OCRL1 for several days. Therefore, we studied polarisation at the point where OCRL1 loss affected maturation by repeating previous experiments in addition to looking at the distribution of a number of polarity markers. However, repeating experiments from the previous chapter yielded different results. In addition to affecting epithelial maturation, OCRL1 loss induced the appearance of vacuolar apical compartments (VACs). These VACs resembled the apical membrane in composition; rich in apical proteins and lipids and associated actin filaments. Although polarity markers were not used previously, the distribution of F-actin was used in the previous chapter to assess cell shape and vacuoles were not observed. The experimental protocol remained the same in both chapters, however a different batch of siRNA used in this chapter may explain the new finding. Maximum OCRL1 depletion with new siRNA appeared to be required for vacuole formation to accompany loss of maturation, suggesting sub-maximal OCRL1 depletion hindered maturation while a greater loss of OCRL1 also induced polarity defects. Alternatively, vacuoles may have been missed in the previous chapter due to poor resolution and grainy appearance of F-actin with Cy5-phalloidin compared to the phalloidin stains used in this chapter which produced clearer and more detailed results.

Studying the location and size of vacuoles over time suggested intracellular apical vacuoles fused with the plasma membrane to form lateral apical lumens. The lateral apical lumens were accompanied by a loss of apical membrane from the cell surface, resembling the organisation of membrane domains in hepatic cell lines with bile canaliculi. The organisation of membrane domains in cells without OCRL1 suggested polarisation along a horizontal rather than vertical plane. In addition, the horizontal arrangement of the microtubule cytoskeleton and the re-positioning of nuclei to ensure maximal distance from the lateral lumen further suggested horizontal orientation. Polarisation appeared unaffected by loss of OCRL1; cells formed distinct apical and basolateral membrane domains kept separate by reorganised bands of tight junction. However, OCRL1 depletion affected the gross organisation of membrane domains, suggesting OCRL1 may be required for the correct orientation of the apical-basal polarity axis.

Discussion

The results of this chapter demonstrate a requirement of OCRL1 for the correct positioning of the apical membrane. OCRL1 depleted cells first formed their apical membrane intracellularly in the form of large vacuoles which appeared to be used at later stages of development to form lateral apical lumens. Intracellular apical domains are frequently observed when apical trafficking pathways are perturbed, whilst lateral apical lumens are less common but may indicate mis-localisation of key polarity proteins responsible for positioning of the apical membrane.

The intracellular apical domains formed when OCRL1 was depleted resemble the vacuolar apical compartments (VACs) formed in calcium switch experiments or when the microtubule cytoskeleton is disrupted (Gilbert et al., 1991; van Zeijl and Matlin, 1990). VACs are large vacuoles which contain microvilli and apical plasma membrane but exclude basolateral membrane markers. Removal of calcium from the extracellular environment blocks calcium dependent adhesive intercellular contacts which in turn prevents polarisation. VACs are thought to accumulate by the fusion of frustrated apical vesicles unable to traffic to the plasma membrane in the absence of cell-cell adhesion. Similarly, disruption of microtubules with nocodazole or colchicine blocks apical trafficking to the cell surface and results in the formation of VACs (Gilbert et al., 1991; van Zeijl and Matlin, 1990). The appearance of VACs in the absence of OCRL1 hints at the possibility that apical trafficking to the plasma membrane may be affected. In addition, OCRL1 has previously been implicated to regulate recycling of megalin and other receptors to the cell surface (Vicinanza et al., 2011). Megalin is normally expressed on the apical plasma membrane of polarised epithelial cells but accumulates in recycling endosomes when OCRL1 is depleted (Vicinanza et al., 2011), suggesting OCRL1 regulates the trafficking of this receptor from recycling endosomes to the plasma membrane. The vacuoles which form in the absence of OCRL1 could potentially be explained if OCRL1 similarly blocks the trafficking of other apical cargo. In the next chapter, the trafficking of apical carriers is studied in OCRL1 depleted cells pre-vacuole formation by looking earlier after OCRL1 depletion.

Although disrupted apical trafficking may explain VAC formation, it was not clear why OCRL1 depleted cells subsequently form lateral lumens. VACs in calcium switch experiments persist only for as long as calcium is absent, when calcium is restored intercellular contacts re-form and VACs are rapidly exocytosed towards the lateral membrane (Vega-Salas et al., 1988). After VAC exocytosis, the apical membrane from the vacuole diffuses towards its final destination at the cell surface (Vega-Salas et al., 1988). Lateral vacuoles are therefore transiently observed in calcium switch experiments as VACs undergo fusion with the lateral membrane. In OCRL1 depleted cells, VACs appeared to similarly fuse with the lateral membrane, though exocytosis of VACs did not lead to reformation of the apical surface. Instead, the vacuoles were maintained in the lateral membrane and subsequently developed into a lateral lumen, however the reason for these differences are not clear.

The formation of lateral lumens is often seen in MDCK cysts grown in 3D culture when it is referred to as the multi-lumen phenotype since insertion of apical membrane into the lateral region between cells of cysts disrupts the formation of a single central lumen. Multiple lumens are formed in MDCK cysts with loss of function of proteins involved in membrane domain segregation or tight junction formation such as Cdc42, Annexin-2, PTEN, aPKC and the apical polarity complex Crumbs (Jaffe et al., 2008; Martín-Belmonte et al., 2007; Schluter et al., 2009), highlighting their role in positioning rather than forming the apical membrane. In addition multiple lumens are also observed in MDCK cysts with defective apical trafficking pathways (Roland et al., 2011). The lateral lumen phenotype is less common when MDCK cells are grown in 2D culture as sheets, likely due to less stringent polarity requirements under these conditions. However, lateral lumens have been reported in epithelial monolayers over-expressing the serine/threonine kinase Par1b, also known as MARK2 and emk1 (Cohen et al., 2003, 2004a, 200b and 2011). Monolayers of MDCK cells over-expressing Par1b convert from a normal columnar epithelial organisation to a hepatic-like appearance, discussed below.

Columnar epithelia, for example in the kidney and intestine, normally position the lumen or apical membrane at the apex of the cell. Other epithelia such as liver hepatocytes position the lumen (bile canaliculi) at sites of intercellular contact in the lateral domain. In addition, the microtubule cytoskeleton in hepatocytes is organised horizontally towards the bile canaliculi, supporting the heavy trafficking demands of the apical membrane (Cohen et al., 2004a). Par1b promotes the transformation of MDCK cells from a normal columnar epithelial polarity to hepatic-like polarity through effects on the microtubule and actin cytoskeleton (Cohen et al., 2994a and 2011). Par1b regulates the microtubule binding activity of several microtubule associated proteins (Drewes and Ebneth, 1998, Illenberger et al., 1996). In addition Par1b regulates the function of insulin receptor tyrosine kinase substrate p53; IRSp53 (Cohen et al., 2011). IRSp53 acts as a scaffold to link the Rho GTPases Cdc42 and Rac1 to their downstream effector molecules involved in actin organisation (Scita et al., 2008). At the basal side of the cell, IRSp53 stimulates the formation of a sub-membraneous actin network to facilitate receptor clustering and signalling from the extracellular matrix (Cohen et al., 2011). The mechanism of Par1b regulation of apical membrane positioning is thought to involve this pathway, although how ECM derived signalling affects positioning of the apical pole is not fully understood.

How OCRL1 depletion might affect events at the basal side of the cell to affect positioning of the apical membrane is not clear. However, both Par1b and IRSp53 interact with lipids; Par1b interacts with acidic lipids via a kinase associated-1 domain (Moravcevic et al., 2010) and IRSp53 binds lipids through an inverted BAR domain (Levtsova et al., 2011). Work carried out in *Drosophila* indicates a potential role for $PI(4,5)P_2$ in mediating membrane recruitment of Par1b; association of Par1b with the plasma membrane required $PI(4,5)P_2$ generation by the PIP5K skittles (Gervais et al., 2008). In this study, depletion of skittles disrupted cytoskeletal organisation and asymmetric transport, suggesting a model where $PI(4,5)P_2$ could mediate interactions between the plasma membrane, Par1b and the cytoskeleton (Gervais et al., 2008). Whether OCRL1 loss affects Par1b localisation through regulation of $PI(4,5)P_2$ is studied in the next chapter. Over-expression of Par1b

appears to convert MDCK monolayers to a hepatic-like epithelium. Although the phenotype of OCRL1 depletion resembles the phenotype of Par1b over-expression, OCRL1 depleted cells do not fully take on the appearance of hepatic cells, suggesting a different underlying mechanism of lumen formation. These differences become apparent when the nature of the intracellular compartments are compared, discussed below.

Calcium switch experiments can be performed on hepatic cells in a similar manner to columnar epithelia. When hepatic cells are grown in low calcium, luminal markers accumulate in an intracellular compartment that re-forms the bile canaliculi when calcium is restored (Tuma et al., 2002). However the hepatic intracellular apical compartment differs from the VACs observed in calcium switch assays performed on columnar epithelial cells. Columnar epithelia form VACs that stain heavily with phalloidin due to the presence of microvilli and exclusively accumulate apical markers. In contrast, the hepatic intracellular apical compartment is devoid of F-actin and the apical markers delivered to this compartment constitutively recycle to the plasma membrane (Tuma et al., 2002). Columnar epithelia and hepatic epithelia have different apical trafficking pathways which might explain the different characteristics of the intracellular apical compartments. For example, unlike columnar epithelia, hepatic cells consistently traffic their apical cargo via the basolateral domain (Maurice et al., 1994).

When MDCK cells over-expressing Par1b are depleted of calcium, they form an intracellular apical compartment that resembles the intracellular compartment formed in hepatic cells (Cohen et al., 2004b). However, the intracellular apical compartments formed in OCRL1 depleted cells were more characteristic of the VACs formed in contact naive MDCK cells; they stained strongly with phalloidin and appeared to completely internalise apical proteins from the cell surface, indicating the absence of recycling through this compartment. Therefore unlike par1b over-expression, MDCK cells depleted of OCRL1 retained kidney epithelial characteristics, suggesting OCRL1 depletion does not induce cells to become hepatic-like, and OCRL1 depleted cells form lumens through a different underlying mechanism. One

possibility is that lumen formation in OCRL1 depleted cells more closely resembles lumenogenesis in MDCK cyst cultures than bile canaliculi formation in hepatic epithelia.

Lumen formation in epithelial cysts occurs when cells are immersed in a uniform environment of extra cellular matrix (O'Brien et al., 2002). In contrast, epithelial cells grown in an asymmetric environment with a plastic support on one side and growth media on the opposing side divide and assemble into sheets with an apical surface in place of a lumen. Therefore detection of asymmetry in the environment appears to be critical in determining the organisation of cells grown in culture. One possibility is that OCRL1 depleted cells lose the ability to detect external polarity cues and grow in 2D culture as though they were growing in 3D culture. This would explain why OCRL1 depleted cells appeared to maintain kidney epithelial cell characteristics.

The position of the apical membrane or lumen is thought to be determined by the absence of cell adhesion, followed by targeting of apical polarity complexes to this region. $PI(4,5)P_2$ has numerous roles in establishing apical membrane identity, recruiting several proteins that regulate expansion of the apical domain. For example, $PI(4,5)P_2$ on the apical surface recruits Annexin-2, which in turn recruits Cdc42 and aPKC to the apical surface. Loss of $PI(4,5)P_2$ from the apical domain prevents normal development of the apical surface and lumen (Martín-Belmonte et al., 2007), indicating the importance of $PI(4,5)P_2$ in regulating apical membrane formation. In addition, there is some evidence to suggest $PI(4,5)P_2$ may regulate membrane recruitment of key polarity proteins such as Par3 (Horikoshi et al., 2011; Krahn et al., 2010; Wu et al., 2007) as well as the exocyst complex (He et al., 2007; Zhang et al., 2008), which is critical for cargo trafficking to the apical membrane. The multiple roles of $PI(4,5)P_2$ in recruitment of apical determinates suggests $PI(4,5)P_2$ is likely to accumulate in the apical membrane early during development.

The accumulation of $PI(4,5)P_2$ in the apical domain requires a low level of $PI(4,5)P_2$ to be maintained on other membranes, so that the apical domain can be identified

as being rich in $PI(4,5)P_2$. If depletion of OCRL1 leads to ectopic accumulation of $PI(4,5)P_2$ in areas other than the apical membrane, one possibility is that key apical membrane determinates become mis-localised, over-riding external polarity cues that normally function to correctly position these complexes. Supporting this possibility is the finding in this chapter that $PI(4,5)P_2$ was unusually enriched in the lateral membrane, a region that normally contains low levels of $PI(4,5)P_2$. A similar function of OCRL1 has been identified in *Drosophila* during cytokinesis. Depletion of dOCRL1 induces ectopic accumulation of $PI(4,5)P_2$ on intracellular membranes, subsequently key components of the cytokinesis machinery are mis-targeted away from the site of cytokinesis towards intracellular compartments (Ben El Kadhi et al., 2011). The function of dOCRL1 during cytokinesis is to down-regulate $PI(4,5)P_2$ on intracellular membranes, allowing the site of cytokinesis to appear comparatively rich in $PI(4,5)P_2$ which recruits multiple contractile ring components to the furrow (Ben El Kadhi et al., 2011). OCRL1 may similarly function in polarisation to enable the correct localisation of multiple apical determinants that interact with $PI(4,5)P_2$. The next chapter examines whether mis-targeting of key apical membrane determinants in OCRL1 depleted cells can explain the lateral lumen phenotype

Chapter Five

OCRL1 regulates apical recycling pathways in MDCK cells

Overview

In the previous chapter, the effect of OCRL1 depletion on cell polarity was studied in mature monolayers of MDCK cells grown in culture for up to 5 days. After 48 hours without OCRL1, MDCK cells incorrectly formed the apical domain intracellularly, resembling the VACs (vacuolar apical compartments) formed in calcium switch experiments (Gilbert et al., 1991; van Zeijl and Matlin, 1990; Vega-Salas et al., 1987). After 72 hours without OCRL1, MDCK cells lost the intracellular apical domain and instead positoned the apical domain between cells, resembling lateral apical lumens.

The formation of VACs in calcium switch experiments is thought to occur by the fusion of frustrated transport vesicles unable to traffic to the plasma membrane (Vega-Salas et al., 1987), suggesting OCRL1 depletion might block apical trafficking to the cell surface. In addition, the eventual formation of the apical domain in the lateral region of the cell suggests OCRL1 may be required for early events in the polarisation process when cells establish an axis of polarity and first mark the sites of apical and basal membrane expasion. Both of these events, forming an axis of polarity and expanding polarised membrane domains, heavily depend on polarised trafficking pathways.

Firstly, this chapter examines the role of apical trafficking in the phenotype of OCRL1 depletion by looking early after RNAi treatment, before intracellular vacuole formation. Secondly, this chapter studies the localisation of some of the key protein polarity complexes involved in apical-basal axis orientation in cells without OCRL1. The aim of these experiments was to find out whether elevated levels of $PI(4,5)P_2$, after OCRL1 depletion, causes re-localisation of any of the polarity complexes that regulate positioning of the apical membrane.

Apical trafficking pathways are disrupted within 24 hours of RNAi treatment

In the previous chapter, OCRL1 was depleted in monolayers of MDCK cells for 48-72 hours. After 72 hours in culture without OCRL1, the cells had undergone extensive rearrangements of the cell cytoskeleton, membrane domains and intercellular junctions. To better understand the events that precede these rearrangements, the RNAi protocol was adapted so that OCRL1 was depleted for shorter amounts of time. Instead of depleting OCRL1 for 48-72 hours, monolayers of MDCK cells were depleted of OCRL1 for 24-48 hours. As in the previous chapter, monolayers depleted of OCRL1 for 48 hours formed perinuclear vacuoles enriched in Gp135 (figure 5.1 second panel). However looking earlier (24 hours following the initiation of RNAi) revealed perinuclear accumulations of vesicular pools of Gp135 not seen previously (figure 5.1 top panel). The timings of these events suggests that the vacuoles predominantly seen at 48 hours after RNAi are formed from the fusion of the smaller vesiclular carriers seen 24 hours earlier. The perinuclear region of the cell houses numerous organelles and compartments involved in trafficking, the accumulation of vesicles carrying apical cargo in such a perinuclear region suggests that apical trafficking pathways are disrupted by loss of OCRL1.

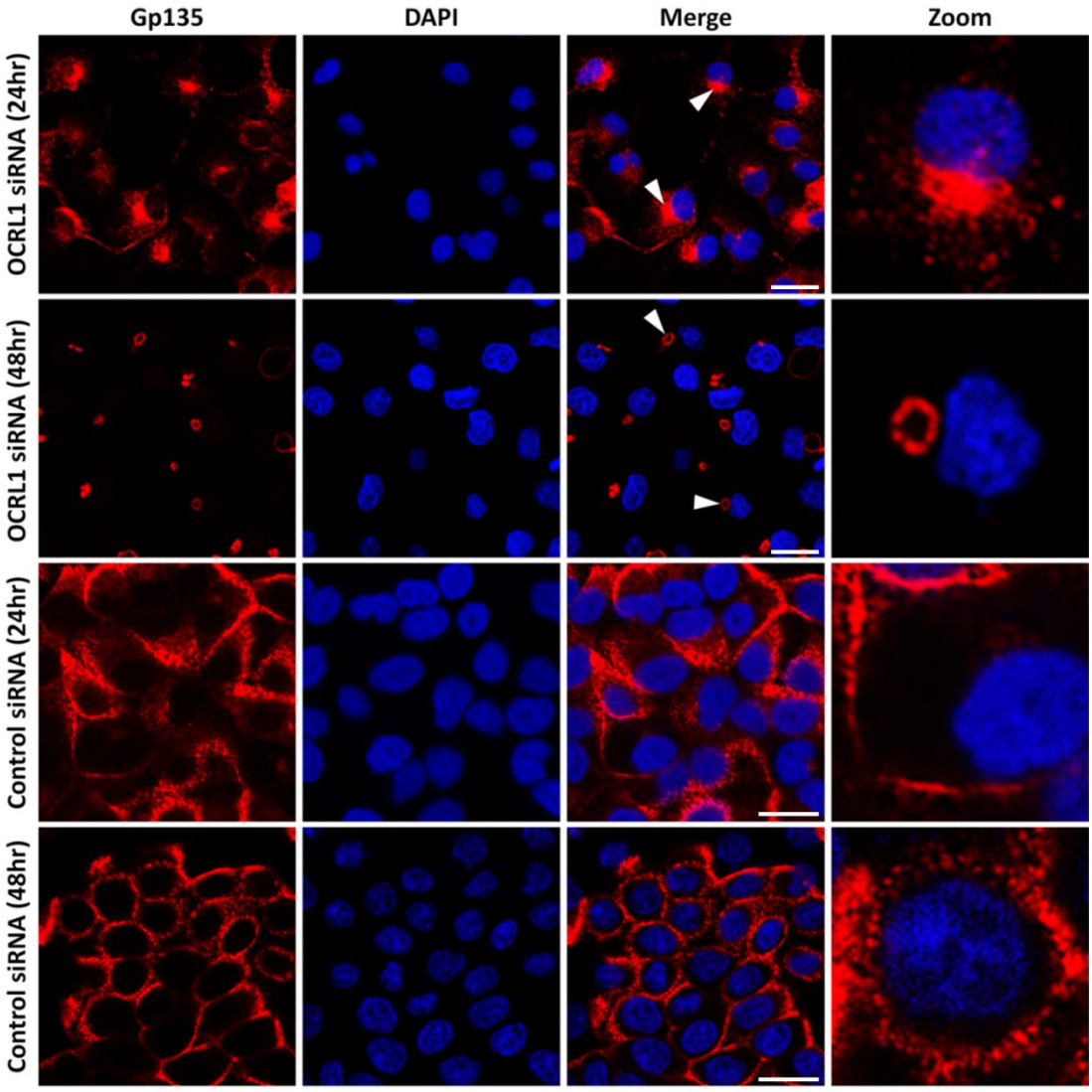

Figure 5.1: OCRL1 depletion disrupts apical trafficking from a perinuclear region. MDCK cells were grown overnight. Cells were transfected with non-targeting control or a pool of OCRL1 siRNA and fixed 24 or 48 hours later. Cells were permeabilised for immunostaining with antibodies to Gp135 (red) and the DNA stain DAPI (blue). Representative single confocal sections are shown from the middle of the monolayers from 2 experiments. Higher magnification images of the merged panels are shown in the last column. White arrows indicate vesicular pools of apical vesicles at 24 hours after OCRL1 RNAi and the vacuoles formed at 48 hours after OCRL1 RNAi. Scale bar 20 µM.

The role of OCRL1 prior to the development of polarity

In the last experiment (figure 5.1) and in the previous chapter, polarisation was studied in monolayers of MDCK cells depleted of OCRL1. These cells had been growing in culture for 24 hours before RNAi and therefore the cells would have already begun polarising normally along a vertical axis before depletion of OCRL1. The process of switching from a vertical to a horizontal axis when OCRL1 is depleted takes approximately 72 hours; lateral apical lumens are fully formed by this time. During the course of approximately 72 hours without OCRL1, cells growing in monolayers initially seem to accumulate apical cargo in a vesicular perinuclear pool before forming perinuclear VACs which appear to be exocytosed in the lateral membrane. For the remainder of this chapter, OCRL1 was depleted in cells which had a limited amount of time to polarise before RNAi. In this new protocol, MDCK cells were plated at a very low density, usually as single cells for just a few hours before OCRL1 depletion. These cells would therefore undergo the earliest stages of polarisation without OCRL1. In addition, fixation and analysis took place 17-24 hours post RNAi, even earlier than above (figure 5.1). These changes made to the protocol limit the oportunity for cells to begin polarising without OCRL1 so that the role of OCRL1 in this process can be better studied.

Due to the short time-frame of the RNAi protocol, some cells on the coverslip remained as single cells at the time of analysis. These single cells had not undergone a cell division during the course of the experiment. Other cells on the coverslip were growing in pairs which may have divided and some cells were growing in small groups. Un-polarised MDCK cells treated with control or silencing oligonucleotides were stained for the apical marker Gp135. In single cells treated with non-targetting control siRNA, Gp135 was enriched on the cell surface, but also intracellularly in a perinuclear pool (figure 5.2A). This perinuclear pool was not seen in polarised monolayers of control cells (figure 5.1) and is likely to be a characteristic of cells early in polarisation (Meder et al.,2005). An XZ reconstruction of a single control cell revealed exclusion of Gp135 from the basal domain where the membrane contacts the underlying support (figure 5.3A). This agrees with

previous findings for Gp135 in single MDCK cells, indicating some level of polarity even at the single cell stage (Meder et al., 2005). In contrast to control cells, OCRL1 depleted cells accumulated Gp135 entirely intracellularly and had no detectable Gp135 on the cell surface (figure 5.2B and figure 5.3B).

In pairs of cells treated with non-targeting control siRNA, Gp135 had polarised to the early apical membrane, and was mostly excluded from the cell-cell contact as well as the basal surface (figure 5.3A). However, in control cells, a faint vesicular pool of Gp135 was seen near the cell-cell contact (figure 5.2A), suggesting some apical cargo is trafficked to this site normally. In paired cells polarising without OCRL1, Gp135 was entirely trafficked to a specific site in the lateral membrane (figure 5.2B). Since lateral lumens are formed in similar regions of OCRL1 depleted cells, it is likely that this pair of cells was undergiong early lumen formation, resembling trafficking of apical carriers to the AMIS (apical membrane insertion site) during early lumen formation (Bryant et al., 2010). Some OCRL1 depleted cells on the coverslip had formed resolvable lumens during the course of the experiment (figure 5.2B and figure 5.3B). Therefore depletion of OCRL1 in un-polarised MDCK cells growing at very low density induced the formation of lateral lumens similar to those seen in the previous chapter, where OCRL1 was depleted in MDCK cells growing as monolayers. Similar results were found in MDCK cells stably expressing GFP-Gp135 (figure 5.4). Plating these cells for just a few hours before RNAi treatment and observing them 17 hours after RNAi resulted in perinuclear accumulations of GFP-Gp135 in single cells and the formation of vacuoles between neighbouring cells treated with OCRL1 siRNA (figure 5.4).

These results indicate that depletion of OCRL1 first results in an accumulation of vesicular Gp135 intracellularly which appears to be trafficked to the site of apical membrane formation on the lateral membrane between paired cells. However, in contrast to cells growing in monolayers (Chapter 4), un-polarised cells depleted of OCRL1 almost always formed lateral lumens without an intermediary VAC stage. Instead, lateral lumens appeared to be formed directly from the vesicular pool of apical material (figure 5.2B). In addition, the process of lumen formation occurred a

lot quicker in un-polarised cells compared to monolayers, with the whole process of repolarisation complete in 24 hours compared to 72 hours. This difference could be due to the requirement for MDCK monolayers to reorient themselves as they switch from a vertical to horizontal plane of polarity. In addition their extensive contacts with neighbouring cells require cells growing in monolayers to coordinate the switch in polarity more so than a lone pair of cells. Therefore, with these additional requirements, lateral lumen formation is likely to take longer in cells growing as monolayers compared to cells growing in isolation. One possibility is that a delay in trafficking of the vesicular pool of Gp135 to the lateral membrane in cells growing as monolayers results in the fusion of these vesicles to form an intermediary VAC-like structure.

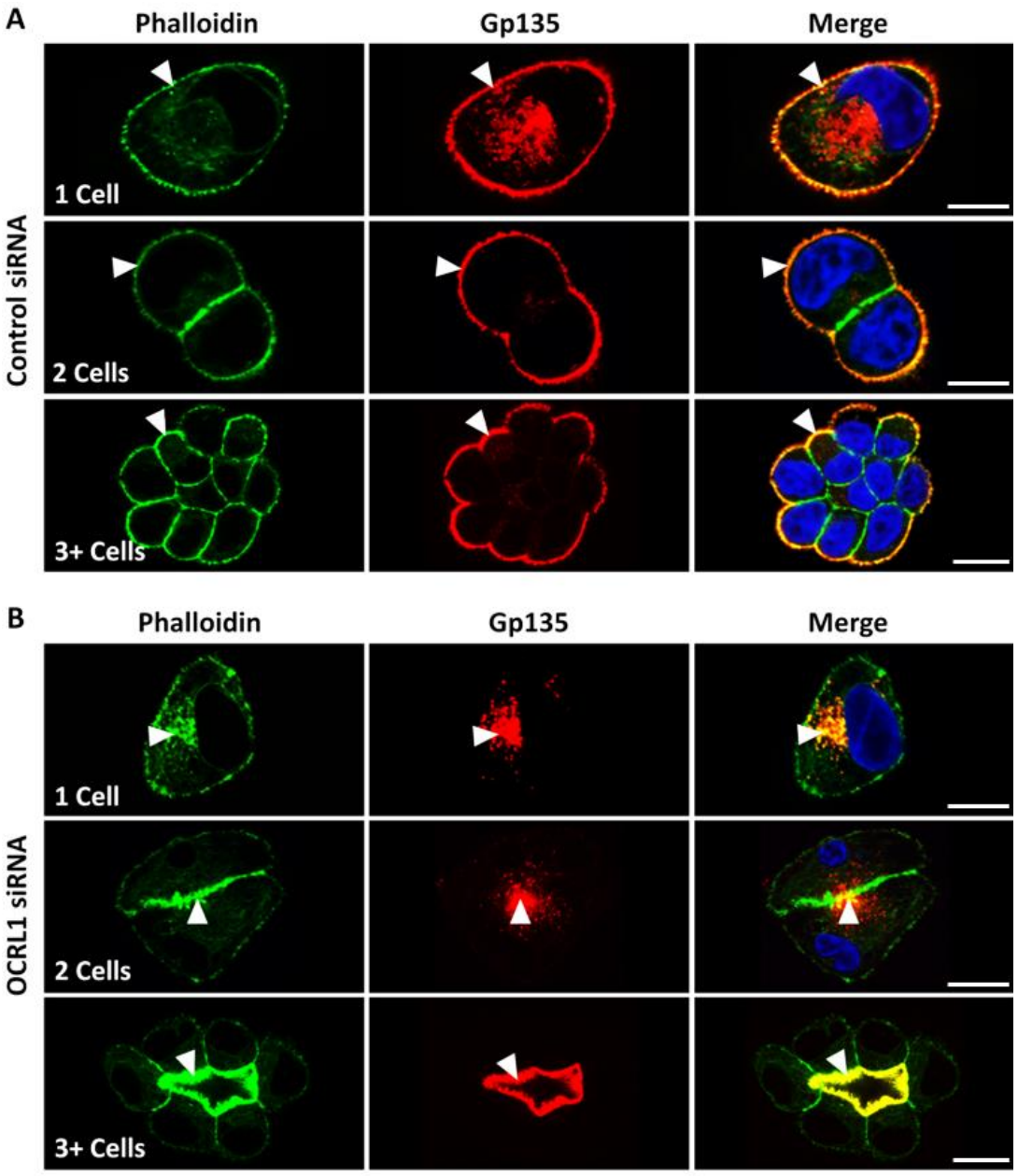

Figure 5.2: Lumen formation in cells plated at low confluence and depleted of OCRL1 for 17 hours. MDCK cells were plated as single cells and grown for 4 hours before treatment with either non-targeting control (A) or a pool of OCRL1 siRNA (B). After 17 hours the cells were fixed and permeabilised for immunostaining with antibodies to Gp135 (red) and F-actin stain phalloidin (green) and the DNA stain DAPI (blue). Representative single confocal sections are shown of single cells, paired cells and cells growing in groups. Experiment repeated twice (n=20 cells observed per treatment). White arrows indicate peripheral membrane localisation of Gp135 in control cells (A) and perinuclear or lateral lumen localisation of Gp135 in OCRL1 depleted cells (B). Scale bar 10 µM.

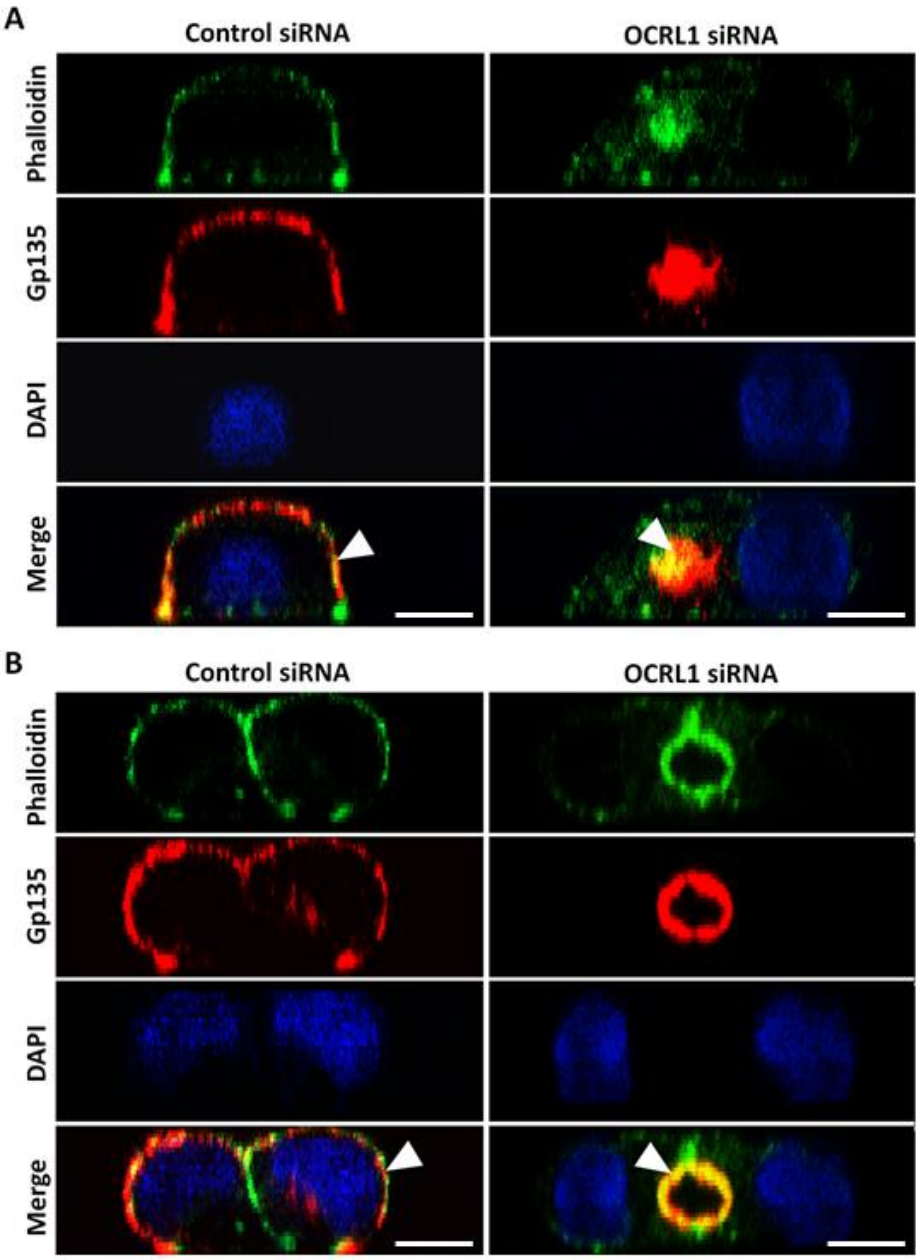

Figure 5.3: XZ constructions of lumen formation in OCRL1 depleted cells. These cells were on the same coverslips as cells in figure 5.2. XZ sections were reconstructed from stacks of 40 single confocal sections. White arrows indicate peripheral membrane localisation of Gp135 in control cells (A) and perinuclear or lateral lumen localisation of Gp135 in OCRL1 depleted cells (B). Experiment repeated twice (n=20 cells observed per treatment). Scale bar 10 µM.

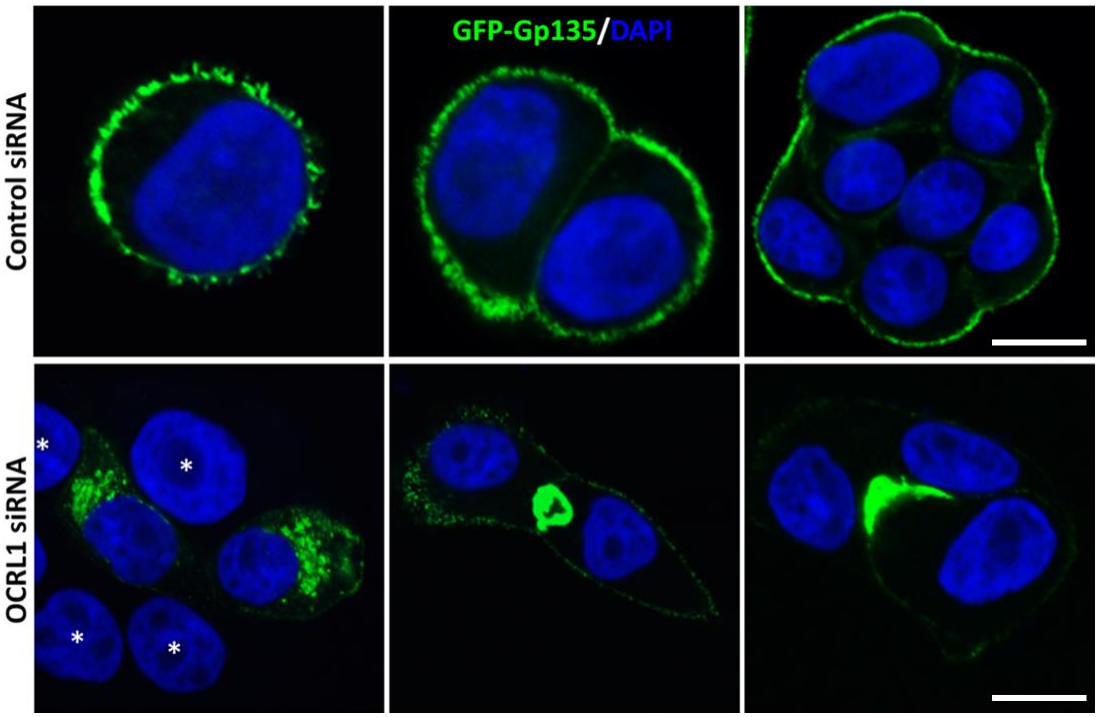

Figure 5.4: GFP tagging of Gp135 has no effect on its trafficking after OCRL1 depletion. MDCK cells stably expressing GFP-Gp135 were grown and subjected to RNAi as in figure 5.2. Cells were fixed and permeabilised for staining with the DNA stain DAPI. Representative confocal sections are shown of a single cell, paired cells and cells growing in small groups expressing GFP-Gp135 (n=20 cells observed for each treatment in a single experiment). Cells not expressing GFP-Gp135 are indicated (*). Scale bar 10 µM.

OCRL1 depletion blocks apical recycling

Without OCRL1, MDCK cells accumulate apical membrane in a perinuclear compartment. This material could be biosynthetic; newly produced Gp135 exiting the TGN, or endocytic from recycling pathways. OCRL1 depletion appears to result in a block in exiting of Gp135 from one of these compartments to the plasma membrane. To determine whether the perinulear Gp135 in OCRL1 depleted cells was endocytic, cells were plated at low density and depleted of OCRL1 in the presence of 10kDa rhodamine dextran in the media. Single cells lacking OCRL1 accumulated rhodamine dextran intracellularly (figure 5.5), and lateral vacuoles formed between cells were also filled with endocytosed fluid (figure 5.5), indicating that MDCK cells depleted of OCRL1 form apical lumens from endocytosed material.

Since a small pool of Gp135 localised to a perinuclear region in control cells (see figure 5.2A), it was possible to carry out FRAP (fluorescence recovery after photobleaching) analysis on live untreated cells stably expressing GFP-Gp135. In this experiment, the perinuclear pool of GFP-Gp135 in one cell was photobleached, but left intact in a neighbouring control cell. The bleached perinuclear region quickly recovered in approximately 15 minutes (figure 5.6). These results indicate that in wild type MDCK cells, Gp135 recycles from a perinuclear region to the plasma membrane, and together with the results above suggest OCRL1 depletion might disrupt this pathway.

To confirm the intracellular pool of Gp135 was endocytic, we tested for localisation of Rab11 to these compartments. In MDCK cells, Rab11A marks the apical recycling endosome (Casanova et al., 1999). In both control cells (figure 5.7A) and OCRL1 depleted cells (figure 5.7B), the intracellular pool of GFP-Gp135 co-localised with Rab11A, agreeing with the previous finding that intracellular Gp135 localises to Rab11 positive compartments (Meder et al., 2005). However, the accumulation of Rab11 in the perinuclear region appeared denser in OCRL1 depleted cells compared to controls (figure 5.7B compared to figure 5.7A). In addition to the co-localisation of GFP-Gp135 with Rab11A in the perinuclear region, more peripheral puncta also

co-localised, indicated in higher magnification images (figure 5.7A/B). Another characteristic marker of apical trafficking pathways in MDCK cells is Rab8, which cooperates with Rab11 to target apical vesicles to the apical membrane (Bryant et al., 2010). Since Rab11 distribution was affected by OCRL1 depletion, we looked to see if Rab8 distribution was also affected. In a similar manner to Rab11, Rab8 accumulated in a perinuclear region and was denser than controls (figure 5.8). Gp135 co-localised with the Rab8 compartment in the perinuclear region of OCRL1 depleted cells (figure 5.8). In addition, double positive vesicles outside the main peri-nuclear region were also observed, indicated in higher magnification images (figure 5.8). These results suggest OCRL1 depletion causes the retention of apical cargo in exaggerated Rab11/Rab8 positive compartments in the perinuclear region of the cell.

In addition to altering the disribution of apical markers, OCRL1 depletion markedly affected the distribution of the cation-independent mannose-6-phosphate receptor (CI-MPR) which normally traffics between the TGN and endosomes. OCRL1 depleted cells lost the central Golgi apparatus pool of MPR which was clearly visible in control cells (figure 5.9). Instead of the Golgi apparatus pool, OCRL1 depleted cells showed an increase in peripheral MPR containing vesicles (figure 5.9), likely to be endosomes, also shown previously (Choudhury et al., 2005; Vicinanza et al., 2011). Therefore OCRL1 depletion appears to affect multiple apical trafficking pathways through a variety of endosome populations.

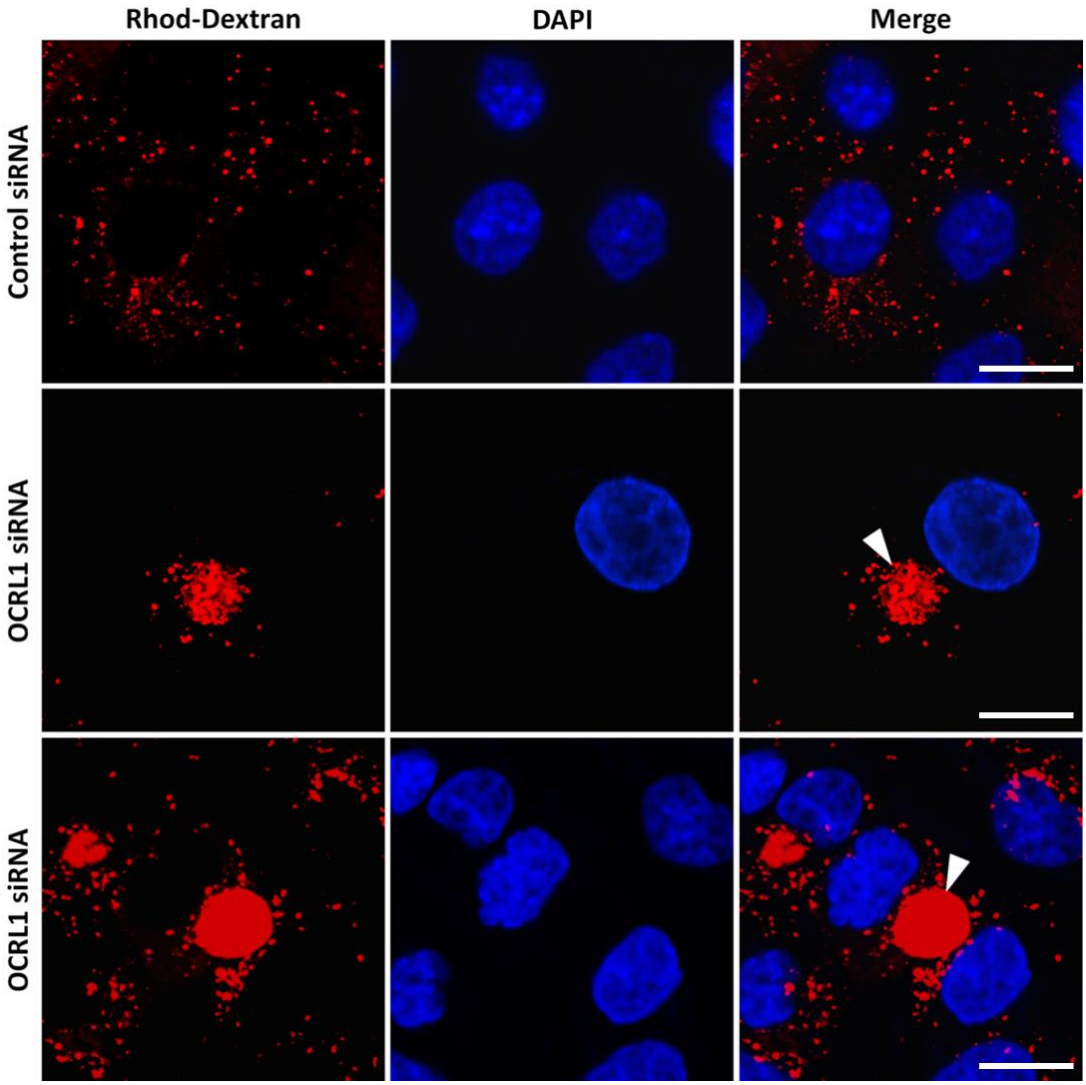

Figure 5.5: Lateral lumens are connected to fluid-phase endocytic pathways. MDCK cells were grown and treated with siRNA as in figure 5.2 in the presence of 10Kda rhodamine dextran for 17 hours and the DNA stain Hoechst 34233 for 30 minutes before fixation. Cells were left un-permeabilised. Representative single confocal sections are shown of a single cell and paired cells on the coverslip. White arrows indicate the perinuclear accumulation of rhodamine dextran in a single cell, and a lateral vacuole formed between paired OCRL1 depleted cells. Representative images are shown from 3 experiments. Scale bar 10 µM.

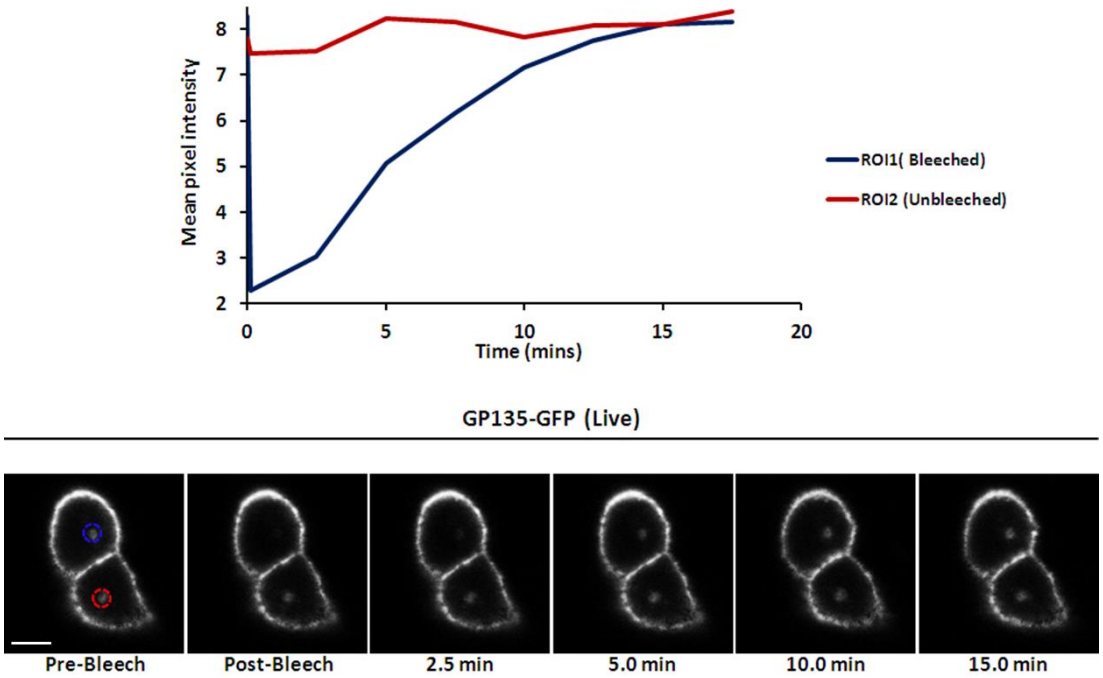

Figure 5.6: GFP-Gp135 recycles rapidly in wild-type MDCK cells. MDCK cells stably expressing GFP-Gp135 were plated on a MaTek dish and grown for 5 hours. Cells were imaged live in phenol free media at 37 ^{o}C with maximum pinhole diameter. One region of interest (ROI) shown in blue was bleached using Leica FRAP software, while the other was left unaffected (red). Images were taken every 2.5 minutes for 17.5 minutes, some of these are shown in black and white. The images were aligned to account for movements in the plane using the StackReg plugin in image J and intensity over time values for the ROI were calculated in image J. Values were normalised against background fluorescence intensity. Representative images are shown from 3 experiments. Scale bar 10 µM.

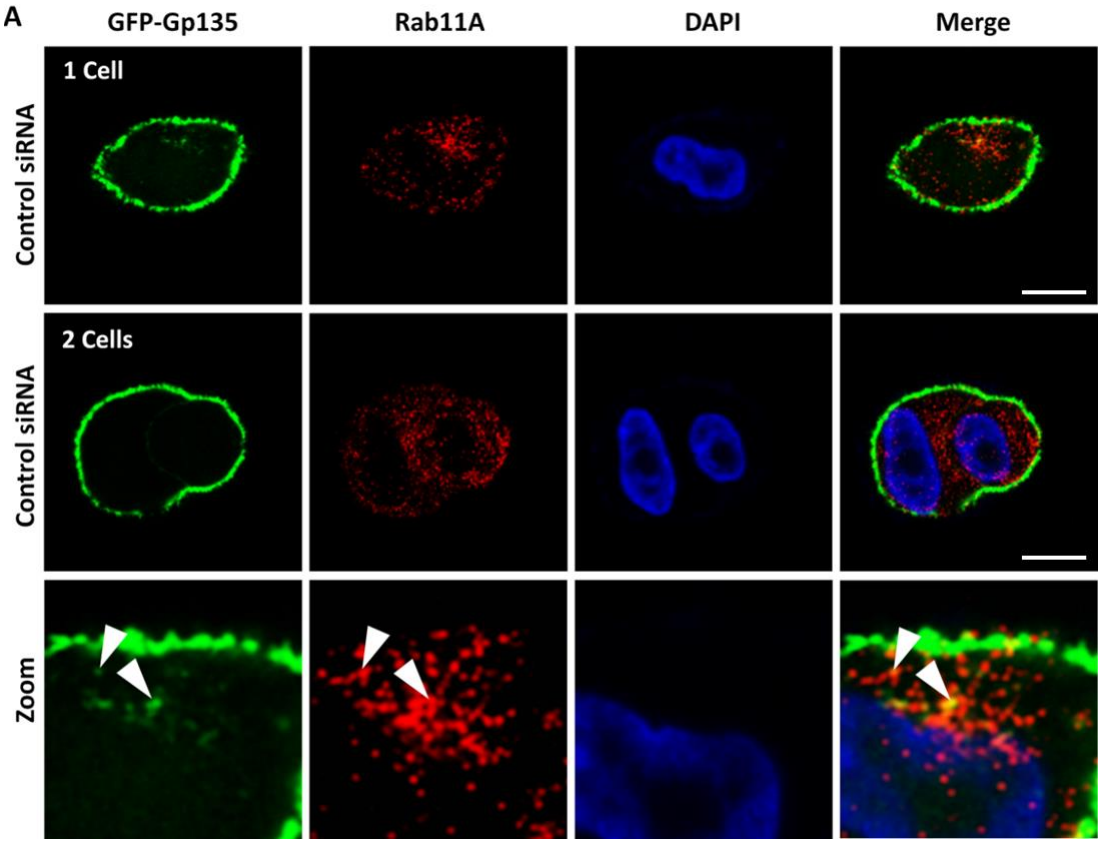

Figure 5.7A: Gp135 traffics through Rab11 positive compartments in control cells. MDCK cells stably expressing GFP-Gp135 were grown and treated with non-targeting control siRNA as in figure 5.2. Cells were fixed and permeabilised for staining with antibodies to Rab11A (red) and the DNA stain DAPI (blue). Representative confocal sections are shown of a single control cell and paired control cells (n=10 cells observed per treatment across 2 experiments). Higher magnification images are shown in the bottom panel. White arrows indicate regions where GFP-Gp135 and Rab11A co-localise. Continued on the next page. Scale bar 10 µM.

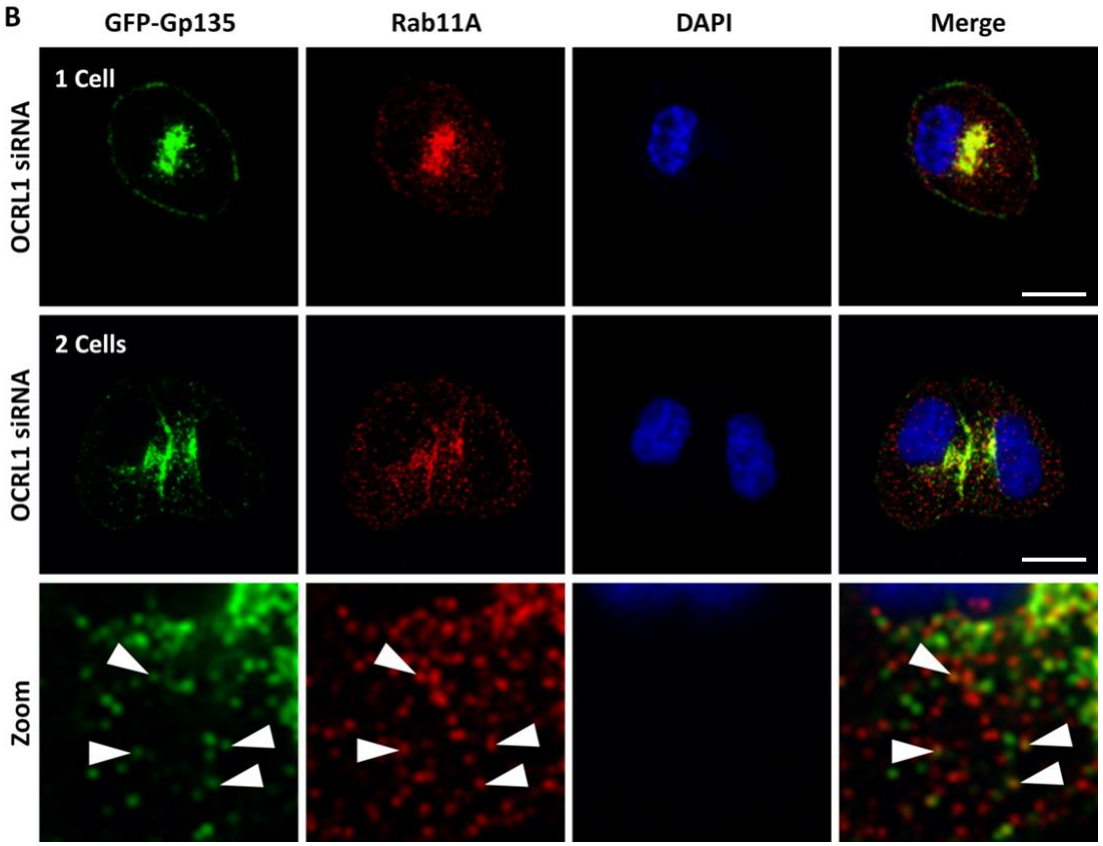

Figure 5.7B: Gp135 accumulates in Rab11 positive compartments without OCRL1. MDCK cells stably expressing GFP-Gp135 were grown and treated with pooled OCRL1 siRNA as in figure 5.2. Cells were fixed and permeabilised for staining with antibodies to Rab11A (red) and the DNA stain DAPI (blue). Representative confocal sections are shown of a single OCRL1 depleted cell and paired OCRL1 depleted cells (n=10 cells observed per treatment across 2 experiments). Higher magnification images are shown in the bottom panel. White arrows indicate regions where GFP-Gp135 and Rab11A co-localise. Scale bar 10 µM.

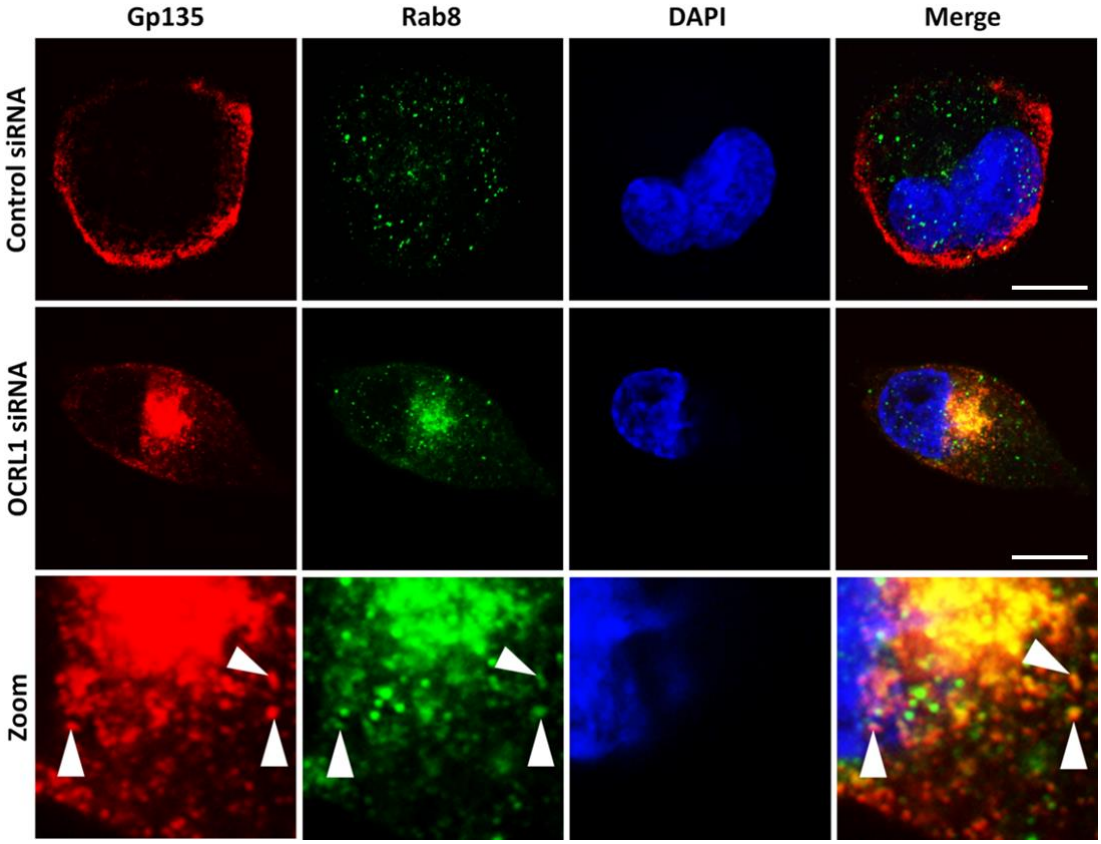

Figure 5.8: Gp135 accumulates in Rab8 positive compartments upon OCRL1 depletion. MDCK cells were grown and subjected to RNAi as in figure 5.2. Cells were fixed and permeabilised for staining with Gp135 (red), Rab8 (green) and the DNA stain DAPI (blue). Representative confocal sections are shown of single OCRL1 depleted cells (n=10 cells observed per treatment across 2 experiments). Higher magnification images are shown of the OCRL1 depleted cell. White arrows indicate punctate regions where Gp135 and Rab8 co-localise. Scale bar 10 µM.

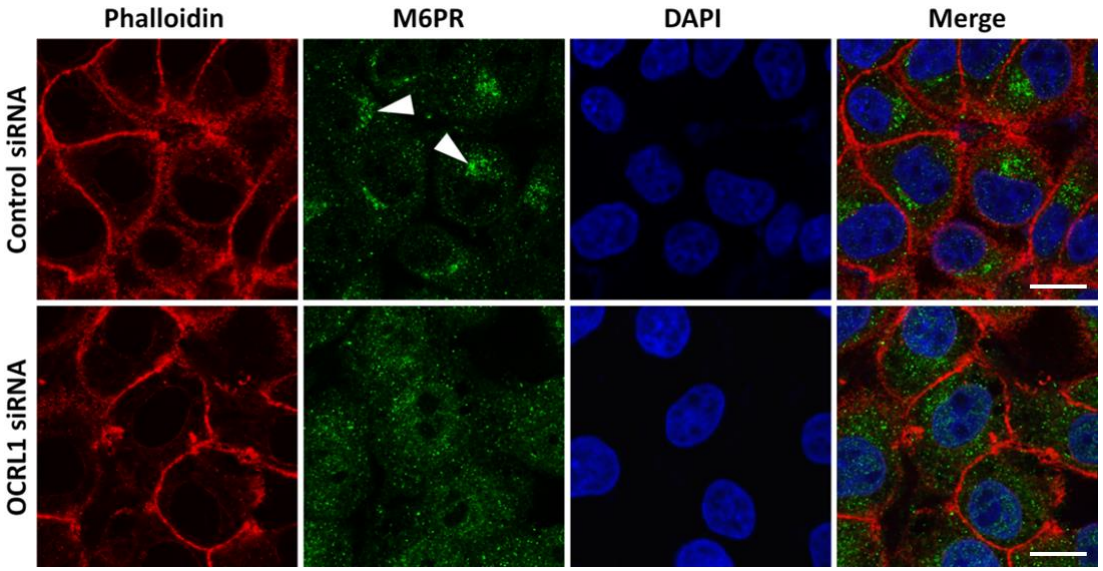

Figure 5.9: OCRL1 depletion redistributes the mannose-6-phosphate receptor. MDCK cells were grown and subjected to RNAi as in figure 5.2. Cells were fixed and permeabilised for staining with phalloidin (red), CI-M6PR (green) and the DNA stain DAPI (blue). Representative confocal sections are shown from the middle of the monolayer. White arrows indicate the perinuclear region of M6PR localisation in control cells which is missing from OCRL1 depleted cells. Scale bar 10 µM.

OCRL1 depletion redistributes apical polarity proteins during early polarisation

Apical–basolateral polarity is initiated by the asymmetric distribution of a number of conserved polarity protein complexes which direct downstream events such as polarised membrane traffic and cytoskeleton organisation. However, the polarised distribution of these protein complexes in turn depends on membrane trafficking (Lalli et al., 2009), highlighting the role that membrane trafficking plays in both initiating and reinforcing cell polarity. A Rab11/Rab8-dependent trafficking pathway has been shown to localise the Par complex to the nascent apical membrane (Bryant et al., 2010). The Par complex is responsible for regulating apical membrane expansion and junction assembly and is composed of aPKC, Par3 and Par6, as well as the Rho family GTPase Cdc42. In addition the Par complex can exist as two separate complexes; Cdc42–Par6–aPKC is associated with the apical surface whereas Par3–aPKC is associated with the tight junction.

Upon depletion of OCRL1, a dense cluster of Rab11/Rab8 positive vesicles accumulate intracellularly and appear to be linked to lateral apical lumen formation. Given the role of the Par complex in apical membrane formation, we decided to investigate whether the abnormal vesicles observed upon depletion of OCRL1 result in a redistribution of Par complex components. This complex is particularly relevant as several of them could be recruited to aberrant pools of internal PI(4,5)P_2 directly, such as Par3 (Horikoshi et al., 2011; Krahn et al., 2010; Wu et al., 2007) or indirectly, such as Cdc42, via Annexin-2 (Martín-Belmonte et al., 2007).

Firstly, we looked at the localisation of Par6 in control and OCRL1 depleted cells that had internalised vesicular pools of Gp135. In control cells, Par6 mostly localised to the plasma membrane, with some cytosolic vesicles (figure 5.10). In OCRL1 depleted cells, Par6 was lost from the plasma membrane and accumulated in a perinuclear cluster of vesicles (figure 5.10). The Par6 positive vesicles co-localised with the perinuclear pool of Gp135 in OCRL1 depleted cells, suggesting that Par6

may be trafficked in the same Rab11/Rab8 pathway previously characterised for Gp135 (figure 5.7 and figure 5.8). Higher magnification images of the OCRL1 depleted cell revealed double positive dots (Par6 and Gp135) outside the main perinuclear region and near the plasma membrane (figure 5.10 bottom panel), further suggesting they are trafficked in the same pathway (figure 5.10)

This perinuclear pool of Par6 in OCRL1 depleted cells was likely to be in complex with aPKC and possibly Cdc42, forming the Cdc42–Par6–aPKC complex. To test for this we checked the localisation of aPKC and Cdc42 in control and OCRL1 depleted cells. The perinuclear accumulations of Par6 which co-localised with Gp135 above (figure 5.10) also co-localised with aPKC (figure 5.11B). Interestingly, the vesicular pool of aPKC and Par6 was only apparent in single OCRL1 depleted cells (figure 5.11B top panel). In pairs of OCRL1 depleted cells a different pattern of localisation was observed. Pairs of OCRL1 depleted cells displayed enriched localisation of Par6 in a region of the lateral membrane (figure 5.11B second panel). This pair of cells may have formed a lateral lumen which was not vet resolvable by confocal microscopy. Control cells showed a similar change in localisation between single and paired cells; in single cells there was a large intracellular pool of aPKC and Par6 which was re-localised to a region near the tight junction in pairs of cells (figure 5.11A XZ images). To localise Cdc42, we expressed Cdc42 as a GFP tagged construct. In OCRL1 depleted cells, some of the vesicular Gp135 was also positive for Cdc42, indicated in higher magnification images (figure 5.12), suggesting the possibility that trafficking of the entire Cdc42–Par6–aPKC complex was disrupted in cells without OCRL1.

In the same experiment as figure 5.11, we localised the basolateral polarity protein scribble in control and OCRL1 depleted cells. In single control cells, scribble primarily localised to the plasma membrane but was re-localised to the lateral border in pairs of cells (figure 5.11A). In OCRL1 depleted cells, scribble was primarily located on the peripheral membrane similarly to controls and was not present on the vesicular pool containing Gp135 and the Par6-aPKC polarity complex (figure 5.11B). These results suggest that OCRL1 depletion does not affect trafficking of

basolateral components and support the specific apical nature of the pathway affected by loss of OCRL1. Since scribble marks the lateral domain and Par6 marks the apical side of the tight junction, their localisation is to distinct regions of the plasma membrane. XZ images of control cells show lateral membrane enrichment of scribble separate from apically localised Par6 and aPKC (figure 5.11A). Similarly in OCRL1 depleted cells, scribble and Par6 localised in a mutually exclusive manner (figure 5.11B). However, lateral scribble was disrupted by the abnormal localisation of Par6 and aPKC in OCRL1 depleted cells, where Par6-aPKC localised laterally, scribble was excluded (figure 5.11B). These findings suggest that separation of the two pathways (apical and basolateral) is maintained after OCRL1 depletion.

In addition to Par6, Par3 is a major component of the Par complex that localises to the tight junction. While in pairs of control cells, Par3 localised to the region of the tight junction, Par3 localisation in OCRL1 depleted cells was perturbed (figure 5.13). In OCRL1 depleted cells, Par3 did not co-localise with the vesicular pool of Gp135, showing a different localisation than Par6 (figure 5.11B). Instead, Par3 seemed to mark the site of delivery for the vesicular apical cargo along the intercellular contact of OCRL1 depleted cells (figure 5.13). However, Par3 did not span the length of the cell-cell contact as in control cells, but was condensed to a region near the middle of the cell contact (figure 5.13). The reorganisation of Par3 can clearly be seen in 3D reconstructions of OCRL1 depleted cells undergoing the early stages of lateral lumen formation (figure 5.14). Pools of vesicular Gp135 accumulated at sites marked by Par3 which appeared to have been reorganised. As lumens were being formed from vesicular apical carriers, Par3 appeared to be reorganised from a single horizontal band, resembling a normal arrangement of the tight junction, to a circular arrangement around the lumen (figure 5.14). These rings of Par3 likely represent the junctional pool of Par3, since rings of Par3 co-localised with ZO-1 in OCRL1 depleted cells that had formed lateral lumens (figure 5.15).

We showed above (figure 5.11B) that abnormal lateral localisations of Par6 and aPKC disrupted the lateral localisation of the basolateral protein scribble. Besides the Scribble complex, there are additional polarity proteins involved in basolateral

membrane formation including Par1b. Par1b is particularly relevant as it has been shown to regulate events at the basement membrane that influence the localisation of the apical membrane. Over-expression of Par1b induced lateral lumens in 2D cultures of MDCK cells similar to depletion of OCRL1 (Cohen et al., 2004a, 200b, 2007 and 2011). In OCRL1 depleted cells, the localisation of Par1b was similar to the localisation of scribble, correctly localising to the lateral membrane but disrupted by aberrant localisation of apical components to the lateral membrane (figure 5.16). Par1b was excluded from the site of early lumen formation in the lateral domain, characterised by trafficking of Gp135 to a region in the cell-cell contact. This can be seen more clearly in XZ images (figure 5.17), showing lateral localisation of Par1b disrupted by a cluster of Gp135 vesicles. Therefore in OCRL1 depleted cells, the tight junction and apical membrane is formed in the lateral membrane between cells which interrupts basolateral determinants such as scribble and Par-1b.

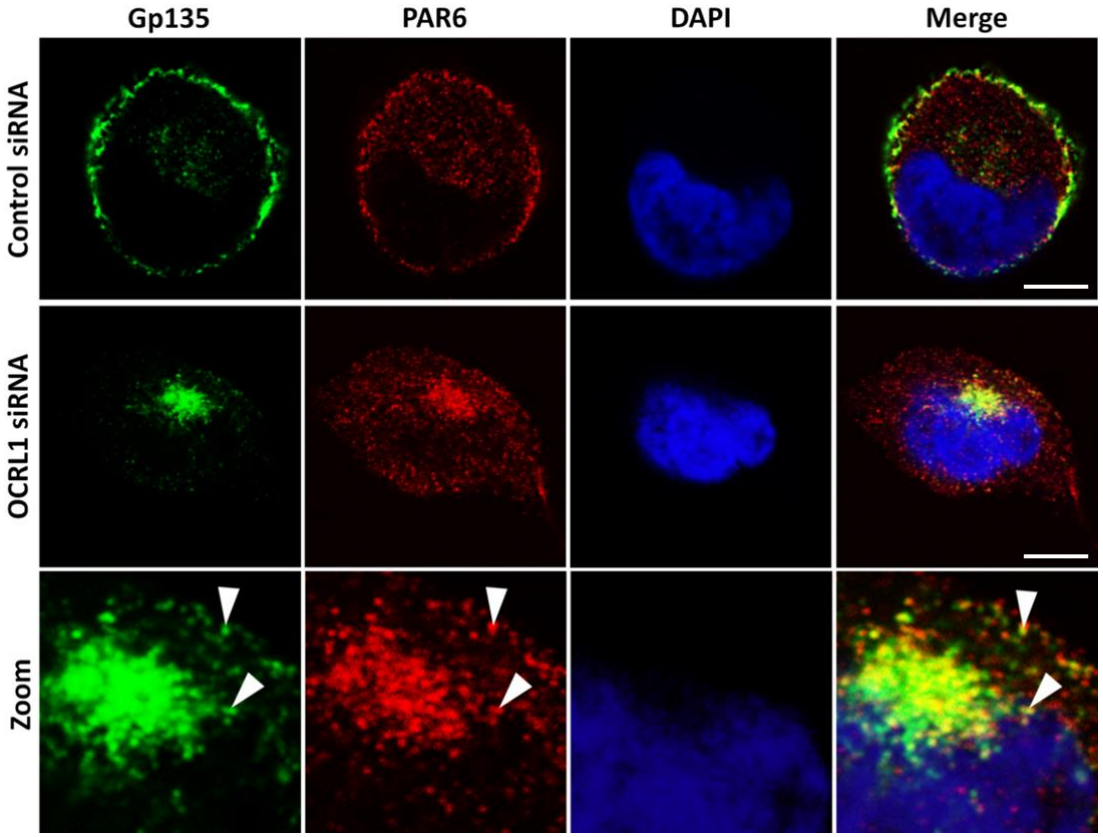

Figure 5.10: OCRL1 depletion redistributes Par6 to a perinuclear region. MDCK cells were grown and subjected to RNAi as in figure 5.2. Cells were fixed and permeabilised for staining with Gp135 antibodies (green), Par6 antibodies (red) and the DNA stain DAPI (blue). Representative single confocal sections are shown (n=10 cells observed per treatment across 1 experiment). Higher magnification images are shown in the bottom panel of the OCRL1 depleted cell. White arrows indicate regions where Gp135 and Par6 co-localise in OCRL1 depleted cells. Scale bar 5 µM.

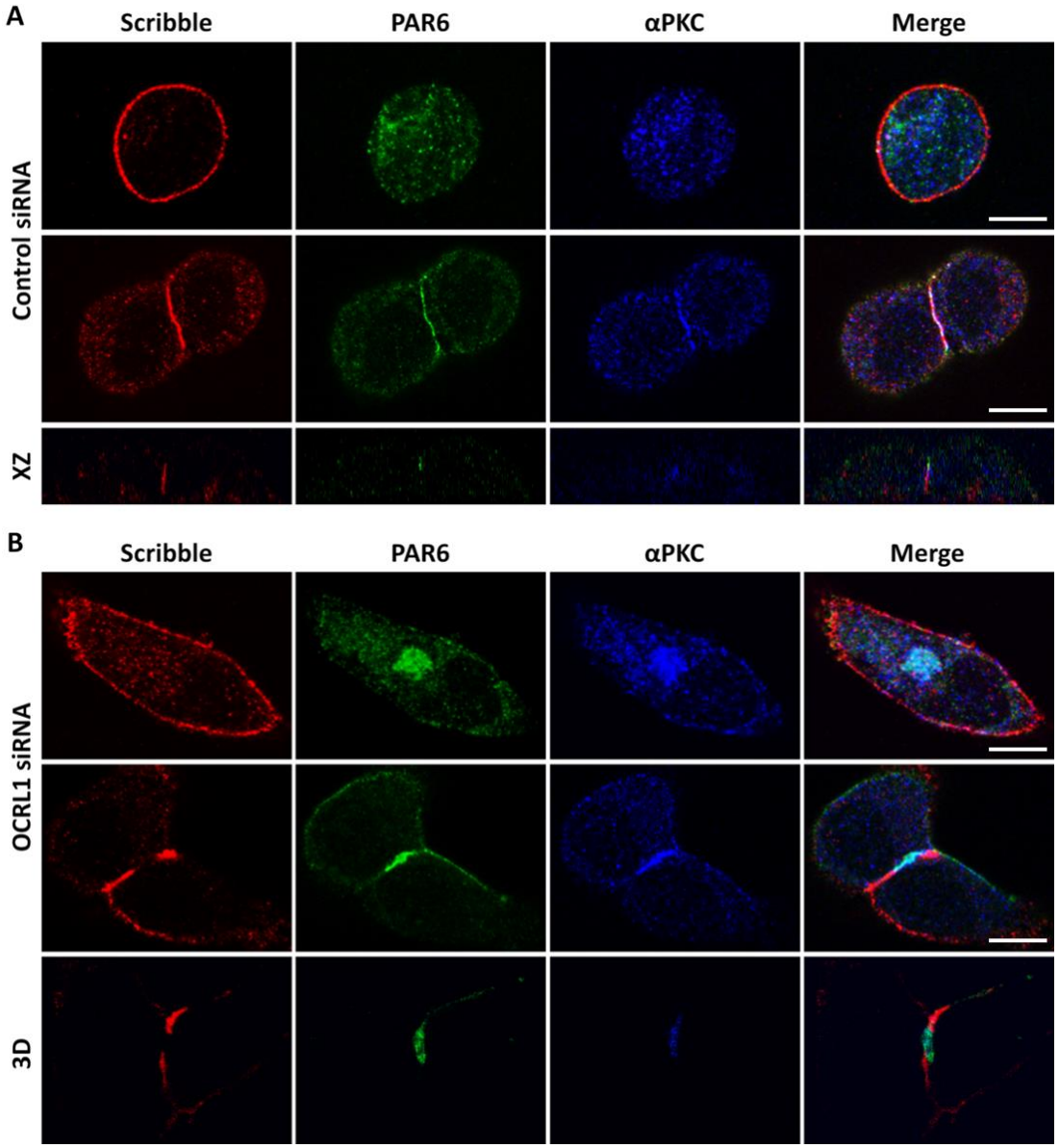

Figure 5.11: Par6 and aPKC are trafficked to lateral lumens. MDCK cells were grown and subjected to RNAi as in figure 5.2. Cells were fixed and stained with antibodies to scribble (red), Par6 (green) and aPKC (blue). Representative single confocal sections are shown of single and paired cells treated with non-targeting control (A) or OCRL1 siRNA (B). n=10 cells observed per treatment across 2 experiments. An XZ reconstruction is shown of a pair of control cells (A) and a 3D reconstruction is shown of a pair of OCRL1 depleted cells (B). Reconstructions were from Z stacks of 20 confocal sections and were carried out in ImageJ. Scale bar 10 μM.

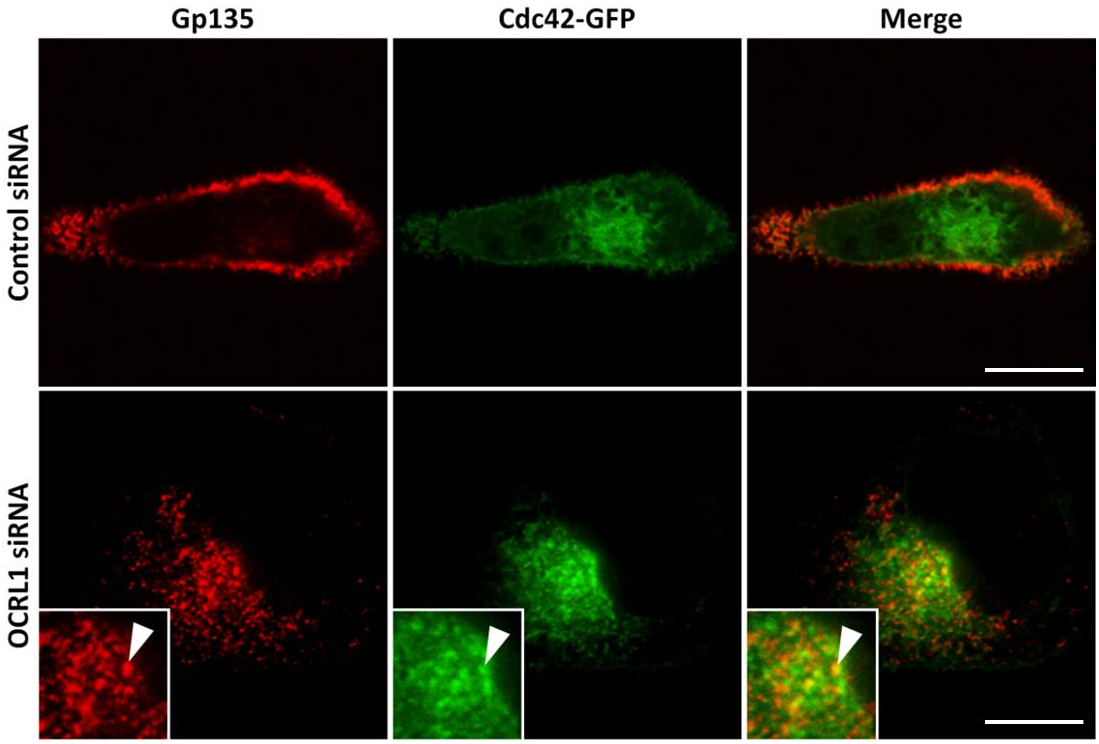

Figure 5.12: Cdc42 partially co-localises with vesicular Gp135. MDCK cells were grown and subjected to RNAi as in figure 5.2. 6 hours after RNAi the cells were transfected with Cdc42-GFP DNA and left for a further 17 hours. Cells were fixed and permeabilised for staining with antibodies to Gp135 (red). Representative single confocal sections are shown of single control and OCRL1 depleted cells (n=10 cells observed per treatment across 3 experiments). Higher magnification images are shown in the inset of the OCRL1 depleted cells. White arrows indicate regions where Gp135 and Cdc42-GFP co-localise. Scale bar 10 µM.

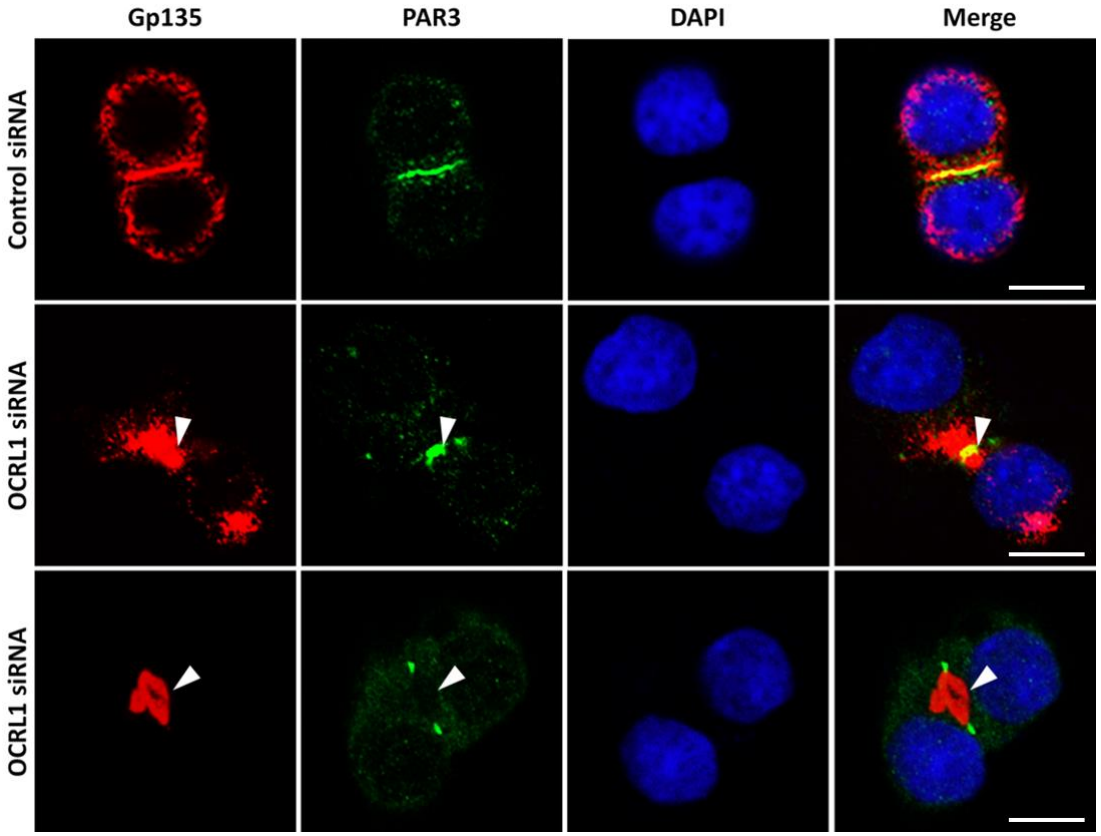

Figure 5.13: Vesicular Gp135 is targeted to Par3 on the lateral membrane. MDCK cells were grown and subjected to RNAi as in figure 5.2. Cells were fixed and permeabilised for staining with antibodies to Gp135 (red), Par3 (green) and the DNA stain DAPI (blue). Images shown are representative of all paired control and OCRL1 depleted cells on the coverslip of a single experiment (n=20). White arrows indicate accumulations of Gp135 between bands of Par3 in OCRL1 depleted cells. Scale bar 10 µM.

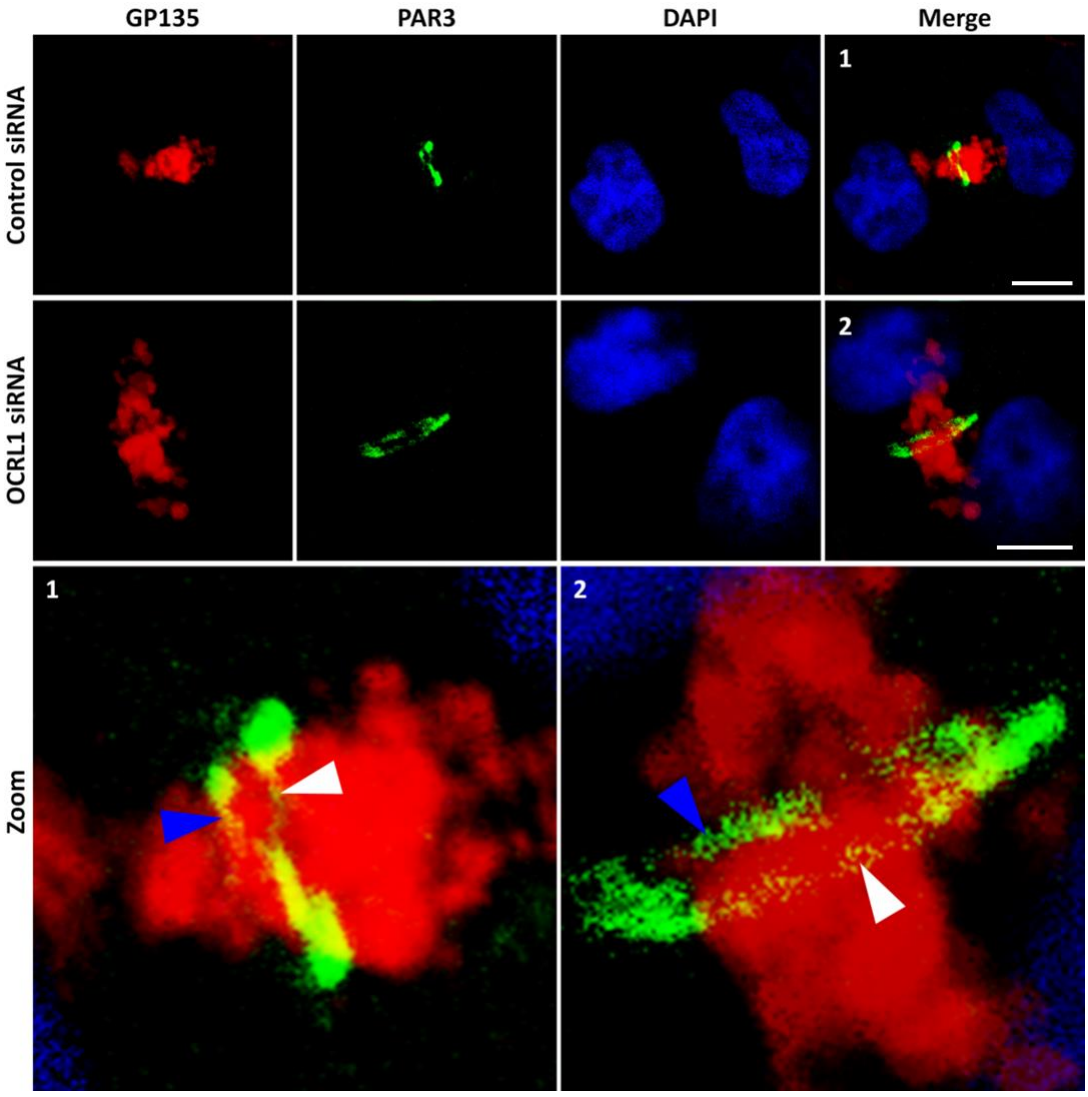

Figure 5.14: Par3 is reorganised as lateral lumens are formed. MDCK cells were grown and subjected to RNAi as in figure 5.2. Cells were fixed and stained with antibodies to Gp135 (red), Par3 (green) and the DNA stain DAPI (blue). All images shown are 3D reconstructions in ImageJ from Z-stacks of 20 confocal sections set to 0% transparency. Regions of image 1 and 2 are shown at higher magnification in the bottom panel. Arrows indicate reorganisation of Par3 into ring-like structures. Blue arrows indicate parts of the ring facing the bottom of the image stack, and white arrows indicate parts of the ring towards the top of the stack. Scale bar 10 µM.

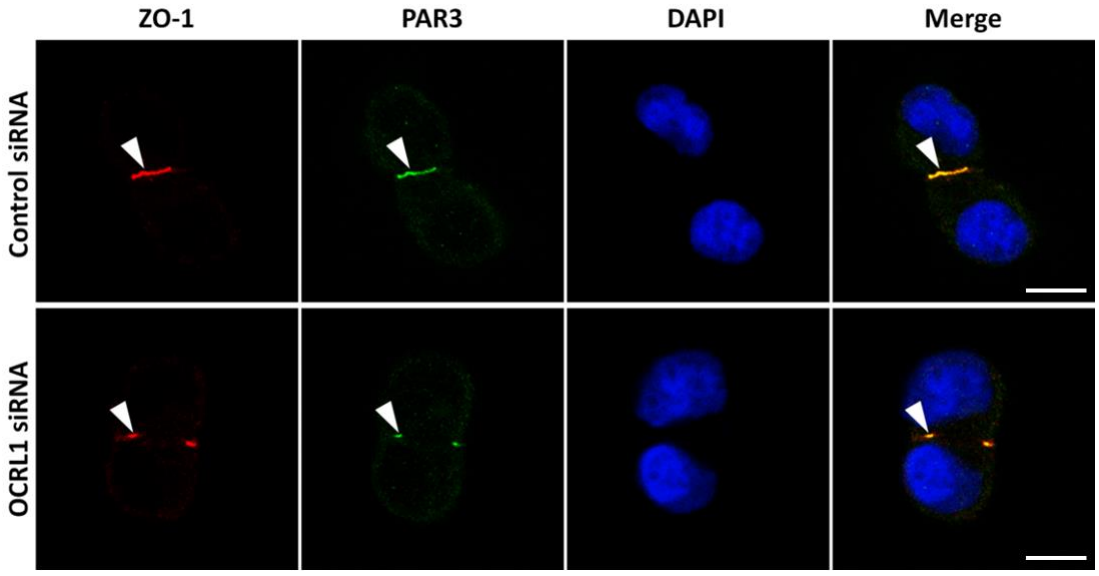

Figure 5.15: Par3 marks the tight junction in cells that have formed lateral lumens. MDCK cells were grown and subjected to RNAi as in figure 5.2. Cells were fixed and permeabilised for staining with antibodies to the tight junction marker ZO-1 (red), Par3 (green) and the DNA stain DAPI (blue). Images shown are representative of all paired control and OCRL1 depleted cells on the coverslip of a single experiment (n=20). White arrows indicate sites of ZO-1 and Par3 co-localisation. Scale bar 10 μM.

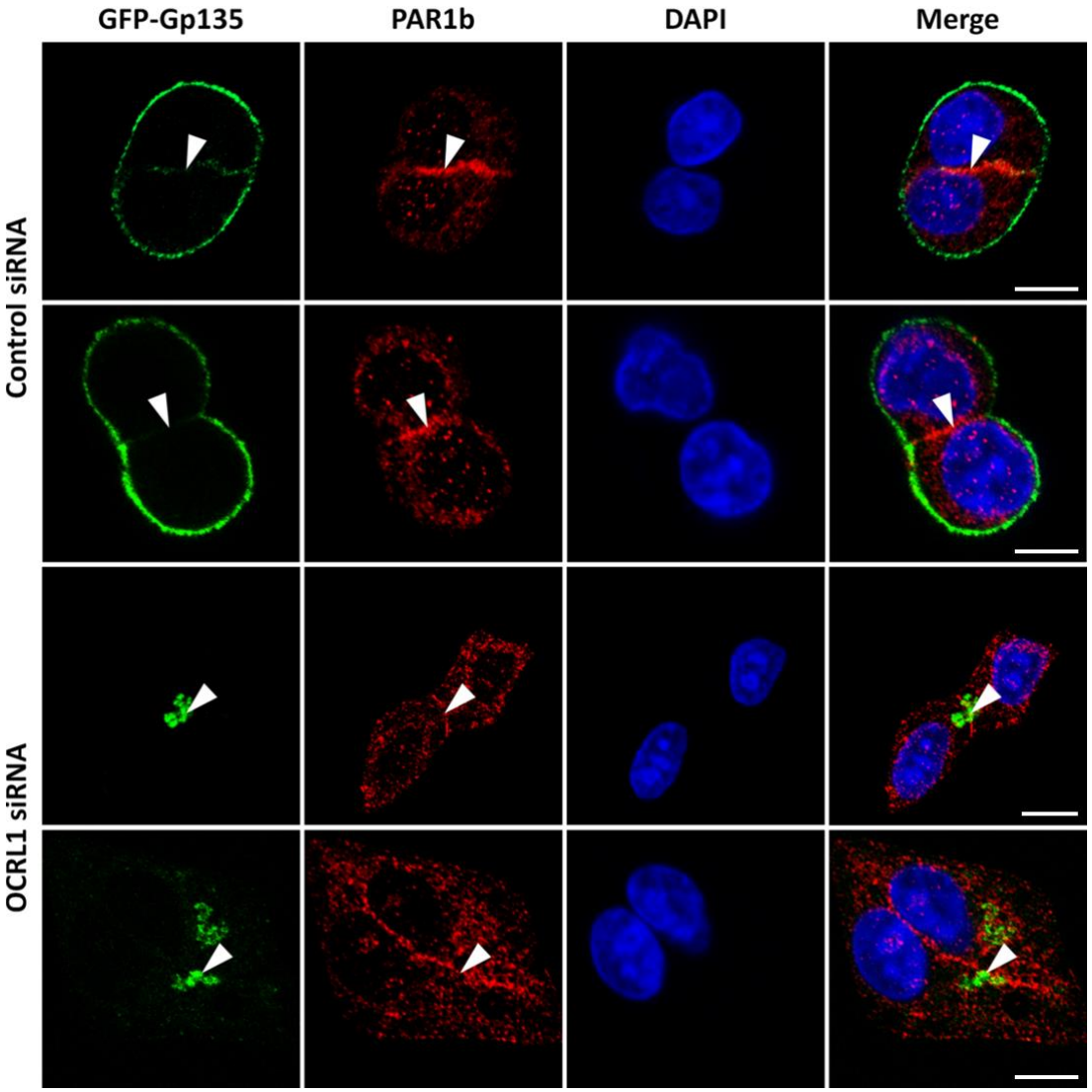

Figure 5.16: Lumen formation initiates in the lateral membrane marked by Par1b. MDCK cells stably expressing GFP-Gp135 were grown and subjected to RNAi as in figure 5.2. Cells were fixed and stained with antibodies to Par1b (red), and the DNA stain DAPI (blue). Images shown are representative of all paired control and OCRL1 depleted cells on the coverslip of a single experiment (n=20). White arrows indicate lateral localisation of Par1b in control cells and sites of Gp135 delivery in OCRL1 depleted cells. Scale bar 10 µM.

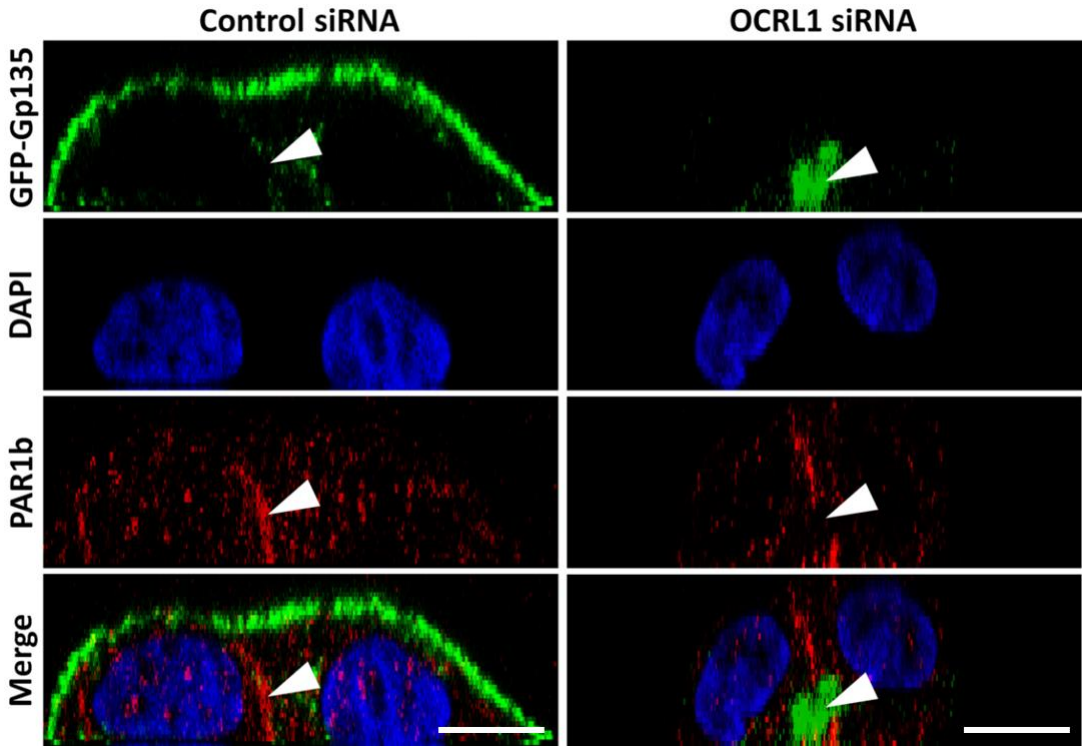

Figure 5.17: XZ images of early lumen formation in the lateral membrane. MDCK cells stably expressing GFP-Gp135 were grown and subjected to RNAi as in figure 5.2. Cells were fixed and stained with Par1b antibodies (red), and the DNA stain DAPI (blue). XZ images were constructed from Z-stacks of 20 single confocal sections. White arrows indicate lateral localisation of Par1b in control cells and sites of Gp135 delivery in OCRL1 depleted cells. Scale bar 10 µM.

PI(4,5)P_2 is enriched on apical carriers when OCRL1 is depleted

OCRL1 is localised to the TGN and a variety of endosome populations. Since OCRL1 is a 5-phosphatase It is likely that OCRL1 functions to regulate the levels of PI(4,5)P_2 on these compartments. Small levels of PI(4,5)P_2 on endosomes is thought to aid the budding process by recruiting proteins involved in membrane curvature and by promoting F-actin organisation near the bud. Therefore PI(4,5)P_2 may be present on the TGN and endosomes normally at a low but functionally important level which would need to be regulated spatially and temporally by phosphatases such as OCRL1.

When OCRL1 is depleted, the population of PI(4,5)P_2 at the Golgi apparatus and endosomes might increase beyond normal levels, affecting endosome function. In yeast, inactivation of synaptojanins results in an accumulation of PI(4,5)P_2 intracellularly due to the lack 5-phosphatase activity (Stefan et al. in 2002). In HeLa cells, OCRL1 depletion results in detectable levels of PI(4,5)P_2 intracellularly, using the GFP tagged PLCδ-PH probe (Vicinanza et al., 2011). The intracellular PI(4,5)P_2 in these cells co-localised with the transferrin receptor, suggesting increasing the level of this phosphoinositide may affect trafficking pathways (Vicinanza et al., 2011). To determine whether OCRL1 depletion effects the intracellular levels of PI(4,5)P_2 in MDCK cells, we also used the PH domain of PLCδ, expressed as a GFP fusion protein, as in figure 4.9. In OCRL1 depleted cells polarising for the first time but lacking OCRL1, pools of PI(4,5)P_2 were visible in a perinuclear region which was clearly absent from control cells (figure 5.18). We next checked whether this pool of PI(4,5)P_2 co-localised with the vesicular Gp135 seen in the absence of OCRL1. This intracellular pool of PI(4,5)P_2 co-localised with the perinuclear Gp135 present when cells were depleted of OCRL1 (figure 5.19), indicating PI(4,5)P_2 enrichment on apical carriers.

Elevated levels of PI(4,5)P_2 on endosomes when OCRL1 is depleted has been reported for other renal proximal tubule cell lines, namely HK-2 cells (Vicinanza et al., 2011). In these cells, the PI(4,5)P_2 induced the accumulation of F-actin on

endosomal membranes (Vicinanza et al., 2011). Images of MDCK cells depleted of OCRL1 above (figure 5.2) suggested F-actin was present intracellularly, co-localising with vesicular Gp135 in the perinuclear region (figure 5.2B). Interestingly, at this early stage in polarisation, when cells were growing in isolation, even control cells had a large perinuclear cluster of Gp135, however no detectable F-actin was present on these structures. These observations suggest the abundance of F-actin in the perinuclear region was specific to loss of OCRL1. We checked to see whether this punctate F-actin co-localised with the PI(4,5)P_2 positive vesicles seen in the absence of OCRL1. In OCRL1 depleted cells, F-actin, PI(4,5)P_2 and Gp135 was all found to be enriched in the perinuclear region of the cell (figure 5.20). Previously the Gp135 compartment was identified as Rab11 and Rab8 positive, expressing the PH domain of PLCδ in OCRL1 depleted cells and staining for Rab11 revealed PI(4,5)P_2 to be present on this endosomal compartment but not at detectable levels in control cells (figure 5.21). In summary, these results suggest that OCRL1 depletion in MDCK cells leads to the accumulation of PI(4,5)P_2 and F-actin on apical recycling endosomes, potentially blocking exit of apical cargo such as Gp135 from this compartment.

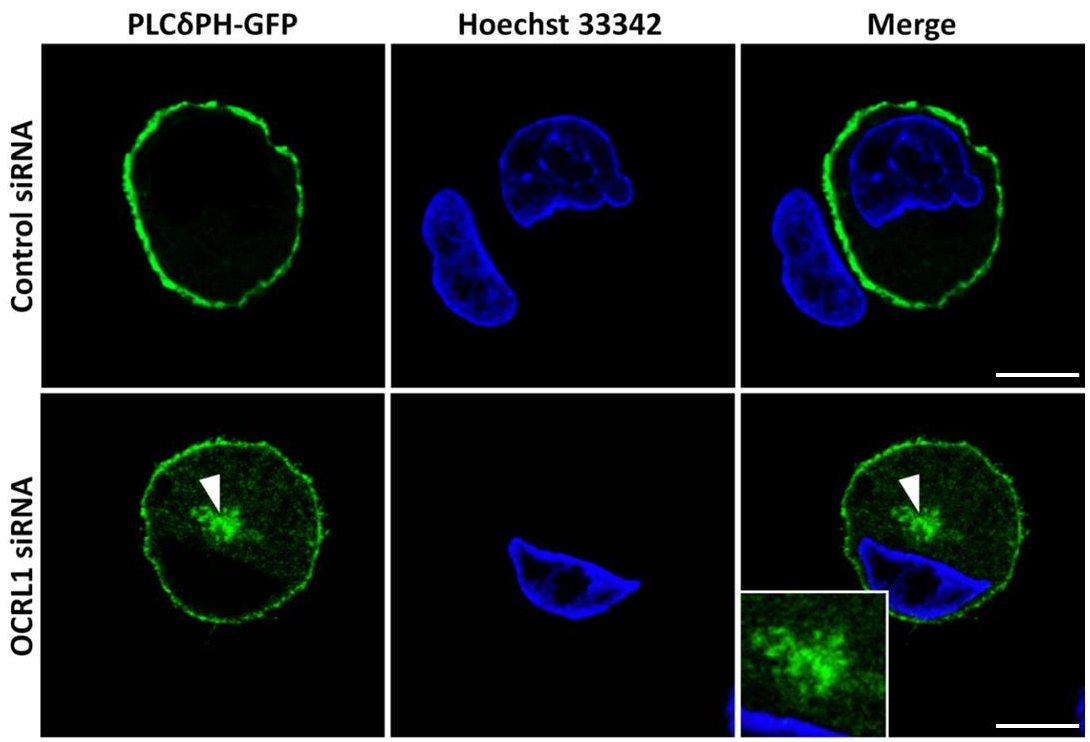

Figure 5.18: PI(4,5)P_2 accumulates intracellularly in live OCRL1 depleted cells. MDCK cells were grown on MaTek dishes and subjected to RNAi as in figure 5.2. 6 hours after RNAi the cells were transfected with PLCδ-PH-GFP DNA (PI(4,5)P_2 binding domain) and left for a further 17 hours. 1 hour before imaging the cells were incubated with the live cell DNA stain Hoechst 33342 (blue) which was washed off before analysis. Cells were imaged in phenol free media on a microscope stage pre-warmed to 37 ^{o}C. Single confocal sections of single cells are shown. A higher magnification image of the OCRL1 depleted cell is shown in the inset. White arrow indicates vesicular accumulations of PI(4,5)P_2 in an OCRL1 depleted cell. Images shown are representative of all control and OCRL1 depleted cells observed in 3 experiment (n=15). Scale bar 10 μM.

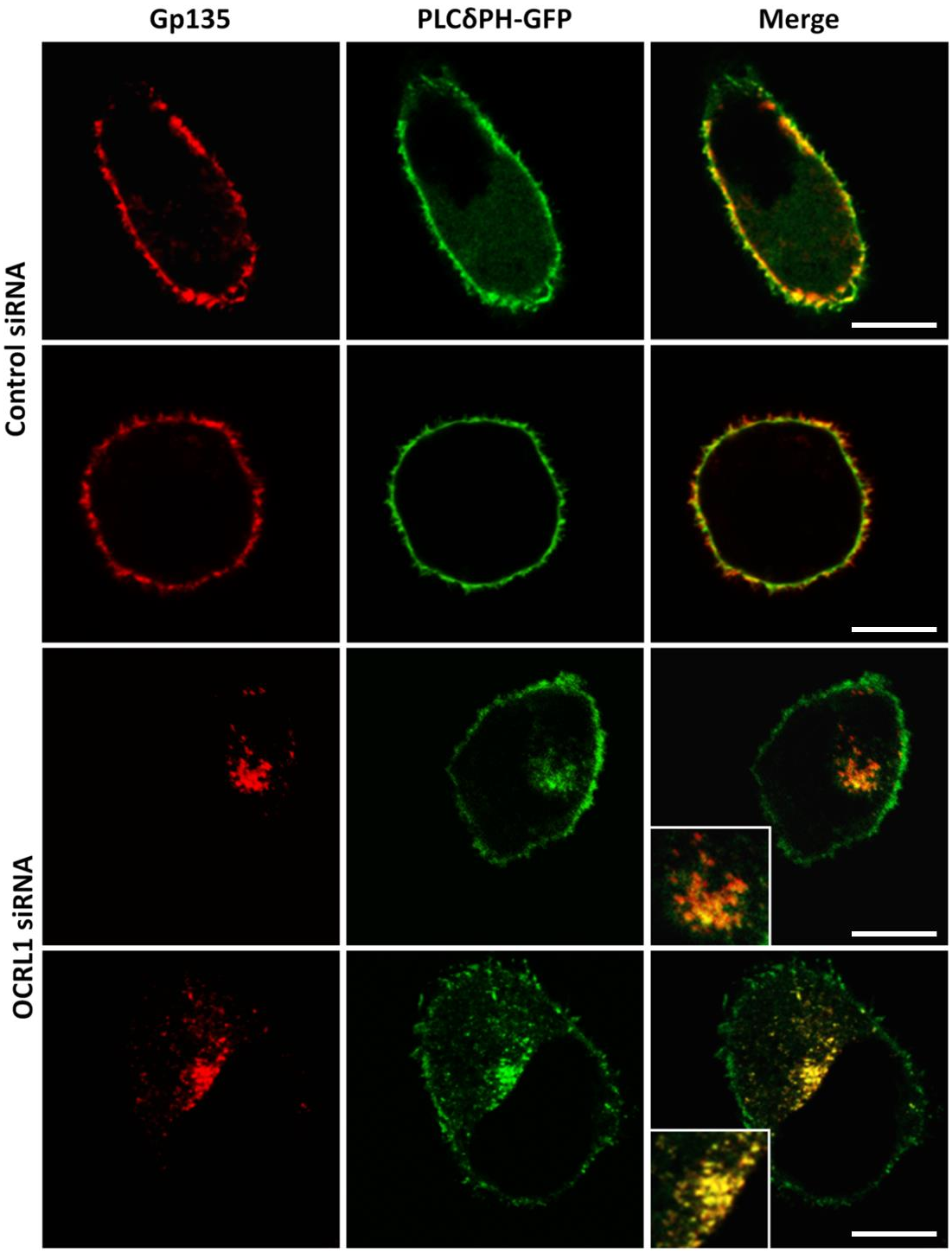

Figure 5.19: PI(4,5)P_2 co-localised with internal Gp135 after OCRL1 depletion. MDCK cells were grown and subjected to RNAi as in figure 5.2 and transfected with PLCδ-PH-GFP DNA (PI(4,5)P_2 binding domain) as in figure 5.18. Cells were fixed and permeabilised for staining with antibodies to Gp135 (red). Single confocal sections are shown of single control and OCRL1 depleted cells (n=10, 2 experiments). Higher magnification images of OCRL1 depleted cells are shown in the insets. Scale bar 10 μM.

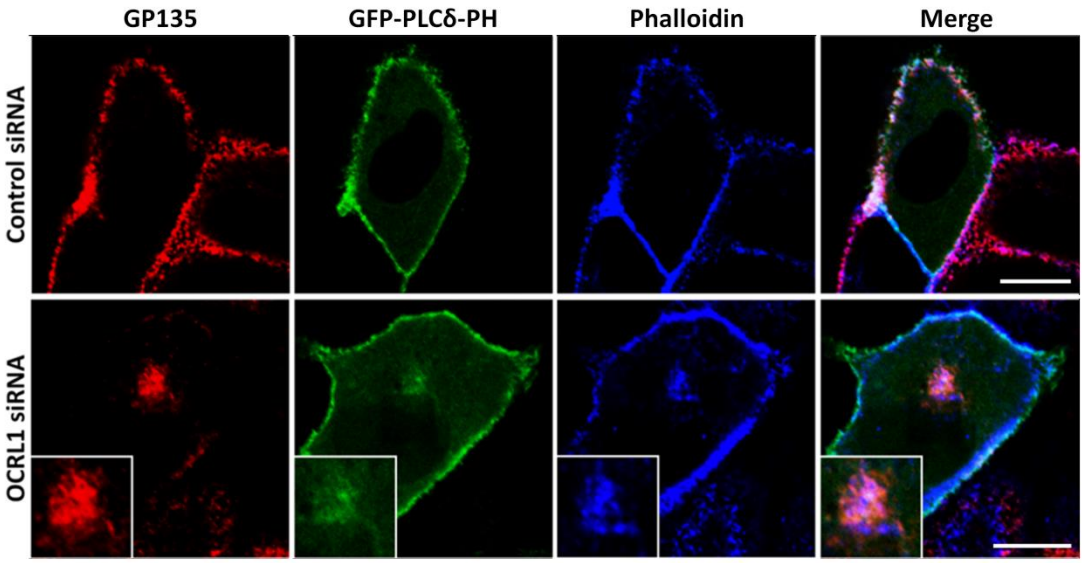

Figure 5.20: F-actin accumulates on PI(4,5)P_2 positive pools of Gp135. MDCK cells were grown and subjected to RNAi as in figure 5.2 and transfected with PLCδ-PH-GFP DNA (PI(4,5)P_2 binding domain) as in figure 5.18. Cells were fixed and permeabilised for staining with antibodies to Gp135 (red) and the actin stain Cy5-phalloidin (blue). Single confocal sections are shown of control and OCRL1 depleted cells (n=10, 2 experiments). Higher magnification images are shown of the OCRL1 depleted cell. Scale bar 10 µM.

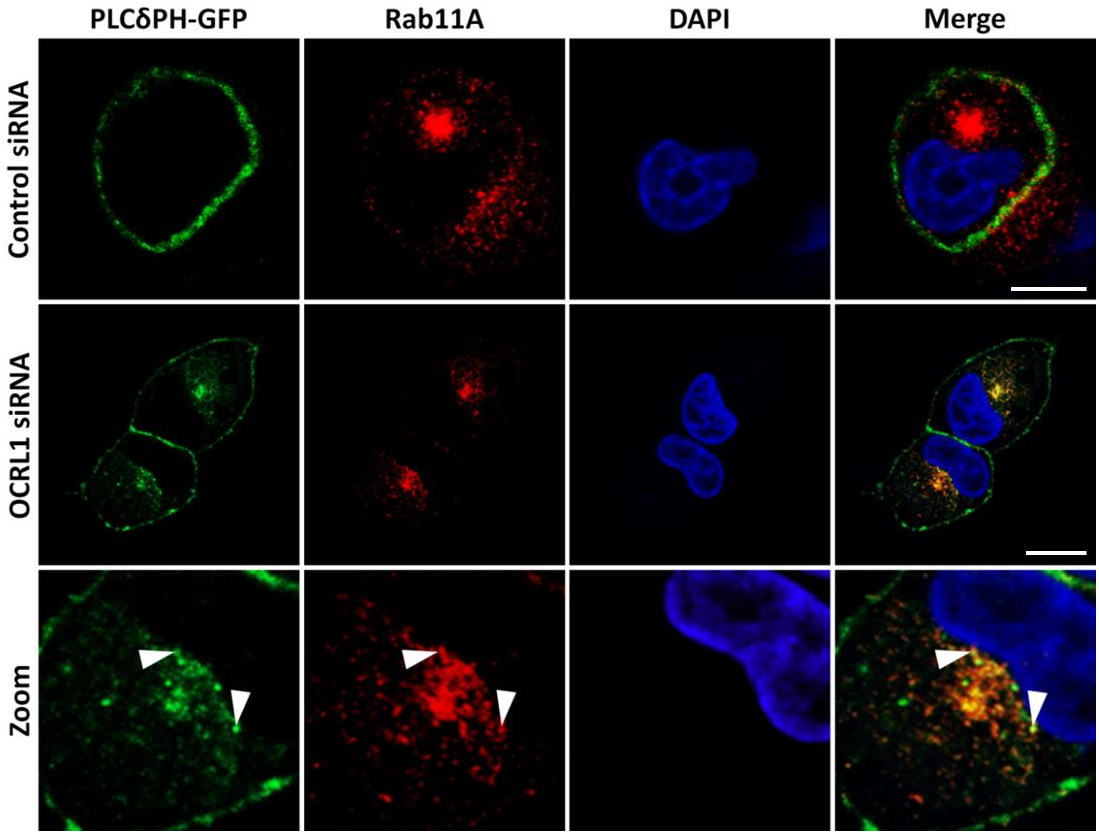

Figure 5.21: Internal PI(4,5)P_2 co-localises with Rab11A upon OCRL1 depletion. MDCK cells were grown and subjected to RNAi as in figure 5.2 and transfected with PLCδ-PH-GFP DNA (PI(4,5)P_2 binding domain) as in figure 5.18. Cells were fixed and permeabilised for staining with Rab11A antibodies (red) and the DNA stain DAPI (blue). Single confocal sections are shown of control and OCRL1 depleted cells (n=10, 2 experiments). Higher magnification images are shown of the OCRL1 depleted cell. White arrows indicate the regions of PI(4,5)P_2 and Rab11A co-localisation in an OCRL1 depleted cell. Scale bar 10 µM.

Apical recycling requires down-regulation of 5-phosphoinositides

Since $PI(4,5)P_2$ and F-actin accumulate on endosomes without OCRL1 (figure 5.20 and figure 5.21), one possibility is that elevated levels of $PI(4,5)P_2$ on the membranes of these compartments blocks exit of apical cargo. To test this, we carried out a series of rescue experiments where endogenous OCRL1 was depleted with siRNA oligos specific for canine OCRL1 and recombinant full length human OCRL1 or a phosphatase-null mutant was re-expressed as a GFP fusion protein. The aim of these experiments was to determine whether the phosphatase domain of OCRL1, which down-regulates the levels of $PI(4,5)P_2$, is required to rescue the apical recycling defect induced by OCRL1 depletion.

Firstly, we co-transfected a GFP expressing plasmid together with control or OCRL1 siRNA to demonstrate that addition of the plasmid DNA did not affect the results of the experiment. OCRL1 depleted cells expressing GFP appeared the same as un-transfected neighbours, accumulating Gp135 entirely in a perinuclear pool (Knock-down; figure 5.22A). Similarly, cells treated with control siRNA and expressing GFP were comparable to neighbouring cells and Gp135 localised to the peripheral membrane (Knock-down control; figure 5.22B). These results can be clearly seen in higher magnification images of GFP expressing cells neighbouring un-transfected cells (figure 5.22A/B).

We next carried out the same experiment using full length OCRL1 tagged with GFP or a phosphatase-null mutant. OCRL1 depleted cells expressing the full length protein with phosphatase domain intact was able to rescue recycling of Gp135. In OCRL1 depleted cells re-expressing the full length protein, Gp135 predominately localised to the plasma membrane (Rescue; figure 5.22C) and these cells were comparable to cells transfected with a combination of non-targeting control siRNA and GFP (Knock-down control; figure 5.22B). Cells not expressing full length OCRL1 and treated with OCRL1 siRNA maintained the recycling defect (Rescue; figure 5.22C), indicating that expression of full length human OCRL1 was responsible for rescuing the phenotype. Cells rescued by re-expressing OCRL1 neighbouring non-

expressing OCRL1 depleted cells are shown in higher magnification images (Rescue; figure 5.22C). These results suggest that re-expression of OCRL1 can rescue the recycling defect seen upon depletion of OCRL1 and indicate that these effects are specific to OCRL1 levels. We next carried out similar rescue experiments with the phosphatase-null mutant OCRL1 (Rescue control; figure 5.22D). Cells depleted of OCRL1 but expressing the phosphatase-null mutant OCRL1 were indistinguishable from neighbouring cells not expressing the protein and were comparable to OCRL1 depleted cells expressing GFP alone (Knock-down control; figure 5.22B); therefore OCRL1 lacking phosphatase activity was unable to rescue the recycling defect caused by loss of the endogenous protein (Rescue control; figure 5.22D). These results suggest that the phosphatase activity of OCRL1 is required to rescue apical recycling in OCRL1 depleted cells.

The results of the rescue experiment can be seen clearly in XZ images of cells in this experiment. Cells expressing GFP and treated with OCRL1 siRNA (Knock down; figure 5.23A) or control siRNA (Knock-down control; figure 5.23B) were similar in appearance to their un-transfected neighbours. However, cells treated with OCRL1 siRNA and transfected with full length OCRL1 were not comparable to their un-transfected neighbours (Rescue; figure 5.23C). In these cells, Gp135 localised to the plasma membrane of the re-expressing cell but was absent from the plasma membrane in the un-transfected neighbour (Rescue; figure 5.23C). In contrast, this effect was not observed with cells re-expressing the phosphatase-null mutant OCRL1. Despite expression of the mutant OCRL1, both the transfected cell and its un-transfected neighbour lost the plasma membrane localisation of Gp135 which accumulated intracellularly (Rescue control; figure 5.23D). These results suggest the phosphatase domain of OCRL1 is required for endosomal recycling of Gp135 to the plasma membrane.

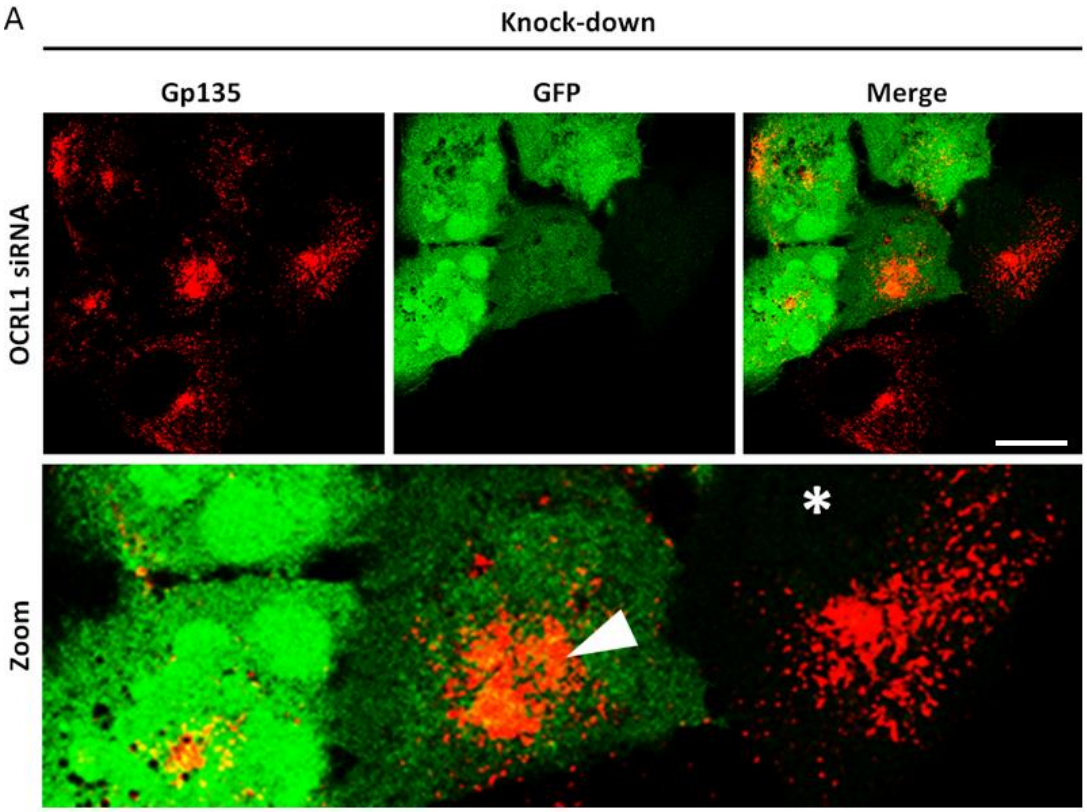

Figure 5.22A: The phenotype of OCRL1 depletion is unaffected by expression of GFP. MDCK cells were grown as in figure 5.2. 6 hours after plating the cells were co-transfected with OCRL1 siRNA and a GFP expressing plasmid and left for a further 17 hours. Cells were fixed and permeabilised for staining with Gp135 antibodies (red). Representative single confocal sections are shown of transfected OCRL1 depleted cells and their un-transfected neighbours (*). Experiment repeated twice, results shown from a single experiment. A higher magnification image is shown of the merged OCRL1 depleted cell. White arrow indicates perinuclear pool of Gp135 in a transfected cell. Scale bar 10 μM.

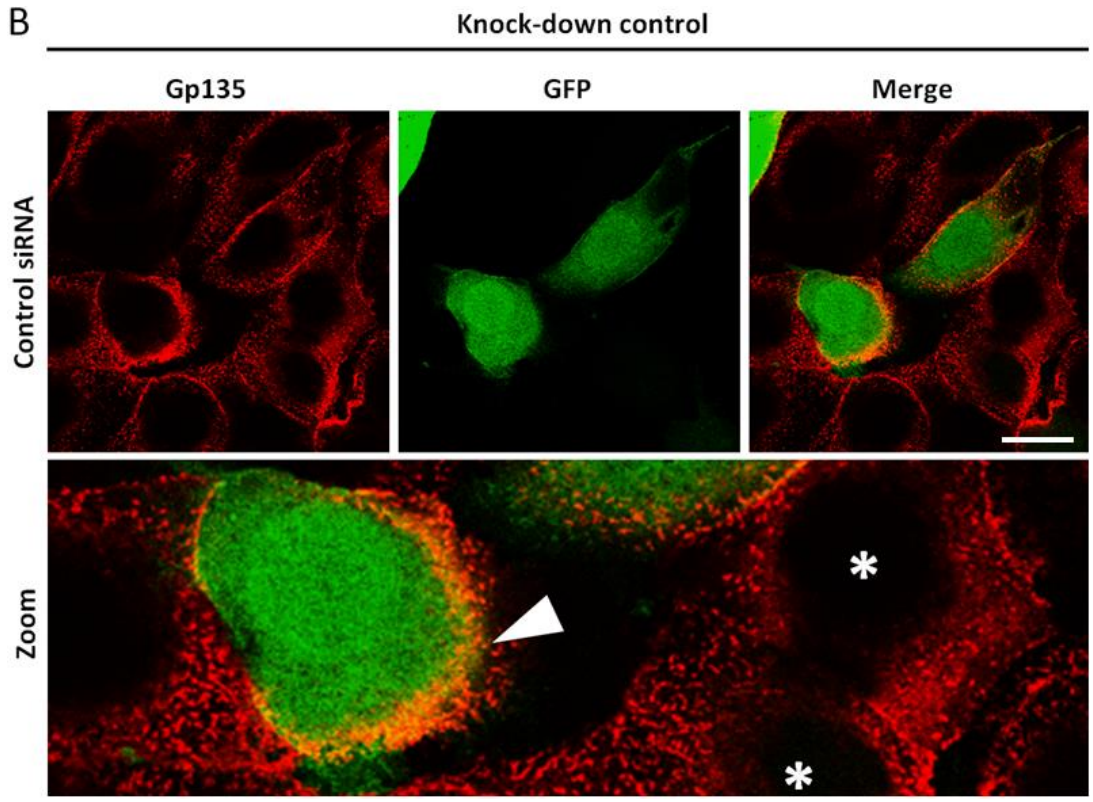

Figure 5.22B: The appearance of control cells is unaffected by expression of GFP. MDCK cells were grown, treated with non-targeting control siRNA, transfected with GFP, fixed and stained as in A. Representative single confocal sections are shown of transfected control cells and their un-transfected neighbours (*).Experiment repeated twice, results shown from a single experiment. A higher magnification image is shown of the merged control cell. White arrow indicates peripheral localisation of Gp135 in transfected cell. Scale bar 10 µM.

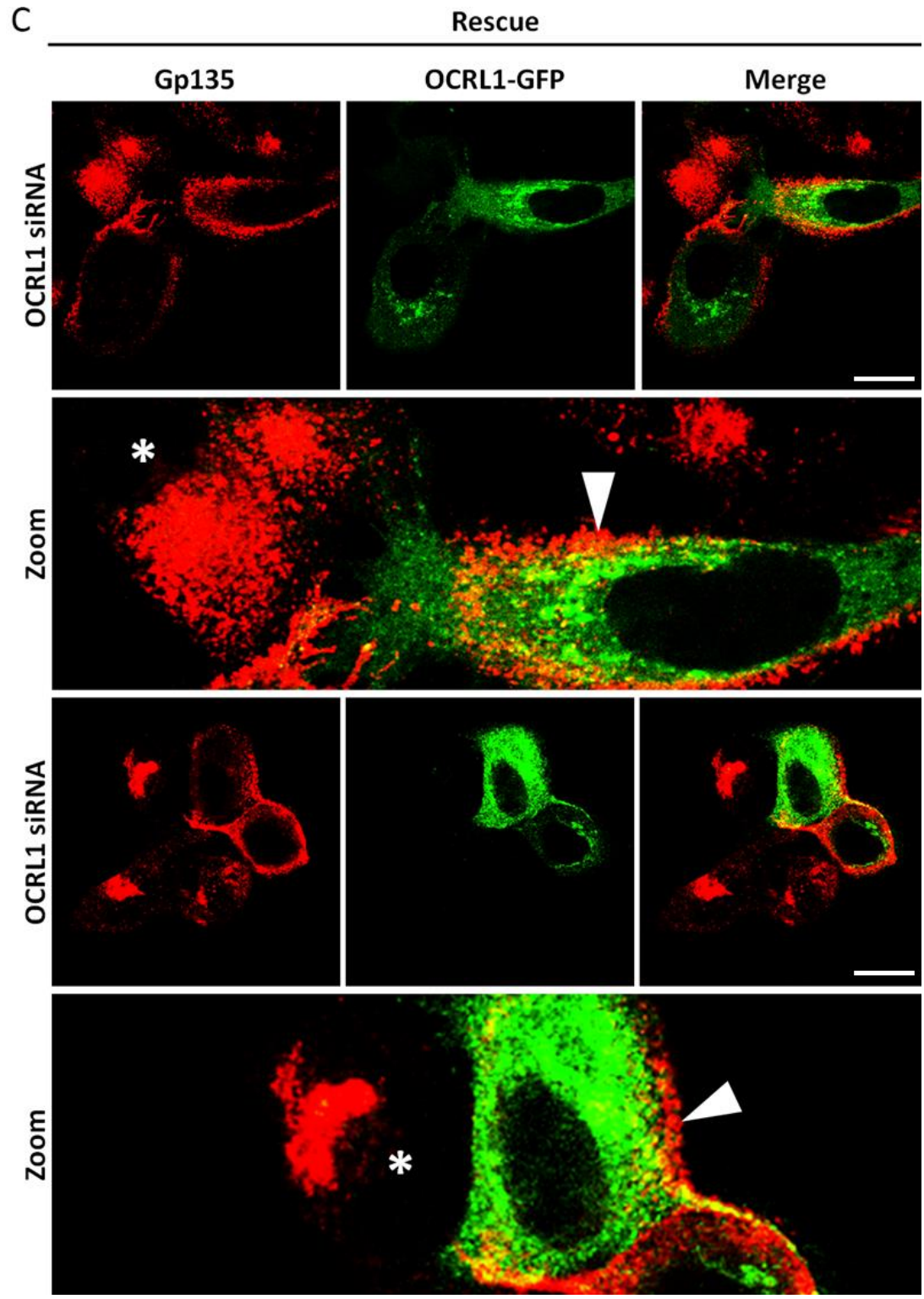

Figure 5.22C: Re-expression of full length OCRL1 rescues apical recycling. MDCK cells were grown, treated with OCRL1 siRNA, transfected with OCRL1-GFP, fixed and stained as in A. Representative confocal sections are shown of transfected cells and their un-transfected neighbours (*).Experiment repeated twice, results shown from a single experiment. Higher magnification images are shown of the merged channels. White arrows indicate peripheral localisation of Gp135 in transfected cells which is absent from un-transfected cells. Scale bar 10 µM.

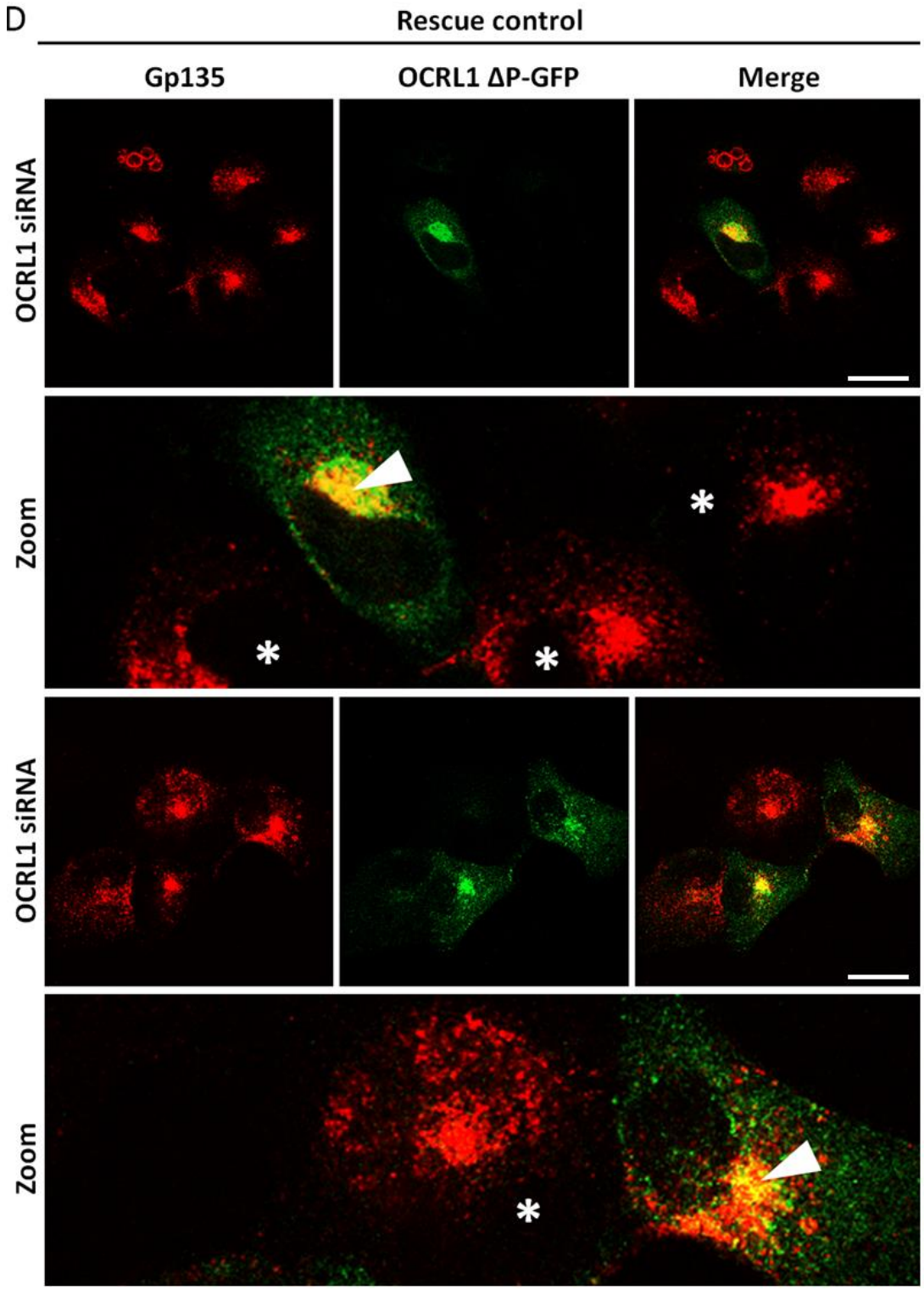

Figure 5.22D: The phosphatase domain of OCRL1 is required to rescue apical recycling. MDCK cells were grown, treated with OCRL1 siRNA, transfected with OCRL1-ΔPhosphatase-GFP, fixed and stained as in A. Representative confocal sections are shown of transfected cells and their neighbours (*). Experiment repeated twice, results shown from a single experiment. Higher magnification images are shown of the merged channels. White arrows indicate perinuclear localisation of Gp135 in transfected cells which is also present in un-transfected cells. Scale bar 10 µM.

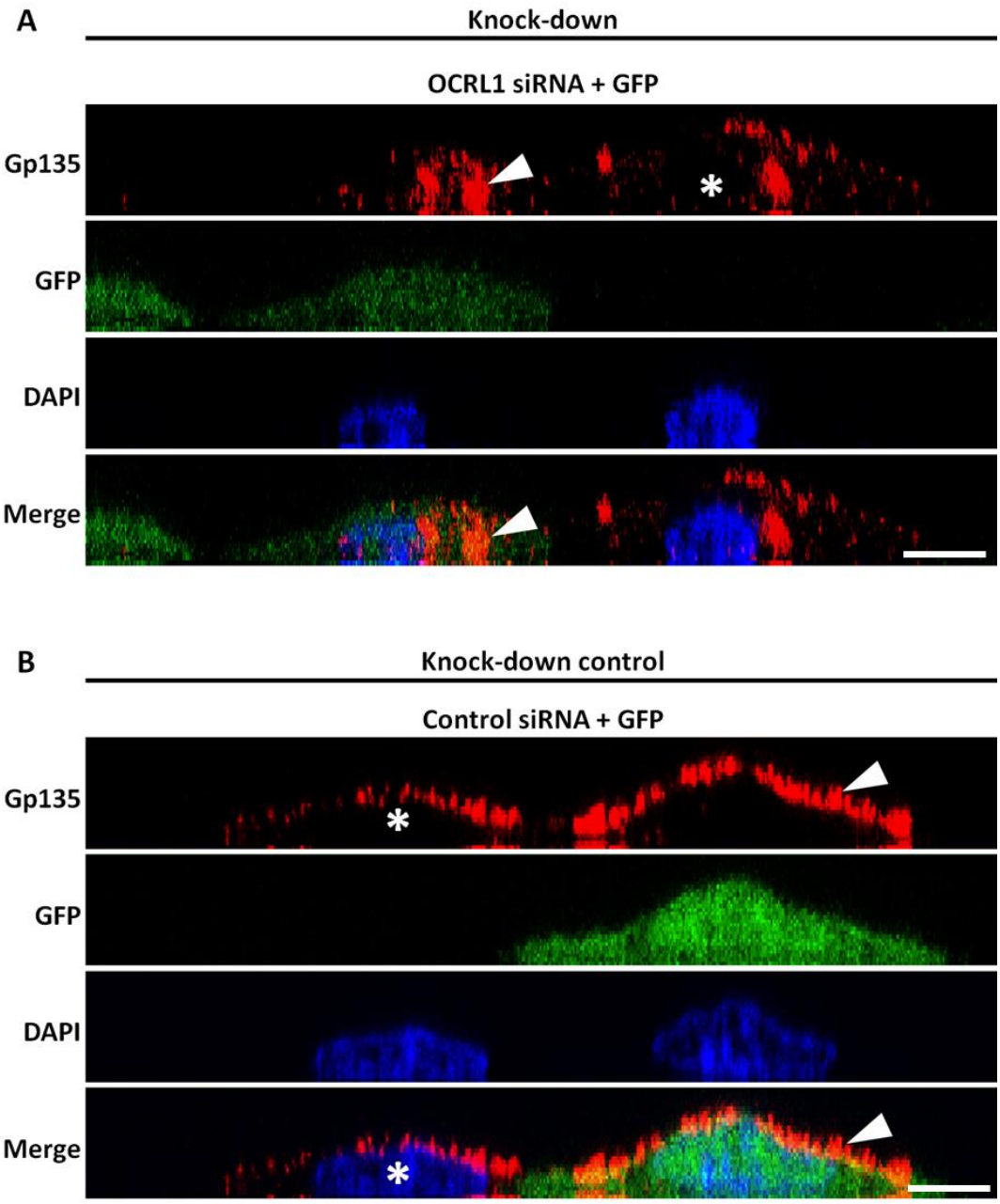

Figure 5.23A-B: XZ images showing the expression of GFP does not affect the phenotype of OCRL1 depletion and control. Cells were from the same coverslips as figure 5.22A and B. MDCK cells treated with OCRL1 siRNA or non-targeting control siRNA were transfected with GFP expression plasmid, fixed and stained with antibodies to Gp135 (red) and the DNA stain DAPI (blue). XZ images were constructed from Z-stacks of 40 confocal sections. A: OCRL1 depleted cells expressing GFP, neighbouring un-transfected cells (*). White arrow indicates perinuclear Gp135 in cell expressing GFP. B: Cells treated with control siRNA expressing GFP, neighbouring un-transfected cells (*). White arrow indicates peripheral localisation of Gp135. Experiment repeated twice, results shown from a single experiment. Scale bar 5 µM.

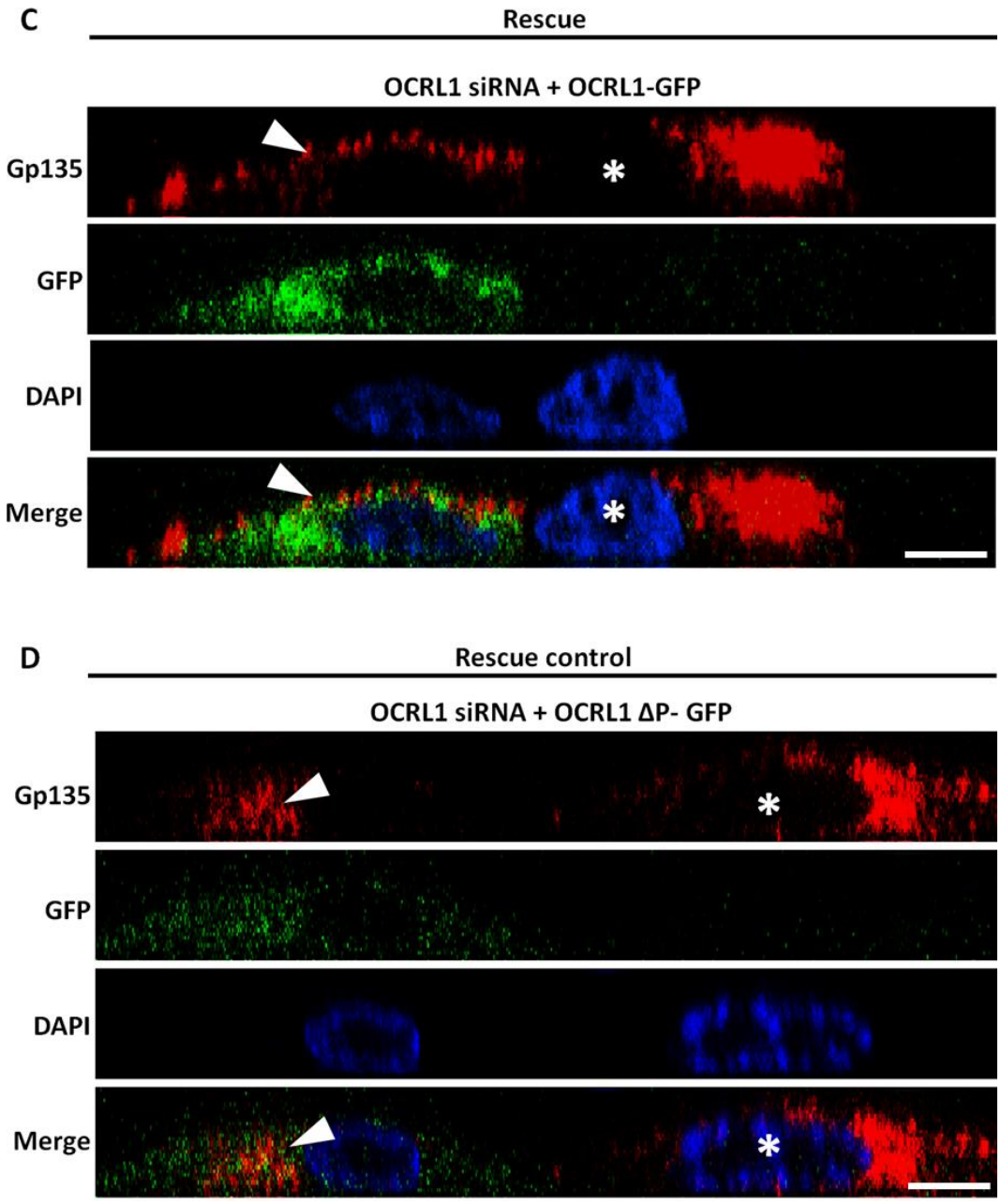

Figure 5.23C-D: XZ images showing full length OCRL1 is required to rescue apical recycling. Cells were from the same coverslips as figure 5.22C and D. MDCK cells treated with OCRL1 siRNA were transfected with recombinant GFP fusion proteins, fixed and stained with antibodies to Gp135 (red) and the DNA stain DAPI (blue). XZ images were constructed from Z-stacks of 40 confocal sections. C: OCRL1 depleted cells expressing full length OCRL1-GFP, neighbouring un-transfected cells (*). White arrow indicates peripheral localisation of Gp135 in cell expressing OCRL1-GFP. D: Cells treated with OCRL1 siRNA expressing Δ-Phosphatase-GFP, neighbouring un-transfected cells (*). White arrow indicates perinuclear localisation of Gp135. Experiment repeated twice, results shown from a single experiment. Scale bar 5 μM.

OCRL1 down-regulates F-actin on vesicular carriers in other renal cell lines.

The results above indicate OCRL1 down-regulates PI(4,5)P_2 and F-actin on apical recycling endosomes in MDCK cells to facilitate cargo exit from this compartment. In this section, we tested whether these results were specific to MDCK cells by looking at the distribution of F-actin in other renal cell lines. There are several human proximal tubular cell lines, such as HK-2, but these have problems with de-differentiation (Orosz et al 2004). We decided to work with a cell line derived from a human renal cell carcinoma where the genetic lesion causing de-differentiation had been reverted by re-expression of von Hippel Lindau protein (VHL). In addition, these cells have good function of their apical junctions (Harten et al 2009). This renal cell line (RCC4) was kindly provided by Prof. Patrick Maxwell (Division of Medicine, Rayne Institute, University College London, UK). OCRL1 was depleted for 48 hours with human specific oligonucleotides and F-actin was visualised by using phalloidin. Without OCRL1, these cells accumulated punctate F-actin in a perinuclear region, not seen in controls (figure 5.24). However, unlike MDCK cells, OCRL1 did not seem to affect cell number within the time-frame of the experiment, suggested by the similar number of nuclei in each confocal section (figure 3.24).

We next looked at the effects of OCRL1 depletion on actin distribution in the hTERT immortalised human renal cell line (NHPTK), used previously in Chapter 3. In Chapter 3 we showed that OCRL1 depletion affected the overall morphology of NHPTK monolayers (figure 3.12). Looking more closely at these cells, we observed punctate F-actin staining on perinuclear vesicles and occasionally perinuclear vacuoles were observed (figure 5.25). These results indicate that OCRL1 might regulate F-actin on trafficking intermediates in other renal cell lines. In addition, the formation of vacuoles in the NHPTK cell line indicates frustrated plasma membrane delivery of cargo from these compartments when OCRL1 is depleted.

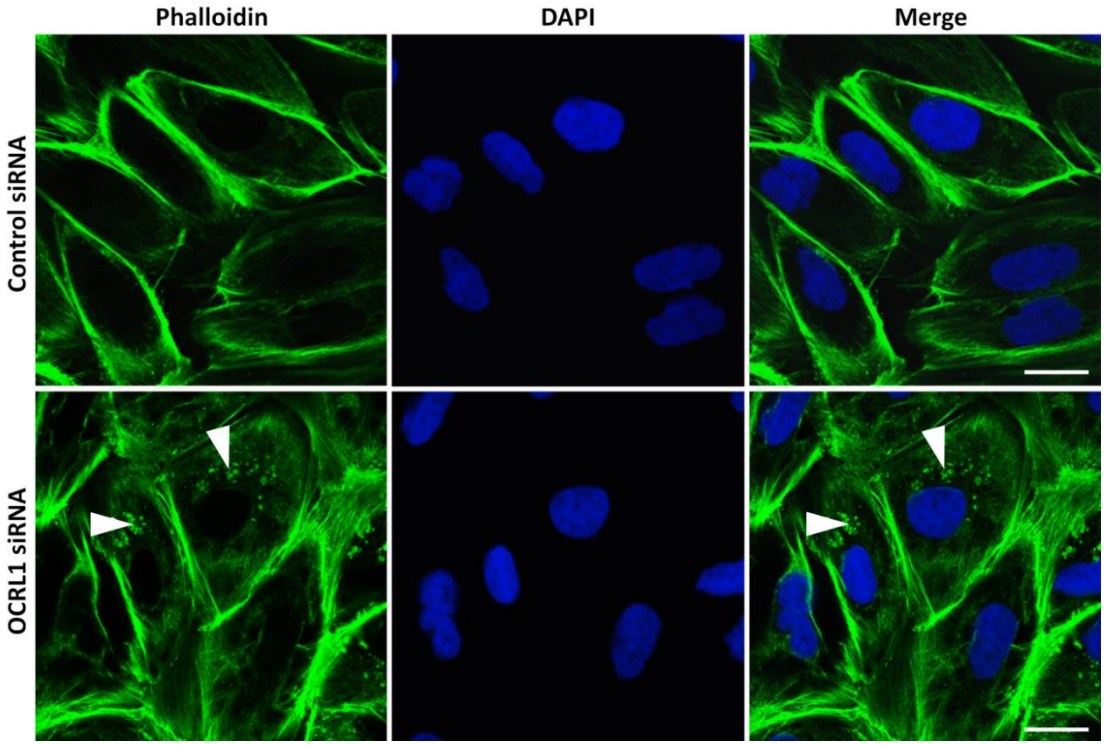

Figure 5.24: OCRL1 depleted RCC4 human renal cells accumulate actin intracellularly. RCC4 stably expressing pVHL were grown for several days. Cells were transfected with non-targeting control or a pool of human specific OCRL1 siRNAs and analysed 48 hours later. Cells were fixed and permeabilised for staining with the F-actin marker phalloidin (green) and the DNA stain DAPI (blue). Representative single confocal sections are shown of cells on the coverslip, experiment repeated twice. White arrows indicate punctate F-actin staining in OCRL1 depleted cells which was absent from controls. Scale bar 10 μM.

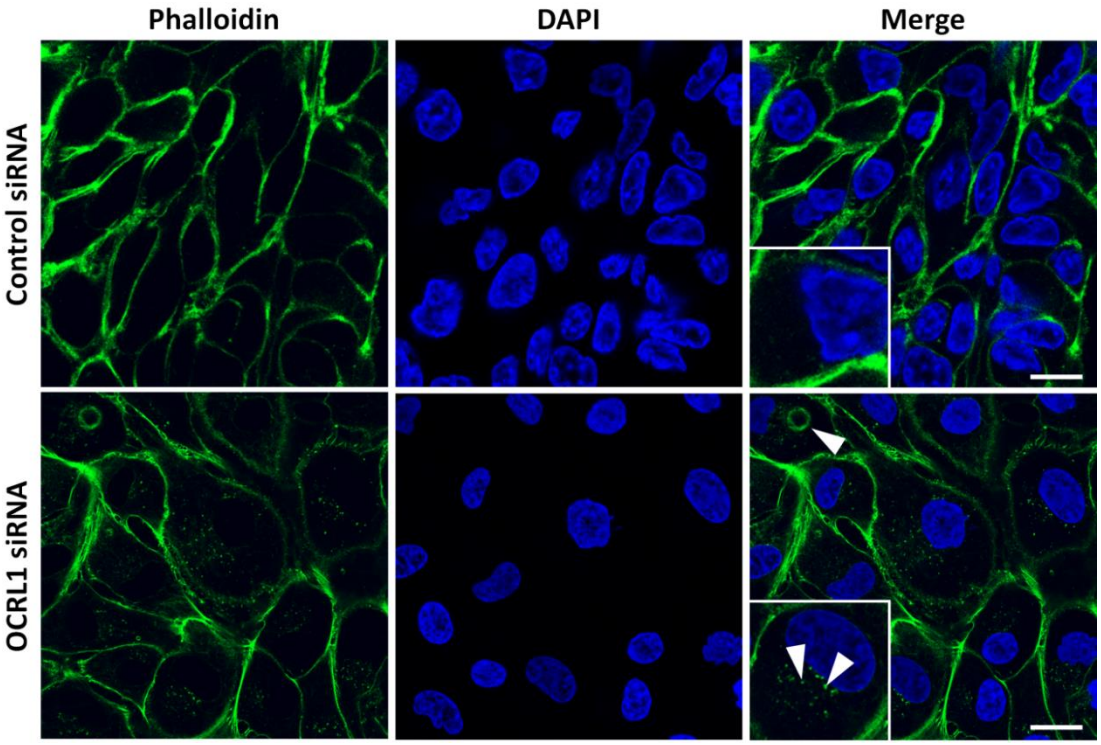

Figure 5.25: OCRL1 depleted NHPTK human renal cells accumulate actin intracellularly. NHPTK cells were grown for several days in culture. Cells were transfected with non-targeting control or a pool of human specific OCRL1 siRNA and analysed 48 hours later. Cells were fixed and stained with the F-actin stain phalloidin (green) and the DNA stain DAPI (blue). Representative single confocal sections are shown of cells on the coverslip, experiment repeated twice. Higher magnification images are shown in the inset. White arrows indicate punctate F-actin staining and vacuoles in OCRL1 depleted cells. Scale bar 10 µM.

Summary

In the previous chapter, loss of OCRL1 affected the gross organisation of polarised membrane domains. OCRL1 depleted cells internalised their apical domain in the form of vacuolar apical compartments (VACs) and subsequently lateralised their apical domain to form lumens between cells. In the previous chapter, VACs and lumens were observed in cells depleted of OCRL1 for several days, suggesting the formation of these structures could be secondary to events that occur sooner after OCRL1 depletion. In this chapter, we aimed to determine the primary role of OCRL1 in polarisation by looking at the first events to occur when the protein was depleted.

In order to study the role of OCRL1 in early polarisation, we made several changes to the experimental protocol used in the previous chapter. Briefly, cells were depleted of OCRL1 for 17-24 hours instead of 48-72 hours, allowing the earliest events to be observed. In addition, rather than depleting monolayers of OCRL1, RNAi was carried out pre-monolayer formation, on single cells growing in isolation. Previously, monolayers were allowed to form intercellular contacts and polarise normally for several days before RNAi. Depletion of OCRL1 in monolayers would require extensive reorganisation of pre-formed junctions and a switch in polarity orientation from a vertical to a horizontal plane. In this chapter, OCRL1 was depleted in un-polarised cells plated for just a few hours before RNAi, so that junction formation and polarisation would begin in the absence of OCRL1, allowing the effects of OCRL1 depletion on these early events to be studied.

Single cells depleted of OCRL1 behaved similarly to monolayers depleted of OCRL1, forming lateral lumens between cells, paired either as a result of cell division or migration on the coverslip. However, lateral lumens developed in monolayers after approximately 72 hours without OCRL1 and formed via an intermediary VAC-like structure. In contrast, when un-polarised cells were depleted of OCRL1, lumens appeared within 24 hours and almost always formed without an intermediary VAC. Instead, vesicular apical cargo was trafficked directly from a perinuclear region to

the site of lumen formation. Interestingly, a similar pool of vesicular apical material was observed pre-vacuole formation in monolayers depleted of OCRL1 for just 24 hours, suggesting the VACs observed at 48 hours are formed from this material. Similarly, in other studies VACs form by the fusion of apical carriers when trafficking to the plasma membrane is prevented (Gilbert et al., 1991; van Zeijl and Matlin, 1990), further suggesting apical trafficking defects in the absence of OCRL1. The requirement for cells growing in monolayers to reorganise junctions and repolarise might delay lateral lumen formation, resulting in the fusion of apical carriers to form VAC-like structures. In contrast, un-polarised cells depleted of OCRL1 begin polarising in the horizontal plane without the need for extensive reorganisation, which might explain the time scale difference of lumen formation between monolayers and single cells. However, the common accumulation of vesicular apical cargo in both experimental systems suggested this may be a primary effect of OCRL1 loss. The rest of the chapter focussed on characterising the vesicular cargo that accumulated upon OCRL1 depletion rather than the vacuoles which formed as a consequence of this effect.

A number of findings suggested OCRL1 depletion disrupted apical recycling pathways, leading to the accumulation of apical vesicles intracellularly. Firstly, the vesicular pool of apical cargo observed upon OCRL1 depletion appeared to originate from a recycling pool of the Rab11/Rab8 apical trafficking pathway. In addition, FRAP analysis confirmed that a small population of apical cargo was subjected to endocytic recycling normally, suggesting the exaggerated pool of apical material observed in OCRL1 depleted cells resulted from an inability to recycle cargo back to the cell surface. OCRL1 has previously been implicated to regulate cargo exit from recycling endosomes by down-regulating $PI(4,5)P_2$ and F-actin on these membranes (Vicinanza et al., 2011). Similarly, expression of PLCδ(PH)-GFP in MDCK cells revealed ectopic accumulations of $PI(4,5)P_2$ and F-actin on recycling endosomes when OCRL1 was depleted. Rescue experiments confirmed that down-regulation of 5-phosphoinostides was required for cargo to exit from endosomes; the catalytic activity of OCRL1 was required to recover apical recycling to the cell surface. These results indicate the block in recycling observed when OCRL1 was depleted was due

to elevated levels of $PI(4,5)P_2$ on endosomes. However these affects were only temporary; eventually the perinuclear apical material was trafficked to the lateral membrane to form a lumen. The rest of this chapter sought to understand the mechanism of lumen formation by studying the distribution of key polarity proteins responsible for positioning the apical membrane.

Apical polarity complexes are thought to be targeted to the apex of the cell early during development where they regulate junction formation and induce expansion of the apical membrane. OCRL1 depleted cells formed intact apical membranes and developed junctions, therefore the function of these polarity complexes appeared to be unaffected by loss of OCRL1. However, the formation of the apical membrane in the wrong place suggested these apical polarity complexes might be aberrantly targeted to the lateral membrane in the absence of OCRL1. We looked at the localisation of a number of these proteins during various stages of lumen formation. Interestingly, the Rab11/Rab8 positive perinuclear cluster of apical cargo also carried the apical polarity complex Par6-aPKC and Cdc42, suggesting this complex is trafficked to the site of lumen formation in a similar manner to Gp135. In contrast, the apical polarity protein Par3 was not present on recycling endosomes of OCRL1 depleted cells; instead Par3 was enriched at the position of lumen formation and appeared to mark the site for insertion of the apical membrane. During early lumen formation, apical cargo including Gp135 and Par6-aPKC was delivered to Par3 on the lateral membrane, which reorganised from a single band to a ring like structure around the lumen as it was formed. Although Par3 localised to the site of lumen formation, it was not clear why the apical membrane was inserted at this site in OCRL1 depleted cells. However, one possibility is for the molecular mechanism of lumen formation in OCRL1 depleted cells to resemble lumenogenesis in cysts, which is well characterised and discussed below.

Discussion

In this chapter, OCRL1 depletion blocked exit of apical cargo from Rab11/Rab8 positive compartments which in MDCK cells correspond to apical recycling endosomes. In a number of recent studies, OCRL1 has been implicated via its 5-phosphatase activity to be essential for endosome function. Depletion of dOCRL1 in *Drosophila* induced the appearance of enlarged endocytic vacuoles enriched in PI(4,5)P_2 and F-actin which caused the subsequent mis-targeting of PI(4,5)P_2 binding proteins to these membranes (Ben El Kadhi et al, 2011). Similarly Lowe Syndrome cells display ectopic accumulations of PI(4,5)P_2 and associated F-actin on endosomes, which cause a number of recycling receptors to be retained intracellularly (Vicinanza et al., 2011). These findings together with the results of this chapter indicate that PI(4,5)P_2 homeostasis is essential for endosome function. However the precise role of OCRL1 at endosomes remains unclear, possible explanations are discussed below.

OCRL1 becomes associated with vesicles early in the endocytic pathway (Erdmann et al., 2007) and appears to persist on these membranes throughout endosome maturation (Vicinanza et al., 2011), suggesting OCRL1 functions during several stages in the endocytic pathway. The finding that PI(4,5)P_2 levels rise on endosomes when OCRL1 is depleted suggests the function of OCRL1 in the endocytic pathway is to facilitate PI(4,5)P_2 turnover. PI(4,5)P_2 is an established regulator of endocytosis, recruiting numerous components of the clathrin machinery (Haucke, 2005), and facilitating invagination by promoting actin polymerisation near the bud (Smythe and Ayscough, 2006). Therefore it is likely that OCRL1 functions post internalisation to remove this functional pool of PI(4,5)P_2, thereby releasing the endocytic machinery from the newly formed vesicle. However, the reason OCRL1 persists on vesicles after internalisation is not clear. One possibility is that OCRL1 facilitates a phosphoinositide switch from plasma membrane derived PI(4,5)P_2 rich endocytic vesicles to endosomes containing PI(3)P. Therefore OCRL1 might function on endosomes to maintain organelle identity by ensuring the plasma membrane and intracellular membranes have distinct populations of phosphoinositides.

Alternatively, the function of OCRL1 at endosomes might be similar to the proposed role of OCRL1 during endocytosis, to regulate a physiologically functional pool of PI(4,5)P_2. An endosomal pool of PI(4,5)P_2 was not observed in our control cells, however PI(4,5)P_2 has previously been detected on endosomes and other intracellular membranes of untreated cells using high resolution techniques (Watt et al., 2002), suggesting low abundance of PI(4,5)P_2 and limited resolution might explain the lack of detection in our control cells. In addition, the observation that a PI(4,5)P_2 synthesising enzyme (PIPKIγi5) localises to endosomes suggests synthesis of 5-phosphoinositides takes place on these membranes (Schill and Anderson, 2009; Sun et al., 2013). Interestingly, one of these studies demonstrated a requirement for PIPKIγi5 to sort the epidermal growth factor receptor (EGFR) from early endosomes into late endocytic compartments (Sun et al., 2013), further suggesting pools of PI(4,5)P_2 on endosomes have functional roles.

Micro-domains of PI(4,5)P_2 on endosomes might facilitate budding and vesicle biogenesis in a manner comparable to the role of PI(4,5)P_2 in endocytosis. For example, PI(4,5)P_2 could mediate cargo sorting into carriers for progression along the endocytic pathway, or it may induce local F-actin polymerisation to facilitate membrane curvature. Evidence for PI(4,5)P_2 having a role in regulating actin polymerisation on endosomes comes from the finding that loss of OCRL1 increased the level of F-actin associated with these membranes in a N-WASP-dependent pathway (Vicinanza et al., 2011). Therefore, loss of OCRL1 in these cells might exaggerate a normal pathway involving PI(4,5)P_2 and N-WASP actin polymerisation. We similarly observed ectopic levels of F-actin on endosomes in OCRL1 depleted cells, however we were unable to rescue recycling with actin depolymerising agents such as Latrunculin-A and Cytochalasin-D (data not shown). Therefore it remains unclear whether F-actin accumulation was responsible for blocking endosome function in our OCRL1 depleted cells.

The first part of this chapter focussed on the recycling defects of apical cargo induced by OCRL1 depletion. In the second part of this chapter we sought to

understand why OCRL1 depleted cells subsequently targeted this material to the lateral membrane. One possibility is that the internalisation of the apical membrane induced a loss of polarity similar to the response of cells when calcium is depleted. Subsequently, OCRL1 depleted cells might attempt to re-establish polarity by targeting the apical vesicles back to the cell periphery. There is some evidence to suggest apical membrane is normally trafficked to the lateral membrane in a region near the junction. For example, the VACs in calcium switch assays are exocytosed near the junction when calcium is restored. In addition, in early polarisation of our control cells, we saw faint clusters of apical vesicles near the cell-cell contact. Although the VACs in calcium switch assays and OCRL1 depleted cells appear to be exocytosed at the same site near the junction, there must be fundamental differences because VAC exocytosis in calcium switch experiments re-form the apical membrane at the cell apex whereas OCRL1 depleted cells maintain the apical membrane from the VAC in the lateral region of the cell.

One possibility is that OCRL1 depletion promotes hepatic-like lumen polarity in a similar manner to over-expression of Par1b (Cohen et al., 2004a, 2004b, 2007 and 2011), discussed in Chapter 4. Interestingly, hepatic cell polarisation occurs in two stages; upon plating at low confluence hepatic cell lines initially adopt columnar polarity similar to MDCK cells (Cohen et al., 2007; Decaens et al., 1996). Then, over a period of approximately two weeks, columnar cells first internalise their apical membrane to become non-polarised before subsequently repolarising with hepatic polarity (Cohen et al., 2007; Decaens et al., 1996). A similar process could occur when OCRL1 is depleted in MDCK cells, whereby a block in apical recycling initially results in cells becoming non-polarised before cells adopt hepatic-like polarity upon re-polarising. However, in this chapter, OCRL1 depleted cells did not appear hepatic-like. In 2D cultures of hepatic cell lines such as WIFB, luminal domains form in the lateral membrane between neighbouring cells (Treyer and Müsch, 2013). Although pairs of OCRL1 depleted cells formed luminal domains between them in the region of the cell-cell contact, additional cell divisions reinforced the apical domain initiated at the 2-cell stage. For example in figure 5.2B, 6 OCRL1 depleted cells shared a single lumen and the cells appeared to have normal cell-cell contacts.

An alternative possibility is that OCRL1 depleted cells behave like cysts grown in 3D culture and lumen formation is a co-ordinated process in these cells. The pathway involved in lumen formation of MDCK cyst cultures contains many of the same components as the pathway identified here for lateral lumen formation of OCRL1 depleted cells. For example, lumen formation in cysts is initiated by delivery of apical determinants such as aPKC-Par6-Cdc42 and Gp135 to the lateral membrane by a Rab8/Rab11 dependent trafficking pathway (Bryant et al., 2010). Another parallel between lumen formation in cysts and OCRL1 depleted cells was the formation of the apical membrane at sites marked by Par3 (Bryant et al., 2010). Although the molecular mechanism of lumen formation in OCRL1 depleted cells appears similar to lumen formation in MDCK cysts, the primary reason for lateral lumen formation in MDCK cells remained unclear. It's possible that lateral lumens are not a product of disrupted apical trafficking pathways, but that loss of OCRL1 induces additional problems leading to mis-localised apical membranes. In the next chapter, other effects of OCRL1 depletion are explored which might explain lateral lumen formation.

Chapter Six

OCRL1 and cell division in MDCK cells

Overview

In the previous chapter, OCRL1 depletion was shown to disrupt polarised trafficking pathways. In polarised epithelia, polarisation is co-ordinated with cell division so that divisions within the epithelium reinforce rather than disrupt cell polarity. Apical lumen formation in 3D culture is initiated at the two cell stage, after mitosis but before the onset of cytokinesis. One possibility is for cells to utilise the cytokinetic machinery to initiate apical membrane formation. For example, prior to cytokinesis, the midbody is positioned between the daughter cells and may act as the spatial cue to form the apical membrane (Datta et al., 2011). Therefore the positioning of the midbody might be important for determining where the apical membrane is initially formed.

OCRL1 depleted cells growing in 2D culture form apical lumens in the lateral membrane rather than at the apex of the cell. As discussed in the previous chapter, the pathway involved in lumen formation of MDCK cysts growing in 3D culture contains many of the same components as the pathway identified for lateral lumen formation of OCRL1 depleted cells. Lateral lumen formation in OCRL1 depleted cells occurs as early as the two cell stage (see figure 5.2 and figure 5.3) and subsequent divisions reinforce the lumen so that as many as six cells contribute to the apical membrane (figure 5.2). Therefore OCRL1 depletion in 2D culture produces lumens similar to those seen in 3D cyst cultures. Lumen formation in OCRL1 depleted cells is preceded by the accumulation of key apical polarity proteins such as the Par polarity complex and luminal proteins such as Gp135 in Rab11 positive recycling endosomes. These apical components appeared to be subsequently trafficked to a region on the lateral membrane between adjacent cells, where the lumen formed. In the previous chapter, it was unclear why the vesicular apical cargo accumulated in this region of the lateral membrane. However, in 3D culture, lumen formation is thought to occur by the targeting of apical vesicles to the site of cytokinesis. Given the link between cytokinesis and apical membrane formation, lumen formation may be co-ordinated with cytokinesis in OCRL1 depleted cells.

Recently OCRL1 has been implicated in multiple stages of cytokinesis. In *Drosophila*, depletion of dOCRL1 resulted in a high failure rate of furrowing and cells were multinucleated (Ben El Kadhi et al., 2011). Furrowing failed in these cells due to ectopic accumulation of $PI(4,5)P_2$ on endosomes which targeted essential components such as RhoA, myosin and anillin towards endosomes at the expense of the cytokinetic ring (Ben El Kadhi et al., 2011). OCRL1 has also been implicated to be involved in the post furrowing stages of cytokinesis. In HeLa cells, OCRL1 is localised to the intercellular bridge by interacting with Rab35 (Dambournet et al., 2011). Depletion of Rab35 or OCRL1 inhibited cytokinesis abscission and was associated with elevated F-actin and $PI(4,5)P_2$ in the intercellular bridge (Dambournet et al., 2011), suggesting that $PI(4,5)P_2$ regulation by OCRL1 is required for successful cytokinesis. This study was carried out in non-polarised cell lines therefore it is not known whether OCRL1 similarly functions in polarised cells. This chapter investigates whether OCRL1 regulates cytokinesis in the MDCK cell line which may explain the polarity defects observed in previous chapters.

OCRL1 depletion delays abscission of the intercellular bridge

To establish whether OCRL1 plays a role in cytokinesis in the MDCK cell line, the microtubules were visualised with α-tubulin antibodies. The midbody and intercellular bridge can be observed as a highly dense structure at the centre of two microtubule bundles between daughter cells. The same siRNA protocol was used in this chapter as the previous chapter, so that the microtubules could be visualised in cells undergoing lumen formation. Cells were plated and depleted of OCRL1 over the course of 24 hours, approximately 4 hours to adhere to the coverslip and 20 hours of siRNA treatment. Following an initial lag phase, MDCK cells have an approximate doubling time of 21 hours during logarithmic growth (Cho et al., 1989), therefore the majority of cells in this experiment would have had the opportunity to begin dividing without OCRL1. We noticed the number of cells connected by a α-tubulin-positive intercellular bridge increased when OCRL1 was depleted, this is shown in figure 6.1 and quantified in figure 6.2. In control cells, 4% of the population was connected by an intercellular bridge compared to 19% after OCRL1 depletion (500 cells per treatment, p = 0.0003, student's T -test). In contrast to the increase in unresolved intercellular bridges, the number of cells undergoing mitosis was not statistically different, 3.5% of the OCRL1 depleted population was undergoing mitosis compared to 4% of the control population (p=0.9, students T-test). These results indicate that only the abscission stage was delayed during the first round of cell division after OCRL1 depletion. Similar results were shown previously in the HeLa cell line, where the number of cells connected by an intercellular bridge increased from 9.1% in control cells to 19.3% after OCRL1 depletion (Dambournet et al., 2011).

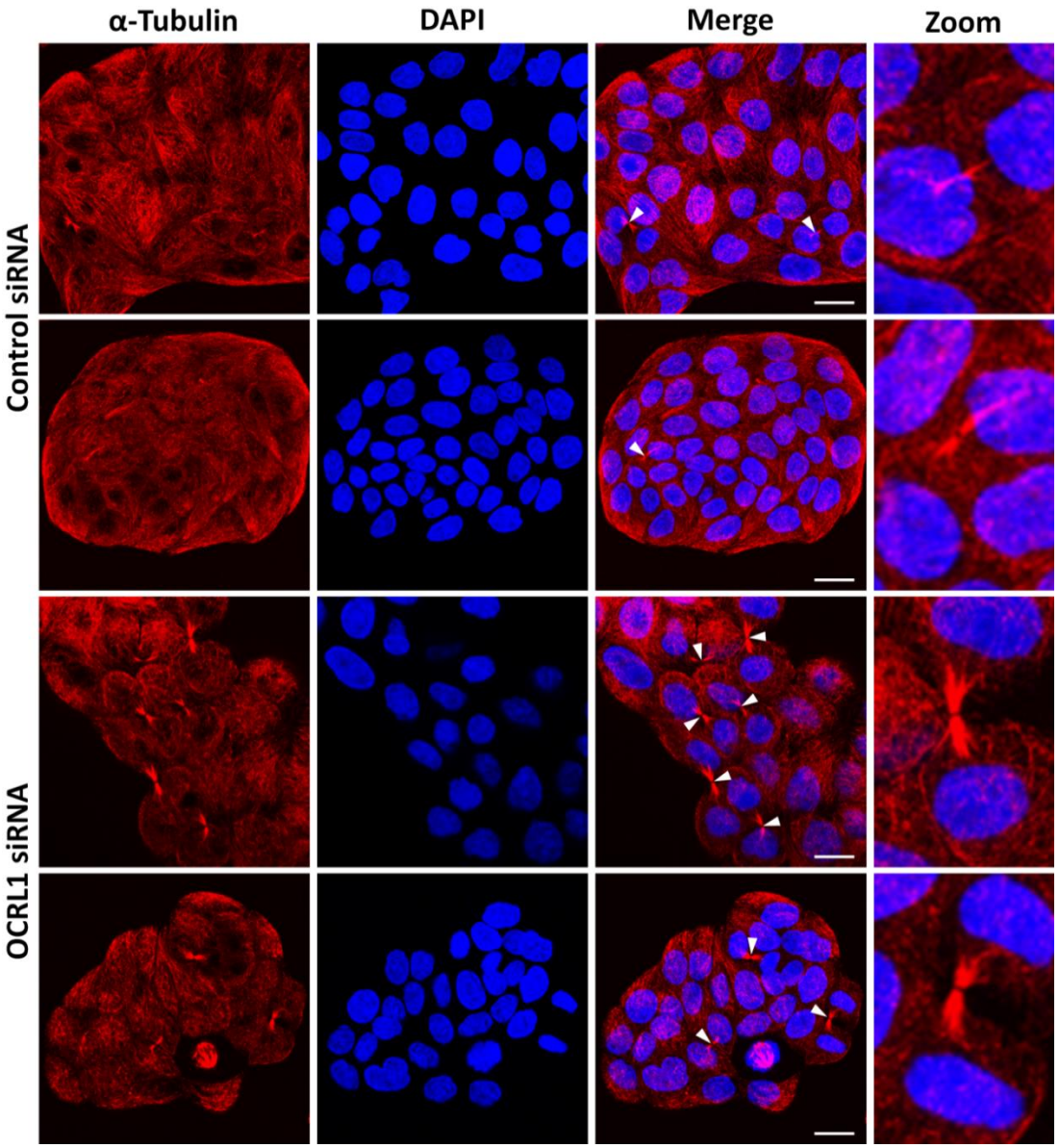

Figure 6.1: OCRL1 depletion delays abscission. MDCK cells were plated for 4 hours before transfection with non-targeting control or OCRL1 siRNA. 20 hours later, the cells were fixed/permeabilised and immunostained with α-tubulin antibodies (red) and the DNA stain DAPI (blue). Images shown are compressed stacks of 10 confocal sections spanning from the bottom to the top of the cell layer from two experiments. White arrows indicate the intercellular bridge formed between pairs of daughter cells. Scale bar 10 µM.

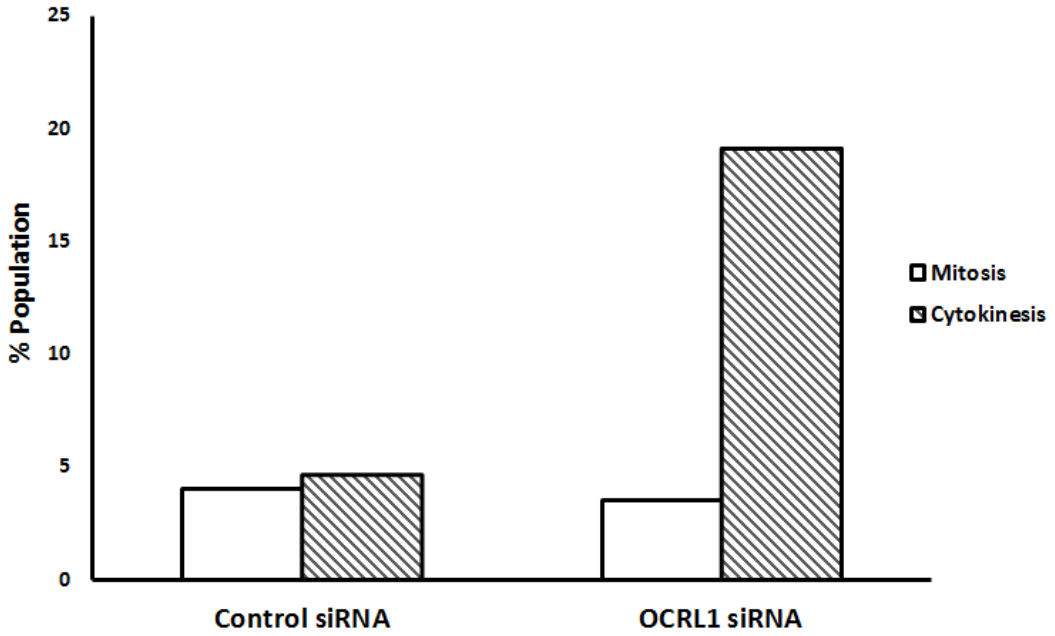

Figure 6.2: Quantification of the abscission defects in OCRL1 depleted cells. Cells were from the same coverslip as Figure 6.1. Confocal stacks containing 10 confocal sections were taken across the coverslip of cells treated with non-targeting control or OCRL1 siRNA in 2 experiments. 10 stacks were used per treatment which amounted to approximately 500 cells per treatment. The number of cells in late stage cytokinesis or mitosis is plotted as a percentage of the total cell count.

OCRL1 localises to spindle poles and the midbody of dividing cells

Previously, OCRL1 was shown to localise to the Golgi apparatus, trafficking intermediates and tight junctions of non-dividing MDCK cells. During cytokinesis of MDCK cells, there was a punctate population of OCRL1 near the midbody of the intercellular bridge (figure 6.3), as shown previously in the HeLa cell line (Dambournet et al., 2011). The midbody is positioned at the centre of the intercellular bridge, identified by the absence of staining with α-tubulin antibodies in contrast to the rest of the intercellular bridge. Higher magnification images of OCRL1 in MDCK cells revealed OCRL1 to be concentrated symmetrically either side of the midbody in two of the intercellular bridges formed between cells (pairs 1 and 3; lower panels figure 6.3) and concentrated more densely on one side of the midbody in one pair of cells (pair 2; lower panels figure 6.3). Several studies report an accumulation of membrane vesicles at the midbody (Goss and Toomre, 2008; Pohl and Jentsch, 2008), with some populations delivered symmetrically by both daughter cells (Goss and Toomre, 2008) and others asymmetrically (Gromley et al., 2005). Therefore the midbody localisation of OCRL1 is likely to correspond to OCRL1 positive vesicles.

In addition to observing the localisation of OCRL1 in cytokinesis, we noticed OCRL1 localised to the spindle poles of mitotic cells prior to cytokinesis (figure 6.4), which was not shown previously (Dambournet et al., 2011). During mitosis, the punctate staining of OCRL1 observed at spindle poles occurred in a region where the centrioles likely reside (figure 6.4). In addition, numerous OCRL1 positive vesicles were focused around the pole, indicated with arrows in the OCRL1 channel only (figure 6.4). During mitosis, the Golgi apparatus fragments into clusters near spindle poles (Seemann et al., 2002), along with recycling endosomes (Hobdy-Henderson et al., 2003; Takatsu et al., 2013). Therefore OCRL1 positive vesicles at spindle poles could correspond to either of these compartments.

In Chapter 5, we showed that OCRL1 depletion resulted in a block of cargo exit from Rab11 and Rab8 positive recycling endosomes. During cytokinesis, this

compartment traffics the cytokinetic machinery to the site and provides the membrane required for furrowing and abscission (Montagnac et al., 2008). Other recycling pathways have been shown to be essential for completing cytokinesis, such as the fast rab35 recycling route (Kouranti et al., 2006). In the HeLa cell line, OCRL1 was targeted to the intercellular bridge in a Rab35 dependent manner (Dambournet et al., 2011). OCRL1 is likely delivered to the midbody by direct interactions with Rab35 on vesicles trafficked to the site (Dambournet et al., 2011). Here we noticed Rab8 also accumulated at the intercellular bridge (figure 6.5), suggesting the possibility that OCRL1 targets the intercellular bridge through interactions with Rab8 GTPase as well as Rab35.

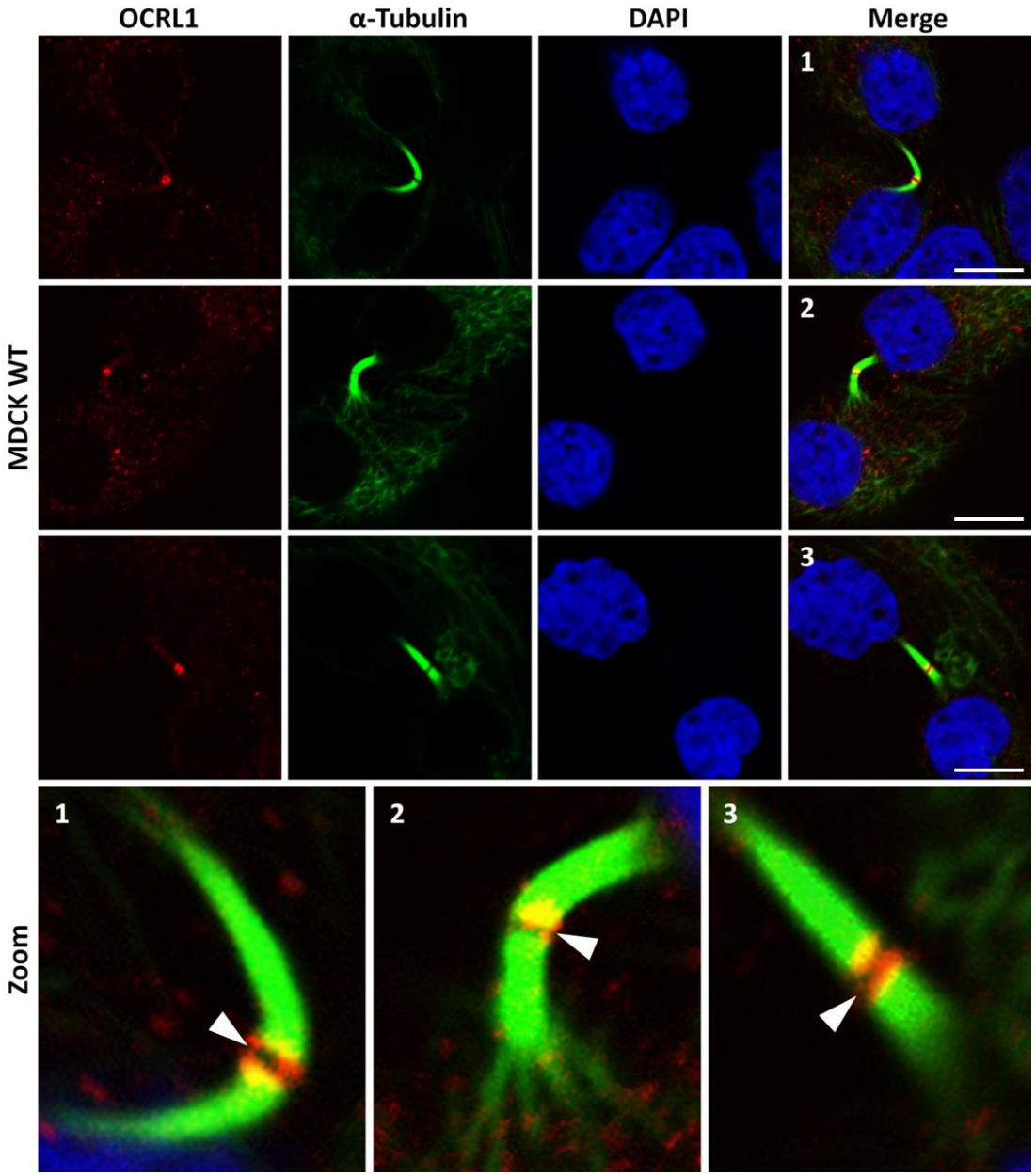

Figure 6.3: OCRL1 localises to the intercellular bridge during cytokinesis. Wild type MDCK cells were grown for 24 hours, fixed and permeabilised for immunostaining with antibodies to α-tubulin (green), OCRL1 (red) and the DNA stain DAPI (blue). Higher magnification images of the merged channels are shown in the bottom panel. White arrows indicate the midbody. Images shown are representative of all cells observed connected by a midbody on the coverslip (n=20) of 2 experiments. Scale bar 10 μM.

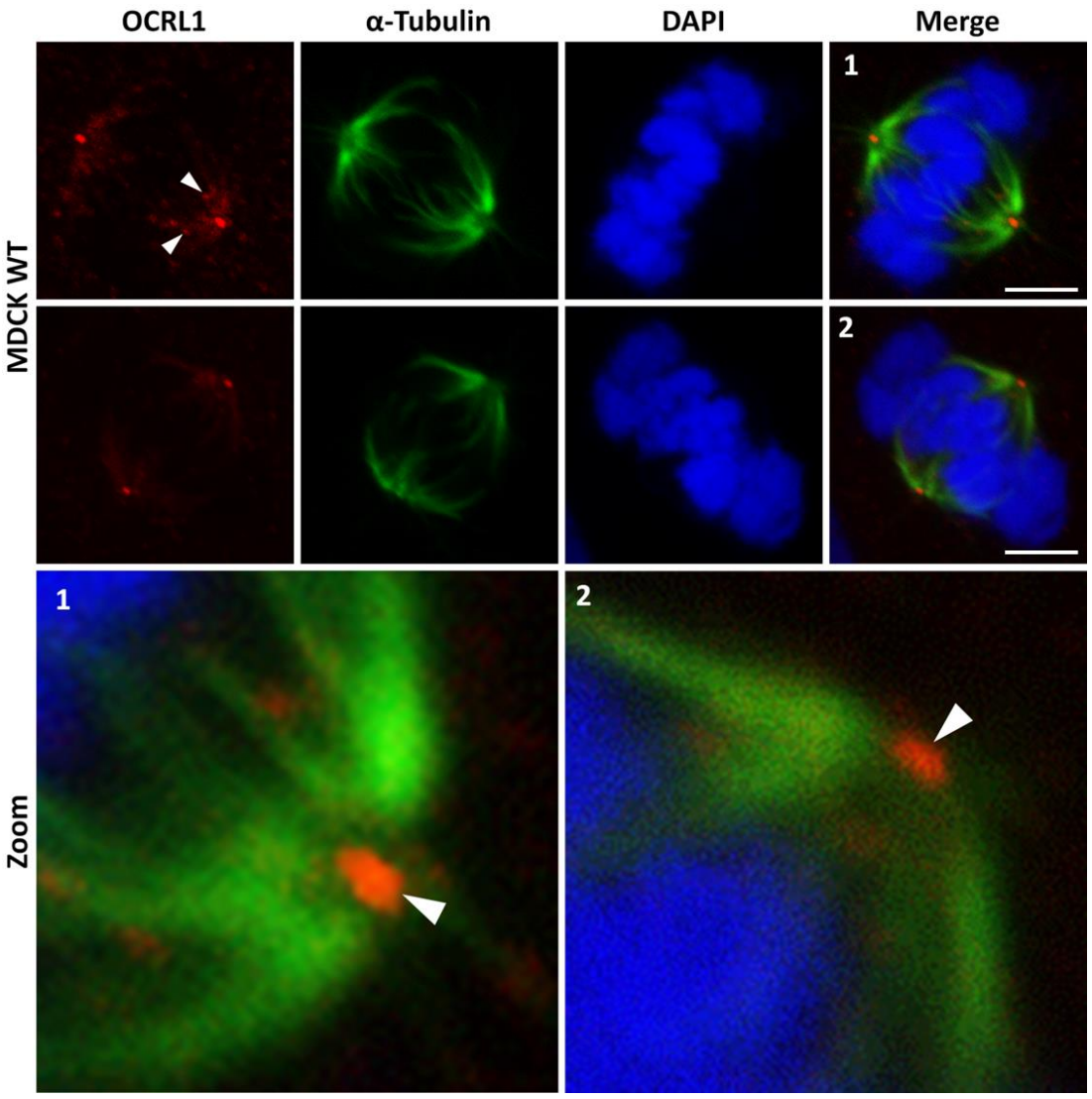

Figure 6.4: OCRL1 localises to the spindle poles during mitosis. Wild type MDCK cells were grown for 24 hours, fixed and permeabilised for immunostaining with antibodies to α-tubulin (green), OCRL1 (red) and the DNA stain DAPI (blue). Images shown are compressed stacks of 4 confocal sections spanning the top and the bottom of the mitotic spindle apparatus. Higher magnification images are shown of the merged channels in the bottom panel. Small white arrows indicate OCRL1 positive vesicles and big white arrows indicate the spindle poles. Images shown are representative of all dividing cells observed on the coverslip (n=10) of 2 experiments. Scale bar 10 μM.

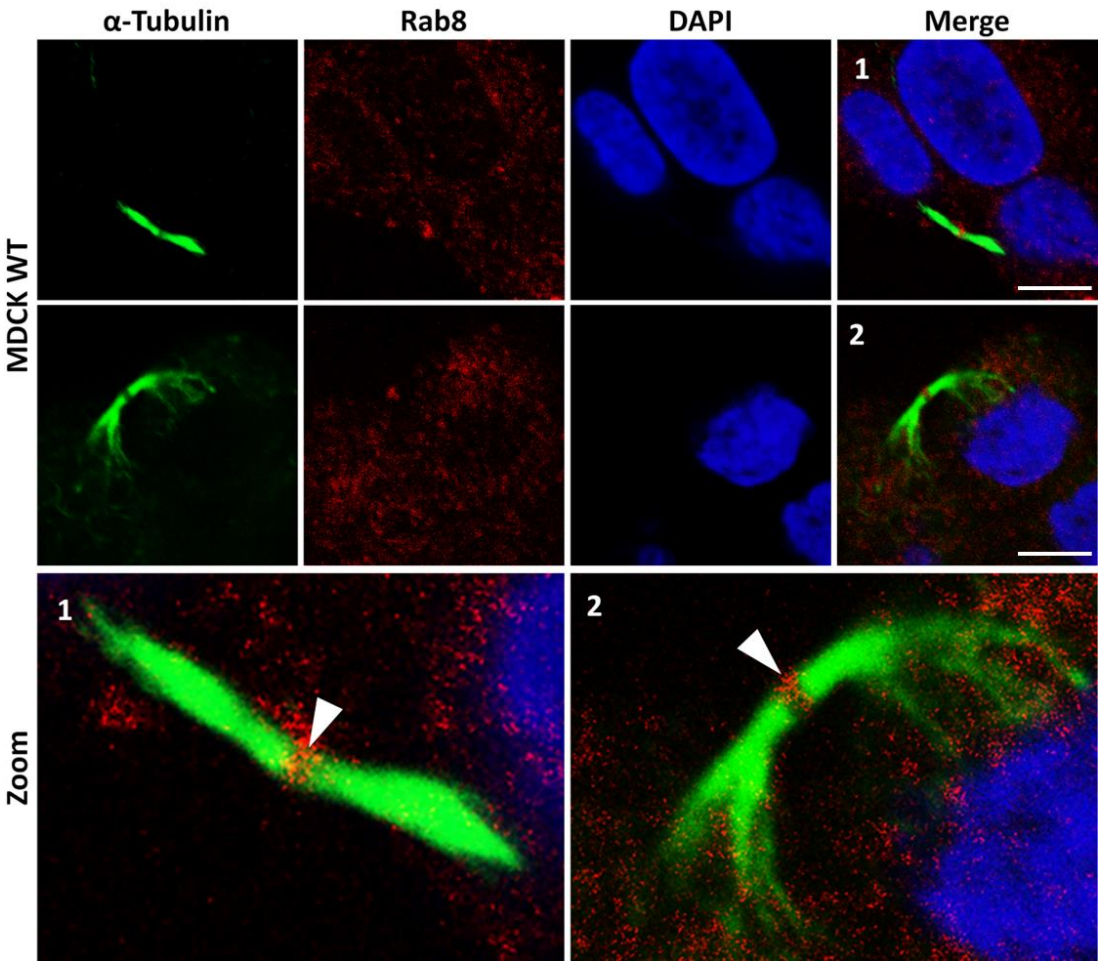

Figure 6.5: Rab8 GTPase localises to the midbody during cytokinesis. Wild type MDCK cells were grown for 24 hours, fixed and permeabilised for immunostaining with antibodies to α-tubulin (green), Rab8 (red) and the DNA stain DAPI (blue). Higher magnification images are shown of the merged channels in the bottom panel (1 and 2). White arrows indicate localisation of the midbody. Images shown are single confocal sections that are representative of all cells observed connected by a midbody on the coverslip (n=20) of 2 experiments. Scale bar 10 µM.

The midbody marks the site of lateral lumen formation

MDCK cells depleted of OCRL1 display defects in both cell polarity and cytokinesis. To determine whether the polarity phenotype is related to the cytokinesis defect we looked at the trafficking of the luminal marker Gp135 in cells during cytokinesis. Previously, pools of Gp135 were shown to target an uncharacterised site in the lateral membrane between pairs of OCRL1 depleted cells (Chapter 5). We studied the localisation of Gp135 again but also looked at the microtubules to indicate stages of cell division. There is some evidence to suggest polarisation of apical and basolateral membranes is maintained throughout cell division, kept in place by tight junctions that remain intact (Reinsch and Karsenti, 1994). When GFP-Gp135 expressing cells underwent cell division, most of the protein remained on the cell surface, with a smaller intracellular pool of vesicles localised to spindle poles (figure 6.6). When OCRL1 depleted cells divided, GFP-Gp135 was absent from the plasma membrane and entirely localised to clusters of vesicles segregated to spindle poles (figure 6.6). In Chapter 5, we observed single OCRL1 depleted cells at interphase accumulate Gp135 in recycling endosomes (figure 5.2 and 5.7B), therefore a block in apical recycling prior to cell division likely results in the accumulation of recycling endosomes which become segregated to spindle poles when OCRL1 depleted cells divide.

We next investigated the localisation of Gp135 in cells undergoing cytokinesis. In control cells connected by an intercellular bridge, Gp135 was mostly localised to the peripheral membrane (figure 6.7), suggesting limited trafficking of apical cargo along the intercellular bridge. In OCRL1 depleted cells, Gp135 accumulated near the midbody of the intercellular bridge (figure 6.7). A 3D reconstruction revealed that these cells also had perinuclear pools of Gp135 (figure 6.7), suggesting the recycling pool of Gp135 that accumulates in the absence of OCRL1 is delivered to the site of abscission when the cell undergoes division. Similar results were found with MDCK cells stably expressing GFP-Gp135 which was present on the plasma membrane of control cells during late stage cytokinesis but accumulated near the midbody in cells depleted of OCRL1 (figure 6.8). Therefore the site of apical membrane trafficking in

cells depleted of OCRL1, as a prelude to aberrant lumen formation, appears to be the site of abscission.

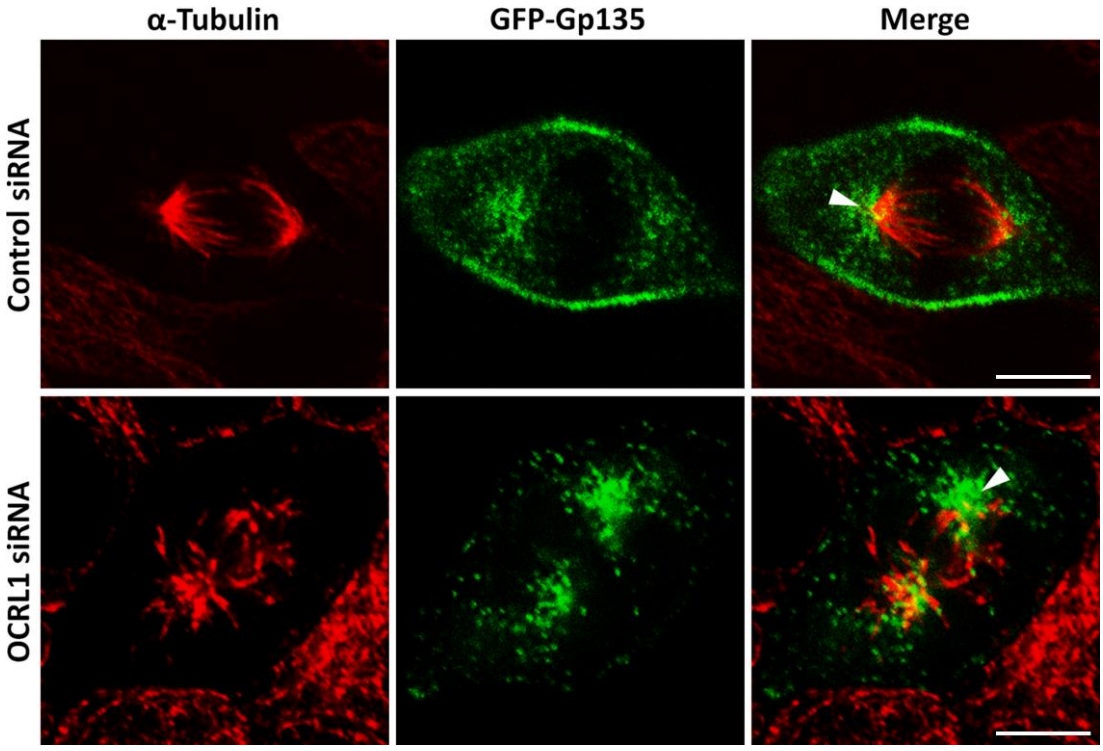

Figure 6.6: Intracellular GFP-Gp135 clusters near spindle poles during mitosis. MDCK cells stably expressing GFP-Gp135 were grown for 4 hours before treatment with non-targeting control siRNA or a pool of OCRL1 siRNA. 20 hours later, cells were fixed and permeabilised for immunostaining with antibodies to α-tubulin (red). Single confocal sections were taken of pairs of GFP-Gp135 expressing cells. Images shown are representative of all expressing cells undergoing division (n=10) from 2 experiments. White arrows indicate vesicular pools of Gp135 near spindle poles. Scale bar 10 μM.

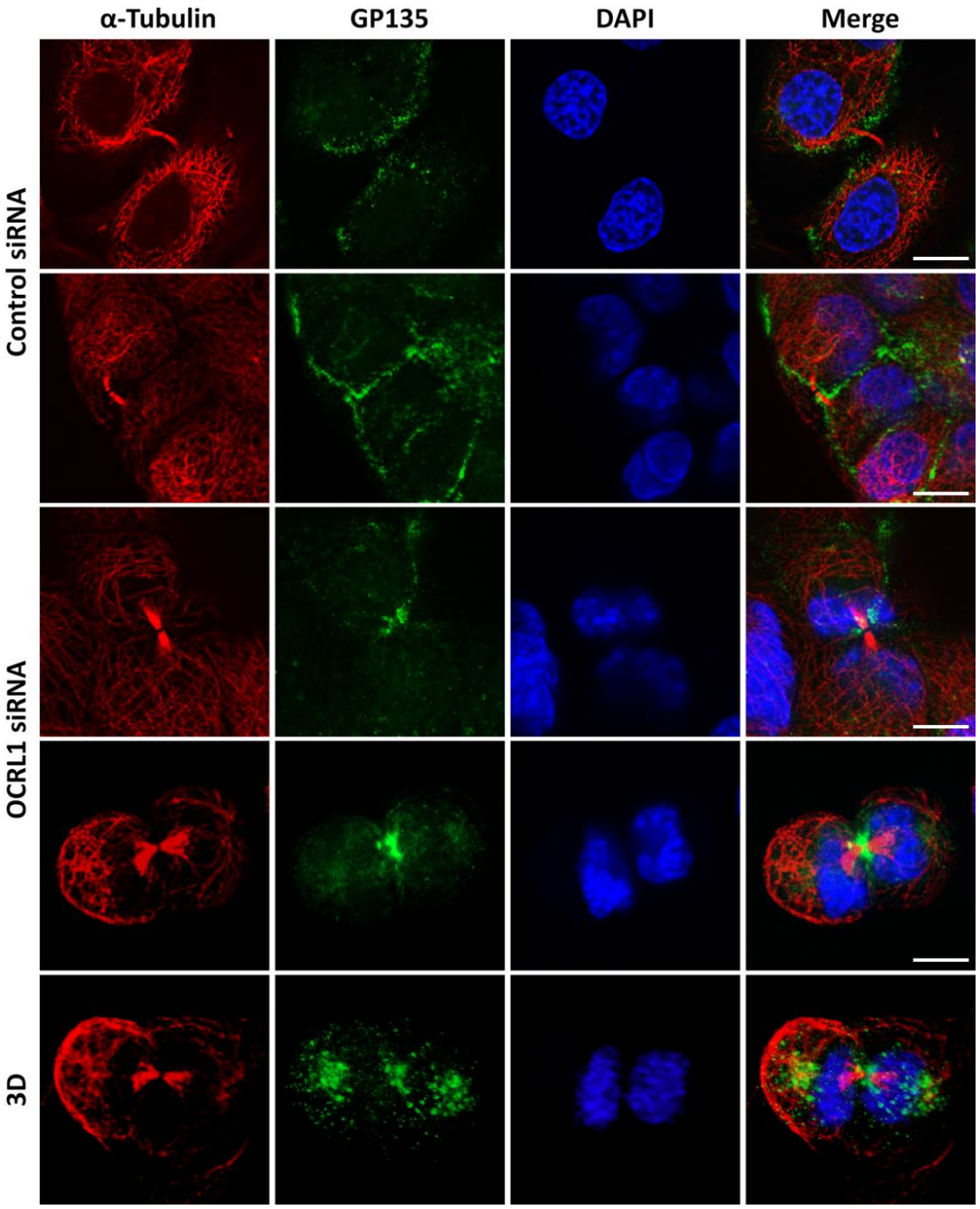

Figure 6.7: Gp135 is trafficked to the midbody in cells depleted of OCRL1. MDCK cells were grown and subjected to RNAi as in figure 6.6. Cells were fixed and permeabilised for immunostaining with antibodies to α-tubulin (red), Gp135 (green) and the DNA stain DAPI (blue). Images shown are single confocal sections of representative cells on the coverslip (n=10 per 2 experiments). The bottom panel is a 3D reconstruction of a pair of OCRL1 depleted cells (ImageJ; Z stack of 20 confocal sections). Scale bar 10 μM.

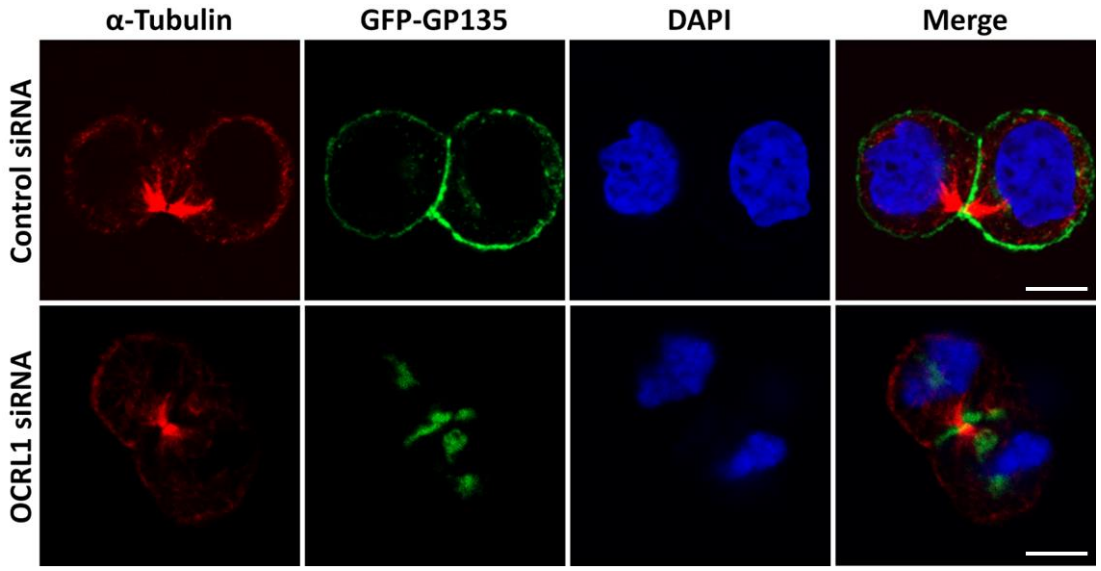

Figure 6.8: GFP-Gp135 is trafficked to the midbody in cells depleted of OCRL1. MDCK cells were grown and subjected to RNAi as in figure 6.6. Cells were fixed and permeabilised for immunostaining with antibodies to α-tubulin (red) and the DNA stain DAPI (blue). Images shown are representative of all expressing cells in late stage cytokinesis (n=5) from a single experiment. Scale bar 10 μM.

OCRL1 depletion disrupts spindle orientation and midbody positioning

Although trafficking of recycling endosomes to the midbody is a normal occurrence, this appears to coincide with lateral lumen formation in OCRL1 depleted cells. A number of key differences might explain the phenotype observed when OCRL1 is depleted. Firstly, recycling endosomes accumulate and secondly they are highly apical in composition, suggesting an excessive amount of apical cargo is delivered to the midbody when OCRL1 depleted cells divide. However, midbodies are expected to be found apically and not in the lateral membrane, leaving the link between midbodies and lateral lumens perplexing. Therefore we next investigated the localisation of midbodies in monolayers of MDCK cells depleted of OCRL1 for 24 hours. Midbodies were only found towards the apical side of control monolayers, but were localised more basally in the absence of OCRL1 (figure 6.9).

Mis-localisation of midbodies has been shown to induce the formation of lateral lumens when Cdc42 is depleted in 3D cultures of MDCK cells (Jaffe et al., 2008; Rodriguez-Fraticelli et al., 2010). Cdc42 regulates the orientation of the mitotic spindle, which determines the location of the midbody (Jaffe et al., 2008; Rodriguez-Fraticelli et al., 2010). In MDCK cells, spindle orientation is tightly controlled, positioned parallel to the plane of the monolayer (Reinsch and Karsenti, 1994). Both spindle poles can usually be seen in a single confocal section less than 0.7 µM depth (Reinsch and Karsenti, 1994). We also observed mitotic spindles parallel to the monolayer in control cells, with spindle poles appearing in the same single confocal section (figure 6.10). However, in the absence of OCRL1, mitotic spindle poles could not be resolved in single confocal sections, with one pole appearing at the basal side of the cell and the other more apically (figure 6.10). This can be seen more clearly in XZ images of mitotic cells, where spindle poles aligned along a horizontal axis in control cells and deviated from this axis in the absence of OCRL1 (figure 6.11). Therefore mis-localised midbodies, possibly due to aberrant spindle orientations, might explain lateral membrane targeting of apical endosomes in the absence of OCRL1.

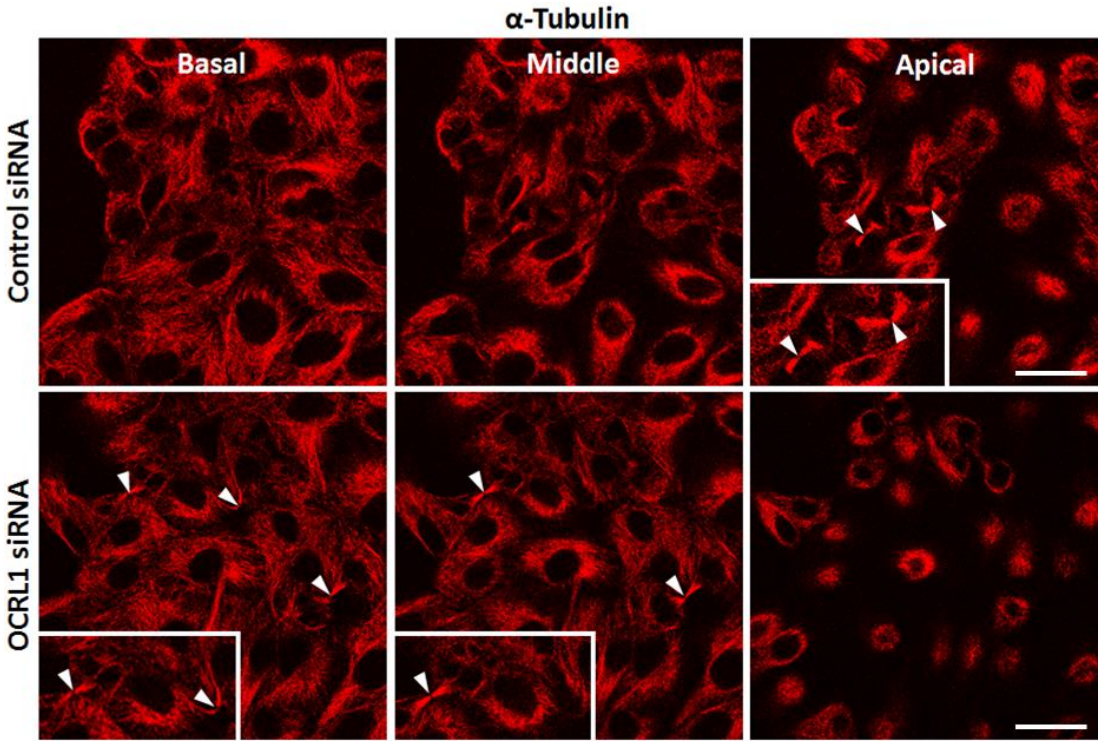

Figure 6.9: OCRL1 depletion disrupts midbody positioning. MDCK cells were grown and subjected to RNAi as in figure 6.6. Cells were fixed and permeabilised for immunostaining with antibodies to α-tubulin (red). Images shown are single confocal sections taken from Z stacks spanning from the bottom to the top of the cell layer. A total of 10 stacks were taken across 2 experiments. The basal, middle and apical side of the monolayers from one experiment are shown. White arrows indicate the midbodies of cells connected by an intercellular bride. Inset images show a zoom of an area of the section containing midbodies. Scale bar 20 μM.

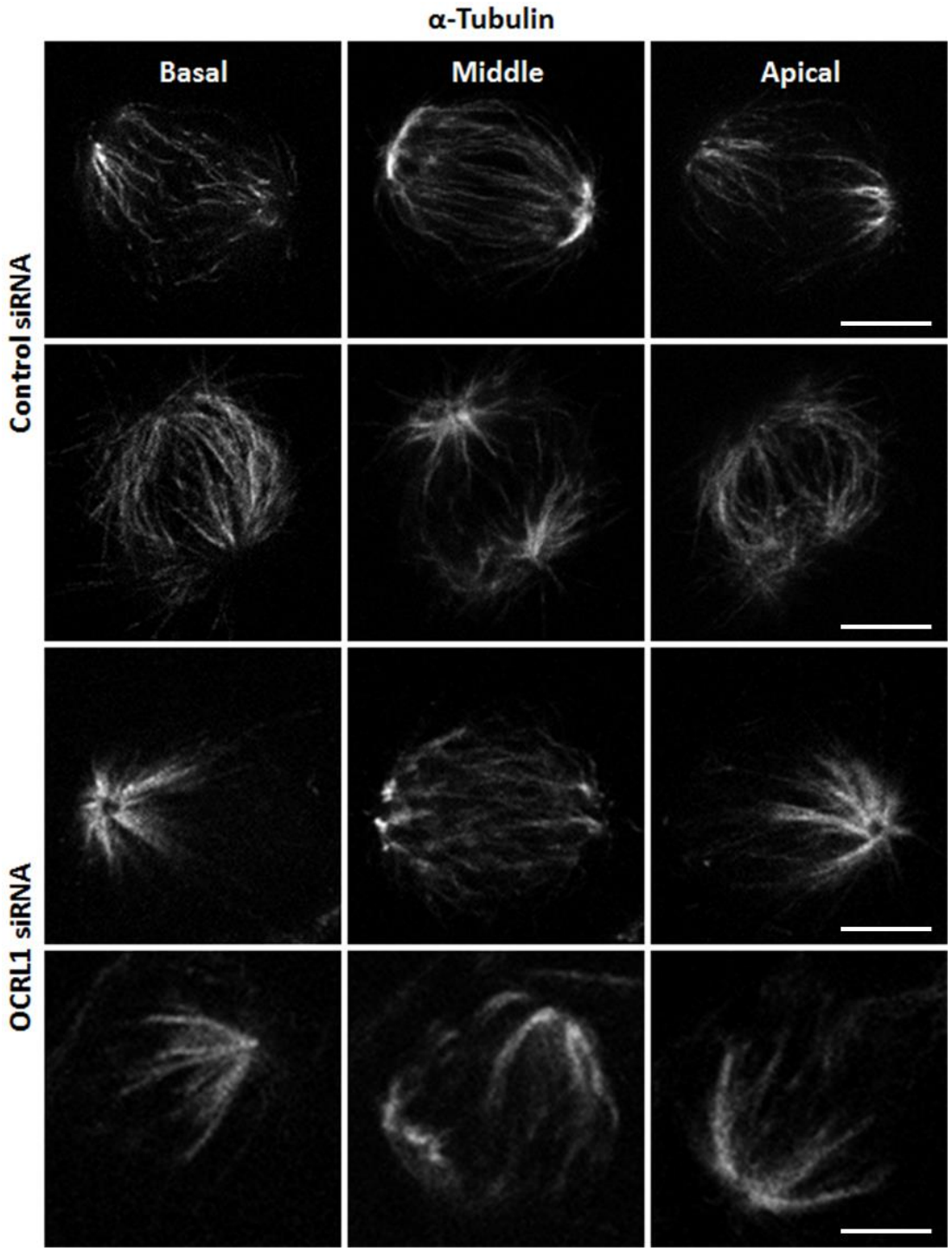

Figure 6.10: OCRL1 depletion disrupts mitotic spindle orientation. MDCK cells were grown and subjected to RNAi as in figure 6.6. Cells were fixed and permeabilised for immunostaining with antibodies to α-tubulin (white). Images shown are single confocal sections taken from Z stacks spanning from the bottom to the top of the cell layer. Images are representative of n=6 cells observed across 2 experiments. The basal, middle and apical side of the spindle pole are shown. Scale bar 10 µM.

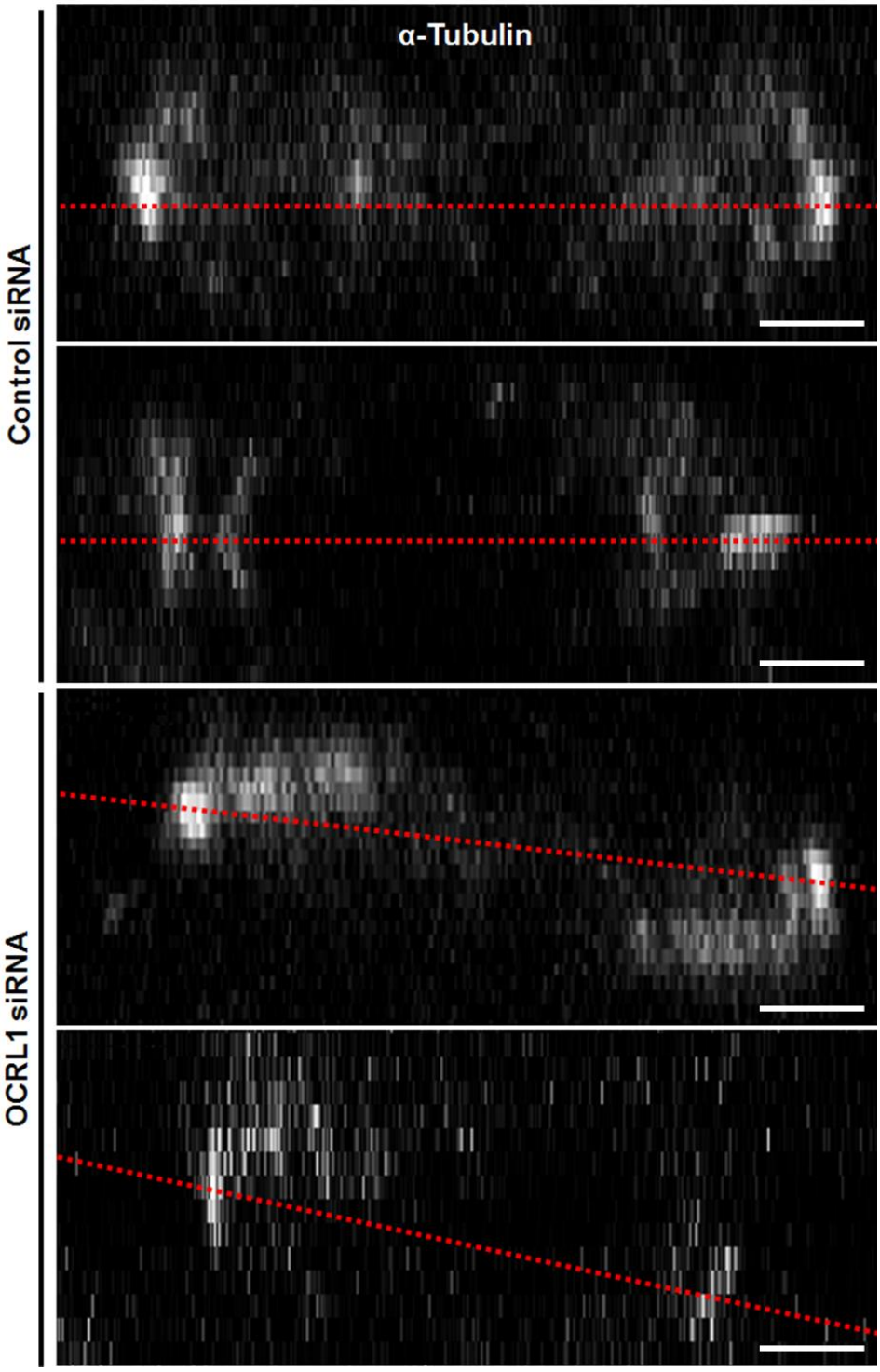

Figure 6.11: XZ images of mitotic spindle orientation. MDCK cells were on the same coverslip as cells in figure 6.10. The microtubules are shown in white. XZ images were reconstructed from Z-stacks of confocal sections spanning from the bottom to the top of the cell layer. The relative orientations of spindle poles are shown by the red line which connects the middle of the brightest point of each spindle. Images are representative of n=6 cells observed across 2 experiments. Scale bar 5 μM.

Summary

This chapter aimed to investigate whether OCRL1 depleted cells with polarity defects also have disrupted cell division. In polarised cell types such as the MDCK cell line, these two processes are closely related. For example, the orientation of cell division has been shown to affect the positioning of the apical membrane (Qin et al., 2010; Rodriguez-Fraticelli et al., 2010). These findings might be explained by the observation that during cell division, trafficking pathways deliver apical cargo along the microtubules of the mitotic spindle and midzone microtubules to the abscission site which normally occurs just beneath the developing lumen (Schlüter et al., 2009). Abnormal orientations of the mitotic spindle apparatus affects the positioning of the midbody in 3D cultures (Jaffe et al., 2008), which directs apical trafficking away from the single developing lumen and results in the multiple lateral lumen phenotype seen in these experiments (Jaffe et al., 2008; Qin et al., 2010; Rodriguez-Fraticelli et al., 2010). In monolayers of MDCK cells, a similar process is thought to occur and abscission takes place just beneath the apical surface (Reinsch and Karsenti, 1994). Since OCRL1 has already been implicated to regulate cytokinesis in non-polarised cells, it was possible that defects in cytokinesis coupled with the recycling defects identified in Chapter 5 could explain the formation of lateral lumens when MDCK cells were depleted of OCRL1 (Chapter 4).

OCRL1 has previously been shown to localise near the midbody during cytokinesis of HeLa cells (Dambournet et al., 2011). Similarly in MDCK cells, we found OCRL1 localised either side of the abscission site during cytokinesis. In addition, we noticed cells in earlier stages of cell division accumulated vesicular pools positive for OCRL1 near the spindle poles, which has not been reported previously. In HeLa cells, OCRL1 localises to the midbody in a Rab35 dependent manner (Dambournet et al., 2011). OCRL1 is likely delivered to the abscission site by direct interactions with Rab35 in endocytic recycling pathways. Similarly, Rab8 and Rab11 pathways have been shown to deliver membrane to the cytokinetic furrow (Fielding et al., 2005; Pohl and Jentsch, 2008). Although we did not look at Rab35, we found Rab8 enriched at the abscission site, highlighting the possibility that interactions with

Rab8 as well as Rab35 endocytic recycling pathways could localise OCRL1 to the midbody. OCRL1 appears to have a functional role in cytokinesis. When we depleted monolayers of MDCK cells of OCRL1, we found an accumulation of cells in the pre-abscission stage, similar to previous findings in the HeLa cell line (Dambournet et al., 2011).

The results of the first part of this chapter indicate that OCRL1 depleted MDCK cells display abscission defects. In the last part of this chapter, we sought to understand whether the defects in cytokinesis were linked to the polarisation defects explored previously. In particular, we showed in the previous chapter that OCRL1 depleted cells delivered apical endosomal membrane to an uncharacterised site between pairs of cells. The results here indicate that this site is marked by the midbody, which appeared to be mis-localised when OCRL1 was depleted, suggesting lateral lumens could result from a combination of recycling and cytokinesis defects, discussed in more detail next.

Discussion

The results of this chapter provide some evidence that MDCK cells without OCRL1 exhibit delayed progression through the final stages of cytokinesis which primarily involves severing of the intercellular bridge. The complete mechanistic details of abscission remain unclear, however it is thought to begin with a secondary ingression of the membrane on one side of the midbody (Neto et al., 2011). Fusion of endosomes with the membrane might contribute to thinning of the intercellular bridge during this process (Schiel et al., 2011). The final membrane scission event is mediated by the ESCRT (endosomal sorting complexes required for transport) machinery. Helices of ESCRT-III are thought to bring the two membranes in close proximity until spontaneous scission occurs (Guizetti et al., 2011). Enrichment of PI(3)P at the midbody facilitates the recruitment of ESCRT-III components to the abscission site (Sagona et al., 2010). However, prior to abscission, PI(4,5)P_2 is the dominant phosphoinositide at the site of cytokinesis. At this stage, PI(4,5)P_2 is essential for recruiting contractile ring components and promoting the assembly of actin filaments required during furrowing (Logan and Mandato, 2006). One possible role for OCRL1 in abscission might be to down-regulate the levels of PI(4,5)P_2 at the midbody to facilitate the change in lipid composition towards PI(3)P. In addition, disassembly of the actin cytoskeleton as well as the microtubules is required to complete cytokinesis (Schweitzer and D'Souza-Schorey, 2004). Since PI(4,5)P_2 promotes actin filament assembly, de-phosphorylation of PI(4,5)P_2 by OCRL1 could mediate disassembly of the actin cytoskeleton during abscission, as suggested by Dambournet and colleagues.

In addition to finding OCRL1 at the midbody, we noticed OCRL1 localised near the spindle poles of dividing cells, where the centrosomes reside. OCRL1 has an ASPM, SPD-2, Hydin (ASH) domain which is frequently present in proteins associated with cilia and centrosomes (Ponting et al., 2006). Consistent with OCRL1 having this domain, OCRL1 has been reported to localise to the basal bodies of cilia (Coon et al., 2012), which are formed from centrioles. The localisation of OCRL1 to spindle poles might resemble the localisation of OCRL1 to cilia basal bodies, which occurs in

a Rab8 dependent manner (Coon et al., 2012). We also noticed OCRL1 in more peripheral puncta around spindle poles; therefore the centrosomal staining of OCRL1 at spindle poles could represent a dense accumulation of OCRL1 positive endosomal vesicles. Since membrane traffic is directed towards the midbody during cytokinesis, it is likely that some of the OCRL1 positive vesicles that accumulate during mitosis are trafficked along this pathway, potentially explaining the midbody localisation of OCRL1.

In the previous chapter, OCRL1 was implicated as a regulator of apical recycling pathways. Cells without OCRL1 accumulated Rab11 and Rab8 positive recycling endosomes and cargo exit from these compartments appeared to be blocked. Recycling endosomes play an important role in cytokinesis, delivering proteins involved in cytokinesis to the abscission site as well as providing the new membrane required (Montagnac et al., 2008). The role of recycling endosomes in cytokinesis appears to be critical since depletion of Rab11 or expression of a dominant-negative mutant causes significant abscission defects (Wilson et al., 2005). Since abscission requires membrane trafficking, the abscission defects observed in this chapter could be secondary to the effects of OCRL1 loss on recycling pathways. Alternatively, the role of OCRL1 in abscission might be distinct from it's role in regulating recycling, as discussed above.

In polarised cell types, there appears to be an additional level of cross-talk, since membrane trafficking and cytokinesis may be co-ordinated with apical membrane formation. One possibility is that the defects in apical recycling coupled with the defects in abscission result in abnormal polarity when OCRL1 is depleted. The next section details how membrane traffic and cytokinesis is co-ordinated with polarisation normally, and then discusses how this might be disrupted with loss of OCRL1.

During cell division, trafficking pathways are modified to accommodate fluctuations in cell volume and plasma membrane surface area. At the onset of mitosis, recycling to the plasma membrane slows, resulting in an intracellular accumulation

of endosomes (figure 6.12A). However whilst the pool of intracellular apical recycling cargo is likely to increase during early mitosis, it is thought that the majority of the apical membrane is maintained on the plasma membrane throughout cell division (Schlüter et al., 2009), indicated in figure 6.12A-E. Our results were in agreement with this view, control cells undergoing mitosis maintained GFP-Gp135 on the cell surface, but also had clusters of vesicular GFP-Gp135 around spindle poles. Recycling resumes during cytokinesis, with traffic directed towards the plane of division (Boucrot and Kirchhausen, 2007), indicated in figure 6.12C-D. In our control cells, the intracellular Gp135 that was seen during mitosis was no longer apparent towards the end of cytokinesis, when cells had formed an intracellular bridge. Instead, Gp135 was only detectable on the cell surface, consistent with the view that apical cargo is re-delivered to the apical membrane during cytokinesis. One way in which cytokinesis is co-ordinated with polarisation is through the apical positioning of the midbody (Fleming et al., 2007; Reinsch and Karsenti, 1994). As the contractile ring furrows asymmetrically (indicated by a black arrow, figure 6.12D), progressing from the basal side, the midbody is formed just near the apical membrane and the junctions rapidly form beneath it (Herszterg et al., 2013), indicated in figure 6.12D. Positioning of the midbody apically ensures any trafficking of apical cargo along midzone microtubules is targeted towards the apical membrane and minimal disruptions occur to the epithelial barrier during abscission.

Our results suggest that in MDCK cells, OCRL1 regulates apical recycling to the plasma membrane from recycling endosomes. Depleting OCRL1 induced a block in apical recycling such that the established apical domain was entirely lost from the cell surface and apical cargo accumulated in Rab11 and Rab8 positive recycling endosomes. Subsequently, when OCRL1 depleted cells divide, the dense pool of apical vesicles were segregated into clusters around spindle poles (figure 6.12G-H), as in control cells. Since Rab11 and Rab8 regulate pathways that traffic to the site of cytokinesis, the apical vesicles appeared to be trafficked to the midbody along this pathway (figure 6.12I). A key difference between control cells and OCRL1 depleted cells at this stage might be the amount of apical cargo present on recycling

endosomes. In OCRL1 depleted cells, the recycling endosomes accumulate key apical determinates such as Par6, aPKC, Cdc42 and Gp135 which are delivered in excess to the midbody during cytokinesis. In addition, there is some evidence that diffusion is limited within the membrane of the cleavage furrow and midbody (Schmidt and Nichols, 2004). The barrier to lateral diffusion of proteins and lipids may be due to the high density of cortical proteins such as the septins in the cleavage furrow (Schmidt and Nichols, 2004). Therefore loss of the apical membrane at the apex of the cell followed by routing of apical traffic during cell division to a region of the membrane where diffusion is limited could further promote localised apical membrane formation at the site of abscission (figure 6.12J). Thus, one possibility is that aberrant traffic is primarily responsible for misplacing apical domains in MDCK cells lacking OCRL1.

However, we noticed a number of additional problems in OCRL1 depleted cells that might contribute to the lateral lumen phenotype. The mitotic spindle appeared mis-orientated in cells without OCRL1 (figure 6.12H), which may explain why midbodies were also mis-localised. Instead of positioning the midbodies apically, OCRL1 depleted cells appeared to position the midbodies laterally (figure 6.12I). These results suggest that without OCRL1, defective recycling coupled with abnormal cytokinesis results in mis-positioning of the apical membrane to form lateral apical lumens.

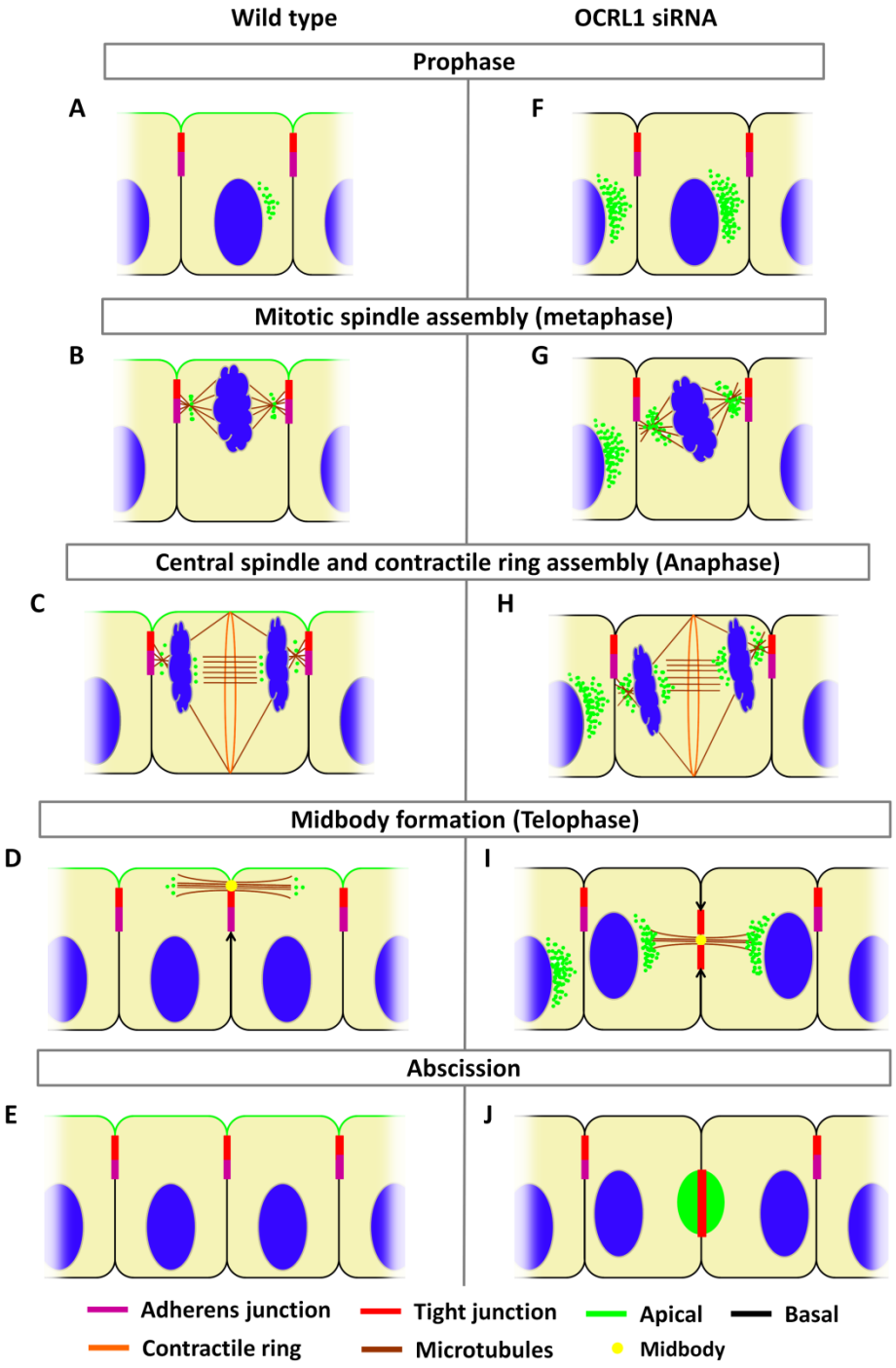

Figure 6.12: Model of OCRL1 depletion and disrupted co-ordination between cell division and polarisation. In MDCK cells, OCRL1 depletion bocks recycling of apical cargo to the plasma membrane. The apical cargo that is internalised as a result is trafficked along midzone microtubules along the normal pathway as OCRL1 depleted cells divide. However a combination of excessive trafficking of apical cargo to the cytokinesis site and mis-localisation of midbodies results in the formation of lateral lumens in OCRL1 depleted cells. See main text for details.

A number of observations support a model that involves both cytokinesis and trafficking defects in the absence of OCRL1. Several studies suggest that apical membrane formation is consistently coupled to cell division. Disrupting the orientation of the mitotic spindle by silencing of Cdc42 leads to the multi-lumen phenotype in 3D cultures (Jaffe et al., 2008, Qin et al., 2010; Rodriguez-Fraticelli et al., 2010). Multiple lumens form when cells no longer co-ordinate apical trafficking to a single common lumen at the cell apex and instead traffic apical cargo to the lateral region between cells. It has been suggested that the apical membrane originates where the midbody is formed during cytokinesis (Schlüter et al., 2009), and lateral apical lumens result from mis-localised midbodies as a result of abnormal spindle orientations (Jaffe et al., 2008, Qin et al., 2010; Rodriguez-Fraticelli et al., 2010). These findings indicate that apical trafficking to the midbody occurs in all cell divisions. The midbody is normally formed just beneath the established apical domain which might ensure correct targeting of apical proteins to the apical membrane during cytokinesis (Fleming et al., 2007; Reinsch and Karsenti, 1994). We found that midbodies were not localised apically in OCRL1 depleted cells. Instead they appeared to form in the middle of the monolayer or more basally. If midbody positioning is key to determining where on the membrane the apical domain develops, mis-localised midbodies may explain lateral lumens in OCRL1 depleted cells.

As mentioned above, one possibility is that OCRL1 depletion disrupts mitotic spindle orientation, resulting in abnormal midbody positioning in a similar manner to Cdc42 depletion. We provided some evidence that this may be the case, since several OCRL1 depleted cells we looked at had mitotic spindle angles that deviated from the horizontal plane. However, other mechanisms are involved in localising the midbody. Asymmetric furrowing of the contractile ring ensures the midbody is formed apically in polarised cell types (Maddox et al., 2007). Components involved in furrowing such as myosin-2 distribute more densely on the basal side which strengthens ingression from this side of the contractile ring (Maddox et al., 2007). The asymmetric distribution of the furrowing machinery appears to be regulated by anillin and the septins since depletion of either of these proteins results in a

symmetric distribution (Maddox et al., 2007). It is not clear how OCRL1 loss would affect the furrowing mechanism. However, one possibility is that OCRL1 depletion disrupts the localisation of anillin. Localisation of anillin to the furrow requires $PI(4,5)P_2$; the PH domain of anillin interacts with $PI(4,5)P_2$, which is normally enriched in the furrow (Liu et al., 2012). Disrupting the levels of $PI(4,5)P_2$ or mutating the PH domain of anillin to disrupt the interaction between anillin and $PI(4,5)P_2$ blocks anillin from localising to the furrow (Ben El Kadhi et al., 2011; Liu et al., 2012). Therefore in MDCK cells, depletion of OCRL1 might disrupt anillin localisation through effects on $PI(4,5)P_2$ levels, which could potentially explain the aberrant localisation of midbodies seen when OCRL1 is depleted. Although the results of this chapter provide a new understanding of the results in Chapter 4 and Chapter 5, we identified additional problems with OCRL1 depleted cells involving cell division. Future work on the role of OCRL1 in cell division is discussed in the next chapter.

Chapter Seven

Final conclusions

Summary

Studying the role of OCRL1 in polarised epithelial cells confirmed the possibility that OCRL1 has specific functions in polarised cells not apparent in other cell types. Firstly, we confirmed the previous finding that a small pool of OCRL1 targeted apical junctions in MDCK cells, existing in a complex with the tight junction protein ZO-1 (Grieve et al., 2011). In addition, our findings suggested that OCRL1 may be required to maintain the normal morphology of tight junctions. Depleting cells of OCRL1 resulted in a larger cytoplasmic pool of vesicular ZO-1 and junctions that appeared thinner, suggesting OCRL1 may play a role in pathways that regulate junction formation.

A key finding in our investigation was that OCRL1 was required for polarisation. Without OCRL1, apical carriers rapidly accumulated intracellularly and a number of observations supported the view that this was due to an inability of cells to traffic apical cargo from recycling endosomes to the plasma membrane. FRAP analysis confirmed that a small population of apical cargo was subjected to endocytic recycling from a perinuclear location. Without OCRL1, this perinuclear pool of apical cargo was exaggerated, and co-localised with Rab8 and Rab11 GTPases, markers of the apical recycling endosome. OCRL1 appears to be recruited to this compartment to down-regulate the levels of $PI(4,5)P_2$. Using the PH domain of PLCδ as a probe for $PI(4,5)P_2$ we showed ectopic accumulations of this phosphoinositide as well as F-actin on recycling endosomes. Rescue experiments confirmed this role for OCRL1, since full length OCRL1 but not a phosphatase null mutant was able to rescue the apical recycling defect. The apical recycling pathway regulated by OCRL1 was responsible for trafficking key apical proteins such as the Par polarity complex, Cdc42 and Gp135. As cells begun to polarise, the disruptions in apical trafficking induced by loss of OCRL1 appeared to have knock-on effects on the organisation of the apical membrane.

As mentioned above, OCRL1 depletion initially affected apical trafficking pathways, but subsequent effects on the overall architecture of cell polarity were observed.

When OCRL1 was depleted in un-polarised cells growing in isolation, single cells displayed apical recycling defects. Upon cell division, polarisation was initiated and cells incorrectly localised the apical membrane. Similarly, when monolayers of cells were depleted of OCRL1, there was a clear progression of events. Cells rapidly accumulated apical cargo intracellularly and formed lateral lumens days later. Overall, these observations suggest the possibility that disruptions in apical trafficking are a primary effect of OCRL1 depletion and lateral lumens may be formed as a consequence.

We next investigated whether lumen formation in OCRL1 depleted cells was co-ordinated with cytokinesis. By observing the state of cell division in cells undergoing lumen formation, we determined the site of lumen formation was marked by the midbody, with apical trafficking directed towards this site. OCRL1 appeared to have a functional role in cytokinesis of MDCK cells. OCRL1 depletion resulted in an accumulation of cells in the pre-abscission stage, suggesting OCRL1 depletion delays progress through the final stages of cytokinesis. In addition, the midbodies of cells without OCRL1 were mis-localised, positioned more basally compared to controls, potentially explaining lateral lumen formation in OCRL1 depleted cells.

In summary, OCRL1 has been implicated to regulate numerous trafficking pathways in un-polarised cells and has been implicated to regulate cytokinesis in HeLa cells. However, the polarised nature of MDCK cells adds additional levels of interplay to these cellular processes. Trafficking in these cells is polarised, with specific pathways for apical and basolateral domains. In addition, polarity needs to be maintained in these cells as they undergo cell division and cytokinesis. To achieve this, regulators of cell polarity and polarised trafficking pathways co-ordinate the completion of cytokinesis and the formation and function of polarised cells. By studying trafficking and cytokinesis in these cells, we revealed that the co-operation between polarisation and cytokinesis was disrupted by loss of OCRL1.

Future Work

A key finding in our investigation was that OCRL1 regulates apical recycling in MDCK cells. Since a phosphatase null mutant OCRL1 was unable to rescue the recycling defect but the full length protein was, our results suggest that OCRL1 facilitates cargo exit from recycling endosomes by down-regulating the levels of $PI(4,5)P_2$. These results together with our finding that $PI(4,5)P_2$ is elevated on recycling compartments in the absence of OCRL1 indicate that excess $PI(4,5)P_2$ underlies the phenotype of OCRL1 depletion. We would like to carry out a screen for rescue of the recycling defect with a kinome siRNA library. Of particular interest would be PI(4)P 5-kinases. Since the levels of $PI(4,5)P_2$ are dependent on both its production and degradation, reducing the cellular level of PI(4)P 5-kinase activity might counteract the rise in $PI(4,5)P_2$ that occurs when OCRL1 is absent. In addition to confirming the role of $PI(4,5)P_2$ in the recycling defect, kinases are typically good therapeutic targets and the results of this screen might identify candidate kinases that when inhibited rescue the effects of OCRL1 loss.

As well as ectopic levels of $PI(4,5)P_2$, recycling compartments were associated with detectable levels of F-actin in OCRL1 depleted cells, not seen in controls. Evidence for $PI(4,5)P_2$ having a role in regulating actin polymerisation on endosomes in HK-2 cells comes from the finding that loss of OCRL1 increased the level of F-actin associated with these membranes in a N-WASP-dependent pathway (Vicinanza et al., 2011). However, as mentioned in Chapter 5, we were unable to rescue recycling with actin depolymerising agents such as Latrunculin-A and Cytochalasin-D (data not shown). Therefore it remains unclear whether F-actin accumulation was responsible for blocking endosome function in our OCRL1 depleted cells. In future studies, we would like to confirm the role of actin polymerisation in the phenotype of OCRL1 depletion by testing for rescue of apical recycling when components of actin polymerisation pathways, such as N-WASP are depleted with siRNA.

The finding that OCRL1 depletion was associated with elevated levels of intracellular F-actin was not unique to MDCK cells. We observed intracellular

punctate F-actin in a number of human renal cell lines depleted of OCRL1, VHL positive RCC4 cells and hTERT immortalised cells (NHPTK). The F-actin positive vesicles were localised to a perinuclear region, similar to MDCK cells. In NHPTK cells, actin rich vacuoles were also observed which are normally associated with disrupted apical trafficking pathways (Vega-Salas et al., 1987). In addition, when NHPTK cells were depleted of OCRL1, F-actin was no longer enriched in the apical membrane, which instead accumulated in the lateral membrane as well as intracellularly. These observations suggest polarisation might be disrupted in NHPTK cells depleted of OCRL1. Being of human origin and proximal tubular in appearance, NHPTK cells are a more suitable model of the renal cells affected by Lowe Syndrome, therefore we would like to use these cells to further investigate the role of OCRL1 in polarisation.

Although MDCK cells rapidly internalised their apical membrane when OCRL1 was depleted, the cells eventually re-polarised. However, instead of polarising along an axis perpendicular to the underlying support, OCRL1 depleted cells polarised along a horizontal plane, appearing more similar to 3D cultures than 2D monolayers. A key difference between these experimental systems is the presence of an asymmetric environment in 2D cultures which is absent when cells are grown in 3D. Therefore, one possibility that we did not investigate is that OCRL1 might be involved in pathways that detect external polarity cues. For example, integrins might be mis-localised in OCRL1 depleted cells which could be tested for. Alternatively, OCRL1 might be involved in organising the sub-membranous cytoskeletal network in the basal domain, which facilitates laminin remodelling. These events are required for proper positioning of the apical membrane and therefore might be involved in the phenotype of OCRL1 depletion.

However, a key development in Chapter 6 indicated that lateral lumen formation was co-ordinated with cell division in OCRL1 depleted cells. Lateral lumens formed at sites marked by the midbody during cytokinesis. In previous chapters, the site of apical trafficking and lumen formation had remained elusive, however this finding raises additional questions. While we made some observations that suggest

cytokinesis may be disrupted by loss of OCRL1, it is not clear whether this is separate from the recycling defect that occurs in OCRL1 depleted cells, since membrane trafficking is required for successful cytokinesis. In addition, although we found both OCRL1 and Rab8 localised to the midbody, it is not clear whether Rab8 is responsible for localising OCRL1 to this site, or whether other GTPases such as Rab35 target OCRL1 to the midbody in MDCK cells, as in HeLa cells (Dambournet et al., 2011). It is possible that the defects in apical recycling and cytokinesis involve different OCRL1 regulated pathways. We would like to determine the interdependence of these events by carrying out a series of rescue experiments designed to check which interactions with OCRL1 are required for rescue of the depletion phenotype. One way a specific interaction can be screened for rescue is by cloning the binding partners into an expression vector, separated by a short linker, allowing the two proteins to adopt their normal confirmation. Initially we would carry out a screen of OCRL1-Rab interactions for rescue of the recycling and cytokinesis defects. From the results in Chapter 5, we suspect that OCRL1 depletion disrupts a Rab8 recycling pathway, however re-expression of OCRL1-Rab8 would confirm whether this interaction is required for apical recycling in MDCK cells. It would then be interesting to assess whether these cells subsequently develop cytokinesis defects, enabling us to determine if the OCRL1-Rab8 interaction is also required for cytokinesis. Similar investigations could be carried out with other GTPases such as Rab35 as well OCRL1 binding partners in the endocytic pathway.

Since the midbody is normally localised apically in polarised epithelial cells, the finding that lateral lumens formed at sites marked by the midbody suggested the possibility that abscission is not only delayed by OCRL1 depletion but that it may also occur in the wrong place. We investigated this briefly and noticed mitotic spindles were mis-orientated in OCRL1 depleted cells and the midbodies were more basally located compared to controls. As well as carrying out accurate measurement of these effects, a more detailed exploration of the role of OCRL1 in mitosis and cytokinesis would be the focus of future studies. These experiments would be designed to understand the pathways involved in spindle orientation and midbody positioning affected by loss of OCRL1. Interestingly, planar orientation of

the mitotic spindle requires intact intercellular junctions, since astral microtubules are anchored to the cell cortex by interactions with junctional components (den Elzen et al., 2008). Given the previous finding of OCRL1 at junctions (Grieve et al., 2011), and the results of Chapter 3, we would like to determine whether junctions appear disrupted in cells with mis-orientated mitotic spindles. A recent study in *Drosophila* suggests junctions also play a role in asymmetrically positioning midbodies (Morais-de-Sá and Sunkel, 2013). During cytokinesis, the apical side of the contractile ring contacts the adherens junctions which were required to recruit the midbody apically (Morais-de-Sá and Sunkel, 2013). Disrupting the adherens junction resulted in more basally localised midbodies and aberrant apical membranes (Morais-de-Sá and Sunkel, 2013). Therefore intercellular junctions are involved in both aspects of cytokinesis that were disrupted by loss of OCRL1 and we would like to look into more detail at the localisation of junctional components in dividing OCRL1 depleted cells. However, OCRL1 might be involved in other pathways that regulate asymmetric furrowing. As discussed in Chapter 6, one possibility is that OCRL1 loss affects asymmetric furrowing by altering the distribution of anillin, which interacts with $PI(4,5)P_2$. Since we observed aberrant localisations of $PI(4,5)P_2$ in OCRL1 depleted cells, anillin may be mis-localised when these cells divide, which is something that could be easily tested for with antibodies.

Discussion

Our objective was to determine the role of OCRL1 in polarised cell types, using cell lines derived from the kidney, which is the organ most affected by Lowe Syndrome and Dents-2 disease. We made a number of observations that suggests OCRL1 has specific roles in polarised cells. As well as localising to junctions, our findings implicate OCRL1 in regulating cell polarity and cell division. These processes are critical for maintaining the architecture of the tissues affected by the disease.

OCRL1 has been implicated in a variety of cellular processes across multiple cell types. In polarised cell types alone, we found OCRL1 localised to tight junctions in mature cells, the Golgi apparatus and trafficking intermediates, and to spindle poles and the midbody during cell division. In addition, our results suggest OCRL1 might have multiple functions in polarised cells, from intercellular junction formation, maturation, apical recycling and cytokinesis. It is likely that OCRL1 is recruited to various different sites in the cell by interacting with specific Rab GTPases and their effector proteins. At these locations, a common function of OCRL1 exists, to couple dephosphorylation of $PI(4,5)P_2$ with membrane identity or cytoskeletal dynamics. While OCRL1 regulates multiple cellular processes, the difficulty is determining which of these are disrupted in Lowe Syndrome and Dents-2 disease.

Since the results of this investigation have been discussed in detail at the end of each chapter, the majority of this final discussion focuses on linking our results to diseases associated with loss of OCRL1. The finding that OCRL1 targets intercellular junctions is potentially interesting because dysfunctional junctions have been connected to kidney disease (Lee et al., 2006). However, whether junctional OCRL1 is a generalised feature of polarised epithelial cells is yet to be determined. Our results suggest a small pool of OCRL1 targets intercellular junctions in MDCK cells. As well as MDCK cells, junctional OCRL1 has been detected in the intestinal epithelial cell line Caco-2 (Grieve et al., 2011). However, as discussed in Chapter 3, several studies of OCRL1 using polarised epithelial cells failed to detect the protein at junctions (Cui et al., 2010; Dressman et al., 2010; Vicinanza et al., 2011).

Similarly, we failed to detect OCRL1 at junctions in a human renal cell line (NHPTK) or a lens epithelial cell line (NTM5). These results suggest that the localisation pattern of OCRL1 is cell type specific. Alternatively, junctional targeting of OCRL1 may occur only temporarily during development. Answering these questions would clarify the importance of junctional OCRL1 in Lowe Syndrome.

One problem in particular is the canine and *distal* tubular origin of MDCK cells, which may display different characteristics to human proximal tubule cells, affected by the disease. For example, the properties of the tight junction varies between distal and proximal cells; higher levels of occludin and ZO-1 in the distal segments make proximal tubule junctions comparatively leaky (Gonzalez-Mariscal et al., 2000; Kiuchi-Saishin et al., 2002). There are several human proximal tubular cell lines which we could use to study OCRL1, such as HK-2, but these have problems with de-differentiation (Orosz et al 2004). We attempted to address this issue by using a human cell line derived from the kidney of a normal adult male (Herbert et al., 2013). These cells were selected for their proximal tubule characteristics (Herbert et al., 2013). However, as mentioned above, we failed to detect OCRL1 at junctions. To elucidate whether junctional OCRL1 is important for Lowe Syndrome, it might be interesting to investigate the appearance of the junctions in sections of affected tissue. With the provision of having a suitable control, the integrity of the junctions could be tested in cells affected by Lowe Syndrome by measurement of the transepithelial electrical resistance (TER); the current across the monolayer. These studies might provide an indication as to whether junctions are disrupted in Lowe Syndrome.

A key finding in our investigation was that OCRL1 depletion perturbed polarisation. In MDCK cells, OCRL1 regulated apical recycling endosome function by down-regulation the levels of $PI(4,5)P_2$. Cells without OCRL1 accumulated apical cargo in exaggerated endosomes associated with ectopic levels of $PI(4,5)P_2$ and F-actin. Interestingly, we observed intracellular punctate F-actin in a number of human renal cell lines depleted of OCRL1. Furthermore, perinuclear punctate F-actin has been reported in OCRL1 depleted HK-2 cells (Vicinanza et al., 2011). The

reproducibility of this finding suggests regulating the levels of $PI(4,5)P_2$ and F-actin on transport intermediates might be a generalised function of OCRL1 and hint at the possibility of trafficking defects in Lowe Syndrome. Our results in particular suggest OCRL1 is required for trafficking of apical components to the apical membrane.

Abnormalities in polarisation have been linked to a variety of diseases. Disrupted polarisation of proteins occurs in polycystic kidney disease. For example, the normally basolateral proteins epidermal growth factor receptor (EGFR) and the Na^+K^+-ATPase are mis-localised to the apical membrane (Wilson et al., 2000). In addition, kidney dysfunction can be due to the failure of cells to traffic proteins to the plasma membrane, resulting in their accumulation intracellularly, such as E-cadherin (Charron et al., 2000). Underlying defects in apical recycling can also lead to disruptions in cell polarity and disease. In microvillus inclusion disease, mutations in myosin-5b block recycling of apical cargo such as the transferrin receptor to the plasma membrane, and cells accumulate large intracellular vacuoles enriched in microvilli (Müller et al., 2008). A similar phenotype is observed in Rab8 knockout mice (Sato et al., 2007). Of particular interest is the finding that Dents disease patients display polarity defects in renal proximal tubule cells (PTCs). Patients with Dents disease have mutations in CLCN-5, and not OCRL1 (when it is referred to as Dents-2). However the renal symptoms of diseases associated with loss of function of OCRL1 and CLCN-5 overlap. In Dents disease, The H^+-ATPase displays inverted polarity in PTCs, localising to the basolateral domain in contrast to is normal apical localisation (Moulin et al., 2003).

Since proper polarisation of epithelial cells lining renal proximal tubules is essential for kidney function, it is possible that our findings with MDCK cells extend to Lowe Syndrome and Dents-2 disease. A role for OCRL1 in regulating apical recycling can potentially explain some phenotypic observations. Analysis of the proximal tubule dysfunction in Lowe Syndrome suggests absorption of substances that rely on vesicular trafficking are more affected than those that are directly released in the cytosol (Bockenhauer et al., 2008). For example, in a sample of patients, loss of low

molecular weight proteins was more extensive than loss of glucose (Bockenhauer et al., 2008), suggesting an underling trafficking defect. Low molecular weight proteins are absorbed from the proximal tubule by receptors such as megalin and cubilin which recycle between the apical plasma membrane and recycling endosomes. If OCRL1 functions to regulate traffic of apical cargo through recycling endosomes, one possibility is that these receptors accumulate intracellularly in Lowe Syndrome patients, resulting in a loss of LMW proteins in the ultrafiltrate.

Several findings support the possibility that the renal symptoms of Lowe Syndrome involve reduced apical recycling. Firstly, patients with Lowe Syndrome have reduced levels of the proteolytic cleavage products of megalin that are normally generated in the apical membrane, suggesting they may have reduced amounts of megalin at the apical surface (Norden et al., 2002). In a CLCN-5 knock out mouse model for Dent's disease, megalin and cubulin appeared redistributed from the brush border to intracellular endosomes, suggesting a block in recycling of megalin and cubulin to the brush border in the apical membrane (Christensen et al., 2003). Furthermore, reduced amounts of megalin have been observed at the apical brush border of the renal tubular epithelium of patients with Dents disease (Santo et al., 2004; Yanagida et al., 2004). Given our findings in MDCK cells, OCRL1 depletion might interfere with the trafficking of apical recycling, including receptors, through recycling compartments. If biopsy specimens could be obtained of the renal tubular epithelium from patients with Lowe Syndrome, the localisation of apical receptors could be examined by immunohistology. In addition, recent advances in animal models of Lowe Syndrome should facilitate progress in these investigations (Bothwell et al., 2011; Ramirez et al., 2012).

In addition to apico–basal polarity, epithelial cells display planar cell polarity. During development of the kidney, formation of tubules requires extensive elongation, involving a period of intense proliferation. This type of tubule elongation requires oriented cell division in which mitotic cells are oriented along an orthogonal axis in the plane of the tissue. Random mitotic spindle orientations interfere with normal elongation, giving rise the dilated tubules associated with some forms of polycystic

kidney disease (Fedeles and Gallagher, 2013). The finding that OCRL1 is potentially involved in pathways that regulate mitotic spindle orientation is worth investigating further. The localisation of OCRL1 to mitotic spindle poles has not been reported before, although it is known that OCRL1 localises to the abscission site during cytokinesis (Dambournet et al., 2011). However, a homologue of OCRL1 (TbOCRL1) is involved in spindle formation and mitosis in Trypanosomes (Abbasi et al., 2011). Like human OCRL1, TbOCRL1 has no GAP activity but interacts with the only Rho GTPase in *Trypanosoma brucei*, linking TbOCRL1 to a homologue of Rho-kinase (Abbasi et al., 2011). In MDCK cells, OCRL1 depletion disrupted the orientation of mitotic spindles, however whether OCRL1 interacts with a mammalian Rho GTPase, such as Rac or Cdc42 in this pathway remains to be determined. It is important to note that patients with Lowe Syndrome do not develop renal cysts. However dilation is sometimes observed in the late stages of Lowe Syndrome but it is not clear whether this is a cause or effect or tubular atrophy (Gropman et al., 2000). As mentioned above, future investigations into the morphology of renal tubules in patients and animal models of Lowe Syndrome will give a better indication of the underlying pathways disrupted.

The aim of this study was to investigate the role of OCRL1 in polarised cell types. Although we focused on the kidney, other tissues affected by Lowe Syndrome are highly polarised. Given our finding that OCRL1 disrupts polarisation in renal cells it would be interesting to carry out similar investigations in cells derived from other tissues affected by Lowe Syndrome. Lens epithelial cells form apical tight junctions with ZO-1 and express the same repertoire of polarity proteins as MDCK cells (Sugiyama et al., 2008). In addition, neurons are highly asymmetric with polarised membrane domains with specialised functions. The endosomal system is crucial for establishing and maintaining neuronal polarity, and it is therefore plausible that OCRL1 regulates polarised membrane trafficking pathways in neurons.

To study OCRL1 in polarised cell types, we primarily used the MDCK cell line, which is widely used as a model of epithelial polarity. In addition to the new finding that OCRL1 is critical for ensuring the proper organisation of polarised membrane

domains, our results provide some evidence that apical membrane formation is co-ordinated with cell division. In addition, our findings strengthen the idea that OCRL1 is involved in the traffic route to the midbody. Whether the dramatic effect of OCRL1 depletion on polarisation is unique to MDCK cells is yet to be determined. However preliminary findings with a human renal cell line (NHPTK) suggest OCRL1 is required for the normal morphology of monolayers. When these cells were depleted of OCRL1, F-actin was no longer enriched in the apical membrane and F-actin accumulated intracellularly on trafficking intermediates, in a similar manner to MDCK cells. These observations suggest a generalised function of OCRL1 in regulating apical trafficking pathways which fits with the renal symptoms of Lowe Syndrome and Dents-2 disease.

References

Abbasi, K., DuBois, K. N., Leung, K. F., Dacks, J. B., & Field, M. C. (2011). A novel Rho-like protein TbRHP is involved in spindle formation and mitosis in trypanosomes. *PLoS One, 6*(11), e26890.

Adams, M., Smith, U. M., Logan, C. V., & Johnson, C. A. (2008). Recent advances in the molecular pathology, cell biology and genetics of ciliopathies. *J Med Genet, 45*(5), 257-267.

Akiyama, C., Shinozaki-Narikawa, N., Kitazawa, T., Hamakubo, T., Kodama, T., & Shibasaki, Y. (2005). Phosphatidylinositol-4-phosphate 5-kinase gamma is associated with cell-cell junction in A431 epithelial cells. *Cell Biol Int, 29*(7), 514-520.

Ali, I. U., Schriml, L. M., & Dean, M. (1999). Mutational spectra of PTEN/MMAC1 gene: a tumor suppressor with lipid phosphatase activity. *J Natl Cancer Inst, 91*(22), 1922-1932.

Ang, A. L., Taguchi, T., Francis, S., Fölsch, H., Murrells, L. J., Pypaert, M., Warren, G., Mellman, I. (2004). Recycling endosomes can serve as intermediates during transport from the Golgi to the plasma membrane of MDCK cells. *J Cell Biol, 167*(3), 531-543.

Apodaca, G., Gallo, L. I., & Bryant, D. M. (2012). Role of membrane traffic in the generation of epithelial cell asymmetry. *Nat Cell Biol, 14*(12), 1235-1243.

Assémat, E., Bazellières, E., Pallesi-Pocachard, E., Le Bivic, A., & Massey-Harroche, D. (2008). Polarity complex proteins. *Biochim Biophys Acta, 1778*(3), 614-630.

Astle, M. V., Seaton, G., Davies, E. M., Fedele, C. G., Rahman, P., Arsala, L., & Mitchell, C. A. (2006). Regulation of phosphoinositide signaling by the inositol polyphosphate 5-phosphatases. *IUBMB Life, 58*(8), 451-456.

Balla, A., Tuymetova, G., Tsiomenko, A., Várnai, P., & Balla, T. (2005). A plasma membrane pool of phosphatidylinositol 4-phosphate is generated by phosphatidylinositol 4-kinase type-III alpha: studies with the PH domains of the oxysterol binding protein and FAPP1. *Mol Biol Cell, 16*(3), 1282-1295.

Barr, F., & Lambright, D. G. (2010). Rab GEFs and GAPs. *Curr Opin Cell Biol, 22*(4), 461-470.

Bartolini, F., & Gundersen, G. G. (2006). Generation of noncentrosomal microtubule arrays. *J Cell Sci, 119*(Pt 20), 4155-4163.

Bement, W. M., Benink, H. A., & von Dassow, G. (2005). A microtubule-dependent zone of active RhoA during cleavage plane specification. *J Cell Biol, 170*(1), 91-101.

Benais-Pont, G., Punn, A., Flores-Maldonado, C., Eckert, J., Raposo, G., Fleming, T. P., Cereijido, M., Balda, M. S., Matter, K. (2003). Identification of a tight junction-associated guanine nucleotide exchange factor that activates Rho and regulates paracellular permeability. *J Cell Biol.* 3;160(5):729-40.

Ben El Kadhi, K., Roubinet, C., Solinet, S., Emery, G., & Carréno, S. (2011). The inositol 5-phosphatase dOCRL controls PI(4,5)P2 homeostasis and is necessary for cytokinesis. *Curr Biol, 21*(12), 1074-1079.

Bershadsky, A. (2004). Magic touch: how does cell-cell adhesion trigger actin assembly? *Trends Cell Biol, 14*(11), 589-593.

Bielas, S. L., Silhavy, J. L., Brancati, F., Kisseleva, M. V., Al-Gazali, L., Sztriha, L., Bayoumi, R. A., Zaki, M. S., Abdel-Aleem, A., Rosti, R. O., Kayserili, H., Swistun, D., Scott, L. C., Bertini, E., Boltshauser, E., Fazzi, E., Travaglini, L., Field, S. J., Gayral, S., Jacoby, M., Schurmans, S., Dallapiccola, B., Majerus, P. W., Valente, E. M., Gleeson, J. G. (2009). Mutations in INPP5E, encoding inositol polyphosphate-5-phosphatase E, link phosphatidyl inositol signaling to the ciliopathies. *Nat Genet, 41*(9), 1032-1036.

Bockenhauer, D., Bokenkamp, A., van't Hoff, W., Levtchenko, E., Kist-van Holthe, J. E., Tasic, V., & Ludwig, M. (2008). Renal phenotype in Lowe Syndrome: a selective proximal tubular dysfunction. *Clin J Am Soc Nephrol, 3*(5), 1430-1436.

Bonilha, V. L., Marmorstein, A. D., Cohen-Gould, L., & Rodriguez-Boulan, E. (1997). Apical sorting of influenza hemagglutinin by transcytosis in retinal pigment epithelium. *J Cell Sci, 110 (Pt 15)*, 1717-1727.

Bothwell, S. P., Farber, L. W., Hoagland, A., & Nussbaum, R. L. (2010). Species-specific difference in expression and splice-site choice in Inpp5b, an inositol polyphosphate 5-phosphatase paralogous to the enzyme deficient in Lowe Syndrome. *Mamm Genome, 21*(9-10), 458-466.

Boucrot, E., & Kirchhausen, T. (2007). Endosomal recycling controls plasma membrane area during mitosis. *Proc Natl Acad Sci U S A, 104*(19), 7939-7944.

Bryant, D. M., Datta, A., Rodríguez-Fraticelli, A. E., Peränen, J., Martín-Belmonte, F., & Mostov, K. E. (2010). A molecular network for de novo generation of the apical surface and lumen. *Nat Cell Biol, 12*(11), 1035-1045.

Bryant, D. M., & Mostov, K. E. (2008). From cells to organs: building polarized tissue. *Nat Rev Mol Cell Biol, 9*(11), 887-901.

Cantley, L. C. (2002). The phosphoinositide 3-kinase pathway. *Science, 296*(5573), 1655-1657.

Cao, X., Surma, M. A., & Simons, K. (2012). Polarized sorting and trafficking in epithelial cells. *Cell Res, 22*(5), 793-805.

Carlton, J. G., & Cullen, P. J. (2005). Coincidence detection in phosphoinositide signaling. *Trends Cell Biol, 15*(10), 540-547.

Cassimeris, L., & Skibbens, R. V. (2003). Regulated assembly of the mitotic spindle: a perspective from two ends. *Curr Issues Mol Biol, 5*(3), 99-112.

Cavey, M., & Lecuit, T. (2009). Molecular bases of cell-cell junctions stability and dynamics. *Cold Spring Harb Perspect Biol, 1*(5), a002998.

Charron, A. J., Nakamura, S., Bacallao, R., & Wandinger-Ness, A. (2000). Compromised cytoarchitecture and polarized trafficking in autosomal dominant polycystic kidney disease cells. *J Cell Biol, 149*(1), 111-124.

Cho, M. J., Thompson, D. P., Cramer, C. T., Vidmar, T. J., & Scieszka, J. F. (1989). The Madin Darby canine kidney (MDCK) epithelial cell monolayer as a model cellular transport barrier. *Pharm Res, 6*(1), 71-77.

Choudhury, R., Diao, A., Zhang, F., Eisenberg, E., Saint-Pol, A., Williams, C., Konstantakopoulos, A., Lucocq, J., Johannes, L., Rabouille, C., Greene, L. E., Lowe, M. (2005). Lowe syndrome protein OCRL1 interacts with clathrin and regulates protein trafficking between endosomes and the trans-Golgi network. *Mol Biol Cell, 16*(8), 3467-3479.

Choudhury, R., Noakes, J C., McKenzie, E., Kox, C., Lowe, M. (2009). Differential Clathrin Binding and Subcellular Localization of OCRL1 Splice Isoforms. *J Biol Chem.* 10; 284(15): 9965–9973.

Christensen, E. I., & Birn, H. (2001). Megalin and cubilin: synergistic endocytic receptors in renal proximal tubule. *Am J Physiol Renal Physiol, 280*(4), F562-573.

Christensen, E. I., & Birn, H. (2002). Megalin and cubilin: multifunctional endocytic receptors. *Nat Rev Mol Cell Biol, 3*(4), 256-266.

Christensen, E. I., Devuyst, O., Dom, G., Nielsen, R., Van der Smissen, P., Verroust, P., Leruth, M., Guggino, W. B., Courtoy, P. J. (2003). Loss of chloride channel ClC-5 impairs endocytosis by defective trafficking of megalin and cubilin in kidney proximal tubules. *Proc Natl Acad Sci U S A, 100*(14), 8472-8477.

Clague, M. J., & Lorenzo, O. (2005). The myotubularin family of lipid phosphatases. *Traffic, 6*(12), 1063-1069.

Clarke, J. (2009). Role of polarized cell divisions in zebrafish neural tube formation. *Curr Opin Neurobiol, 19*(2), 134-138.

Clarke, J. H., Letcher, A. J., D'santos, C. S., Halstead, J. R., Irvine, R. F., & Divecha, N. (2001). Inositol lipids are regulated during cell cycle progression in the nuclei of murine erythroleukaemia cells. *Biochem J, 357*(Pt 3), 905-910.

Clément, S., Krause, U., Desmedt, F., Tanti, J. F., Behrends, J., Pesesse, X., Sasaki, T., Penninger, J., Doherty, M., Malaisse, W., Dumont, J. E., Le Marchand-Brustel, Y., Erneux, C., Hue, L., Schurmans, S. (2001). The lipid phosphatase SHIP2 controls insulin sensitivity. *Nature, 409*(6816), 92-97.

Cohen, D., Brennwald, P. J., Rodriguez-Boulan, E., & Müsch, A. (2004a). Mammalian PAR-1 determines epithelial lumen polarity by organizing the microtubule cytoskeleton. *J Cell Biol, 164*(5), 717-727.

Cohen, D., Fernandez, D., Lázaro-Diéguez, F., & Müsch, A. (2011). The serine/threonine kinase Par1b regulates epithelial lumen polarity via IRSp53-mediated cell-ECM signaling. *J Cell Biol, 192*(3), 525-540.

Cohen, D., & Müsch, A. (2003). Apical surface formation in MDCK cells: regulation by the serine/threonine kinase EMK1. *Methods, 30*(3), 269-276.

Cohen, D., Rodriguez-Boulan, E., & Müsch, A. (2004b). Par-1 promotes a hepatic mode of apical protein trafficking in MDCK cells. *Proc Natl Acad Sci U S A, 101*(38), 13792-13797.

Cohen, D., Tian, Y., & Müsch, A. (2007). Par1b promotes hepatic-type lumen polarity in Madin Darby canine kidney cells via myosin II- and E-cadherin-dependent signaling. *Mol Biol Cell, 18*(6), 2203-2215.

Coon, B. G., Hernandez, V., Madhivanan, K., Mukherjee, D., Hanna, C. B., Barinaga-Rementeria Ramirez, I., Lowe, M., Beales, P. L., Aguilar, R. C. (2012). The Lowe syndrome protein OCRL1 is involved in primary cilia assembly. *Hum Mol Genet, 21*(8), 1835-1847.

Coon, B. G., Mukherjee, D., Hanna, C. B., Riese, D. J., Lowe, M., & Aguilar, R. C. (2009). Lowe syndrome patient fibroblasts display Ocrl1-specific cell migration defects that cannot be rescued by the homologous Inpp5b phosphatase. *Hum Mol Genet, 18*(23), 4478-4491.

Cramm-Behrens, C. I., Dienst, M., & Jacob, R. (2008). Apical cargo traverses endosomal compartments on the passage to the cell surface. *Traffic, 9*(12), 2206-2220.

Cui, S., Guerriero, C. J., Szalinski, C. M., Kinlough, C. L., Hughey, R. P., & Weisz, O. A. (2010). OCRL1 function in renal epithelial membrane traffic. *Am J Physiol Renal Physiol, 298*(2), F335-345.

Czech, M. P. (2000). PIP2 and PIP3: complex roles at the cell surface. *Cell, 100*(6), 603-606.

D'Avino, P. P. (2009). How to scaffold the contractile ring for a safe cytokinesis - lessons from Anillin-related proteins. *J Cell Sci, 122*(Pt 8), 1071-1079.

Dambournet, D., Machicoane, M., Chesneau, L., Sachse, M., Rocancourt, M., El Marjou, A., Formstecher, E., Salomon, R., Goud, B., Echard, A., (2011). Rab35 GTPase and OCRL phosphatase remodel lipids and F-actin for successful cytokinesis. *Nat Cell Biol, 13*(8), 981-988.

Das, B., Shu, X., Day, G. J., Han, J., Krishna, U. M., Falck, J. R., & Broek, D. (2000). Control of intramolecular interactions between the pleckstrin homology and Dbl homology domains of Vav and Sos1 regulates Rac binding. *J Biol Chem, 275*(20), 15074-15081.

Datta, A., Bryant, D. M., & Mostov, K. E. (2011). Molecular regulation of lumen morphogenesis. *Curr Biol, 21*(3), R126-136.

Decaens, C., Rodriguez, P., Bouchaud, C., & Cassio, D. (1996). Establishment of hepatic cell polarity in the rat hepatoma-human fibroblast hybrid WIF-B9. A biphasic phenomenon going from a simple epithelial polarized phenotype to an hepatic polarized one. *J Cell Sci, 109 (Pt 6)*, 1623-1635.

den Elzen, N., Buttery, C. V., Maddugoda, M. P., Ren, G., & Yap, A. S. (2009). Cadherin adhesion receptors orient the mitotic spindle during symmetric cell division in mammalian epithelia. *Mol Biol Cell, 20*(16), 3740-3750.

Dragsten, P. R., Blumenthal, R., & Handler, J. S. (1981). Membrane asymmetry in epithelia: is the tight junction a barrier to diffusion in the plasma membrane? *Nature, 294*(5843), 718-722.

Dressman, M. A., Olivos-Glander, I. M., Nussbaum, R. L., & Suchy, S. F. (2000). Ocrl1, a PtdIns(4,5)P(2) 5-phosphatase, is localized to the trans-Golgi network of fibroblasts and epithelial cells. *J Histochem Cytochem, 48*(2), 179-190.

Drewes, G., Ebneth, A., Preuss, U., Mandelkow, E. M., & Mandelkow, E. (1997). MARK, a novel family of protein kinases that phosphorylate microtubule-associated proteins and trigger microtubule disruption. *Cell, 89*(2), 297-308.

Dunster, K., Toh, B. H., & Sentry, J. W. (2002). Early endosomes, late endosomes, and lysosomes display distinct partitioning strategies of inheritance with similarities to Golgi-derived membranes. *Eur J Cell Biol, 81*(3), 117-124.

Durgan, J., Kaji, N., Jin, D., & Hall, A. (2011). Par6B and atypical PKC regulate mitotic spindle orientation during epithelial morphogenesis. *J Biol Chem, 286*(14), 12461-12474.

El Sayegh, T. Y., Arora, P. D., Ling, K., Laschinger, C., Janmey, P. A., Anderson, R. A., & McCulloch, C. A. (2007). Phosphatidylinositol-4,5 bisphosphate produced by PIP5KIgamma regulates gelsolin, actin assembly, and adhesion strength of N-cadherin junctions. *Mol Biol Cell, 18*(8), 3026-3038.

Erdmann, K. S., Mao, Y., McCrea, H. J., Zoncu, R., Lee, S., Paradise, S., Modregger, J., Biemesderfer, D., Toomre, D., De Camilli, P. (2007). A role of the Lowe syndrome protein OCRL in early steps of the endocytic pathway. *Dev Cell, 13*(3), 377-390.

Etienne-Manneville, S. (2004). Cdc42--the centre of polarity. *J Cell Sci, 117*(Pt 8), 1291-1300.

Faucherre, A., Desbois, P., Nagano, F., Satre, V., Lunardi, J., Gacon, G., & Dorseuil, O. (2005). Lowe syndrome protein Ocrl1 is translocated to membrane ruffles upon Rac GTPase activation: a new perspective on Lowe syndrome pathophysiology. *Hum Mol Genet, 14*(11), 1441-1448.

Faucherre, A., Desbois, P., Satre, V., Lunardi, J., Dorseuil, O., & Gacon, G. (2003). Lowe syndrome protein OCRL1 interacts with Rac GTPase in the trans-Golgi network. *Hum Mol Genet, 12*(19), 2449-2456.

Fededa, J. P., & Gerlich, D. W. (2012). Molecular control of animal cell cytokinesis. *Nat Cell Biol, 14*(5), 440-447.

Fedeles, S., & Gallagher, A. R. (2013). Cell polarity and cystic kidney disease. *Pediatr Nephrol, 28*(8), 1161-1172.

Feng, W., Wu, H., Chan, L. N., & Zhang, M. (2008). Par-3-mediated junctional localization of the lipid phosphatase PTEN is required for cell polarity establishment. *J Biol Chem, 283*(34), 23440-23449.

Ferguson, S. M., & De Camilli, P. (2012). Dynamin, a membrane-remodelling GTPase. *Nat Rev Mol Cell Biol, 13*(2), 75-88.

Ferrari, A., Veligodskiy, A., Berge, U., Lucas, M. S., & Kroschewski, R. (2008). ROCK-mediated contractility, tight junctions and channels contribute to the conversion of a preapical patch into apical surface during isochoric lumen initiation. *J Cell Sci, 121*(Pt 21), 3649-3663.

Field, S. J., Madson, N., Kerr, M. L., Galbraith, K. A., Kennedy, C. E., Tahiliani, M., Wilkins, A., Cantley, L. C. (2005). PtdIns(4,5)P2 functions at the cleavage furrow during cytokinesis. *Curr Biol,* 15(15), 1407-1412.

Fielding, A. B., Royle, S. J. (2013). Mitotic inhibition of clathrin-mediated endocytosis. *Cell Mol Life Sci.,* 70(18):3423-33.

Fielding, A. B., Schonteich, E., Matheson, J., Wilson, G., Yu, X., Hickson, G. R., Srivastava S, Baldwin, S. A., Prekeris, R., Gould, G. W. (2005). Rab11-FIP3 and FIP4 interact with Arf6 and the exocyst to control membrane traffic in cytokinesis. *EMBO J, 24*(19), 3389-3399.

Fleming, E. S., Zajac, M., Moschenross, D. M., Montrose, D. C., Rosenberg, D. W., Cowan, A. E., & Tirnauer, J. S. (2007). Planar spindle orientation and asymmetric cytokinesis in the mouse small intestine. *J Histochem Cytochem, 55*(11), 1173-1180.

Fujii, M., Ohtsubo, M., Ogawa, T., Kamata, H., Hirata, H., & Yagisawa, H. (1999). Real-time visualization of PH domain-dependent translocation of phospholipase C-delta1 in renal epithelial cells (MDCK): response to hypo-osmotic stress. *Biochem Biophys Res Commun, 254*(2), 284-291.

Fukuda, M., Kanno, E., Ishibashi, K., & Itoh, T. (2008). Large scale screening for novel rab effectors reveals unexpected broad Rab binding specificity. *Mol Cell Proteomics, 7*(6), 1031-1042.

Gaidarov, I., & Keen, J. H. (1999). Phosphoinositide-AP-2 interactions required for targeting to plasma membrane clathrin-coated pits. *J Cell Biol, 146*(4), 755-764.

Garrard, S. M., Capaldo, C. T., Gao, L., Rosen, M. K., Macara, I. G., & Tomchick, D. R. (2003). Structure of Cdc42 in a complex with the GTPase-binding domain of the cell polarity protein, Par6. *EMBO J, 22*(5), 1125-1133.

Gassama-Diagne, A., Yu, W., ter Beest, M., Martin-Belmonte, F., Kierbel, A., Engel, J., & Mostov, K. (2006). Phosphatidylinositol-3,4,5-trisphosphate regulates the formation of the basolateral plasma membrane in epithelial cells. *Nat Cell Biol, 8*(9), 963-970.

Gerke, V., Creutz, C. E., & Moss, S. E. (2005). Annexins: linking Ca2+ signalling to membrane dynamics. *Nat Rev Mol Cell Biol, 6*(6), 449-461.

Gerke, V. Weber, K. (1984). Identity of p36K phosphorylated upon Rous sarcoma virus transformation with a protein from brush borders; calcium-dependent binding to nonerythroid spectrin and F-actin. *EMBO J*. 3, 227-233

Gervais, L., Claret, S., Januschke, J., Roth, S., & Guichet, A. (2008). PIP5K-dependent production of PIP2 sustains microtubule organization to establish polarized transport in the Drosophila oocyte. *Development, 135*(23), 3829-3838.

Gilbert, T., & Rodriguez-Boulan, E. (1991). Induction of vacuolar apical compartments in the Caco-2 intestinal epithelial cell line. *J Cell Sci, 100 (Pt 3)*, 451-458.

Gillooly, D. J., Morrow, I. C., Lindsay, M., Gould, R., Bryant, N. J., Gaullier, J. M., Parton, R. G., Stenmark, H. (2000). Localization of phosphatidylinositol 3-phosphate in yeast and mammalian cells. *EMBO J, 19*(17), 4577-4588.

Glotzer, M. (2005). The molecular requirements for cytokinesis. *Science, 307*(5716), 1735-1739.

Goetz, S. C., & Anderson, K. V. (2010). The primary cilium: a signalling centre during vertebrate development. *Nat Rev Genet, 11*(5), 331-344.

Goldstein, B., & Macara, I. G. (2007). The PAR proteins: fundamental players in animal cell polarization. *Dev Cell, 13*(5), 609-622.

Gonzalez-Mariscal, L., Namorado, M. C., Martin, D., Luna, J., Alarcon, L., Islas, S., Valencia, L., Muriel, P., Ponce, L., Reyes, J. L. (2000). Tight junction proteins ZO-1, ZO-2, and occludin along isolated renal tubules. *Kidney Int, 57*(6), 2386-2402.

Goss, J. W., & Toomre, D. K. (2008). Both daughter cells traffic and exocytose membrane at the cleavage furrow during mammalian cytokinesis. *J Cell Biol, 181*(7), 1047-1054.

Green, K. J., Getsios, S., Troyanovsky, S., & Godsel, L. M. (2010). Intercellular junction assembly, dynamics, and homeostasis. *Cold Spring Harb Perspect Biol, 2*(2), a000125.

Grieve, A. G., Daniels, R. D., Sanchez-Heras, E., Hayes, M. J., Moss, S. E., Matter, K., Lowe, M., Levine, T. P. (2011). Lowe Syndrome Protein OCRL1 Supports Maturation of Polarized Epithelial Cells. *PLoS One, 6*(8), e24044.

Gromley, A., Yeaman, C., Rosa, J., Redick, S., Chen, C. T., Mirabelle, S., Guha, M., Sillibourne, J., Doxsey, S. J. (2005). Centriolin anchoring of exocyst and SNARE complexes at the midbody is required for secretory-vesicle-mediated abscission. *Cell, 123*(1), 75-87.

Gropman, A., Levin, S., Yao, L., Lin, T., Suchy, S., Sabnis, S., Hadley, D., Nussbaum, R. (2000). Unusual renal features of Lowe syndrome in a mildly affected boy. *Am J Med Genet, 95*(5), 461-466.

Guizetti, J., Schermelleh, L., Mäntler, J., Maar, S., Poser, I., Leonhardt, H., Muller-Reichert, T., Gerlich, D. W. (2011). Cortical constriction during abscission involves helices of ESCRT-III-dependent filaments. *Science, 331*(6024), 1616-1620.

Habermann, B. (2004). The BAR-domain family of proteins: a case of bending and binding? *EMBO Rep, 5*(3), 250-255.

Hagemann, N., Hou, X., Goody, R. S., Itzen, A., & Erdmann, K. S. (2012). Crystal structure of the Rab binding domain of OCRL1 in complex with Rab8 and functional implications of the OCRL1/Rab8 module for Lowe syndrome. *Small GTPases, 3*(2), 107-110.

Hao, Y., Du, Q., Chen, X., Zheng, Z., Balsbaugh, J. L., Maitra, S., Shabanowitz, J., Hunt, D. F., Macara, I. G. (2010). Par3 controls epithelial spindle orientation by aPKC-mediated phosphorylation of apical Pins. *Curr Biol, 20*(20), 1809-1818.

Harten, S. K., Shukla, D., Barod, R., Hergovich, A., Balda, M. S., Matter, K., Esteban, M. A., Maxwell, P. H. (2009). Regulation of renal epithelial tight junctions by the von Hippel-Lindau tumor suppressor gene involves occludin and claudin 1 and is independent of E-cadherin. *Mol Biol Cell, 20*(3), 1089-1101.

Hartsock, A., & Nelson, W. J. (2008). Adherens and tight junctions: structure, function and connections to the actin cytoskeleton. *Biochim Biophys Acta, 1778*(3), 660-669.

Hayes, M. J., Shao, D. M., Grieve, A., Levine, T., Bailly, M., & Moss, S. E. (2009). Annexin A2 at the interface between F-actin and membranes enriched in phosphatidylinositol 4,5,-bisphosphate. *Biochim Biophys Acta, 1793*(6), 1086-1095.

He, B., Xi, F., Zhang, X., Zhang, J., & Guo, W. (2007). Exo70 interacts with phospholipids and mediates the targeting of the exocyst to the plasma membrane. *EMBO J, 26*(18), 4053-4065.

Hehnly, H., & Doxsey, S. (2012). Polarity sets the stage for cytokinesis. *Mol Biol Cell, 23*(1), 7-11.

Heo, W. D., Inoue, T., Park, W. S., Kim, M. L., Park, B. O., Wandless, T. J., & Meyer, T. (2006). PI(3,4,5)P3 and PI(4,5)P2 lipids target proteins with polybasic clusters to the plasma membrane. *Science, 314*(5804), 1458-1461.

Herbert, B. S., Grimes, B. R., Xu, W. M., Werner, M., Ward, C., Rossetti, S., Harris, P., Bello-Reuss, E., Ward, H. H., Miller, C., Gattone, V. H., Phillips, C. L.,

Wandinger-Ness, A., Bacallao, R. L. (2013). A telomerase immortalized human proximal tubule cell line with a truncation mutation (Q4004X) in polycystin-1. *PLoS One, 8*(1), e55191.

Herszterg, S., Leibfried, A., Bosveld, F., Martin, C., & Bellaiche, Y. (2013). Interplay between the dividing cell and its neighbors regulates adherens junction formation during cytokinesis in epithelial tissue. *Dev Cell, 24*(3), 256-270.

Hilpelä, P., Vartiainen, M. K., & Lappalainen, P. (2004). Regulation of the actin cytoskeleton by PI(4,5)P2 and PI(3,4,5)P3. *Curr Top Microbiol Immunol, 282*, 117-163.

Hobdy-Henderson, K. C., Hales, C. M., Lapierre, L. A., Cheney, R. E., & Goldenring, J. R. (2003). Dynamics of the apical plasma membrane recycling system during cell division. *Traffic, 4*(10), 681-693.

Hogan, B. L., & Kolodziej, P. A. (2002). Organogenesis: molecular mechanisms of tubulogenesis. *Nat Rev Genet, 3*(7), 513-523.

Hoopes, R. R., Shrimpton, A. E., Knohl, S. J., Hueber, P., Hoppe, B., Matyus, J., Simckes, A., Tasic, V., Toenshoff, B., Suchy, S. F., Nussbaum, R. L., Scheinman, S. J. (2005). Dent Disease with mutations in OCRL1. *Am J Hum Genet, 76*(2), 260-267.

Horikoshi, Y., Suzuki, A., Yamanaka, T., Sasaki, K., Mizuno, K., Sawada, H., Yonemura, S., Ohno, S. (2009). Interaction between PAR-3 and the aPKC-PAR-6 complex is indispensable for apical domain development of epithelial cells. *J Cell Sci, 122*(Pt 10), 1595-1606.

Hou, X., Hagemann, N., Schoebel, S., Blankenfeldt, W., Goody, R. S., Erdmann, K. S., & Itzen, A. (2011). A structural basis for Lowe syndrome caused by mutations in the Rab-binding domain of OCRL1. *EMBO J, 30*(8), 1659-1670.

Hua, W., Sheff, D., Toomre, D., & Mellman, I. (2006). Vectorial insertion of apical and basolateral membrane proteins in polarized epithelial cells revealed by quantitative 3D live cell imaging. *J Cell Biol, 172*(7), 1035-1044.

Hutagalung, A. H., & Novick, P. J. (2011). Role of Rab GTPases in membrane traffic and cell physiology. *Physiol Rev, 91*(1), 119-149.

Hyvola, N., Diao, A., McKenzie, E., Skippen, A., Cockcroft, S., & Lowe, M. (2006). Membrane targeting and activation of the Lowe syndrome protein OCRL1 by rab GTPases. *EMBO J, 25*(16), 3750-3761.

Ikonomov, O. C., Sbrissa, D., & Shisheva, A. (2006). Localized PtdIns 3,5-P2 synthesis to regulate early endosome dynamics and fusion. *Am J Physiol Cell Physiol, 291*(2), C393-404.

Illenberger, S., Drewes, G., Trinczek, B., Biernat, J., Meyer, H. E., Olmsted, J. B., Mandelkow, E. M., Mandelkow, E. (1996). Phosphorylation of microtubule-associated proteins MAP2 and MAP4 by the protein kinase p110mark. Phosphorylation sites and regulation of microtubule dynamics. *J Biol Chem, 271*(18), 10834-10843.

Itoh, T., & De Camilli, P. (2006). BAR, F-BAR (EFC) and ENTH/ANTH domains in the regulation of membrane-cytosol interfaces and membrane curvature. *Biochim Biophys Acta, 1761*(8), 897-912.

Itoh, T., Koshiba, S., Kigawa, T., Kikuchi, A., Yokoyama, S., & Takenawa, T. (2001). Role of the ENTH domain in phosphatidylinositol-4,5-bisphosphate binding and endocytosis. *Science, 291*(5506), 1047-1051.

Jacoby, M., Cox, J. J., Gayral, S., Hampshire, D. J., Ayub, M., Blockmans, M., Pernot, E., Kisseleva, M. V., Compere, P., Schiffmann, S. N., Gergely, F., Riley, J. H., Perez-Morga, D., Woods, C. G., Schurmans, S. (2009). INPP5E mutations cause primary cilium signaling defects, ciliary instability and ciliopathies in human and mouse. *Nat Genet, 41*(9), 1027-1031.

Jaffe, A. B., Kaji, N., Durgan, J., & Hall, A. (2008). Cdc42 controls spindle orientation to position the apical surface during epithelial morphogenesis. *J Cell Biol, 183*(4),625-633.

Jamora, C., & Fuchs, E. (2002). Intercellular adhesion, signalling and the cytoskeleton. *Nat Cell Biol, 4*(4), E101-108.

Janke, M., Herrig, A., Austermann, J., Gerke, V., Steinem, C., & Janshoff, A. (2008). Actin binding of ezrin is activated by specific recognition of PIP2-functionalized lipid bilayers. *Biochemistry, 47*(12), 3762-3769.

Jean, S., Cox, S., Schmidt, E. J., Robinson, F. L., & Kiger, A. (2012). Sbf/MTMR13 coordinates PI(3)P and Rab21 regulation in endocytic control of cellular remodeling. *Mol Biol Cell, 23*(14), 2723-2740.

Jean, S., & Kiger, A. A. (2012). Coordination between RAB GTPase and phosphoinositide regulation and functions. *Nat Rev Mol Cell Biol, 13*(7), 463-470.

Jeanes, A., Smutny, M., Leerberg, J. M., & Yap, A. S. (2009). Phosphatidylinositol 3'-kinase signalling supports cell height in established epithelial monolayers. *J Mol Histol, 40*(5-6), 395-405.

Jefferson, A. B., & Majerus, P. W. (1995). Properties of type II inositol polyphosphate 5-phosphatase. *J Biol Chem, 270*(16), 9370-9377.

Johnson, J. L., Erickson, J. W., & Cerione, R. A. (2012). C-terminal di-arginine motif of Cdc42 protein is essential for binding to phosphatidylinositol 4,5-bisphosphate-containing membranes and inducing cellular transformation. *J Biol Chem, 287*(8), 5764-5774.

Johnson, J. M., Castle, J., Garrett-Engele, P., Kan, Z., Loerch, P. M., Armour, C. D., Santos, R., Schadt, E. E., Stoughton, R., Shoemaker, D. D. (2003). Genome-

wide survey of human alternative pre-mRNA splicing with exon junction microarrays. *Science, 302*(5653), 2141-2144.

Jänne, P. A., Suchy, S. F., Bernard, D., MacDonald, M., Crawley, J., Grinberg, A., Wynshaw-Boris, A., Westphal, H., Nussbaum, R. L. (1998). Functional overlap between murine Inpp5b and Ocrl1 may explain why deficiency of the murine ortholog for OCRL1 does not cause Lowe syndrome in mice. *J Clin Invest, 101*(10), 2042-2053.

Kaksonen, M., Toret, C. P., & Drubin, D. G. (2005). A modular design for the clathrin- and actin-mediated endocytosis machinery. *Cell, 123*(2), 305-320.

Kamberov, E., Makarova, O., Roh, M., Liu, A., Karnak, D., Straight, S., & Margolis, B. (2000). Molecular cloning and characterization of Pals, proteins associated with mLin-7. *J Biol Chem, 275*(15), 11425-11431.

Kaur, S., Fielding, A. B., Gassner, G., Carter, N. J. & Royle, S.J. (2014) An unmet actin requirement explains the mitotic inhibition of clathrin-mediated endocytosis. *eLife.* in press.

Kemphues, K. J., Priess, J. R., Morton, D. G., & Cheng, N. S. (1988). Identification of genes required for cytoplasmic localization in early C. elegans embryos. *Cell, 52*(3), 311-320.

King, W. G., Mattaliano, M. D., Chan, T. O., Tsichlis, P. N., & Brugge, J. S. (1997). Phosphatidylinositol 3-kinase is required for integrin-stimulated AKT and Raf-1/mitogen-activated protein kinase pathway activation. *Mol Cell Biol, 17*(8), 4406-4418.

Kiuchi-Saishin, Y., Gotoh, S., Furuse, M., Takasuga, A., Tano, Y., & Tsukita, S. (2002). Differential expression patterns of claudins, tight junction membrane proteins, in mouse nephron segments. *J Am Soc Nephrol, 13*(4), 875-886.

Kizhatil, K., & Bennett, V. (2004). Lateral membrane biogenesis in human bronchial epithelial cells requires 190-kDa ankyrin-G. *J Biol Chem, 279*(16), 16706-16714.

Klarlund, J. K., Tsiaras, W., Holik, J. J., Chawla, A., & Czech, M. P. (2000). Distinct polyphosphoinositide binding selectivities for pleckstrin homology domains of GRP1-like proteins based on diglycine versus triglycine motifs. *J Biol Chem, 275*(42), 32816-32821.

Knust, E., & Bossinger, O. (2002). Composition and formation of intercellular junctions in epithelial cells. *Science, 298*(5600), 1955-1959.

Kouranti, I., Sachse, M., Arouche, N., Goud, B., & Echard, A. (2006). Rab35 regulates an endocytic recycling pathway essential for the terminal steps of cytokinesis. *Curr Biol, 16*(17), 1719-1725.

Kovacs, E. M., Ali, R. G., McCormack, A. J., & Yap, A. S. (2002). E-cadherin homophilic ligation directly signals through Rac and phosphatidylinositol 3-kinase to regulate adhesive contacts. *J Biol Chem, 277*(8), 6708-6718.

Krahn, M. P., Klopfenstein, D. R., Fischer, N., & Wodarz, A. (2010). Membrane targeting of Bazooka/PAR-3 is mediated by direct binding to phosphoinositide lipids. *Curr Biol, 20*(7), 636-642.

Kumar, N. M., & Gilula, N. B. (1996). The gap junction communication channel. *Cell, 84*(3), 381-388.

Kutateladze, T. G. (2010). Translation of the phosphoinositide code by PI effectors. *Nat Chem Biol, 6*(7), 507-513.

Lafont, F., Burkhardt, J. K., & Simons, K. (1994). Involvement of microtubule motors in basolateral and apical transport in kidney cells. *Nature, 372*(6508), 801-803.

Lalli, G. (2009). RalA and the exocyst complex influence neuronal polarity through PAR-3 and aPKC. *J Cell Sci, 122*(Pt 10), 1499-1506.

Lanzetti, L. (2007). Actin in membrane trafficking. *Curr Opin Cell Biol, 19*(4), 453-458.

Lapierre, L. A., Kumar, R., Hales, C. M., Navarre, J., Bhartur, S. G., Burnette, J. O., Provance, D. W., Mercer, J. A., Bahler, M., Goldenring, J. R. (2001). Myosin vb is associated with plasma membrane recycling systems. *Mol Biol Cell, 12*(6), 1843-1857.

Lee, D. B., Huang, E., & Ward, H. J. (2006). Tight junction biology and kidney dysfunction. *Am J Physiol Renal Physiol, 290*(1), F20-34.

Lemmon, M. A. (2003). Phosphoinositide recognition domains. *Traffic, 4*(4), 201-213.

Lemmon, M. A. (2008). Membrane recognition by phospholipid-binding domains. *Nat Rev Mol Cell Biol, 9*(2), 99-111.

Leung, S. M., Ruiz, W. G., & Apodaca, G. (2000). Sorting of membrane and fluid at the apical pole of polarized Madin-Darby canine kidney cells. *Mol Biol Cell, 11*(6), 2131-2150.

Levtsova, O. V., Davletov, I. D., Sokolova, O. S., & Shaĭtan, K. V. (2011). A molecular dynamics study of the interaction between domain I-BAR of the IRSp53 protein and negatively charged membranes. *Biofizika, 56*(2), 242-247.

Lichter-Konecki, U., Farber, L. W., Cronin, J. S., Suchy, S. F., & Nussbaum, R. L. (2006). The effect of missense mutations in the RhoGAP-homology domain on ocrl1 function. *Mol Genet Metab, 89*(1-2), 121-128.

Lietzke, S. E., Bose, S., Cronin, T., Klarlund, J., Chawla, A., Czech, M. P., & Lambright, D. G. (2000). Structural basis of 3-phosphoinositide recognition by pleckstrin homology domains. *Mol Cell, 6*(2), 385-394.

Lin, D. C., Quevedo, C., Brewer, N. E., Bell, A., Testa, J. R., Grimes, M. L., Miller, F. D., Kaplan, D. R. (2006). APPL1 associates with TrkA and GIPC1 and is required for nerve growth factor-mediated signal transduction. *Mol Cell Biol, 26*(23), 8928-8941.

Liu, J., Fairn, G. D., Ceccarelli, D. F., Sicheri, F., & Wilde, A. (2012). Cleavage furrow organization requires PIP(2)-mediated recruitment of anillin. *Curr Biol, 22*(1), 64-69. doi: 10.1016/j.cub.2011.11.040

Liu, Y., & Bankaitis, V. A. (2010). Phosphoinositide phosphatases in cell biology and disease. *Prog Lipid Res, 49*(3), 201-217.

Lizarbe, M. A., Barrasa, J. I., Olmo, N., Gavilanes, F., & Turnay, J. (2013). Annexin-phospholipid interactions. Functional implications. *Int J Mol Sci, 14*(2), 2652-2683.

Logan, M. R., & Mandato, C. A. (2006). Regulation of the actin cytoskeleton by PIP2 in cytokinesis. *Biol Cell, 98*(6), 377-388.

Loi, M. (2006). Lowe syndrome. *Orphanet J Rare Dis, 1*, 16.

Lou, X., McQuistan, T., Orlando, R. A., & Farquhar, M. G. (2002). GAIP, GIPC and Galphai3 are concentrated in endocytic compartments of proximal tubule cells: putative role in regulating megalin's function. *J Am Soc Nephrol, 13*(4), 918-927.

Lowe, C. U., Terrey, M., & MacLachlan, E. A. (1952). Organic-aciduria, decreased renal ammonia production, hydrophthalmos, and mental retardation; a clinical entity. *AMA Am J Dis Child, 83*(2), 164-184.

Lowe, M. (2005). Structure and function of the Lowe syndrome protein OCRL1. *Traffic, 6*(9), 711-719.

Luo, N., West, C. C., Murga-Zamalloa, C. A., Sun, L., Anderson, R. M., Wells, C. D., Weinreb, R. N., Travers, J. B., Khanna, H., Sun, Y. (2012). OCRL localizes to the primary cilium: a new role for cilia in Lowe syndrome. *Hum Mol Genet, 21*(15), 3333-3344.

Maddox, A. S., Lewellyn, L., Desai, A., & Oegema, K. (2007). Anillin and the septins promote asymmetric ingression of the cytokinetic furrow. *Dev Cell, 12*(5), 827-835.

Mailleux, A. A., Overholtzer, M., & Brugge, J. S. (2008). Lumen formation during mammary epithelial morphogenesis: insights from in vitro and in vivo models. *Cell Cycle, 7*(1), 57-62.

Mao, Y., Balkin, D. M., Zoncu, R., Erdmann, K. S., Tomasini, L., Hu, F., Jin, M. M., Hodsdon, M. E., De Camilli, P. (2009). A PH domain within OCRL bridges clathrin-mediated membrane trafficking to phosphoinositide metabolism. *EMBO J, 28*(13), 1831-1842.

Mao, Y. S., & Yin, H. L. (2007). Regulation of the actin cytoskeleton by phosphatidylinositol 4-phosphate 5 kinases. *Pflugers Arch, 455*(1), 5-18.

Margolis, B., & Borg, J. P. (2005). Apicobasal polarity complexes. *J Cell Sci, 118*(Pt 22), 5157-5159.

Martin-Belmonte, F., Gassama, A., Datta, A., Yu, W., Rescher, U., Gerke, V., & Mostov, K. (2007). PTEN-mediated apical segregation of phosphoinositides controls epithelial morphogenesis through Cdc42. *Cell, 128*(2), 383-397.

Martín-Belmonte, F., Yu, W., Rodríguez-Fraticelli, A. E., Ewald, A. J., Ewald, A., Werb, Z., Alonso, M. A., Mostov, K. (2008). Cell-polarity dynamics controls the mechanism of lumen formation in epithelial morphogenesis. *Curr Biol, 18*(7), 507-513.

Marzesco, A. M., Dunia, I., Pandjaitan, R., Recouvreur, M., Dauzonne, D., Benedetti, E. L., Louvard, D., Zahraoui, A. (2002). The small GTPase Rab13 regulates assembly of functional tight junctions in epithelial cells. *Mol Biol Cell, 13*(6), 1819-1831.

Masuda-Hirata, M., Suzuki, A., Amano, Y., Yamashita, K., Ide, M., Yamanaka, T., Sakai, M., Imamura, M., Ohno, S. (2009). Intracellular polarity protein PAR-1 regulates extracellular laminin assembly by regulating the dystroglycan complex. *Genes Cells, 14*(7), 835-850.

Matter, K., & Balda, M. S. (2003). Signalling to and from tight junctions. *Nat Rev Mol Cell Biol, 4*(3), 225-236.

Matter, K., Brauchbar, M., Bucher, K., & Hauri, H. P. (1990). Sorting of endogenous plasma membrane proteins occurs from two sites in cultured human intestinal epithelial cells (Caco-2). *Cell, 60*(3), 429-437.

Maurice, M., Schell, M. J., Lardeux, B., & Hubbard, A. L. (1994). Biosynthesis and intracellular transport of a bile canalicular plasma membrane protein: studies in vivo and in the perfused rat liver. *Hepatology, 19*(3), 648-655.

McConkey, D. J., Choi, W., Marquis, L., Martin, F., Williams, M. B., Shah, J., Svatek, R., Das, A., Adam, L., Kamat, A., Siefker-Radtke, A., Dinney, C. (2009). Role of epithelial-to-mesenchymal transition (EMT) in drug sensitivity and metastasis in bladder cancer. *Cancer Metastasis Rev, 28*(3-4), 335-344.

McMahon, H. T., & Gallop, J. L. (2005). Membrane curvature and mechanisms of dynamic cell membrane remodelling. *Nature, 438*(7068), 590-596.

Meder, D., Shevchenko, A., Simons, K., & Füllekrug, J. (2005). Gp135/podocalyxin and NHERF-2 participate in the formation of a preapical domain during polarization of MDCK cells. *J Cell Biol, 168*(2), 303-313.

Mizuno-Yamasaki, E., Rivera-Molina, F., & Novick, P. (2012). GTPase networks in membrane traffic. *Annu Rev Biochem, 81*, 637-659.

Montagnac, G., Echard, A., & Chavrier, P. (2008). Endocytic traffic in animal cell cytokinesis. *Curr Opin Cell Biol, 20*(4), 454-461.

Morais-de-Sá, E., Mirouse, V., & St Johnston, D. (2010). aPKC phosphorylation of Bazooka defines the apical/lateral border in Drosophila epithelial cells. *Cell, 141*(3), 509-523.

Morais-de-Sá, E., & Sunkel, C. (2013). Adherens junctions determine the apical position of the midbody during follicular epithelial cell division. *EMBO Rep, 14*(8), 696-703.

Moravcevic, K., Mendrola, J. M., Schmitz, K. R., Wang, Y. H., Slochower, D., Janmey, P. A., & Lemmon, M. A. (2010). Kinase associated-1 domains drive MARK/PAR1 kinases to membrane targets by binding acidic phospholipids. *Cell, 143*(6), 966-977.

Moulin, P., Igarashi, T., Van der Smissen, P., Cosyns, J. P., Verroust, P., Thakker, R. V., Scheinman, S. J., Courtoy, P. J., Devuyst, O. (2003). Altered polarity and expression of H+-ATPase without ultrastructural changes in kidneys of Dent's disease patients. *Kidney Int, 63*(4), 1285-1295.

Müller, T., Hess, M. W., Schiefermeier, N., Pfaller, K., Ebner, H. L., Heinz-Erian, P., Ponsting, l. H., Partsch, J., Röllinghoff, B., Köhler, H., Berger, T., Lenhartz, H., Schlenck, B., Houwen, R. J., Taylor, C. J., Zoller, H., Lechner, S., Goulet, O., Utermann, G., Ruemmele, F. M., Huber, L. A., Janecke, A. R. (2008). MYO5B mutations cause microvillus inclusion disease and disrupt epithelial cell polarity. *Nat Genet, 40*(10), 1163-1165.

Müsch, A. (2004). Microtubule organization and function in epithelial cells. *Traffic, 5*(1), 1-9.

Nakanishi, H., & Takai, Y. (2008). Frabin and other related Cdc42-specific guanine nucleotide exchange factors couple the actin cytoskeleton with the plasma membrane. *J Cell Mol Med, 12*(4), 1169-1176.

Nelson, W. J. (2003). Adaptation of core mechanisms to generate cell polarity. *Nature, 422*(6933), 766-774.

Neto, H., & Gould, G. W. (2011). The regulation of abscission by multi-protein complexes. *J Cell Sci, 124*(Pt 19), 3199-3207.

Noakes, C. J., Lee, G., & Lowe, M. (2011). The PH domain proteins IPIP27A and B link OCRL1 to receptor recycling in the endocytic pathway. *Mol Biol Cell, 22*(5), 606-623.

Noda, Y., Okada, Y., Saito, N., Setou, M., Xu, Y., Zhang, Z., & Hirokawa, N. (2001). KIFC3, a microtubule minus end-directed motor for the apical transport of annexin XIIIb-associated Triton-insoluble membranes. *J Cell Biol, 155*(1), 77-88.

Norden, A. G., Lapsley, M., Igarashi, T., Kelleher, C. L., Lee, P. J., Matsuyama, T., Scheinman, S. J., Shiraga, H., Sundin, D. P., Thakker, R. V., Unwin, R. J., Verroust, P. Moestrup, S. K. (2002). Urinary megalin deficiency implicates abnormal tubular endocytic function in Fanconi syndrome. *J Am Soc Nephrol, 13*(1), 125-133.

Nussbaum, R. L., Orrison, B. M., Jänne, P. A., Charnas, L., & Chinault, A. C. (1997). Physical mapping and genomic structure of the Lowe syndrome gene OCRL1. *Hum Genet, 99*(2), 145-150.

O'Brien, L. E., Jou, T. S., Pollack, A. L., Zhang, Q., Hansen, S. H., Yurchenco, P., & Mostov, K. E. (2001). Rac1 orientates epithelial apical polarity through effects on basolateral laminin assembly. *Nat Cell Biol, 3*(9), 831-838.

O'Brien, L. E., Zegers, M. M., & Mostov, K. E. (2002). Opinion: Building epithelial architecture: insights from three-dimensional culture models. *Nat Rev Mol Cell Biol, 3*(7), 531-537.

Ojakian, G. K., & Schwimmer, R. (1988). The polarized distribution of an apical cell surface glycoprotein is maintained by interactions with the cytoskeleton of Madin-Darby canine kidney cells. *J Cell Biol, 107*(6 Pt 1), 2377-2387.

Olivos-Glander, I. M., Janne, P. A. and Nussbaum, R. L. (1995). The oculocerebrorenal syndrome gene product is a 105-kD protein localized to the Golgi complex. Am. J. Hum. Genet. 57, 817–823

Orosz, D. E., Woost, P. G., Kolb, R. J., Finesilver, M. B., Jin, W., Frisa, P. S., Choo, C. K., Yau, C. F., Chan, K. W., Resnick, M. I., Douglas, J. G., Edwards, J. C., Jacobberger, J. W., Hopfer, U. (2004). Growth, immortalization, and

differentiation potential of normal adult human proximal tubule cells. *In Vitro Cell Dev Biol Anim, 40*(1-2), 22-34.

Oztan, A., Silvis, M., Weisz, O. A., Bradbury, N. A., Hsu, S. C., Goldenring, J. R., Yeaman, C., Apodaca, G. (2007). Exocyst requirement for endocytic traffic directed toward the apical and basolateral poles of polarized MDCK cells. *Mol Biol Cell, 18*(10), 3978-3992.

Padrick, S. B., & Rosen, M. K. (2010). Physical mechanisms of signal integration by WASP family proteins. *Annu Rev Biochem, 79*, 707-735.

Pandey, K. N. (2010). Small peptide recognition sequence for intracellular sorting. *Curr Opin Biotechnol, 21*(5), 611-620.

Pearson, M. A., Reczek, D., Bretscher, A., & Karplus, P. A. (2000). Structure of the ERM protein moesin reveals the FERM domain fold masked by an extended actin binding tail domain. *Cell, 101*(3), 259-270.

Pirruccello, M., Swan, L. E., Folta-Stogniew, E., & De Camilli, P. (2011). Recognition of the F&H motif by the Lowe syndrome protein OCRL. *Nat Struct Mol Biol, 18*(7), 789-795.

Pohl, C., & Jentsch, S. (2008). Final stages of cytokinesis and midbody ring formation are controlled by BRUCE. *Cell, 132*(5), 832-845.

Ponting, C. P. (2006). A novel domain suggests a ciliary function for ASPM, a brain size determining gene. *Bioinformatics, 22*(9), 1031-1035.

Prigent, M., Dubois, T., Raposo, G., Derrien, V., Tenza, D., Rosse, C., Camonis, J., Chavrier, P. (2003). ARF6 controls post-endocytic recycling through its downstream exocyst complex effector. *J Cell Biol, 163*(5), 1111-1121.

Qin, Y., Capaldo, C., Gumbiner, B. M., & Macara, I. G. (2005). The mammalian Scribble polarity protein regulates epithelial cell adhesion and migration through E-cadherin. *J Cell Biol, 171*(6), 1061-1071.

Qin, Y., Meisen, W. H., Hao, Y., & Macara, I. G. (2010). Tuba, a Cdc42 GEF, is required for polarized spindle orientation during epithelial cyst formation. *J Cell Biol, 189*(4), 661-669.

Ramirez, I. B., Pietka, G., Jones, D. R., Divecha, N., Alia, A., Baraban, S. C., Hurlstone, A. F., Lowe, M. (2012). Impaired neural development in a zebrafish model for Lowe syndrome. *Hum Mol Genet, 21*(8), 1744-1759.

Raucher, D., Stauffer, T., Chen, W., Shen, K., Guo, S., York, J. D., Sheetz, M. P., Meyer, T. (2000). Phosphatidylinositol 4,5-bisphosphate functions as a second messenger that regulates cytoskeleton-plasma membrane adhesion. *Cell, 100*(2), 221-228.

Rbaibi, Y., Cui, S., Mo, D., Carattino, M., Rohatgi, R., Satlin, L. M., Szalinski, C. M., Swanhart, L. M., Folsch, H., Hukriede, N. A., Weisz, O. A. (2012). OCRL1 modulates cilia length in renal epithelial cells. *Traffic, 13*(9), 1295-1305.

Reaves, B. J., Bright, N. A., Mullock, B. W. and Luzio, J. P. (1996). The effect of wortmannin on the localisation of lysosomal type I integral membrane glycoproteins suggests a role for phosphoinositide 3-kinase activity in regulating membrane traffic late in the endocytic pathway. *J. Cell Sci.* 109, 749-762.

Reinsch, S., & Karsenti, E. (1994). Orientation of spindle axis and distribution of plasma membrane proteins during cell division in polarized MDCKII cells. *J Cell Biol, 126*(6), 1509-1526.

Rescher, U., Ruhe, D., Ludwig, C., Zobiack, N., & Gerke, V. (2004). Annexin 2 is a phosphatidylinositol (4,5)-bisphosphate binding protein recruited to actin assembly sites at cellular membranes. *J Cell Sci, 117*(Pt 16), 3473-3480.

Revenu, C., Ubelmann, F., Hurbain, I., El-Marjou, F., Dingli, F., Loew, D., Delacour, D., Gilet, J., Brot-Laroche, E., Rivero, F., Louvard, D., Robine, S. (2012). A new role for the architecture of microvillar actin bundles in apical retention of membrane proteins. *Mol Biol Cell, 23*(2), 324-336.

Richards, W. G., Sweeney, W. E., Yoder, B. K., Wilkinson, J. E., Woychik, R. P., & Avner, E. D. (1998). Epidermal growth factor receptor activity mediates renal cyst formation in polycystic kidney disease. *J Clin Invest, 101*(5), 935-939.

Ridley, A. J. (2006). Rho GTPases and actin dynamics in membrane protrusions and vesicle trafficking. *Trends Cell Biol, 16*(10), 522-529.

Rink, J., Ghigo, E., Kalaidzidis, Y., & Zerial, M. (2005). Rab conversion as a mechanism of progression from early to late endosomes. *Cell, 122*(5), 735-749.

Rodriguez-Boulan, E., Kreitzer, G., & Musch, A. (2005). Organization of vesicular trafficking in epithelia. *Nat Rev Mol Cell Biol, 6*(3), 233-247.

Rodriguez-Boulan, E., & Nelson, W. J. (1989). Morphogenesis of the polarized epithelial cell phenotype. *Science, 245*(4919), 718-725.

Rodriguez-Fraticelli, A. E., Vergarajauregui, S., Eastburn, D. J., Datta, A., Alonso, M. A., Mostov, K., & Martín-Belmonte, F. (2010). The Cdc42 GEF Intersectin 2 controls mitotic spindle orientation to form the lumen during epithelial morphogenesis. *J Cell Biol, 189*(4), 725-738.

Rodriguez-Gabin, A. G., Ortiz, E., Demoliner, K., Si, Q., Almazan, G., & Larocca, J. N. (2010). Interaction of Rab31 and OCRL-1 in oligodendrocytes: its role in

transport of mannose 6-phosphate receptors. *J Neurosci Res, 88*(3), 589-604.

Roh, M. H., Fan, S., Liu, C. J., & Margolis, B. (2003). The Crumbs3-Pals1 complex participates in the establishment of polarity in mammalian epithelial cells. *J Cell Sci, 116*(Pt 14), 2895-2906.

Roh, M. H., Liu, C. J., Laurinec, S., & Margolis, B. (2002). The carboxyl terminus of zona occludens-3 binds and recruits a mammalian homologue of discs lost to tight junctions. *J Biol Chem, 277*(30), 27501-27509.

Rohatgi, R., Ho, H. Y., & Kirschner, M. W. (2000). Mechanism of N-WASP activation by CDC42 and phosphatidylinositol 4, 5-bisphosphate. *J Cell Biol, 150*(6), 1299-1310.

Rojas, R., Ruiz, W. G., Leung, S. M., Jou, T. S., & Apodaca, G. (2001). Cdc42-dependent modulation of tight junctions and membrane protein traffic in polarized Madin-Darby canine kidney cells. *Mol Biol Cell, 12*(8), 2257-2274.

Roland, J. T., Bryant, D. M., Datta, A., Itzen, A., Mostov, K. E., & Goldenring, J. R. (2011). Rab GTPase-Myo5B complexes control membrane recycling and epithelial polarization. *Proc Natl Acad Sci U S A, 108*(7), 2789-2794.

Roy, A., & Levine, T. P. (2004). Multiple pools of phosphatidylinositol 4-phosphate detected using the pleckstrin homology domain of Osh2p. *J Biol Chem, 279*(43), 44683-44689.

Sagona, A. P., Nezis, I. P., Pedersen, N. M., Liestøl, K., Poulton, J., Rusten, T. E., Skotheim, R. I., Raiborg, C., Stenmark, H. (2010). PtdIns(3)P controls cytokinesis through KIF13A-mediated recruitment of FYVE-CENT to the midbody. *Nat Cell Biol, 12*(4), 362-371.

Santo, Y., Hirai, H., Shima, M., Yamagata, M., Michigami, T., Nakajima, S., & Ozono, K. (2004). Examination of megalin in renal tubular epithelium from patients with Dent disease. *Pediatr Nephrol, 19*(6), 612-615.

Sato, T., Mushiake, S., Kato, Y., Sato, K., Sato, M., Takeda, N., Ozono, K., Miki, K., Kubo, Y., Tsuji, A., Harada, R., Harada, A. (2007). The Rab8 GTPase regulates apical protein localization in intestinal cells. *Nature, 448*(7151), 366-369.

Schiel, J. A., Park, K., Morphew, M. K., Reid, E., Hoenger, A., & Prekeris, R. (2011). Endocytic membrane fusion and buckling-induced microtubule severing mediate cell abscission. *J Cell Sci, 124*(Pt 9), 1411-1424.

Schill, N. J., Anderson, R. A. (2009). Two novel phosphatidylinositol-4-phosphate 5-kinase type Igamma splice variants expressed in human cells display distinctive cellular targeting. *Biochem J*. 422:473–482.

Schlüter, M. A., Pfarr, C. S., Pieczynski, J., Whiteman, E. L., Hurd, T. W., Fan, S., Liu, C. J., Margolis, B. (2009). Trafficking of Crumbs3 during cytokinesis is crucial for lumen formation. *Mol Biol Cell, 20*(22), 4652-4663.

Schmidt, K., & Nichols, B. J. (2004). A barrier to lateral diffusion in the cleavage furrow of dividing mammalian cells. *Curr Biol, 14*(11), 1002-1006.

Schonteich, E., Wilson, G. M., Burden, J., Hopkins, C. R., Anderson, K., Goldenring, J. R., & Prekeris, R. (2008). The Rip11/Rab11-FIP5 and kinesin II complex regulates endocytic protein recycling. *J Cell Sci, 121*(Pt 22), 3824-3833.

Schweitzer, J. K., Burke, E. E., Goodson, H. V., & D'Souza-Schorey, C. (2005). Endocytosis resumes during late mitosis and is required for cytokinesis. *J Biol Chem, 280*(50), 41628-41635.

Schweitzer, J. K., & D'Souza-Schorey, C. (2004). Finishing the job: cytoskeletal and membrane events bring cytokinesis to an end. *Exp Cell Res, 295*(1), 1-8.

Scita, G., Confalonieri, S., Lappalainen, P., & Suetsugu, S. (2008). IRSp53: crossing the road of membrane and actin dynamics in the formation of membrane protrusions. *Trends Cell Biol, 18*(2), 52-60.

Seemann, J., Pypaert, M., Taguchi, T., Malsam, J., & Warren, G. (2002). Partitioning of the matrix fraction of the Golgi apparatus during mitosis in animal cells. *Science, 295*(5556), 848-851.

Sharma, N., Low, S. H., Misra, S., Pallavi, B., & Weimbs, T. (2006). Apical targeting of syntaxin 3 is essential for epithelial cell polarity. *J Cell Biol, 173*(6), 937-948.

Shen, L., Weber, C. R., & Turner, J. R. (2008). The tight junction protein complex undergoes rapid and continuous molecular remodeling at steady state. *J Cell Biol, 181*(4), 683-695.

Shrimpton, A. E., Hoopes, R. R., Knohl, S. J., Hueber, P., Reed, A. A., Christie, P. T., Igarashi, T., Lee, P., Lehman, A., White, C., Milford, D. V., Sanchez, M. R., Unwin, R., Wrong, O. M., Thakker, R. V., Scheinman, S. J. (2009). OCRL1 mutations in Dent 2 patients suggest a mechanism for phenotypic variability. *Nephron Physiol, 112*(2), p27-36.

Siller, K. H., & Doe, C. Q. (2009). Spindle orientation during asymmetric cell division. *Nat Cell Biol, 11*(4), 365-374.

Simon, G. C., & Prekeris, R. (2008). The role of FIP3-dependent endosome transport during cytokinesis. *Commun Integr Biol, 1*(2), 132-133.

Simonsen, A., Lippé, R., Christoforidis, S., Gaullier, J. M., Brech, A., Callaghan, J., Toh, B. H., Murphy, C., Zerial, M., Stenmark, H. (1998). EEA1 links PI(3)K

function to Rab5 regulation of endosome fusion. *Nature, 394*(6692), 494-498.

Sirajuddin, M., Farkasovsky, M., Hauer, F., Kühlmann, D., Macara, I. G., Weyand, M., Stark, H., Wittinghofer, A. (2007). Structural insight into filament formation by mammalian septins. *Nature, 449*(7160), 311-315.

Skop, A. R., Liu, H., Yates, J., Meyer, B. J., & Heald, R. (2004). Dissection of the mammalian midbody proteome reveals conserved cytokinesis mechanisms. *Science, 305*(5680), 61-66. Smythe, E., & Ayscough, K. R. (2006). Actin regulation in endocytosis. *J Cell Sci, 119*(Pt 22), 4589-4598.

Smith C, M., Chircop, M. (2012) Clathrin-mediated endocytic proteins are involved in regulating mitotic progression and completion. *Traffic.* 13(12):1628-41.

Sorokin, S. (1962). Centrioles and the formation of rudimentary cilia by fibroblasts and smooth muscle cells. *J Cell Biol, 15*, 363-377.

Straight, S. W., Shin, K., Fogg, V. C., Fan, S., Liu, C. J., Roh, M., & Margolis, B. (2004). Loss of PALS1 expression leads to tight junction and polarity defects. *Mol Biol Cell, 15*(4), 1981-1990.

Strilić, B., Eglinger, J., Krieg, M., Zeeb, M., Axnick, J., Babál, P., Muller, D. J., Lammert, E. (2010). Electrostatic cell-surface repulsion initiates lumen formation in developing blood vessels. *Curr Biol, 20*(22), 2003-2009.

Strilić, B., Kucera, T., Eglinger, J., Hughes, M. R., McNagny, K. M., Tsukita, S., Dejana, E., Ferrara, N., Lammert, E. (2009). The molecular basis of vascular lumen formation in the developing mouse aorta. *Dev Cell, 17*(4), 505-515.

Suchy, S. F., & Nussbaum, R. L. (2002). The deficiency of PIP2 5-phosphatase in Lowe syndrome affects actin polymerization. *Am J Hum Genet, 71*(6), 1420-1427.

Suchy, S. F., Olivos-Glander, I. M., & Nussabaum, R. L. (1995). Lowe syndrome, a deficiency of phosphatidylinositol 4,5-bisphosphate 5-phosphatase in the Golgi apparatus. *Hum Mol Genet, 4*(12), 2245-2250.

Sugiyama, Y., Lovicu, F. J., & McAvoy, J. W. (2011). Planar cell polarity in the mammalian eye lens. *Organogenesis, 7*(3), 191-201.

Sugiyama, Y., Prescott, A. R., Tholozan, F. M., Ohno, S., & Quinlan, R. A. (2008). Expression and localisation of apical junctional complex proteins in lens epithelial cells. *Exp Eye Res, 87*(1), 64-70.

Sun, Y., Carroll, S., Kaksonen, M., Toshima, J. Y., & Drubin, D. G. (2007). PtdIns(4,5)P2 turnover is required for multiple stages during clathrin- and actin-dependent endocytic internalization. *J Cell Biol, 177*(2), 355-367.

Sun, Y., Hedman, A. C., Tan, X., Schill, N. J., & Anderson, R. A. (2013). Endosomal Type Iγ PIP 5-Kinase Controls EGF Receptor Lysosomal Sorting. *Dev Cell, 25*(2), 144-155.

Swan, L. E., Tomasini, L., Pirruccello, M., Lunardi, J., & De Camilli, P. (2010). Two closely related endocytic proteins that share a common OCRL-binding motif with APPL1. *Proc Natl Acad Sci U S A, 107*(8), 3511-3516.

Takatsu, H., Katoh, Y., Ueda, T., Waguri, S., Murayama, T., Takahashi, S., Shin, H. W., Nakayama, K. (2013). Mitosis-coupled, microtubule-dependent clustering of endosomal vesicles around centrosomes. *Cell Struct Funct, 38*(1), 31-41.

Taylor, M. J., Perrais, D., & Merrifield, C. J. (2011). A high precision survey of the molecular dynamics of mammalian clathrin-mediated endocytosis. *PLoS Biol, 9*(3), e1000604. do

TerBush, D. R., Maurice, T., Roth, D., & Novick, P. (1996). The Exocyst is a multiprotein complex required for exocytosis in Saccharomyces cerevisiae. *EMBO J, 15*(23), 6483-6494.

Treyer, A., & Müsch, A. (2013). Hepatocyte polarity. *Compr Physiol, 3*(1), 243-287.

Tuma, P. L., Finnegan, C. M., Yi, J. H., & Hubbard, A. L. (1999). Evidence for apical endocytosis in polarized hepatic cells: phosphoinositide 3-kinase inhibitors lead to the lysosomal accumulation of resident apical plasma membrane proteins. *J Cell Biol, 145*(5), 1089-1102.

Ungewickell, A., Ward, M. E., Ungewickell, E., & Majerus, P. W. (2004). The inositol polyphosphate 5-phosphatase Ocrl associates with endosomes that are partially coated with clathrin. *Proc Natl Acad Sci U S A, 101*(37), 13501-13506.

Utech, M., Ivanov, A. I., Samarin, S. N., Bruewer, M., Turner, J. R., Mrsny, R. J., Parkos, C. A., Nusrat, A. (2005). Mechanism of IFN-gamma-induced endocytosis of tight junction proteins: myosin II-dependent vacuolarization of the apical plasma membrane. *Mol Biol Cell, 16*(10), 5040-5052.

Utsch, B., Bokenkamp, A., Benz, M. R., Besbas, N., Dötsch, J., Franke, I., Fründ, S., Gok, F., Hoppe, B., Karle, S., Kuwertz-Broking, E., Laube, G., Neb, M., Nuutinen, M., Ozaltin, F., Rascher, W., Ring, T., Tasic, V., van Wijk, J. A., Ludwig, M. (2006). Novel OCRL1 mutations in patients with the phenotype of Dent disease. *Am J Kidney Dis, 48*(6), 942.e941-914.

van Rahden, V. A., Brand, K., Najm, J., Heeren, J., Pfeffer, S. R., Braulke, T., Kutsche, K. (2012). The 5-phosphatase OCRL mediates retrograde transport of the mannose 6-phosphate receptor by regulating a Rac1-cofilin signalling module. *Hum Mol Genet,* 1;21(23):5019-38.

van Weering, J. R., Verkade, P., & Cullen, P. J. (2010). SNX-BAR proteins in phosphoinositide-mediated, tubular-based endosomal sorting. *Semin Cell Dev Biol, 21*(4), 371-380.

van Zeijl, M. J., & Matlin, K. S. (1990). Microtubule perturbation inhibits intracellular transport of an apical membrane glycoprotein in a substrate-dependent manner in polarized Madin-Darby canine kidney epithelial cells. *Cell Regul, 1*(12), 921-936.

Vega-Salas, D. E., Salas, P. J., & Rodriguez-Boulan, E. (1987). Modulation of the expression of an apical plasma membrane protein of Madin-Darby canine kidney epithelial cells: cell-cell interactions control the appearance of a novel intracellular storage compartment. *J Cell Biol, 104*(5), 1249-1259.

Vega-Salas, D. E., Salas, P. J., & Rodriguez-Boulan, E. (1988). Exocytosis of vacuolar apical compartment (VAC): a cell-cell contact controlled mechanism for the establishment of the apical plasma membrane domain in epithelial cells. *J Cell Biol, 107*(5), 1717-1728.

Vega-Salas, D. E., San Martino, J. A., Salas, P. J., & Baldi, A. (1993). Vacuolar apical compartment (VAC) in breast carcinoma cell lines (MCF-7 and T47D): failure of the cell-cell regulated exocytosis mechanism of apical membrane. *Differentiation, 54*(2), 131-141.

Vicinanza, M., Di Campli, A., Polishchuk, E., Santoro, M., Di Tullio, G., Godi, A., Levtchenko, E., De Leo, M. G., Polishchuk, R., Sandoval, L., Marzolo, M. P., De Matteis, M. A. (2011). OCRL controls trafficking through early endosomes via PtdIns4,5P_2-dependent regulation of endosomal actin. *EMBO J, 30*(24), 4970-4985.

von Stein, W., Ramrath, A., Grimm, A., Müller-Borg, M., & Wodarz, A. (2005). Direct association of Bazooka/PAR-3 with the lipid phosphatase PTEN reveals a link between the PAR/aPKC complex and phosphoinositide signaling. *Development, 132*(7), 1675-1686.

Voronov, S. V., Frere, S. G., Giovedi, S., Pollina, E. A., Borel, C., Zhang, H., Schmidt, C., Akeson, E. C., Wenk, M. R., Cimasoni, L., Arancio, O., Davisson, M. T., Antonarakis, S. E., Gardiner, K., De Camilli, P., Di Paolo, G. (2008). Synaptojanin 1-linked phosphoinositide dyshomeostasis and cognitive deficits in mouse models of Down's syndrome. *Proc Natl Acad Sci U S A, 105*(27), 9415-9420.

Walther, R. F., & Pichaud, F. (2010). Crumbs/DaPKC-dependent apical exclusion of Bazooka promotes photoreceptor polarity remodeling. *Curr Biol, 20*(12), 1065-1074.

Wang, E., Brown, P. S., Aroeti, B., Chapin, S. J., Mostov, K. E., & Dunn, K. W. (2000). Apical and basolateral endocytic pathways of MDCK cells meet in acidic

common endosomes distinct from a nearly-neutral apical recycling endosome. *Traffic, 1*(6), 480-493.

Wang, Q., & Margolis, B. (2007). Apical junctional complexes and cell polarity. *Kidney Int, 72*(12), 1448-1458.

Wang, Y. J., Wang, J., Sun, H. Q., Martinez, M., Sun, Y. X., Macia, E., Kirchhausen, T., Albanesi, J. P., Roth, M. G., Yin, H. L. (2003). Phosphatidylinositol 4 phosphate regulates targeting of clathrin adaptor AP-1 complexes to the Golgi. *Cell*, 114, 299–310.

Watanabe, S., Ando, Y., Yasuda, S., Hosoya, H., Watanabe, N., Ishizaki, T., & Narumiya, S. (2008). mDia2 induces the actin scaffold for the contractile ring and stabilizes its position during cytokinesis in NIH 3T3 cells. *Mol Biol Cell, 19*(5), 2328-2338.

Watt, S. A., Kular, G., Fleming, I. N., Downes, C. P., & Lucocq, J. M. (2002). Subcellular localization of phosphatidylinositol 4,5-bisphosphate using the pleckstrin homology domain of phospholipase C delta1. *Biochem J, 363*(Pt 3), 657-666.

Weber, K. L., Fischer, R. S., & Fowler, V. M. (2007). Tmod3 regulates polarized epithelial cell morphology. *J Cell Sci, 120*(Pt 20), 3625-3632.

Wenk, M. R., Lucast, L., Di Paolo, G., Romanelli, A. J., Suchy, S. F., Nussbaum, R. L., Cline, G. W., Shulman, G. I., McMurray, W., De Camilli, P. (2003). Phosphoinositide profiling in complex lipid mixtures using electrospray ionization mass spectrometry. *Nat Biotechnol, 21*(7), 813-817.

Willenborg, C., Jing, J., Wu, C., Matern, H., Schaack, J., Burden, J., & Prekeris, R. (2011). Interaction between FIP5 and SNX18 regulates epithelial lumen formation. *J Cell Biol, 195*(1), 71-86.

Wilson, P. D. (1997). Epithelial cell polarity and disease. *Am J Physiol, 272*(4 Pt 2), F434-442.

Wilson, P. D., Devuyst, O., Li, X., Gatti, L., Falkenstein, D., Robinson, S., Fambrough, D., Burrow, C. R. (2000). Apical plasma membrane mispolarization of NaK-ATPase in polycystic kidney disease epithelia is associated with aberrant expression of the beta2 isoform. *Am J Pathol, 156*(1), 253-268.

Wu, H., Feng, W., Chen, J., Chan, L. N., Huang, S., & Zhang, M. (2007). PDZ domains of Par-3 as potential phosphoinositide signaling integrators. *Mol Cell, 28*(5), 886-898.

Wu, S., Mehta, S. Q., Pichaud, F., Bellen, H. J., & Quiocho, F. A. (2005). Sec15 interacts with Rab11 via a novel domain and affects Rab11 localization in vivo. *Nat Struct Mol Biol, 12*(10), 879-885.

Wu, X., Hepner, K., Castelino-Prabhu, S., Do, D., Kaye, M. B., Yuan, X. J., Wood, J., Ross, C., Sawyers, C. L., Whang, Y. E. (2000). Evidence for regulation of the PTEN tumor suppressor by a membrane-localized multi-PDZ domain containing scaffold protein MAGI-2. *Proc Natl Acad Sci U S A, 97*(8), 4233-4238.

Yamada, S., & Nelson, W. J. (2007). Localized zones of Rho and Rac activities drive initiation and expansion of epithelial cell-cell adhesion. *J Cell Biol, 178*(3), 517-527.

Yamamura, R., Nishimura, N., Nakatsuji, H., Arase, S., & Sasaki, T. (2008). The interaction of JRAB/MICAL-L2 with Rab8 and Rab13 coordinates the assembly of tight junctions and adherens junctions. *Mol Biol Cell, 19*(3), 971-983.

Yamashita, K., Suzuki, A., Satoh, Y., Ide, M., Amano, Y., Masuda-Hirata, M., Hayashi, Y. K., Hamada, K., Ogata, K., Ohno, S. (2010). The 8th and 9th tandem spectrin-like repeats of utrophin cooperatively form a functional unit to interact with polarity-regulating kinase PAR-1b. *Biochem Biophys Res Commun, 391*(1), 812-817.

Yanagida, H., Ikeoka, M., Kuwajima, H., Wada, N., Tabata, N., Sugimoto, K., Okada, M., Takemura, T. (2004). A boy with Japanese Dent's disease exhibiting abnormal calcium metabolism and osseous disorder of the spine: defective megalin expression at the brushborder of renal proximal tubules. *Clin Nephrol, 62*(4), 306-312.

Yasuda, T., Ohtsuka, T., Inoue, E., Yokoyama, S., Sakisaka, T., Kodama, A., Takaishi, K., Takai, Y. (2000). Importance of spatial activation of Cdc42 and rac small G proteins by frabin for microspike formation in MDCK cells. *Genes Cells, 5*(7), 583-591.

Yeaman, C., Grindstaff, K. K., Wright, J. R., & Nelson, W. J. (2001). Sec6/8 complexes on trans-Golgi network and plasma membrane regulate late stages of exocytosis in mammalian cells. *J Cell Biol, 155*(4), 593-604.

Yin, H. L., & Janmey, P. A. (2003). Phosphoinositide regulation of the actin cytoskeleton. *Annu Rev Physiol, 65*, 761-789.

Yonemura, S. (2011). Cadherin-actin interactions at adherens junctions. *Curr Opin Cell Biol, 23*(5), 515-522.

Yoshida, S., Bartolini, S., & Pellman, D. (2009). Mechanisms for concentrating Rho1 during cytokinesis. *Genes Dev, 23*(7), 810-823.

Yu, W., Shewan, A. M., Brakeman, P., Eastburn, D. J., Datta, A., Bryant, D. M., Fan, Q. W., Weiss, W. A., Zegers, M. M., Mostov, K. E. (2008). Involvement of

RhoA, ROCK I and myosin II in inverted orientation of epithelial polarity. *EMBO Rep, 9*(9), 923-929.

Zhang, X., Bi, E., Novick, P., Du, L., Kozminski, K. G., Lipschutz, J. H., & Guo, W. (2001). Cdc42 interacts with the exocyst and regulates polarized secretion. *J Biol Chem, 276*(50), 46745-46750.

Zhang, X., Hartz, P. A., Philip, E., Racusen, L. C., & Majerus, P. W. (1998). Cell lines from kidney proximal tubules of a patient with Lowe syndrome lack OCRL inositol polyphosphate 5-phosphatase and accumulate phosphatidylinositol 4,5-bisphosphate. *J Biol Chem, 273*(3), 1574-1582.

Zhang, X., Orlando, K., He, B., Xi, F., Zhang, J., Zajac, A., & Guo, W. (2008). Membrane association and functional regulation of Sec3 by phospholipids and Cdc42. *J Cell Biol, 180*(1), 145-158.

Zheng, Z., Zhu, H., Wan, Q., Liu, J., Xiao, Z., Siderovski, D. P., & Du, Q. (2010). LGN regulates mitotic spindle orientation during epithelial morphogenesis. *J Cell Biol, 189*(2), 275-288.